University of Helsinki
Dissertationes Universitatis Helsingiensis 29/2026

Integrin signalling mediates bi-directional metabolic and functional changes in immune cells

Guillem Saldo Rubio

ACADEMIC DISSERTATION

To be presented, with the permission of the Faculty of Biological and Environmental Sciences of the University of Helsinki, for public examination in lecture room 2402, University of Helsinki, Biokeskus 3,
on 9th January 2026, at 13:00.

Helsinki 2026

Pre-examiners

Professor Marko Salmi, University of Turku

Professor Jari Ylänne, University of Jyväskylä

Custos

Professor Susanna C. Fagerholm, University of Helsinki

Supervisors

Professor Susanna C. Fagerholm, University of Helsinki

Dr. Heidi Harjunpää, University of Helsinki

Opponent

Tenured Scientist Dr. Miguel Vicente Manzanares, Consejo Superior de Investigaciones Científicas

Publisher: University of Helsinki
Series: Dissertationes Universitatis Helsingiensis 29/2026

ISBN 978-952-84-1832-0 (Paper back)
ISBN 978-952-84-1831-3 (PDF)
ISSN 2954-2898 (Print)
ISSN 2954-2952 (PDF)
PunaMusta, Joensuu 2026

Abstract

Immune cells alter their gene expression and metabolic profiles in response to pathogens but also in response to changes in their environment, leading to immune cell activation. One of the environmental sensor systems in immune cells is that created by integrins, which are cell surface adhesion proteins. Integrins allow immune cells to sense their environment as well as play a central role in their extravasation from blood vessels into the sites of inflammation.

The aim of this thesis was to study the role of β2 integrins in immune cell activation, polarization and metabolic reprogramming using an Itgb2 TTT/AAA knock-in mouse line where the kindlin-3 binding site in the cytoplasmic domain of β2 integrin has been mutated. It was previously shown that the TTT/AAA mutation leads to loss of dendritic cell adhesion but results in increased activation of these cells. These dendritic cells also display increased migration to lymph nodes and increased T-cell activation. We show here that somewhat paradoxically these KI dendritic cells displayed a suppressed metabolic profile, i.e. a significant decrease in both glycolysis and oxidative phosphorylation. We found that mimicking this suppressed metabolic profile with a low concentration of the glycolysis inhibitor 2DG (2-deoxy-D-glucose) resulted in wild type dendritic cell activation in a similar way as the KI mutation. 2DG also made dendritic cells more migratory *in vitro* and was shown to generate stronger antitumoral responses *in vivo*, showing that this suppressed metabolic profile is immunologically relevant.

We wondered if similar effects of integrins on immune cell phenotype as those seen in dendritic cells might be at play also in other immune cells. In stroke, microglial responses cause an inflammatory response which is one of the main causes of neuronal damage. Therefore, we studied the effects of the integrin mutation on microglial phenotype and stroke outcome *in vivo*. Interestingly, it was found that the integrin mutation led to decreased inflammation and resulted in neuroprotection following haemorrhagic stroke. The integrin KI microglia displayed a reduced inflammatory response, showing that while integrin signalling regulates the immune system, the effects need not be the same across different immune cell types.

Immune cells constantly interact with each other and with other cells. There existed no assay that would allow for the quantification of the biomechanical parameters in heterogeneous cell clusters, such as those formed by dendritic cells and T-cells in lymph nodes. Having studied the effects of impaired integrin adhesion and signalling in different immune cells, we decided to partner with a biomechanics research group to develop a new assay to investigate the biomechanical properties of immune cell clusters. This assay was then used this to study the effects of different T-cell activation regimens and the integrin KI mutation on the stiffness of immune aggregates. This novel assay is now available as a tool for further studies.

Integrin signalling remains an interesting field of study, with new evidence provided here that deficiencies in integrin function result in immunometabolic changes and immunomodulatory effects in different tissue-specific response pathways.

Acknowledgements / Preface / List of abbreviations / List of symbols

2DG	2-deoxy-D-glucose
ADAM17	α disintegrin metalloproteinase 17
AKT	Protein Kinase B
APC	Antigen-presenting cell
BCR	B-cell receptor
BMDC	Bone-marrow-derived dendritic cell
CalDAG-GEFI	Calcium-Diacylglycerol Guanine Nucleotide Exchange Factor I
cDC	Conventional dendritic cell
COVID	Coronavirus disease
CSF1	Colony stimulating factor 1
CSF1R	Colony stimulating factor 1 receptor
cSMAC	Central supramolecular activation cluster
CTLD	C-type lectin domain
DAG	Diacylglycerol
DC	Dendritic cell
ECAR	Extracellular acidification rate
ECM	Extracellular matrix
EGF	Epidermal growth factor
ERM	Ezrin, radixin, moesin
FAK	Focal adhesion kinase
FAO	Fatty acid oxydation
FERM	4.1 protein, ezrin, radixin, moesin
FERMT3	Kindlin-3 gene
GLUT1	Glucose transporter 1
HSC	Haematopoietic stem cell
IgSF	Immunoglobulin-like superfamily
ILK	Integrin-linked kinase
iNOS	Inducible nitric oxide kinase
IP_3	Inositol 1,4,5-trisphosphate
ITGB2	β2 integrin gene
KI	*Knock-in* (Referencing ITGB2 TTT/AAA mutants)
LAD I	Leukocyte adhesion deficiency 1
LAD II	Leukocyte adhesion deficiency 2
LAD III	Leukocyte adhesion deficiency 3
LC	Langerhans cell

LFA1	Lymphocyte function-associated antigen-1
LPS	Lipopolysaccharide
Mac1	Macrophage antigen 1
MAPK	Mitogen-activated protein kinase
MDP	Macrophage and dendritic cell progenitor
MHCI	Major histocompatibility complex 1
MHCII	Major histocompatibility complex 2
MIDAS	Metal-ion dependent adhesion site
MLC	Myosin light chain
MLCK	Myosin light chain kinase
moDC	Monocyte-derived dendritic cell
mTOR	Mammalian target of rapamycin
mTORC1	Mammalian target of rapamycin complex 1
mTORC2	Mammalian target of rapamycin complex 2
MYTP1	Myosin phosphatase target subunit 1
NET	Neutrophil extracellular trap
NK cell	Natural killer cell
NO	Nitic oxide
OCR	Oxygen-consumption rate
OXPHOS	Oxidative phosphorylation
PAR4	Protease-activated receptor 4
pDC	Plasmacytoid dendritic cell
PfkI	Phosphofructokinase 1
PINCH	Particularly interesting cysteine- and histidine-rich protein
PIP2	Phosphatidylinositol 4,5-bisphosphate
PKC	Protein kinase C
Pkm	Pyruvate kinase
PLC	Phospholipase C
PMA	Phorbol 12-myristate 13-acetate
PSGL1	P-selectin glycoprotein ligand-1
pSMAc	Peripheral supramolecular activation cluster
qPCR	Quantitative polymerase chain reaction
RAP1	Ras-proximate-1
RIAM	Rap1-GTP-interacting adaptor molecule
ROS	Reactive oxygen species
SHC	Src homology 2 domain-containing transforming protein 1
SRC	SRC proto-oncogene, non-receptor tyrosine kinase
TAZ	Transcriptional coactivator with PDZ-binding motif
TCR	T-cell receptor
TLR	Toll-like receptor
TNF	Tumour necrosis factor
VEGF-R1	Vascular endothelial growth factor receptor 1
VEGF-R1	Vascular endothelial growth factor receptor 2
VWA	von Willebrand domain A
vWF	von Willebrand factor
WT	*Wild type* (Referencing ITGB2)
YAP	Yes-associated protein

Index

List of original publications

This thesis is based on the following publications, which are referred to in the text by their roman numerals:

I Harjunpää, H., Somermäki, R.*, Saldo Rubio, G.*, Fusciello, M., Feola, S., Faisal, I., Nieminen, A. I., Wang, L., Llort Asens, M., Zhao, H., Eriksson, O., Cerullo, V., & Fagerholm, S. C. (2024). Loss of β2-integrin function results in metabolic reprogramming of dendritic cells, leading to increased dendritic cell functionality and anti-tumor responses. *OncoImmunology*, *13*(1). https://doi.org/10.1080/2162402X.2024.2369373

Prepared dendritic cell suspensions for peritumoral injection, performed translation rate analysis and cell migration assay. Collaborated with co-authors in dendritic cell culture and isolation, ROS assay, flow cytometry, qPCR, analyses as well as the associated data analysis of the aforementioned experiments. Wrote the materials and methods of the experiments for which I was solely responsible and participated in the review of the manuscript together with the co-authors.

II Harjunpää, H., Tallberg, R., Cui, Y., Guenther, C., Liew, H.-K., Seelbach, A., Saldo Rubio, G., Airavaara, M., & Fagerholm, S. C. (2024). β2-Integrins Regulate Microglial Responses and the Functional Outcome of Hemorrhagic Stroke In Vivo. *The Journal of Immunology*, *213*(4), 519–525. https://doi.org/10.4049/JIMMUNOL.2300815

Performed cell culture and isolation of leukocytes and microglia cells together with H.H. and C.Y. Helped analyse the cylinder test paw usage with H.H and C.Y.. Participated in the review of the manuscript together with the co-authors.

III Askari, S.*, Saldo Rubio, G.*, Datar, A., Harjunpää, H., Fagerholm, S. C., & Backholm, M. (2025). Soft matter mechanics of immune cell aggregates. *Journal of the Royal Society Interface*, *22*(228). https://doi.org/10.1098/RSIF.2025.0231

Performed the T-cell culture and isolation, the translation rate analysis, the flow cytometry and their respective statistical analyses. Aided in the operation and optimization of the force assay along with the experimental design. Wrote the parts of the manuscript pertaining to biology with the physics sections written by A.S.

*Equal contribution

1 Brief overview of the immune system

Immunity and how it functions was brought to the forefront of human consciousness with the COVID pandemic. All readers will be aware that evolution has granted us a complex system of threat-recognition mechanisms to be able to respond to foreign cells and viruses entering our bodies and with the ability to form an increasingly effective response against recurring threats. In short, mammals have two sets of immune components, those which recognize specific antigens (adaptive immunity) and those which recognize molecular patterns (innate immunity).

The components of innate immunity range from barrier systems, like our skin which separates our insides from all the bacteria and viruses in the environment, to cells that process these foreign agents to be able to mount a tailored immune response. Most of these immune cells come from stem cells located in the bone marrow as described in Figure 1, while embryonic precursors instead being the origin for most tissue-resident macrophages, including microglial cells[1,2].

The innate immune system is ready to respond to foreign bodies and damage much faster than the adaptive immune system, though their responses are not as specific as antigen-specific T- and B-cell responses. The adaptive immune system meanwhile gets more efficient with subsequent challenges by the same antigen, with memory cells expanding their population with repeated challenges. Therefore, each subsequent challenge by the same antigen is met with a faster and more vigorous response. This increase in immune response efficiency is due to both the 20-1000 times increase in the number of antigen-specific memory cells and faster activation kinetics compared to the first challenge with a given antigen[3–7].

The innate immune system contains cells such as basophils, eosinophils and neutrophils, which in simplistic terms cause inflammation, kill parasites and eat intruding cells, respectively. It also contains cells which after phagocytizing bacteria and aberrant cells (infected and cancerous ones) are able to break them down and present their fragments to T and B lymphocytes to evoke the adaptive immunity. These professional antigen presenting cells (APCs) express Major Histocompatibility Complex II (MHCII)[8] and include dendritic cells (DCs), macrophages (including microglia) and B-cells[9,10]. MHCII serves to present antigens of extracellular source taken up by APCs via endocytosis and processed into small immunogenic peptides[8]. These presented peptides can engage cognate T

cell receptors (TCRs) and generate a specific response against the bacteria or aberrant cells expressing the peptide. On the contrary to MHCII, MHCI is expressed in all nucleated cells and constantly presents self-antigens and any other antigens of internal origin such as parts of any viruses that may have infected the cell[8]. This presentation of endogenous antigens allows for targeted cytotoxicity when viral or tumour antigens are being presented on the cell surface[11]. In addition, APCs are able to utilize MHCI molecules to present exogenous or externally derived antigens in a process termed cross-presentation which is vital for mounting efficient immune response against virally infected or cancer cells[12].

Among the professional APCs, there exist differences in the context and efficiency in mounting an immune response. DCs excel at presenting antigens and are responsible for initiating most adaptive immune responses[13]. Macrophages present antigens to the adaptive immune system through MHCII and participate in both tolerogenic and inflammatory responses while also being vital for the correct development and homeostasis of many tissues[13–16]. Microglia cells are brain-residing macrophages with a highly specialized neuron-housekeeping role[13,17]. B-cells can uptake and process antigens through the MHCII pathway as other APCs but can also uniquely capture antigens from the extracellular space via their B-cell receptors (BCR) and endocytose them for MHCII presentation if they match their specific BCR[13,18].

Recently, it has become evident, that the function of an immune cell is tightly connected to the metabolic status of the cell[19–24]. During an infection, T- and B-cells for example modify their metabolism away from oxidative phosphorylation (OXPHOS) and towards glycolysis to meet the energetic and biosynthetic needs of rapid cell expansion[25,26]. This cell replication results in a large increase of cells capable of responding to the specific threat that activated them and allows for a tailored immune response of tightly orchestrated T- and B-cell responses. After the infection is cleared, the number of immune cells reactive to those antigens remains higher than before due to the establishment of memory T- and B-cells[27,28]. The metabolism of these memory cells however returns to one dominated by OXPHOS and fatty acid oxidation (FAO), exemplifying how the immunological activation of cells closely correlates with their metabolic state[29].

This overview, however, is a very simple version of a very complex system of which we are still learning from. One example of this limited simplicity is the fact that even among the innate immune cells there exists a level of memory termed "trained immunity"[30,31]. This trained immunity differs from adaptive immunity in that instead of being centred around a more efficient response to a specific antigen, it is able to respond more effectively in an antigen agnostic way. This memory capacity of innate immune cells is caused by epigenetic reprogramming during infection, causing a shift in their metabolic profile towards glycolysis to meet the metabolic needs of increased production of cytokines and rapid activation and cell

division[28,32–35]. Different to the adaptive immune memory, which can last for a lifetime, the longest trained immunity is believed to last up to 5 years with months being the more common timeframe[36].

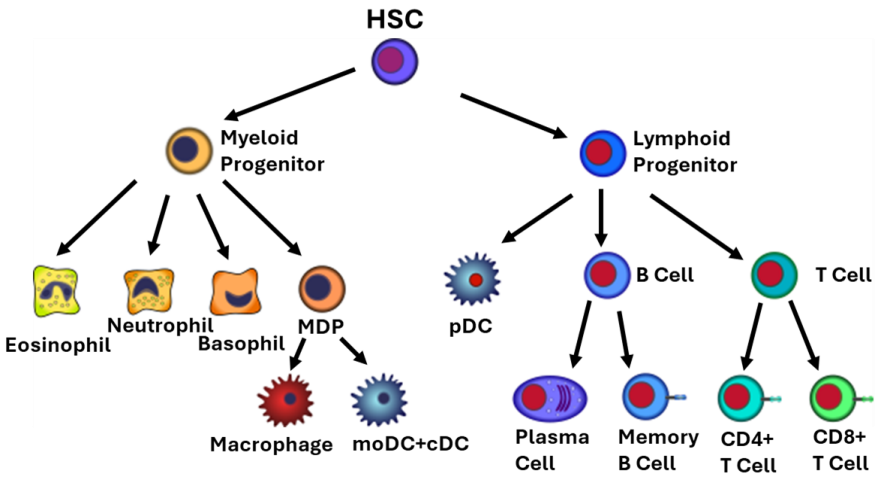

Figure 1. Haematopoietic cells derived from bone marrow haematopoietic stem cells (HSC), branching first to myeloid and lymphoid progenitor cells. From there myeloid progenitors differentiate to eosinophils, neutrophils, basophils and macrophage and dendritic cell progenitor (MDP) the latter of which gives rise to both (some) macrophages, monocyte-derived dendritic cells (moDC) and myeloid/conventional dendritic cells (cDC). Lymphoid progenitors meanwhile differentiate to produce plasmacytoid dendritic cells (pDCs), B-cells and T-cells. T-cells differentiate into CD4 or CD8 naïve, effector or memory cells and B-cells maturing to either plasma cells or memory B-cells[37].

2 Adhesion molecules in immunology

2.1 Adhesion molecules

Cells interact with their environment through adhesion, and this adhesion is mediated by a vast array of functionally and structurally distinct adhesion molecules. The molecules are divided into four families according to both structural similarities and ligand types: integrins, selectins, cadherins and the immunoglobulin superfamily (IgSF) including nectins. As an added level of complexity, many of these adhesion proteins are capable of making bonds that get stronger (catch bonds) or weaker (slip bonds) when force is applied, or ones whose adhesion force stays the same regardless of tension (ideal bonds)[38]. A list of some adhesion molecules relevant to immunity, their ligands and families can be found at Table 1.

Table 1. A selection of immunologically relevant adhesion proteins tabulated together with some of the components of the extracellular matrix (ECM) or structural components they bind to as well as the adhesion molecule family they belong to. In parentheses are other common names for the adhesion proteins.

Adhesion protein	ECM or structural component	Adhesion molecule family
α1β1 (VLA-1)	Collagen, Laminin [39–41]	Integrin
α2β1 (VLA-2)	Collagen, Laminin, Chondroadherin [39–41]	Integrin
α3β1 (VLA-3)	Collagen, Laminin, Reelin, Thrombospondin 1, Fibronectin [39–41]	Integrin
α4β1 (VLA-4)	Fibronectin, Osteopontin, VCAM-1[39]	Integrin
α9β1 (RLC)	Collagen, Laminin, Tenascin, Osteopontin [39–41]	Integrin
αLβ2 (LFA-1, CD11a/CD18)	ICAM-1/2/3/4/5, JAM-A[39–41]	Integrin
αMβ2 (MAC-1, CR3, CD11b/CD18)	ICAM-1, iC3b, Fibrinogen, Plasminogen, MPO [39–41]	Integrin
αXβ2 (P150, CR4, CD11c/CD18)	Fibrinogen, VCAM-1, ICAM-1	Integrin
P-selectin	P-selectin glycoprotein ligand-1 (PSGL-1)[42,43]	Selectin

E-selectin	PSGL-1, E-selectin ligand (ESL-1), and CD44[44]	Selectin
L-selectin	PSgl-1, CD34, GlyCAM-1[45]	Selectin
E-cadherin	E-cadherin, αEβ7 and α2β1[46,47]	Cadherin
Desmocollin	Desmocollin, desmoglein[48]	Cadherin
Desmoglein	Desmoglein, desmocollin[48]	Cadherin
CD2 (LFA-2)	CD58 (LFA-3)[49]	Immunoglobulin superfamily
CD4	MHCII[50,51]	Immunoglobulin superfamily
ICAM-1 (CD54)	LFA-1 (αLβ2)[51,52]	Immunoglobulin superfamily
Nectin-1	Tactile[53]	Nectin
Nectin-2 (PVRL2)	PVRIG, TIGIT, DNAM1 [53,54]	Nectin
Nectin-3	TIGIT [53]	Nectin
Nectin-4	TIGIT [53]	Nectin
Necl-2	CRTAM [53]	Nectin
Necl-5 (PVR)	TIGIT[53,54]	Nectin

Integrins are heterodimeric transmembrane adhesion proteins that bind to a wide variety of extracellular matrix components which is why sometimes they are called matrix adhesion proteins. The α-subunit seems to be a primary determinant of extracellular ligand binding specificity, whereas the β-tail is the main moderator of intracellular interactions. Integrins form catch bonds that transition to slip bonds as tension increases[55]. Integrins will be discussed at length later on as they are the main focus of the thesis work.

Selectins are monomeric transmembrane cell adhesion proteins that mediate cell-cell adhesion by binding specific carbohydrate polymers in a catch-bond manner[56]. They are divided into three subtypes P, E and L selectins depending on what cells express them: platelets (P) (and endothelial cells), endothelial cells (E) and leukocytes (L), respectively[57,58]. Each selectin possesses an N-terminal calcium-dependent (C-type) lectin domain (CTLD), an epidermal growth factor (EGF)-like domain, a varying number of short complement-like repeat (SCR) domains, a transmembrane domain and a short cytoplasmic tail[59]. Selectins undergo extensive post-translational modifications with L-selectin having a protein weight of 30 kDa but an observed weight of 70-100 kDa depending on the cell type[43]. Interestingly, it is the N- and O- linked glycosylation which largely determines the binding specificity of selectins[44,60,61]. L-selectin binds to CD34 by attaching to the sulphated sialyl-Lewis^X that is part of the O-glycan attached to CD34. P-selectin binds to the O-linked glycan in the N terminus of P-selectin glycoprotein ligand-1 (PSGL-1) when the sialyl-Lewis^X and nearby tyrosines are modified with sulphate[62]. E-selectin, being the most versatile of the family, can bind to sialyl-Lewis^X attached to

either PSGL-1, CD43 or CD44[62]. In blood vessels, L-selectin on leukocytes undergoes sub-second changes in bond lifetime with its ligand under flow conditions, categorised into "catch" and "slip" bonds[43]. Initial contact between the CTLD and ligand on the leading edge of the cell exerts a low tensile strength[63]. Under optimal shear stress conditions (0.3–1.0 dyne per cm^2), the tensile force between the CTLD and its ligand increases to unfold and expose a greater region for ligand binding[64]. By this point, ligand interaction is directly under the rolling cell. The bond lifetime increases under this condition and forms a canonical "catch" bond. Later, the tensile force between the CTLD and ligand increases further as the leukocyte rolls over the initial site of contact and as such the bond originally at the leading edge is now at the trailing edge. As the tensile force exceeds the limit for catch bonds, the bond lifetime decreases and "slips" to release the CTLD from its ligand. Under conditions of abundant ligand availability, a new catch bond will form at the new leading edge allowing the process to repeat, culminating in classic cell rolling behaviour[43,44,65]. This rolling effectively decreases the speed at which leukocytes move through blood vessels. This slower movement gives the opportunity for more complex adhesions to take place at for example sites of inflammation[66,67].

In neutrophils the ectodomains of L-selectins can be cleaved off in response to external stimuli leading selectins to lose their adhesion capabilities to ligands. The minimal structural determinant for a selectin ligand is composed of a branched tetra saccharide, called sialyl Lewis x (sLe^x), containing sialic acid, galactose, fucose and N-acetyl glucosamine (expressed as: Siaα2,3Galβ1,4 (Fucα1,3)GlcNAc)[43]. L-selectin binds to sulphated variants of sLe^x with higher affinity than to un-sulphated variants. This allows, for example, the homing of neutrophils to lymph nodes as the endothelial cells lining the venules leading to peripheral lymph nodes constitutively express sulphated-sLe^x. Neutrophil activation with pro-inflammatory stimuli like formyl peptides (from Gram negative bacteria or mitochondria), tumour necrosis factors (TNFs) or toll-like receptors (TLR) agonists leads to rapid shedding of L-Selectin ectodomains via cleavage at the membrane-proximal ends. The main enzymes responsible for the cleavage of L-selectin are α disintegrin and metalloproteinase 17 (ADAM17)[68] which are expressed and stored in vesicles in numerous leukocyte subtypes and can be rapidly mobilised to the plasma membrane in response to cell-activating stimuli.

In leukocytes, ADAM17 activity is controlled by two major kinases: protein kinase C (PKC) and p38 mitogen-activated protein kinase (MAPK)[68,69]. PKC-induced shedding of L-selectin is strongly dependent on regulatory elements within the cytoplasmic tail of L-selectin (serine phosphorylation and ERM binding), whereas p38 MAPK-induced shedding requires threonine phosphorylation of the ADAM17 cytoplasmic tail[68,69]. The nature of the activating signal dictates the kinase pathway that will ultimately be responsible for the shedding, with N-

Formylmethionyl-leucyl-phenylalanine/lipopolysaccharide (LPS)/TNF-induced shedding mediated more through p38 MAPK and T-cell receptor signalling-induced shedding of L-selectin being driven by PKCα [70]. Calmodulin acts as a negative regulator of shedding and its constitutive association with the L-selectin tail in resting cells keeps the selectin cleavage site in a conformation resistant to proteolytic attack by ADAM17 [71]. The cleavage coincides with the downregulation of production of further L-selectins and the upregulation of αMβ2. This upregulation is largely achieved by the recruitment of internal vesicles rich in αMβ2 to the cell surface from where the integrins can participate in outside-in signalling and leukocyte arrest.

Cadherins are dimeric transmembrane cell adhesion proteins whose name reflects their reliance on extracellular calcium to maintain a conformation which allows binding. There are over one hundred types of cadherins in humans alone[72]. And to help manage this complexity they are often classified into four groups: Classical cadherins, desmosomal cadherins, protocadherins, and unconventional cadherins.

Classical cadherins are the group that contains the first characterized cadherins. These cadherins are transmembrane dimeric proteins that have five calcium-binding extracellular domains which stiffen when binding calcium[47,73]. Following calcium binding, these cadherins form zipper-like bonds with cadherins in a nearby cell by having the five calcium-binding repeats adhere along the length of the protein[47,74]. Desmosomal cadherins form the transmembrane protein components of desmosomes and are comprised of all types of desmocollin and desmoglein. They tend to form heterodimers and contain four extracellular calcium-binding repeats that bind the opposing trans heterodimer, with desmocollin binding to desmogleins in the cis and trans dimer[75]. Protocadherins generally exhibit weaker binding forces than classical or desmosomal cadherins and can even be calcium independent[74]. Unconventional cadherins are all the rest of the cadherins which cannot be characterized into the other groups[47].

Immunoglobulin superfamily adhesion proteins are a widely diverse family of adhesion molecules. They comprise of either several immunoglobulin-like extracellular repeats bound to a fibronectin type III domain, which links them to a membrane-anchoring glycosylphosphatidylinositol[51], or immunoglobin-like extracellular repeats bound to an alpha chain transmembrane domain and one or more intracellular signalling domains[49,52,76]. This superfamily of adhesion proteins can make up to 50% of the total leukocyte surface glycoproteins[77]. To make sense of this diversity, they are often classified by their binding types: homotypic binding and heterotypic binding. Homotypic binding occurs between two identical adhesion

proteins in opposing cell faces. Examples of this adhesion mode include NCAM, CEA, CD31 and CD66 though the degree of overlap and number of immunoglobulin domains involved in binding varies. Heterotypic binding has been studied at length as many leukocyte adhesions are formed between an immunoglobulin family protein and an adhesion protein of another type. Among these, CD2/CD58, CD4/MHCII and ICAM-1/αLβ2 are the most studied.

Nectins are a distinct subgroup of immunoglobulin adhesion proteins which are transmembrane adhesion proteins containing three Ig-like extracellular domains. Similar to cadherins, nectins form cis-dimers which then interact with trans dimers on the reciprocal binding surface. However, nectins are calcium independent and therefore form ideal bonds[78,79]. There have been 9 different nectins identified to date, with Nectin 1-4 being able to bind afadin (cytoskeleton linker protein) cytoplasmically and Necl (nectin-like) 1-5 lacking afadin interaction[80].[70]. Nectins form cell-cell junctions and are vital for tissue integrity in organs such as kidneys[81]. Nectins (particularly nectins-2 and -4) are ligands for immune checkpoint receptors such as TIGIT and CD96, being thus important in cancer immunology[82]. However, the role of all nectins is not yet fully understood, and some, such as Necl-1, have not been conclusively found expressed in any non-cancerous tissue[80] .

2.2 Integrins

Integrins were first identified through their role in integrating the cytoskeleton to the extracellular matrix. This identification was done by Richard Hynes, Erkki Ruoslahti, and Timothy Springer in the 80s and earned them the Albert Lasker Basic Medical Research Award in 2022. Since those early experiments much more research has been conducted, and techniques have evolved enabling to know the position of each atom in an integrin and to identify every existing integrin in mammals[83–86].

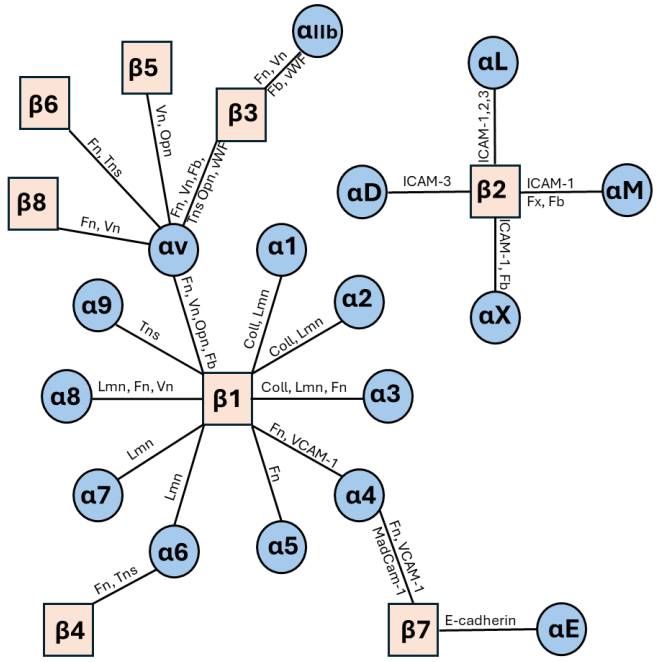

Figure 2. Integrin chains, dimers and their canonical ligands. Integrin α-β dimers represented by joining the chains via a line containing the canonical ligands of each heterodimer. Ligand abbreviations used: Coll (Collagen), Fb (Fibrinogen), Fn (Fibronecrtin), Fx (Factor X), ICAM-1,2,3 (Intracellular Adhesion Molecule-1,2,3), Lmn (Laminin), MadCam-1 (Mucosal ADdressin Cell Adhesion Molecule-1) Opn (Osteopontin), Tns (Tenascin), VCAM-1 (Vascular Cell Adhesion Molecule-1), Vn (Vitronectin) and vWF (von Willebrand's Factor).

In mammals, integrins exist as 24 different heterodimers of an α and a β chain as shown on Figure 2. There are sixteen α and eight β chains with the α chains being responsible for ligand specificity and the more conserved β chains mostly responsible for signal transduction[87]. Each subunit, whether α or β, has a broadly similar structure with one large multi-domain extracellular segment, one transmembrane helix, and a short cytoplasmic tail. The extracellular region interacts with ECM ligands, ligands on other cells or soluble ligands, and is composed of approximately 1104 (700–1100) amino acid residues long α subunit and 778 residues long β subunit[88]. The N-terminal extracellular domain of each integrin monomer forms a globular "head" connected to the membrane by an elongated ~170 Å "stalk". All β subunits (β1-8) and half of the mammalian α subunits (α1,2,10,11,D,E,M,L and X) contain an additional domain not present in the other half (α 3-9,IIb and V), which is an approximately 190 amino acid domain termed the von Willebrand A domain (VWA). VWO acts as a metal-ion dependent adhesion site (MIDAS) motif and is also known as the I-domain (Inserted domain)[89] (Figure 3). The MIDAS motifs show certain imperfection in β chains and

may not be fully functional as MIDAS[90]. Nevertheless, these motifs are where α and β subunits interface in the extracellular space and together comprise the binding site for ligands. The MIDAS-positive α subunits can be divided into two groups. Integrins α1, α2, α10, and α11 associate with integrin β1 subunit to form receptors for collagen. Integrins αL, αM, αD, αX complex with the β2 subunit, whereas αE complexes with β7, these five integrins are expressed on leukocytes where they mediate cell interactions.

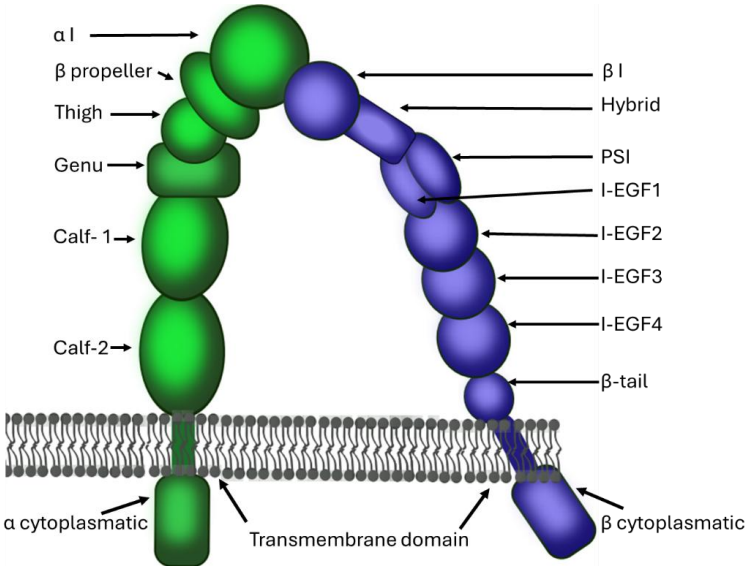

Figure 3. Domains of a prototypic MIDAS-positive integrin dimer, pictured here in the open high affinity conformation. The α chain is depicted in green and the β one in blue.

2.3 Inside-out signalling

2.3.1 General inside-out signalling

High-affinity binding of integrins to ligands is not constitutive but requires a conformational switch of the ligand-binding site. Integrins are constitutively found in a closed state with the ligand-binding site largely hidden. This regulatory mechanism allows leukocytes and platelets, for example, to circulate in the blood without pathologically adhering to each other or to the vascular wall. The switch to the high-affinity state is rapid, with a sub-second time frame, is reversible in under a minute, and is triggered from within the cell in response to extracellular chemical and/or mechanical stress signals[91]. This dimension of environmental interaction is

known as inside-out signalling[92–94]. Integrins are the most well-studied proteins capable of inside-out signalling (Figure 4).

As mentioned, integrins are generally found in their closed conformation in homeostatic conditions, preventing binding of the ECM and other binding partners. Depending on the cell type, different signals can trigger a signalling cascade that results in integrin conformational change and stable binding. The intracellular tails of the integrins are known to have electrostatic interactions between the Arg 995 of αIIb and Asp 723 of β3 (and equivalent positions in other α and β chains) which keep the tails together and as a result, the extracellular domains in the closed conformation [95]. Similarly, the helix-helix transmembrane interaction between the α and β integrins allows them to be close enough for the intracellular electrostatic interaction to take place. It has been confirmed that it is both the intracellular and transmembrane interactions between the α and β chains that are needed to maintain the closed interaction as when the transmembrane domains are mutated to hinder the helix-helix interaction, the integrins are left constitutionally active [96]. For this combined role of the cytoplasmic and transmembrane domains of integrin dimers, they are often termed as the inner and outer membrane clasp [96]. The binding of both being necessary to maintain the inactivity of the integrin [96].

Integrin clasps can be disrupted by different biological processes, for example, by the binding of talin[93,97–100]. Talin is an important regulator of integrin activity as its binding to the β chain disrupts the closed conformation and promotes the activation of the integrin dimer. The exact mechanism by which this is achieved remains in contention but is most likely a combination of the following three mechanisms. 1) Talin binds the β chain and the membrane and promotes a tilt in the bound integrin which disrupts the inner and outer membrane clasp[101]. 2) Talin binds the integrin in a way that talin's Lys 324 is close to Asp 723 on β3 integrin and thus is able to affect the salt bridge between Arg 995 and Asp 723 in αIIbβ3 (equivalent positions on other integins)[102]. 3) Simple steric interference between talin and the cytoplasmic tail of α integrin in such a way that the tails of the integrin dimer are wedged apart[103].

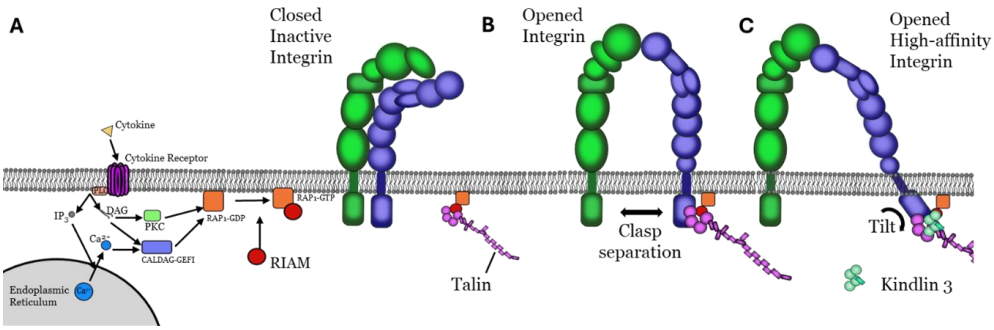

Figure 4. Inside-out activation of integrins. A) Chemokine signalling causes phospholipase C (PLC) to cleave membrane lipids into phosphoinositol-triphosphate (IP_3) and diacylglycerol

(DAG). IP_3 leads to the release of calcium from the endoplasmic reticulum. From there DAG and Ca^{2+} activate either protein kinase C (PKC) or calcium and diacylglycerol-regulated guanine-nucleotide exchange factor 1 (CALDAG-GEFI), leading to the exchange of GDP to GTP on Ras-related protein 1 (RAP1). RAP1-GTP can then recruit Rap1-GTP-interacting Adaptor Molecule (RIAM). RIAM in turn recruits both talin and kindlin which favour the opening of the integrins via the separation of the membrane clasp (B) and tilt of the trans-membrane β integrin to yield a high-affinity open state(C)[104,105].

Talin exists at rest as an antiparallel homodimer with each monomer consisting of a 270 kDa protein with a globular head and a rod-shaped c-terminal tail[98]. The domain responsible for Talin's binding affinity is the globular FERM (protein 4.1, ezrin, radixin, moesin) which contains the (ezrin, radixin and moesin) structure common to all ERM proteins. Talin's affinity for the tail of β integrins can be regulated by the state of talin as in its resting state the integrin-binding "head" is masked by its tail. This inhibiting tail can be cleaved off from talin by the proteases calpain or thrombin in response to certain stimuli which increases affinity for integrins sixfold[106]. The C-terminal tail can also be induced to unmask the head of talin via ERM protein phosphorylation, Rho-dependent signalling and PIP2 (phosphatidylinositol 4,5-bisphosphate). Talin in its autoinhibited form is recruited to the cell membrane through binding to RIAM (Rap1-GTP-interacting Adaptor Molecule). RIAM is an effector of Rap1 (Ras-related protein 1), which when activated by phosphorylation via Src (proto-oncogene tyrosine-protein kinase) or FAK (Focal Adhesion Kinase), can interact with the membrane-linked Rap1[103,107–109]. RIAM seems to recruit both kindlin and talin to the cell membrane, allowing for their coordinated interaction with the tails of β integrins[110]. The activation of Rap1 hinges on the inactive GDP bound to it at rest being exchanged for a GTP via a GEF (Guanine nucleotide-exchange factor) action. This nucleotide exchange is the most common nexus between different signalling cascades which share CalDAG-GEF1 (calcium and diacylglycerol-regulated GEF1)[105] (Figure 4, A). The N-terminal domain of talin has been shown to bind to layilin[111], focal adhesion kinases[112], polyphosphoinositides[113], and to integrin β1 and β3 cytoplasmic domains[114,115]. Similarly, the C-terminal domain binds also to the integrin cytoplasmic domain and, in addition, to vinculin[116] and to actin filaments[117]. All of these interactions serve to modulate the interaction between talin and the cytoplasmic tails of β integrins, to affect integrin clustering and signalling as a result.

Once the integrins are activated and their cytoplasmic tails are pulled apart, they unfold, revealing their ligand-binding sites in a process taking altogether less than a second[118,119]. Structural studies have shown that the I domains on integrin dimers are coordinated with each other in such a way that "pulling" on the β chain from within the cell is enough to induce a conformation change in both chains of the dimer[120]. The presence of magnesium ions in the metal coordination locus of MIDAS has been shown to reduce the energy threshold needed to unfold integrins as it reduces the stiffness of the hybrid hinge-like domain[121].

2.3.2 Cell-specific inside-out integrin activation

In T-cells, TCR activation leads to integrin activation[122]. APCs interface with T-cells by means of the immunological synapse. The immunological synapse is a highly organized structure of clustered TCRs ringed by αLβ2. Within minutes of TCR stimulation there is a change in integrin conformation leading to adhesion without the need for changes in cell surface integrin levels. In resting T-cells, both the inactive and active forms of αLβ2 are mobile on the cell surface while the intermediate activation state of αLβ2 (Figure 4, B) is anchored to the cytoskeleton and immobile[123]. Calpain activation unlinks the intermediate form of αLβ2 but promotes the cytoskeletal anchoring of the active form which allows for the formation of the active immunological synapse[123].

Integrin clustering is important for reinforcing adhesion signalling and can occur both by multiple integrins binding the same extracellular ligand (usually a matrix component) or through the sharing of the same intracellular integrin-associated proteins[123–125]. Classical examples of integrin clustering are focal complexes as well as both fibrillar and focal adhesions in fibroblasts, the aforementioned immunological synapses in activated T-cells, podosomes in macrophages and adherent osteoclasts, and invadopodia in cancer cells. Talin binding to integrin as a homodimer provides a potential mechanism by which talin may cross-link integrins at the same time as it activates them, with each N-terminal talin head of the dimer binding to a different integrin[126].

Platelets express a variety of integrins including $\alpha_2\beta_1$, $\alpha_5\beta_1$, $\alpha_6\beta_1$, $\alpha_v\beta_3$ and $\alpha_{IIb}\beta_3$. $\alpha_{IIb}\beta_3$ is unique to platelets and megakaryocytes. $\alpha_{IIb}\beta_3$ has fibrinogen, fibrin, fibronectin and von Willebrand factor as binding partners which allows it to crosslink platelets and enable platelet aggregation[127]. In resting platelets, the integrin is maintained in the low affinity closed conformation and opens in response to inside-out activation. Initially thrombin binds to PAR4 (Protease-Activated Receptor 4 in mice, in humans Protease-Activated Receptor 1) which causes phospholipid hydrolysis and therefore the local production of IP_3 (Inositol-3-Phosphate) and DAG (Diacylglycerol) which together increase intracellular Ca^{2+} levels activating PKC and CALDAG-GEFI. CALDAG-GEFI then exchanges GDP from RAP1-GDP with GTP to produce RAP1-GTP which allows it to recruit RIAM (RAP1-GTP Interacting Adaptor Molecule). Talin 1 and kindlin-3 are RIAM's binding partners at the membrane which are able to activate the integrin. Other activating stimuli converge in the increase of intracellular calcium and from there the activation cascade of $\alpha_{IIb}\beta_3$ remains the same[127,128]. Figure 4A describes leukocyte integrin activation, but this activation is very similar in platelets.

2.4 Outside-in signalling

Integrins are also able to be activated from the extracellular space as the closed conformation of integrins does not fully hide the ligand binding site. Once the extracellular domain of integrins bind to their ligand, the inner and outer membrane clasps separate[41,93,94]. To reinforce this opening, talin is recruited and it stabilizes the open conformation of the integrin dimer[93,94,121]. Once bound to integrins, however, talin is not static as it has been found to unfold to promote stable activation and integrin cross-linking upon transduction of mechanical traction forces from actomyosin to the ECM[129]. This unfolding of talin is responsible for the catch-bond behaviour of integrins. The entire ECM-integrin-talin-actin complex is often described as the integrin clutch; a complex that reacts in different ways to different levels of force[130–133] (Figure 5). Talin unfolds its three hinge-like helical domains R1-3, with R3 being the mechanosensing one. It unfolds at ~5 pN which is the *in-vivo* force of a single myosin molecule[116]. After R3 unfolds and exposes vinculin-binding sites, vinculin is able to readily bind talin. Vinculin thus prevents talin's re-folding and establishes long-term integrin activation. Increasing forces sequentially unfold R1-2, revealing yet more vinculin binding sites and accommodating the increased traction until a threshold around 25 pN after which increased tension renders the α-coils into random coils and disintegrates the vinculin binding sites. If force was reduced after that point, talin can re-fold obviating the vinculin binding, providing therefore the mechanical basis for the catch-bond to slip-bond transition behaviour observed in integrins[55].

The increase in membrane-proximal Ca^{2+} levels and activation of PKC lead to the production of phosphoinositol-biphosphate which together with the high calcium activates calpain, a protease which cuts talin and cytoplasmic β tails of integrins[106,134,135]. The cleavage of talin separates the head from the rod domain, activating integrins but abrogating talin's integrin bundling functions. The cleavage of integrin tails acts as a limiting factor in extended integrin mechano-signalling. In focal adhesions talin is found almost exclusively in the cleaved form with only talin heads localizing to the focal adhesion[106,135–138].

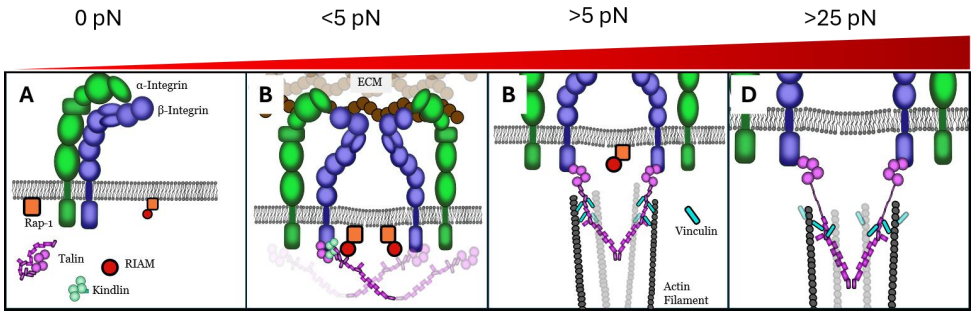

Figure 5. Outside-in mechano-signalling of integrins. A) At a force of 0 pN the integrins are in the closed confirmation. RIAM recruits both talin and kindlin to the plasma membrane in a Rap1-GTP-dependent manner via binding of RIAM to the R2–R3 domains of talin. At the membrane talin autoinhibition is relieved by interactions with acidic membrane phospholipids and the FERM domain is revealed. Talin can then activate integrins. B) From 0 to 5 pN talin has engaged the integrins and started to cluster them through the action of antiparallel talin dimers. At this force, talin is still bound to RIAM. Active integrins can bind to extracellular ligands which can be components of the ECM or cell-bound ligands. C) At and above 5 pN talin captures the retrograde flow of actin through vinculin cross-linking. At ~5 pN, the force of a single actomyosin contraction, the R3 domain of talin is destabilized and this reduces RIAM binding whilst exposing the high affinity vinculin binding site which then binds vinculin allowing for the binding of actin. Above 5 PN, more vinculin binding sites are engaged and with them more force can be transmitted through the bond. D) Above 25 pN domains R1-R3 of talin unfold to a random coil, rendering their respective vinculin binding sites inexistent [119,135,139–141].

Kindlin synergizes with talin and binds β chain's cytoplasmic tail at the membrane distal end while talin binds the membrane proximal one at NPXY motiffs[104,142]. There are three kindlin genes in mammals, each with distinct tissue expression: Kindlin-1 being expressed in epithelial cells, kindlin-2 being prevalent in most tissues and kindlin-3 being restricted to hematopoietic lineage cells[93,142,143]. Kindlins contain FERM domains that allow them to interact with the cell membrane, and an F3 domain that resembles talin's phosphotyrosine-binding domain, granting it the ability to recognize all β integrin cytoplasmic tails at a membrane distal point. It has been found, however, that despite its interaction with the cell membrane and the tail of integrins, kindlin alone is not sufficient for integrin activation[144]. Instead, it is understood that kindlin's role is a synergistic one with talin. Talin by itself is not able to fully activate integrins and overexpression of talin in absence of kindlin yields no activation of integrins beyond the baseline activation achieved by small concentrations of talin[145]. Based on the displacement model of integrin activation[146], migfilin could dislodge filamin and make β chain cytoplasmic tail accessible to talin and kindlin binding. Kindlins are vital for integrin signalling as it is kindlins that act as cytoskeletal linkers by interacting with ILK (Integrin-linked kinase) and migfilin which is a filamin-binding protein. ILK interacts with the cytoplasmic tails of β1 and β3 chains and facilitates the recruitment of the ILK-PINCH-Parvin complex (IPP). Among the downstream

targets of ILK activation there is Akt/PKB, GSK3β, β-catenin, p44/42 MAP kinases, myosin light chain and MYTP1 in the Hippo pathway[147–151].

Activated Akt is a potent promoter of cell survival so through this axis integrins binding to the ECM reinforce cell survival in tissues[152]. This is obviously more complex in cells not bound to a constant matrix such as lymphocytes. Activation of Akt is caused by phosphorylation of Thr 308 and Ser 473 by PI3-kinase[153,154], the Rictor-mTOR (mammalian target of rapamycin) complex and the ILK-Rictor complex. Akt is involved in staving off anoikis cell death (the programmed cell death of tissue cells when adhesion is lost) as has been shown in endothelial cells[153]. Anoikis being the cell death triggered by lack of integrin binding, migratory cells need a system to avoid it when not attached. Macrophages prevent this form of apoptosis by receiving constant cytokine signalling when immature and prevent it without the need for external reinforcement after polarization[155]. Other migrating cells such as DCs are understood to stave off apoptosis through similar mechanisms[155,156].

GSK3β is inactivated by ILK-mediated phosphorylation at Ser 9, regulating transcription factors such as β-Catenin, CREB and AP-1[148]. AP-1 itself upregulates genes encoding for matrix metalloproteinases (MMP-9 and MMP-2) which allow cells to degrade the extracellular matrix to facilitate migration[148,157].

Other targets of ILK are P44/42 (ERK1/2) and ELK1 transcription factors which are phosphorylated only in adherent conditions, downstream of integrins[158]. ERK localization to the nucleus is impaired by nonadherent conditions as its phosphorylation licenses it for nuclear translocation[159]. ILK and myosin light chain kinase (MLCK) can both phosphorylate myosin light chains at the same sites[160]. The phosphorylation of myosin IIa is required for the formation of β1 integrin focal adhesions[154]. Phosphorylated myosin light chain 6 meanwhile interacts with kindlin-3 and is required to support integrin αIIbβ3[161]. This leads to increased myosin II-mediated contraction and bundling of actin.

Integrin signalling inhibits the Hippo tumour suppression pathway by having ILK phospho-inhibit MYPT1 which when inactive results in the inhibition of Merlin[149]. Merlin (encoded in NF2) is a linker between transmembrane proteins and the actin cytoskeleton. The main target of the Hippo kinase cascade however are the Yap/Taz transcription factors, the phosphorylation of which sequesters them in the cytoplasm via interaction with 14-3-3 proteins and ubiquitin-dependent proteasomal degradation[162].

Common to all integrin types are two related conserved transcription factors the YAP (Yes-Associated Protein) and the paralog TAZ (transcription factor with PDZ-binding motif) known as the YAP/TAZ mechanosensory pathway[163,164]. Together, YAP and TAZ are able to translate mechanical information, from shear stress to cell shape and extracellular matrix rigidity into cell-specific gene expression changes. YAP and TAZ act as transcriptional co-regulators by binding to enhancer elements,

using TEAD transcription factors to bind to DNA[165–167] and are shared among multiple signalling pathways usually bundled as the Hippo signalling pathway. The Hippo signalling cascade (also known as the Salvador-Warts-Hippo pathway) consists of a series of kinases that start with MST1/2 binding to SAV1/WW45 to form an active kinase to phosphorylate and thus activate LATS1/2 kinases. MST1/2 also phosphorylate MOB1A/B which together with LATS1/2 in turn form a LATS1/2-MOB1A/B complex which delivers an inactivating phosphorylation to both YAP and TAZ[162–168]. Once phosphorylated, YAP/TAZ are excluded from the nucleus and marked for proteasomal degradation [169–172]. YAP/TAZ can also be phosphorylated by kinases AKT and JNK[173,174] as well as Yes/Src/c-Abl kinases[175,176]. Another method of control of YAP/TAZ is the sequestration into the β-catenin destruction complex regulated by Wnt signalling[177,178].

A notable upstream inhibitor of YAP/TAZ is Merlin which is found co-localized with tight and adherens junctions in epithelial cells [179]. Merlin promotes the formation of protein scaffolds that result in the LATS-mediated phosphor-inactivation of YAP[180]. Another key inactivator is Scribble, which proximal to the cell membrane, functions as an adaptor to facilitate the formation of the MST/LATS/TAZ complex which phospho-inactivates TAZ[181]. The involvement of integrins with these pathways starts at the clustering of integrins and the related activation of Syc, FAK and Src kinases (Figure 5). Integrin-FAK signalling allows for microtubule stabilization and the subsequent Rho signalling (explained later)[182]. Integrins couple with Fyn and Yes activate in turn FAK which together with Src-family kinases forms the SHC (Src homology and collagen homology) pathway which involves Syc[183]. YAP/TAZ activity can also be regulated by Rho-GTPases[163,168] as seen when inhibitors of MYLCK or ROCK (Rho-associated kinase) result in a YAP phospho-inactivation[184,185]. Altogether, integrins both by associating directly with kinases and by acting as the linkages for stress fibres are able to tightly regulate the activation of the YAP/TAZ nuclear or cytosolic localization and therefore control genetic program activation.

Another major transcription factor downstream of integrins is SRF, the master regulator of a multitude of cytoskeletal genes and even β2 integrins themselves in some cells [186–188]. The majority of these SRF gene transcription effects have been found to be dependent on MRTF-A acting as a cofactor[186]. MRTF-A/SRF pathway is activated in response to external cell stimuli which initiates F-actin polymerization downstream of RhoA activation and microtubule reorganization[182,186,189]. In the cytoplasm MRTF-A is bound to G-actin while F-actin polymerization releases MRTF-A, enabling it to translocate to the nucleus where it can influence gene expression[190,191].

2.4.1 Integrins in mechanosensing

Mechanotransduction is the process by which external biophysical stimuli are translated into intracellular biochemical signals[192]. These stimuli can be sensed through immunoreceptors as they bind to cells and the ECM or can be sensed through other systems. Mechanical clues such as substrate stiffness (measured as Young's modulus) intrinsically relate to the tissue in question, or its state. For example, the bone marrow and brain have a Young's modulus close to 4 kPa while bone and cartilage have a Young's modulus above 1 MPa[193].

Tissue stiffness is sensed by many cell types through integrins. For example, endothelial cells use integrins to sense an increase of matrix stiffness past a 3-5 kPa threshold. This leads to both cell-spreading and YAP nuclear localization[194]. The increase in endothelial cell spreading and signalling is positively correlated with matrix stiffness up to a plateau localized around 10 kPa [194]. Migratory immune cells meanwhile have been shown to modulate their migration speed and morphology in response to matrix stiffness in the ranges of 1-8 kPa[195,196]. These stiffness ranges are biologically relevant as most tissues have a Young's modulus under 5 kPa while skin, spleen and lymph nodes have a stiffness close to 10 kPa[195]. For macrophages, soft substrates result in suppression of M1-related genes and an increase in M2-related genes when compared to a stiff substrate[197]. Integrin mechanosensing is also known to regulate both DC and macrophage metabolism and function through YAP-induced mTOR activation. In these cells, higher stiffness leads to increased proinflammatory signalling and a switch to glycolysis[195,196,198–200].

Mechanosignaling can also occur through deformation of the cell nucleus which reflects the tension of the cytoskeleton[201]. Stiffer substrates cause higher forces to be translated through actin and result in the deformation and elongation of the nucleus. This allows for nuclear deformation to act as a mechanosensor[201]. Yap, one of the transcription factors downstream of integrin signalling, can also act here as a mechanosensor itself without needing to be phosphorylated by the Hippo pathway[202]. Nuclear localization of Yap increases as substrate stiffness increases and the nucleus is deformed, allowing Yap to affect gene transcription in response to nuclear deformation[202].

Fluid shear stress can also be a mechanical signal translated through a multitude of cell-surface proteins such as VEGF receptor 1 (VEGF-R1) and -2 (VEGF-R2)[203–205]. The PI3K/Akt/mTOR signal transduction pathway is activated by VEGF-R2 in conditions of high shear stress, increasing adhesion, proliferation, and differentiation in endothelial progenitors[205].

The final mechanosignal covered here is viscosity. Viscosity is the measure of internal friction within a fluid, and it increases together with osmotic pressure and fluid density in most biological systems. It nevertheless constitutes a distinct signal from those, as has been demonstrated with liver cell lines where media of the same osmotic pressure but differing viscosity led to differing responses[206]. One of the

mechanosensors of viscosity is once again integrins. Integrins enhance cell spreading in high viscosity, causing actin cytoskeleton re-arrangements, nuclear flattening, and nuclear translocation of YAP and β-catenin proteins[206–209].

2.4.2 Cell-specific outside-in signalling

In platelets, activated $\alpha_{IIb}\beta_3$ binding to either fibrinogen, fibrin or von Willebrand Factor allows these extracellular ligands to act as cross-linkers and form a mesh-like platelet aggregate[210]. Some cytoplasmic interactions of these integrins require the phosphorylation of Tyr 773 and Tyr 785 in the β3 cytoplasmic domain by Src family kinases. Mutation of the corresponding tyrosine residues in mice produces platelets with impaired clot retraction and a tendency to re-bleed from sites of tail bleeding[211]. Fibrinogen binding to the extracellular domain of activated $\alpha_{IIb}\beta_3$ stimulates an increase in the activity of Src family kinases and Syk[212]. Studies of platelets from mice lacking these kinases suggest that these events are required for the initiation of outside-in signalling and for full platelet spreading, irreversible aggregation and clot retraction. There is also evidence that the ITAM-containing receptor, FcγRIIa, is the link between Src family kinase and Syk activation in human platelets activated by $\alpha_{IIb}\beta_3$[213]. Beside the signalling cascades of $\alpha_{IIb}\beta_3$ mentioned above, there are certain signalling events dependent on integrin clustering such as the modulation of avidity. The origin of integrin clustering, despite being extremely common in outside-in signalling and being known to affect the signalling, does not yet have an agreed cause of formation[214]. There are arguments for the cause being intracellular protein-protein interactions[215], the recruitment of multivalent proteins to the integrin tails[216,217] or by homomeric transmembrane domain interactions[218]. All the above mechanisms are seen in cases of integrin clustering and disruption of either abrogates clustering, therefore they all play an indispensable role in integrin clustering. $\alpha_{IIb}\beta_3$ clustering complements ligand binding to drive full outside-in signalling, which cannot be induced by monovalent ligands[210,215,216,219]. $\alpha_{IIb}\beta_3$ outside-in signalling drives processes essential for haemostasis, including platelet spreading, stable thrombus formation and clot retraction.

In T cells, integrins participate in migration as they do in all lymphocytes but here they also participate in TCR function. Integrins are found in close cooperation with the TCR, αLβ2 engagement with ICAM-1 sustaining and enhancing TCR-induced tyrosine phosphorylation, phosphatidylinositol-specific phospholipase-γ1 (PLC-γ1) activation, and calcium signalling, as well as phosphatidylinositol-3-kinase (PI3K) activity[220–224].

The endocytosis of iC3b opsonized particles by phagocytes is αMβ2 dependent and requires the activation of Ras homolog family member A GTPase (RhoA) [225,226]. In this case the phagocytosis is started by αMβ2 integrin engaging iC3b and its Rho-

mediated cytoskeletal rearrangement allowing for phagocytosis followed by antigen processing[13,225]. IgG opsonized cells cause Rho-independent phagocytosis which depend instead on the Rac1 GTPase (Ras-related C3 botulinum toxin substrate 1)[225]. This Rac1-dependent phagocytosis starts by IgG recognition at Fc receptors which then signal the inside-out activation of αVβ5 and ultimately actin polymerization through Rac1[225,227].

3 Integrins mediate immune cell activation and effector functions

3.1 T-Cells

In T-cells, integrin α4β1 is important for the rolling of lymphocytes on endothelial cells as well as stalling and extravasation in naive cells, but it is overcome by αLβ2 in activated T-cells[228]. Both α4β1 and αLβ2 follow similar inside-out activation, first activated by chemokines and then fully engaged when bound to VCAM-1 and ICAM-1 respectively[229]. α4β1 is found to localize in its fully active form at the leading edge of migrating lymphocytes together with chemokine receptors[39,229]. Engagement of α4β1 to VCAM-1 or fibronectin induces the production and secretion of MMP-2 and -9 through FAK signalling[230,231]. These proteases then can cleave a range of ECM components including fibronectin, allowing for un-impeded migration. Cytokines activate αLβ2 through G-protein-coupled receptor allowing it to bind ICAM-1 and undergo the prototypical lymphocyte rolling and arrest[130,232,233].

The integrin functions that are unique to T-cells are those that occur in the immunological synapse that forms between APCs and T-cells. The immunological synapse is a highly regulated structure, and forms when an antigen-loaded MHCI or MHCII on an APC interacts with an antigen-specific TCR and is a structure that requires integrins to form correctly[234,235]. Co-stimulatory molecules are recruited to the forming synapse with CD28 being recruited to the immunological synapse from its uniform distribution across the cell membrane after its binding to CD80 and CD86 on APCs[236,237]. The inhibiting receptor CTLA4 is both recruited from intracellular vesicles and its expression increases following T cell activation after which it can be recruited to the T-cell surface through binding of CD80 to CD28 at a lower speed than the co-stimulatory CD28, helping regulate the duration of the immunological synapse[236–239]. Part of the downstream signalling following engagement of these initial molecules is to increase the membrane-proximal levels of Ca^{2+}, activating PKC-θ and eventually leading to activation of the transcription factors NFAT and NF- κB which regulate T-cell proliferation[236,240,241]. NFAT controls the expression of, among others, IL-2 and IFN-ɣ which are released into the synapse in a polarized fashion and IL-4 and TNF-α which are secreted in a non-directional manner by T-cells[242]. The immunological synapse forms as a radially

symmetric structure with a core containing MHCII-TCR and CD28/CTLA4-CD80/CD86 in a so-called "central supramolecular activation cluster", shortened to cSMAC. Around cSMAC, can be found peripheral SMAC (pSMAC) where αLβ2 on the T-cell binds to ICAM-1 on the APC[234,235,243]. This second ring is itself ringed by a third ring enriched in CD45[244]. The complex interplay between the strength, duration and number of interactions between the T-cell and APC are responsible for eliciting specific T-cell responses[234].

Studies with *Itgb2*-null mice indicate that T-cells fail to activate in response to MHC alloantigens or staphylococcal enterotoxin A, but that bypassing TCR activation via phorbol myristate acetate (PMA) still allows for T-cell activation. These results show that β2 integrin is vital for the formation of an effective immunological synapse [245].

The polarization of the actin cytoskeleton of the T-cell towards the APC is also vital for the formation of an adequate immunological synapse. Cytoskeletal rearrangement follows immunological synapse formation and is necessary for its success[234,235,243]. Along with the polarization of actin, Golgi apparatus and mitochondria are also aligned with the immunological synapse[234]. Furthermore, receptors are further recruited to the synapse along with vesicles. These receptors include traditional components of the synapse (TCR, αLβ2 integrin, and CD28) along with some transporters such as GLUT-1 (Glucose Transporter Type-1)[234].

3.2 Neutrophils

Neutrophils are polymorphonuclear myeloid cells that comprise 70% of circulating leukocytes in humans and 10-25% in mice[246]. Neutrophils extravasate at sites of inflammation through a process common to all leukocytes (explained in detail later) which relies on integrins. Neutrophils however express less α4β1 compared to other leukocytes, making them reliant on β2 integrins to extravasate[247–249]. This is demonstrated by the lack of pus formation, which is otherwise comprised mostly of neutrophils, in patients suffering from a pathological β2 integrin mutation[250,251]. Once at the site of infection, neutrophils eliminate pathogens via phagocytosis or through extracellular killing. Neutrophils have the capacity to kill the invaded microorganism by secreting their toxic granular content (degranulation), producing reactive oxygen species (ROS) to damage microbial components, or releasing their DNA and subsequently forming neutrophil extracellular traps (NETs) in a process of cell death known as NETosis[247,252,253]. This phagocytic function is generally reserved for pathogens opsonized with IgG or iC3b. αMβ2 on neutrophils binds to iC3b and initiates phagocytic function[254]. The cytotoxic release of granules onto antibody-labelled cells involves integrins after they become activated by IgG receptors (Fc*γ* receptor IIa or IIIb) through the recruitment and activation of PI3K [255,256]. Both αMβ2 and αLβ2 integrins regulate granule release after binding ICAM-

1 on the opsonized cell[255,256]. The increase in oxygen consumption that forms the respiratory burst which results in the formation of ROS is not fully understood in terms of how it is linked to integrin function [253]. However, it is well established that there is a link, as neutrophils with dysfunctional integrins and integrin signalling are unable to successfully undergo this respiratory burst[251,257,258].

3.3 Antigen presenting cells: Dendritic Cells and Macrophages (including Microglia)

APCs must be present at the sites of injury either through pre-existing tissue residence or through active migration after injury, be able to phagocytize antigens, migrate to lymph nodes (microglia skip this step[259]) and present the antigens to T- and B-cells to conduct their antigen presentation roles effectively. Despite their name and main role, APCs do not only present antigens, they also play vital roles in tissue homeostasis. The best studied example of this is the role of macrophages, which exist in three distinct lineages: tissue-resident macrophages seeded from either the yolk sac or embryonal liver and macrophages originating from monocytic bone marrow precursors[16,260]. Tissue resident macrophages have been shown to be needed not only for the maintenance of tissue homeostasis but also for the correct initial development of some tissues such as the pancreas and mammary glands[15].

For the antigen-presenting role to be effective, APCs need to uptake the antigens in the first place. This uptake is integrin dependent, with both αMβ2 and αXβ2 able to bind iC3b and IgG opsonized cells and induce phagocytosis[225,226]. In the brain, microglia cells trigger the Rho-dependent endocytosis and proteolysis of small β-amyloid aggregates in a β2 integrin-dependent pathway wherein integrins react to the stiffness of the amyloid "crystals" in the same manner as was originally studied with uric acid crystals[261,262]. This integrin-dependent phagocytic pathway promotes both clearing harmful debris and uptaking antigens.

ROS and RNS (Reactive Oxygen and Nitrogen Species) are both produced by phagocytes to directly act in antimicrobial activity and in signalling pathways within the phagocytes themselves, affecting their pro-inflammatory cytokine production[258,263,264]. The antimicrobial activity of ROS and RNS is similar to the one seen in neutrophils mentioned above: oxidative damage causing failure of cellular components. The pro-inflammatory effects of ROS are mediated through inflammasome activation and assembly, containing ASC (adaptor protein apoptosis-associated speck-like protein containing a CARD). Once assembled, the inflammasome is able to recruit and initiate autocatalytic activation of caspase-1 and finally elicit inflammation via release of IL-1β and IL-18[265]. The inflammasome activation is downstream of ROS production, which can be initiated through integrin mechanosensing of stiff substrates[262,266–269]. ROS-induced post-translational modifications on cysteines (S-nitrosylation, palmitoylation,

glutathionylation, and oxidation) have been shown to be at least partially responsible for the switch to a more inflammatory glycolytic immunometabolic profile[22,270–272].

Integrins function in concert with different toll-like receptors (TLRs) via activation of reinforcing signalling cascades. α9β1 has been reported to induce Th17 cell promoting cytokines in DCs and macrophages in synergy with TLR2 and TLR4 through the ERK pathway[273], whilst β2 integrins aid in TLR4 signalling by co-localizing to the TLR4-LPS binding site and reinforcing their endocytosis in DCs[274–277].

Macrophages exhibit two broad phenotypes (*in-vitro*[278]) designated as M1 and M2 with both types existing as ideals and most macrophages existing in a polarization spectrum between the two extremes. M1 macrophages are pro-inflammatory and express high levels of CD80, CD86, FcγRII/III (CD32/16) and are capable of secreting pro-inflammatory cytokines[279]. Meanwhile, M2 macrophages are classified as anti-inflammatory, and express arginase-1 (Arg-1), mannose receptor (CD206), IL-10 and chemokines CCL17 and CCL22. Recently, however, it has been recognized that this simple pro/anti-inflammatory dichotomy does not capture the phenotypes seen in-vivo where the lineage, activation regimen and culture conditions of the macrophages impact the expression of hundreds of genes which together constitute the different phenotypes seen *in-vivo*[278]. Due to this emerging complexity, and the focus of this work on cells other than macrophages, it has been deemed beyond the scope of this work.

Microglia are the macrophages which are seeded to the nascent brain from yolk sac progenitors in the early embryo[280]. At steady state microglia are able to self-renew in the central nervous system without any contribution from the bone-marrow[280]. No cell-surface markers are unique to microglia that could separate them from other APCs as microglial expression of markers can be transient and depend on the cellular context. The transcription factors Pu.1 and Irf8 control the genetic program characteristic of microglia[281]. Like other tissue-resident macrophages, microglia play an important role in the homeostasis and structuring of the tissue they reside in. They participate in gliogenesis, vasculogenesis, neurogenesis, myelination, release of soluble factors and conduct phagocytosis[282,283]. In the healthy brain, microglia are homogeneously distributed. Their cell bodies are largely sessile, but they extend protrusions to "scan" the nearby parenchyma[284]. Much like other APC groups, there exist a growing number of distinct microglial states with characteristic immune and metabolic profile. Many of these are being named after the disruption to homeostasis in which they were originally identified (e.g. human Alzheimer's disease microglia being termed HAM)[284,285]. There exists confusion in the field regarding the role of microglia when activated as many authors define any presence of MHCII on microglia as a marker of inflammation and imminent neurodegeneration but there exists a growing pool

of evidence that such a definition is context-dependent[286–289]. One good example is that of stroke. Immediately upon the event of stroke neurons release excessive amounts of glutamate. This glutamate is both directly toxic to other neurons and activates microglia through N-methyl-D-aspartate receptor binding[288,289]. Glutamate signalling results in both the release of more glutamate from within the microglial cell and the production of TNF-α[288,289]. This feedback and the activation of microglia from ligation of necrotic debris to different TLRs results in more generalized neuronal death than the initial injury would have otherwise caused[288,289]. The role of microglia does not stop with the pro-inflammatory role. Microglia are also responsible for recovery after stroke. In this context, microglia increase neuroblast differentiation into neurons through the production of IL-4[286]. A switch between these two roles of microglia, from the neurodegenerative to the neuroprotective has been found to only require extended temporal exposure to the stressor, from acute to chronic[288,290,291].

Dendritic cells can be divided into conventional dendritic cells (cDCs, divided into cDC1 and cDC2 sub-groups), plasmacytoid dendritic (pDCs) cellsand monocyte-derived dendritic cells (moDCs)[9,292]. Broadly speaking, cDC1s promote cytotoxic CD8+ T cell responses, while cDC2s generate CD4+ T-Cell reponses[292,293].

pDCs arise from the same common dendritic cell precursor but differ in that they express the transcription factor E2-2[294]. pDCs specialize in producing type I IFNs following recognition of nucleic acids through Toll-like receptor 7 (TLR7) and TLR9 and are also known as interferon-producing dendritic cells[295].

moDCs can differentiate from monocytes after being exposed to GM-CSF and IL-4[296]. They are a highly heterogeneous group and there exist some debate as to whether the observed heterogenicity calls for distinct activation stages or if they are all functionally the same cells[296]. The types currently under debate depending on the type and location of the infection and the inflammatory setting are termed monocyte-derived cells, TNF/iNOS-producing DC (Tip-DC), or inflammatory DCs[9,297,298]. The BMDCs that are used in this thesis resemble moDCs, though the method of differentiating them also yields macrophages[299].

3.4 Metabolic changes during immune cell activation

When B- and T-cells are activated through their antigen receptors, they both recruit the glucose transporter GLUT-1 to the immunological synapse[234,300]. The recruitment of GLUT-1 forms part of the metabolic reprogramming that these cells undergo upon activation. Their metabolism shifts away from OXPHOS toward glycolysis. This produces energy to meet the heightened demands of the activated cells and to provide useful metabolic intermediaries for biosynthetic purposes[20,301–303]. As introduced earlier, this switch towards glycolysis lasts only for the acute

phase of cell activation and proliferation. As the cells transition to memory B- and T- cells the cells again start to use OXPHOS [29]. One factor that is at the core of this metabolic switch to glycolysis is the activation of mTOR, often referred to as the master metabolic regulator[304]. The activation of this Ser/Thr kinase in B- and T-cells results in a comprehensive upregulation of all rate-limiting enzymes involved in glycolysis and a concomitant decrease in those involved in OXPHOS[304,305]. In T-cells, mTOR activation is needed for commitment to Th1, Th2 and Th17 effector cell lineages while mTOR-deficient $CD4^+$ T-cells preferentially differentiate towards a regulatory (Treg) phenotype [306–308].

Resting APCs use mostly OXHPHOS for energy production, but activated APCs switch largely to glycolysis [309–311]. Upon activation, APCs simultaneously upregulate the uptake of glucose through an increase in GLUT-1 in the cell membrane and an increase in the translation of glycolytic enzymes such as phosphofructokinase[312]. Sustained glycolysis supports the survival of APCs through the decrease in OXPHOS and provides materials for the biosynthesis of fatty acids[312]. Robust nitric oxide (NO) production by inducible NO synthase (iNOS) causes mTOR activation. mTOR in turn acts as the central hub for the metabolic switch into glycolysis[313–315].

Finally, there is ample evidence that APCs respond not only to their internal metabolism but to organism-wide metabolic alterations as seen with the effects of the diabetes drug metformin[316–318]. Metformin has been found to have profound effects in reprogramming both macrophages and dendritic cells towards tolerogenic profiles through immunometabolic reprogramming and found to boost their antitumoral activity[318–320]. This has led to increasing research into the potential use of metabolic or dietary interventions as forms of immunomodulation[321–326].

4 Leukocyte adhesion diseases

4.1 Leukocyte adhesion cascade

There exist three distinct Leukocyte Adhesion Deficiencies (LAD) in humans, each with a wide array of symptoms stemming from distinct integrin adhesion deficiencies. Here the effect of different types of LAD are studied in relation to their effects on leukocyte extravasation. Other functions affected by LAD are covered later. The transfer of leukocytes from the bloodstream to tissues occurs in four steps (Figure 6):

First, under flow conditions, loose adhesion between the endothelium and vessel wall causes the leukocyte to roll. This process is mediated by P and E selectins which are expressed on activated endothelium and bind to the constitutively activated sialylated ligands on leukocytes, while L-selectin instead being expressed in leukocytes and binding endothelial sialylated, fucosylated ligands[327–329]. The same sialylated ligands which are missing fucosylation in LAD II[330].

The second step is the activation of the leukocytes they come into contact with multiple chemokines and cytokines during rolling, leading to the inside-out activation of integrins[331]. The activated integrins in turn bind to ICAMs and form more firm bonds, which arrest the rolling and leads to extravasation. LAD III is caused by a mutation in kindlin-3 which prevents integrin activation and signalling[332].

The third step is the arrest of the leukocytes through strong adhesion with the vessel walls. This adhesion takes place chiefly between integrins (αLβ2, αMβ2) on the leukocyte and ICAMs on the vessel walls[65,329,333,334]. Neutrophils, monocytes, and lymphocytes adhere to endothelium and undergo a change from a spherical to a flattened morphology[329]. This is required for firm adhesion and for transmigration through the endothelium[335]. Mutations in β2 integrins in LAD I interfere with this step as they prevent entirely or hinder their binding to ligands[336,337].

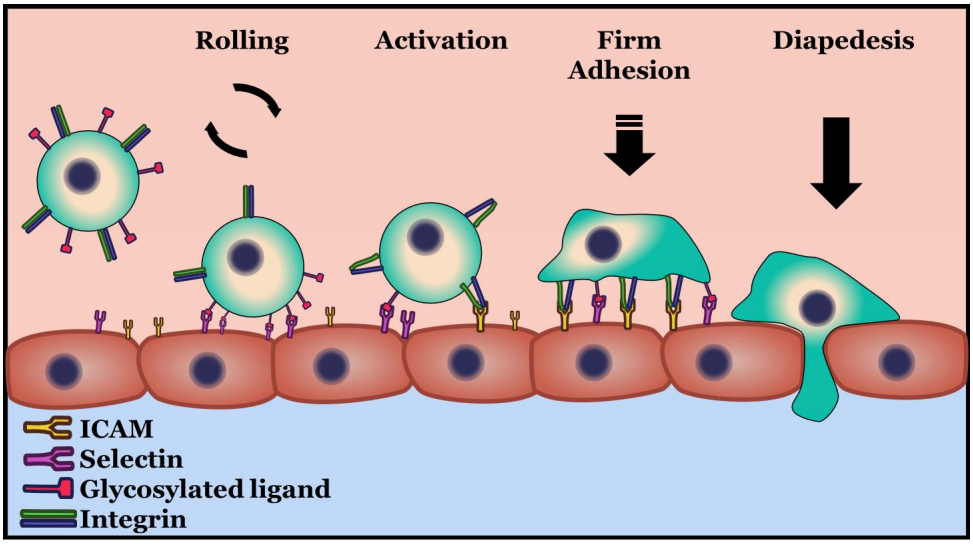

Figure 6. Leukocyte adhesion cascade shown as a prototypical leukocyte extravasating at a site of injury. The endothelial cells in dark red which line the blood vessel above them have been activated and express ICAM-1/2 as well as E/P-Selectin. The leukocyte, which constitutively expresses ligands for both and L-selectin, is first slowed down via binding of selectins (loss of their sialylated ligands in LAD II results in failure at this step). The binding of selecting triggers inside-out activation of integrins in a kindlin-3-dependent manner (LAD III results in failure at this point) with firm adhesion following soon after (LAD I cells are unable to complete this integrin-dependent step). From there leukocytes can move over brief distances until diapedesis across the blood vessel walls and into the surrounding tissue takes place.

The fourth and final step in extravasation is trans-endothelial migration which can take place[338] between (paracellular migration) or through the endothelial cells (trans-cellular migration)[333]. As the leukocyte interacts with the endothelium in the previous steps, the endothelium also responds by clustering VCAM-1 and ICAM-1 (ligands for α4β1 and αLβ2/αMβ2 respectively). This clustering requires Src-dependent phosphorylation of actin-binding cortactin and the engagement of ICAM-1 promotes this same phosphorylation in a self-reinforcing loop[334,339]. The loosening of endothelial cell junctions is required for paracellular migration, engaging ICAM-1 and VCAM-1 on the endothelial cells stimulating an increase in Ca^{2+} in the cytosol which among other effects activates MLCK (Myosin light-chain kinase) leading to actin-myosin fibre contraction. This is believed to help endothelial cells pull apart from each other making gaps in the order of hundreds of Ångstroms, enabling leukocytes to actively "crawl" through the gaps formed[340]. The increased calcium leads to the activation of RAC-1 and PKC which cause the phosphorylation of VE-cadherin, un-linking it from the actin cytoskeleton[341]. From there it is understood that the leukocytes move through the space between endothelial cells along with the lateral endothelial recycling compartment

membrane so that the focal adhesions are pushed to the side rather than separated[342]. Trans-cellular migration has been found to happen through the formation of a transient pores across the endothelial cells but the molecular process that causes them has not been fully elucidated yet[343].

Scanning electron microscopy of neutrophils and macrophages revealed that these cells have numerous surface wrinkles and folds, which means that the actual surface area of these cells greatly exceeds that of a sphere of the same diameter. Biophysical studies about the properties of the neutrophil plasma membrane have been performed using suction of the plasma membrane into micropipettes[344–346], showing that force is able to un-wrinkle these cells. The distribution of two surface molecules, which are important for leukocyte rolling and adhesion, L-selectins and β2-integrins, is influenced profoundly by the wrinkles as selectins are located only on the raised edges of the wrinkles and integrins in the valleys between wrinkles[347]. Thus, the un-wrinkling of these cells allows for the presentation and binding of a greater proportion of integrins which allows for a strong bond to form between the cells and the endothelium. Lymphocytes also have a membrane surface area much greater than their volumes at rest require. In their case however it seems L-selectin and PSGL1 are localized to the raised membrane protrusions (microvilli) and CD44 is localized to the cell body[348]. In all these cell types, the existence of extensive excess membrane at rest allows for rapid cell volume increase upon activation without the requirement to produce new membrane at the same speed.

4.2 LAD I

Mutations inβ2 integrins (missense, pre-mature truncation, etc.) lead to defective leukocyte function. LAD I was one of the first immunodeficiencies for which the genetic defect was identified[251,349]. The disease presents with recurring bacterial infections, severe gingivitis and periodontitis in the patients who survive past infancy[350,351]. Bacterial and fungal infections present absent of pus. Complete loss of β2 integrin expression leads to death before the age of one while impaired expression of β2 integrins leads to clinical features of varying severity matching the degree of β2 integrin functional impairment[352]. The role of β2 integrins in the formation of specific T-cell responses is evident in LAD I patients as they present an increase in Th17 response in the gums which leads to periodontal bone loss and severe periodontitis[353,354]. LAD I patients present a failure of recruitment of neutrophils to the gums which results in gums harbouring lesions with dense inflammatory infiltrate made up of lymphocytes and largely devoid of neutrophils[354]. Cytokines linked to IL-17A expression (Il-6, IL1β and Il-23) were expressed in LAD I periodontitis, with IL-6 and IL-23 being significantly overexpressed when compared to both gingivitis and periodontitis in non-LAD I patients[354]. IL-17 and IL-23 were not detected above normal levels in blood and

were instead localized to the oral mucosa[354]. Cytokines and chemokines related to neutrophil granulopoiesis and recruitment (G-CSF, CXCL2 and CXCL5) were significantly up-regulated in LAD I, but owing to the lack of β2 integrin function, this does not result in the intended recruitment of neutrophils but instead causes significant neutrophilia in blood [355]. In addition, LAD I patients with mild forms of the disorder have neutrophils that fail to phagocytize opsonized cells as αMβ2 on neutrophils fails to bind to iC3b and initiate phagocytic function[254].

A mouse model for LAD I is the β2 integrin null mouse. It replicates the known pathology of LAD I in humans, with up to 40% perinatal mortality, severe gingivitis, skin lesions and lack of pus formation[356]. In addition, these mice recapitulate the severe periodontal bone loss seen in human LAD I patients and show the same localized increase in IL-17 and IL-23 in the oral mucosa. The causal link between the increased levels of IL-17 and IL-23 was conclusively established in the CD11a knockout model when local gingiva treatment with either anti-IL-17 or anti-IL-23 antibodies resulted in abrogation of periodontal bone loss of the knockout phenotype and later translated into human treatments with the IL-23-blocking drug, Ustekinumab[354,357]. The prevention of the bone degeneration obtained with Ustekinumab correlated with higher sequestration of osteoclast growth factors and a reduction in the levels of anaerobic bacteria[354].

4.3 LAD II

LAD II is an adhesion deficiency caused by mutations in the fucose transporter in the Golgi, which leads to absence of Sialyl Lewis X, the ligand for selectins[62]. In this variant of LAD, the rolling phase of leukocyte adhesion is affected. The syndrome presents with recurrent infections which improve with age, periodontitis, Bombay blood type (absence of antigen H), mental retardation, growth delay and clinical stigmata[358]. The clinical stigmata characteristic of LAD II are long eyelashes, a broad and depressed nasal bridge, a simian crease, and dorsally positioned second toes. There are very few patients globally identified as having LAD II (less than 10 reported cases) so the creation of mouse models deficient in Slc35C1 (GDP-Fucose transporter) has been vital for the study of this disorder.

Dietary fucose supplementation was first attempted in 1999 by Marquardt et. al. in a patient with LAD II [359]. The supplementation successfully recovered the levels of Sialyl Lewis X expression to functional levels without causing the expression of the fucosylated H antibodies[359]. This was critical as this patient had the Bombay blood type (lack of H antigen in their erythrocytes and presence of anti-H antibodies)[359]. In addition to the re-expression of selectin ligands on neutrophils, the disease's elevated peripheral neutrophil counts reduced to normal levels, no

episodes of fever occurred after beginning of the therapy, and psychomotor capabilities and growth of the patient improved[359].

As more patients with LAD II have been identified since, other milder forms of the disease have been found where the mutations are not in the same location[360,361]. In these patients the haematologic defects were minimal, they did not exhibit the Bombay blood type, but they presented with short stature and developmental delay. A recent (2022) study by Tahata et. al. focused on the effects of fucose supplementation on patients with this minimal LAD II phenotype[361]. This study found that the developmental defects were reversed and there was an overall increase in fucosylated proteins including Sialyl Lewis X and antigen H from barely detectable to equivalent to those of healthy individuals[361]. These two findings together show that fucose supplementation is a viable and valuable treatment for LAD II.

4.4 LAD III

LAD III is an adhesion defect caused by activation defects in multiple types of integrins without the integrins themselves being deficient and is the rarest in this family of disorders. It presents with recurrent infections, bleeding tendency, leucocytosis, hepato-splenomegaly, platelet aggregation deficiency, osteopetrosis and IL-17 overproduction[362] . The cause of LAD III was initially attributed to *RASGRP2* as mutations of this gene were found in most LAD III patients [363,364]. Later studies however found that kindlin-3, one of the cytoplasmic integrin tail adaptors, is needed for integrin function. Mutation analysis of the gene encoding for kindlin-3 (*FERMT3*) revealed homozygous mutations in it in all LAD III patients. These analyses also revealed that all the patients who had the *RASGRP2* mutations also had *FERMT3* nonsense mutations and that both of these were likely inherited together as the genes for both are located close to each other on the same arm of chromosome 11[365,366]. A study of a LAD III patient of Sudanese background with a novel kindlin 3 splicing mutation shows that differences in the mutations affecting kindlin 3 were responsible for differences in symptomatology between LAD III patients [367]. Bleeding disorders and recurrent infections are common to all LAD III patients, whilst osteopetrosis is not present in all patients.

An initial mouse model of LAD III was developed by creating a knockout of CalDAG-GEFI which recapitulated the loss of function of all three β integrins present in haematopoietic cells (β1, β2 and β3). Neutrophils failed to successfully adhere to activated venules, and their platelets were unable to form thrombus and therefore these mice experienced severe bleeding[363]. The CalDAG-GEFI knockout fails to activate Rap1-GTP.

A second mouse model was generated by knocking out kindlin-3. These mice presented as entirely normal in heterozygosis but in homozygosis they presented

severe osteopetrosis, and severe bleeding which caused death within a week after birth[368,369]. The symptoms resembled LAD III but were so severe that most insights need to be obtained with the help of other mouse lines. Foetal liver cells from FERMT3-/- were transplanted into lethally irradiated wild-type mice to study the functionality of platelets. Platelets were found to be unable to aggregate properly and cause clot retraction[370].

Deficiency of kindlin-3 impacts the function of β_1, β_2 and β_3 integrins though it has been shown that kindlin-3 expression levels of as low as 5% are able to maintain basal function of these integrins and prevent spontaneous bleeding[368]. The 5% expression level of kindlin-3 however is insufficient to prevent defects in infection response or platelet aggregation in stress conditions, with the impairments being less severe at higher levels of kindlin-3 expression[371].

4.5 Current treatments for LAD

As mentioned above the only currently pharmacologically treatable LAD is LAD II with fucose supplementation being effective only as long as it is continued. LAD patients are symptomatically treated with broad-spectrum antibiotics[350]. Hematopoietic stem cell transplants from a healthy donor (bone marrow transplant) is the only permanent cure for all three variants of the disease as it replaces the defective cells with functional ones [351,372,373]. The bleeding disorders of patients with LAD III are treated with recombinant factor VIIa, either leading up to a more permanent solution like the aforementioned transplant or as a lifelong treatment[374,375].

5 Aims

The research aims of this doctoral project were to comprehensively study the role of β2 integrin mechanotransduction and its effects on immune cell activation, polarization and metabolic reprogramming using an ITGB2 TTT/AAA KI mouse line. More specifically, the aims were to:

- Study the role of β2 integrins in DC metabolic reprogramming and polarization *in-vivo*.
- Identify signalling pathways driving β2 integrin-regulated DC maturation and applications for antitumour responses.
- Study the role of β2 integrins in microglial polarization *in-vivo*.
- Establish a novel method of assaying cell-cell adhesion forces of T-cells and correlating adhesive forces with cell activation state.

6 Materials and Methods

Table 2. Methods I personally carried out either alone or in combination with other researchers from among those in the original publications comprising this thesis and where to find them.

Method	Publication where it can be found
Murine sampling and bone marrow collection	I, II, III
BMDC culture	I
Preparation of cells for peritumoral injection	I
Translation rate analysis	I, III
ROS measurements	I
Flow cytometry	I, III
ELISA	I
qRT-PCR	I
Cell migration assay	I
Isolation of leukocytes from the CNS	II
Microglial isolation by MACS	II
Cylinder test paw usage	II
T-cell isolation by MACS	III
T-cell cluster formation	III
Statistical analyses	I, II, III

7 Results and discussion

7.1 Integrin signalling regulates immune cells

7.1.1 Dendritic cells

Through integrins, cells interact with their physical environment and respond to it accordingly. The Fagerholm research group has been using a mouse model which consists of a C57BL/6N with homozygous T759A, T760A, and T761A knock-in (KI) mutations in exon 16 of *Itgb2*, corresponding to the β2 integrin binding site for kindlin-3[376]. This mutation results in reduced binding of β2 integrins to ligands[376]. This allows us to study the effects of defective integrin signalling on leukocyte function. This mouse model presents no significant comorbidities beside an observable, but not pathologic splenomegaly. Homozygous *wild-type Itgb2* (WT) mice of the same genetic background were used as controls. β2 integrins have been previously shown to regulate dendritic cell activation using this model[377,378]. KI DCs have been shown to express increased levels of T-cell co-stimulatory molecules CD40, CD80, CD86 and MHCII when compared to WT[377]. It has been established that the *Itgb2* KI DCs promote a stronger TH1 response (Interferon ɣ) and a weaker TH2 response (IL-4, IL-5 and IL-13) than the respective WT cells when challenged with TH1 or TH2 response-eliciting factors (heat-killed *Propionibacterium acnes* for Th1/17 and schistosome soluble egg antigen for Th2)[377]. It has also been established that the *Itgb2* KI DCs induce a stronger antitumor response *in vivo*[378].

Here we show that β2 integrins regulate DC metabolism through T759-761A mediated functions. Mass spectrometry of bone-marrow-derived dendritic cells (BMDCs) from these mice showed differences in metabolites between the WT and KI BMDCs (I, Figs. 1d, e). Chief among them were increases in arginine, proline, serine and glycine metabolism in KI BMDCs and a decrease in both ATP and ADP levels concomitant with an increase in phosphocreatine (I, Fig. 1e). Indeed, other experiments confirmed that the KI BMDCs present a supressed metabolic state mainly evidenced by the decreases in both oxidative phosphorylation and glycolysis which were measured both in terms of lower ECAR (Extracellular Acidification Rate) and OCR (Oxygen Consumption Rate). ECAR being a common proxy measurement of glycolysis as glycolytic byproducts are acidic and expelled from cells, similarly OCR is an indirect measurement of OXPHOS as respiration is the

main user of oxygen in animal cells[379,380]. Another indirect measurement of metabolic capacity in these cells was the lowered total protein translation as measured through puromycin incorporation (I, Fig. 2)[381].

The metabolic reprogramming was instilled at the level of transcription, with PfkI (phosphofructokinase-1), Pkm (Pyruvate kinase) and Glut1 (Glucose transporter protein type 1) being significantly under-expressed in KI vs WT BMDCs. PfkI being of specific note as it is the rate-limiting step in glycolysis. The functionality of the Glut1 transporter was found to be lowered in accordance with its lower expression (I, Fig 3). Furthermore, the OXPHOS-supressing iNOS was found to be increased at the mRNA level in KI BMDCs when performing qPCRs (I, Fig. 4c). A shift from a balanced metabolic profile with a preference for OXPHOS towards one where glycolysis is the preferred energy source has long been a marker of dendritic cell maturation[382]. In our studies however we found that the KI phenotype led to both a decrease in OXPHOS and glycolysis without impairing the co-stimulatory or migratory ability of the BMDCs (rather, these were increased). The β2-integrin dysfunction led to an overall reduction in metabolic activity and not a Warburg effect priming the cells for glycolysis.

The pathways responsible for this metabolic shift were investigated starting with Akt and mTOR which were both found to be upregulated in KI BMDCs (I, Fig. 4a). The AMPK pathway is known to oppose mTOR and respond to energy stress such that cell proliferation is curtailed [383,384]. The AMPK pathway was found to be slightly downregulated in KI cells (I, Fig. 4b), which agrees with the increase seen in mTOR. It was found that despite this, mTOR was not responsible for the differences in metabolism between WT and KI as treatment of KI cells with rapamycin (inhibitor of mTOR) did not only not revert their metabolic phenotype but further reduced their overall metabolic rate as seen by decreases in ECAR and OCR (I, Fig. 4d-7, Fig. S1d).

As had been previously established[385–387], the Ikaros transcription factor plays a major role in DC function and development and RNA-seq revealed 64 genes repressed by Ikaros also to be downregulated in KI BMDCs (I, Fig. 5a). These genes mostly belong to glycolytic processes, cytokine production and cell migration. Indeed, treatment of KI BMDCs with the Ikaros inhibitor lenalidomide increased the overall metabolism of KI cells as seen in the increases in ECAR and OCR (I, Fig. 5c-e) thus partially reversing the metabolic profile of KI cells. Significantly however, Ikaros was not responsible for all the metabolic differences between WT and KI BMDCs as the differences in Glut1 and glucose-uptake seen in KI cells did not revert to those seen in WT (I, Fig. 3b-c) after treatment with lenalidomide (I, Fig. S1g-h). From these findings we understand that Ikaros is one of the transcription factors downstream of β2 integrin signalling and partially responsible for the metabolic reprogramming seen in KI cells but is not the only one responsible.

7.1.2 Metabolic state regulates DC functionality

Since the exact link between the integrin signalling and metabolic shift was not completely clear as KI BMDCs didn't increase their Glut1 expression to WT levels after Ikaros was inhibited, we endeavoured to explore this glucose uptake difference between phenotypes by inhibiting the first steps of glycolysis through the use of the hexokinase inhibitor 2DG (2-deoxy-D-glucose). Previous research has shown that impairing glycolysis in dendritic cells (and macrophages) with a glycolysis-blocking concentration of 10 mM 2DG stunts their activation after being challenged by LPS. Dendritic cells under such conditions fail to upregulate the production of costimulatory CD40, CD80 and CD86[388].

We observed the effects on activation markers at different concentrations of 2DG to establish if the KI phenotypical differences in activation markers were dose-dependent on glycolytic activity. Surprisingly, we found that the lowest concentration used produced the greatest effect. An overnight treatment of WT BMDCs with 2.5 mM 2DG increased CCR7 and IL-12 expression at the mRNA and protein levels (I, Fig. 6a-c) while the higher,11.1 mM[389,] concentration had no such effect. This result revealed that it was not complete glycolysis blocking that caused these effects but instead it was the starvation-like effect of partial inhibition. This is in accordance with published research which shows that fasting is capable of activating phagocytic cells to render them better antigen-presenting cells[321–323].

In previous studies by the Fagerholm group, it was established that KI BMDCs express more dendritic cell activation markers even in the absence of antigenic stimuli[378,390]. The markers assayed were CD40, CD80, CD86, CCR7 and MHCII as well as the production of IL-12. Interestingly, CCR7 and IL-12 were also found to increase in WT BMDCs after overnight treatment with low-level 2DG (2.5 mM), with the levels of these markers in the WT BMDCs thus treated being similar to the KI cells (I, Fig. 6).

Beside these markers, functional assays confirmed that the BMDCs treated with low doses of 2DG were more migratory and were more efficient at stimulating CD4 T-cell proliferation (I, Fig. 6 d,f) *in-vitro*. As had been previously shown[378], BMDCs expressing a mature migratory and co-stimulatory phenotype (KI BMDCs in that case) are able to curtail the growth of B16-OVA and B16-F10 melanomas in mice when BMDCs were injected peritoumorally. In this study, after having found that 2.5 mM 2DG overnight (o/n) was able to stimulate WT BMDCs in a manner making them similar to the previously established KI BMDCS, we investigated these cells in a DC immunotherapy approach. The effectiveness of WT BMDCs treated with 2DG as antitumour agents exceeded those seen with the non-treated WT BMDCs as B16-OVA tumour growth was slowed in all BMDC treatment groups but in three of the 2DG WT BMDC the tumour became undetectable (I, Fig. 7 a-d). Immune cell infiltration of the tumour sites was assayed via flow cytometry and overall, 2.5 mM 2DG BMDC-treated tumours had higher infiltration by CD45+ leukocytes. The

levels of CD44 T-Cell memory markers in the tumours was similarly raised. Additionally, the levels of activated CD4+ and CD8+ T-Cells were both increased in the tumours treated with 2.5 mM 2DG BMDCs, confirming that the antitumoral activity observed was due to a complex immune response being successfully triggered (I, Fig. 7 e).

7.1.3 Microglia

Having established these differences between BMDCs with and without functional β2 integrins, the potential differences between microglia cells in these two mice was established by studying the differences between Itgb2 KI and WT mice when challenged with a pro-inflammatory injury to the brain. We settled on inducing a haemorrhagic stroke on their right striatum according to the standard haemorrhagic stroke protocol[391]. As expected, both WT and KI mice showed a decrease in their immediate well-being as assayed by loss of weight 1-3 days following the stroke (II, Fig. 1a). The functional impairment however differed between WT and KI mice at 24h as assayed by the use of left paw (impaired by the motor-governing right striatum) in a cylinder test. Significant left paw motor impediment was observed in WT mice with only ~20% left-paw use, while there was virtually no impediment in KI mice with ~50% left paw usage (II, Fig. 1b)

The study of pro-inflammatory cytokine expression in right striatum RNA extracts 3 days post-stroke showed a significant reduction in TNFα, IL-6 and IL-10 in KI mice compared to the WT controls (II, Fig. 2a-c). Flow cytometry of microglia cells extracted from healthy WT and KI mice showed no difference in the percentage of total brain leukocytes that are microglia cells (II, Fig. 3a) but show that the KI microglia express significantly lower levels of pro-inflammatory and co-stimulatory markers MHCII, CD86 and CD16/32 (II, Fig. 3b-d).

In-vitro studies on microglia cultures sourced from healthy un-treated WT or KI murine brains corroborated that there is indeed a difference in response between microglia cells of these two genotypes. LPS stimulation increased the expression of TNF-α of both WT and KI microglial cells, but the KI cells consistently expressed lower levels of TNF-α when stimulated (II, Fig. 4). There is extensive literature showing that β2 integrin antibody blockage or integrin absence leads to neuroprotective outcomes after both haemorrhagic and ischaemic brain injury[392–397]. Here we showed that these neuroprotective effects of β2-integrin impairment are related to altered microglial polarization towards an “M2” phenotype which exogenous activation was found to be neuroprotective[398].

7.2 A new dimension of integrin functional studies

When studying the effects of integrin mechanosignalling, existing studies have been limited to investigating either cell-surface interactions in different formats or cell-cell interactions[399]. This has proven somewhat limiting as in-vivo all interactions occur in three dimensions. Many cell-cell interactions such as T-cell aggregation at the early steps of their activation need to be maintained that their biological purpose can be fulfilled[400,401]. In the case of T-cells, their close interaction with each other allows them to share IL-2[402] ,and the sharing thereof is required to form an effective immune response. To address the unmet need for an assay method that would allow for force-measurement of multicellular clusters in a way that would allow complex heterogeneous cell clusters to be analysed, we developed a mesoscale (ø 30–120 μm) force-measuring system and validated it with readily obtainable cell clusters, T-cells in the early stages of post-TCR activation. These cell clusters were chosen as their internal adhesion relies on integrins, namely αLβ2 and disruption thereof results in impaired T-cell activation[403–405].

CD4+ T-cells were isolated from mouse spleens, and their clustering was induced by anti-CD3 activating antibodies or PMA and Ionomycin to obtain T-cell clusters of a regular size (III, Fig. 1a-b). The calmodulin inhibitor W-7 was added to the PMA + Ionomycin activated T-cells to study its effect on cytoskeletal rearrangements. All three treatment groups showed similar T-cell activation with the early activation marker CD69 reaching its peak expression at 5h post-induction while CD25, a late activation marker, was highest at the longest timepoint assayed of 24h post-induction (III, Fig. 1c,d).

These clusters of T-cells obtained with different activation methods and ostensibly the same activation state as measured by activation marker flow cytometry readouts were then used in a novel force-measuring assay recently developed for the potential assay of cells or small organisms[406,407]. This assay consists of a pair of glass micropipettes connected to a suction system, with one being stationary and one connected to a linear motor. The motorized pipette is straight and used to impart tension on the system, the stationary pipette is L-shaped and has been force-calibrated such that it is know what forces upon it cause what levels of deflection. These two pipettes are set up in front of a microscope such that the micropipettes sit in a chamber that holds cell cluster suspensions (III, Fig. 2a).

The cell clusters, once placed between both pipettes in the assay chamber, were approximated to a homogeneous cylinder which extends and thins as tension is applied to it (III, Figs. 2,3). From the deflection of the L-pipette and the measurements of the radius and length of the cell cluster cylinder, the stress and strain of the system can be obtained. Stress in this context referring to the physical quantity that describes the force present during deformation while strain is the relative deformation an object experiences under stress. Their relation is often expressed as the stress/strain ratio, also known as Young's modulus. A higher

Young's modulus describing a stiffer material which is less easily deformed. Repeated measurements showed that two consistent measurements could be gleamed from the stress/strain curve, the main one being the Young's modulus of the initial linear elastic deformation of the cluster and the second being the ultimate tensile strength of the cluster before cell-cell bonds start to fail in sequence and the ultimate rupture of the cluster occurs (III, Fig. 2b,c). The consistency of the mechanical readouts at different times post-induction and the fact the measures are intrinsic to the cell clusters themselves and do not vary with time can be seen in III Figure 4. Similarly, the Young's modulus and ultimate tensile strength of the T-cell clusters were measurements that were repeatable over different experimental days, a true intrinsic property of the type of cluster being studied (III, Fig. 5).

To assess if the measurements we were obtaining related directly to the activation and signalling of integrins (mainly αLβ2 in case of T-cells[122,124,125]) an attempt to prime the integrins through pre-stretching of the clusters before pulling on them with the pipettes was carried out. This was to stimulate the known catch-bond properties of integrins and yield stronger integrin binding[408]. However, it was found that the clusters became softer after pre-stretching (III, Fig. 6). There was also no difference in terms of Young's modulus or ultimate tensile strength between WT and KI CD4 T-cells activated with PMA + Ionomycin (III, Fig. S1). The lack of a difference in the stiffness of these cells after attempted integrin catch-bond mechanical priming between KI and WT point to these measurements being independent of kindlin-mediated integrin activation and signalling.

Finally, the Young's modulus of the T-cell clusters was higher in T-cells activated with PMA + Ionomycin when these had also been treated with W-7 than when they had not (III, Fig. 7a). The gentler [409] activation with anti-CD3 yielded the softest T-cell clusters (III, Fig. 7b). In all of the above cases, the ultimate tensile strength was not noticeably different between the different treatment groups. Similarly, there was no significant difference in the protein translation of these cells with or without the W-7 (III, Fig. S2). The increase in stiffness observed may be caused by the effects calmodulin usually has upon caldesmon, the latter being a cross-linker of myosin II and actin-tropomyosin filaments[410]. By this method, W-7 might prevent the inhibition of caldesmon and lead to higher than usual cross-linking of the cytoskeletal stress fibres[410], rendering the T-Cell clusters stiffer.

We therefore proved that we can reliably measure the stiffness of T-cell clusters and that such stiffness is different depending on activation regiment. When putting this together with recent mechanobiological studies in which the stiffness of T-cells over time was linked to different levels of T-cell activation[411] we can see how we can employ this method to study the efficiency of T-cell activation methods.

With this new method, the door opens to studying the immunomodulatory effects of antigen presentation between DCs and T-cells in different adhesion strength contexts. For example, such studies might reveal how alterations to

integrins such as the lack of proper *Itgb2* expression in LAD I leads to TH-17 responses and if other adhesion-force interventions might result in in similar TH-17 responses.

8 Conclusions and future perspectives

The finding that low dose 2DG could elicit a profound metabolic reprogramming in BMDCs similar to that seen in KI mice which replicates the findings of other[412,413]. Metabolic reprogramming is not simply downstream of DC activation. Metabolic reprogramming is inducible by DC maturation and DC maturation is itself inducible by metabolic reprogramming.

The finding that metabolically reprogrammed BMDCs have superior antitumoral activity *in-vivo* opens a possible avenue for the creation of antigen-agnostic cancer vaccines. This being the holy-grail of cancer vaccines as the existing dendritic-cell cancer vaccines suffer from poorly-antigenic antigen choice or from experimental selection-bias when tumour lysates are used to load antigens onto dendritic cells prior to injection into the patient[414–417]. Another issue with existing DC vaccines is the fact they migrate poorly, with some studies showing that less than 5% of injected cells make it to a draining lymph node[418]. Our research into metabolically reprogrammed dendritic cells found them to be more migratory and express more CCR7, showing improved homing to lymph nodes.

Research aiming to translate these findings in human DCs has already started in our research group and we expect others are also following the same path if recent publications are any indication. Niveau et. al. having published in the last months that modulation of mTOR pathways in melanoma patients successfully reprogrammed their dendritic cells away from a tumour-quiescent reliance on OXPHOS and onto an antitumoral reliance on glycolytic metabolism[419]. Zhou et. al. which published a month after them that a lysosomal permeant dendritic cell vaccine adjuvant had its adjuvant effect by reprogramming (even in the absence of antigens) dendritic cells to a more glycolytic and immunologically mature phenotype[420]. Our experiments however saw an increase in both mTORC1 and 2 activities (mammalian target of rapamycin complex 1 and 2). mTOR1 is known to cause a Warburg-like metabolic shift but the metabolic effects of mTORC2 are less well known due to the lack of mTORC2-specific antagonists. The lack of mTOR subtype-specific inhibitors and need to use the pan-inhibitor rapamycin might explain why the effects we saw that rapamycin caused a further decrease in ECAR and OCR in KI BMDCs. Some data about the effects of mTORC2 inhibition can be gleamed however from genetic models deficient in Rictor as it is a major component of mTORC2. The mouse Rictor-/- knockout model has been found to have increased

both glycolysis and OXPHOS in their DCs[421]. If this effect is symmetric, it could be responsible for the decrease in both glycolysis and OXPHOS we see simultaneously in our KI DCs and 2DG WT DCs. It has been reported that ILK can mediate the phosphorylation of AKT directly, skipping the need for mTORC2[422]. This would link integrin activation to mTORC2 activity; however the opposite would also be possible as PIP_3 is known to activate both mTORC2 and kindlin-3. As both of these PIP_3-binding proteins exist in the membrane-proximal space, the lack of kindlin-3 presence following the mutation preventing interaction with β2 integrin might cause what PIP_3 exists to activate mTORC2 instead. There is evidence that 2DG can cause AKT phosphorylation through IGF1R[423,424]. These indications however are hard to rely on as other groups report either no effect on p-AKT following 2DG treatment or even a decrease[314,425,426]. Overall, it seems that the effects of mTOR modulation are mixed or tissue-dependent so more studies with the same cell types and comparable methodologies are needed to elucidate these pathways[313].

In our research we found the Ikaros transcription factor overexpressed in KI DCs and there was a significant increase in mRNA transcripts of Ikaros's targets and concomitant decrease in the transcripts inhibited by it. It is known that one such gene inhibited by Ikaros is *Ship1*, the protein it encodes being responsible for the degradation of PIP_3[427]. Degradation of PIP_3 preventing the membrane interaction of p-AKT and leading to effects similar to those seen with prevention of AKT phosphorylation[427]. Some of these metabolic effects of Ikaros are seen in cells lacking it which upon restitution of Ikaros function proceed to decrease protein levels of Glut1, Hk2 and Pfkl among others[428–430]. Ikaros however is known to regulate many genes which could both increase and decrease cell metabolism, more study with specific gene silencing will be needed to elucidate which of the many genes regulated by Ikaros is responsible for the effects seen in our KI cells[431].

The pathway(s) responsible for the supressed metabolism in our KI DCs and 2DG WT cells has not been conclusively identified. However, there are some potential pathways such as mTORC2 as described above which require further study. Another interesting avenue of study is on the potential post-translational modifications blocked by low doses of 2DG such as N-glycosylation. The antigen-agnostic maturation of the experimental BMDCs stands in contrast with the previous established knowledge that APCs require undergoing a Warburg-like metabolic reprogramming. Future research must endeavour to find out if this effect is unique to the BMDC cell types we used in our research or if it is a behaviour that exists in other APCs and has hitherto remained undiscovered.

Research published by Jiang et. al. after the microglia paper has independently corroborated that β2 integrin dysfunction (full knock-out and antibody blockade in their case[432]) leads to neuroprotective outcomes through microglial polarization. As we had previously established that β2 integrins regulate metabolism and it in turn regulates immune function in another APC; we wondered if a similar mechanism

might be at play in microglia cells. Other research groups have established that for microglia even very low doses (1 mM) of 2DG are able to significantly push them away from pro-inflammatory responses to LPS or haemorrhagic stroke[17,425,433–436]. Furthermore, and linking to the aforementioned effects of organism-wide fasting signals, it was found that ketogenic diets lead to neuroprotective results in brain injury with reduced inflammation and lessened cognitive impairment as a result[21,437,438]. At the same time there has been research showing that metformin, which was initially developed to treat type-II diabetes, effectively metabolically reprograms microglia cells which itself is a causative factor in the neuroprotective effects seen in patients and laboratory animals after stroke[317,439,440]. Both due to the similar antigen-presenting roles of dendritic cells and microglia as well as their observed metabolic reprogramming after β2 integrin impairment, it is possible therefore that the mechanisms at play are common to microglia and dendritic cells. Future studies will reveal if there is a difference in metabolic state between KI and WT microglia, with the less OXPHOS-dependent cells relying on glycolysis correlating with lessened inflammation and neuroprotection.

In the field of mechanobiology, the assay of T-cell clusters with the micropipette force sensor proved its accuracy and precision as results from different cells were consistently alike within each group while different from each other. In the future we plan to use this method to study the stiffness of DC and T-cell co-culture cell clusters to correlate their biomechanical properties with more traditional marker-based antigen-presentation efficiency after metabolic reprogramming. We expect other research groups to also find it a useful method which should unseat the probe+static surface methods that had until now been competing for standardization in mechanobiological studies of single cells or mesoscale clusters[399]. An example of the unmet need for new mechanical force assays can be seen in Fritzche and Kruse's perspectives article from 2024 where they go over the role of adhesion force in early TCR activation and resulting immunological outcomes and lament at the fact there existed no assay to adequately measure adhesion force in contexts such as these[441].

9 References

1. Hoeffel G, Ginhoux F. Ontogeny of Tissue-Resident Macrophages. Front Immunol. 2015;6(SEP):486. doi:10.3389/FIMMU.2015.00486

2. Rodrigues PF, Trsan T, Cvijetic G, Khantakova D, Panda SK, Liu Z, Ginhoux F, Cella M, Colonna M. Progenitors of distinct lineages shape the diversity of mature type 2 conventional dendritic cells. Immunity. 2024;57(7):1567-1585.e5. doi:10.1016/j.immuni.2024.05.007

3. Campos M, Godson DL. The effectiveness and limitations of immune memory: understanding protective immune responses. Int J Parasitol. 2003;33(5–6):655–661. doi:10.1016/S0020-7519(03)00066-3

4. Campos M, Godson DL. The effectiveness and limitations of immune memory: understanding protective immune responses. Int J Parasitol. 2003;33(5–6):655–661. doi:10.1016/S0020-7519(03)00066-3

5. Grove DI, Hamburger J, Warren KS. Kinetics of Immunological Responses, Resistance to Reinfection, and Pathological Reactions to Infection with Trichinella spiralis. J Infect Dis. 1977;136(4):562–570. doi:10.1093/INFDIS/136.4.562

6. De Silva NS, Klein U. Dynamics of B cells in germinal centres. Nat Rev Immunol. 2015;15(3):137–148. doi:10.1038/NRI3804;SUBJMETA

7. Kurosaki T, Kometani K, Ise W. Memory B cells. Nat Rev Immunol. 2015;15(3):149–159. doi:10.1038/NRI3802;SUBJMETA

8. Rock KL, Reits E, Neefjes J. Present Yourself! By MHC Class I and MHC Class II Molecules. Trends Immunol. 2016;37(11):724–737. doi:10.1016/J.IT.2016.08.010

9. Guilliams M, Ginhoux F, Jakubzick C, Naik SH, Onai N, Schraml BU, Segura E, Tussiwand R, Yona S. Dendritic cells, monocytes and macrophages: A unified nomenclature based on ontogeny. Nat Rev Immunol. 2014;14(8):571–578. doi:10.1038/nri3712

10. Rastogi I, Jeon D, Moseman JE, Muralidhar A, Potluri HK, McNeel DG. Role of B cells as antigen presenting cells. Front Immunol. 2022;13:954936. doi:10.3389/FIMMU.2022.954936

11. Jhunjhunwala S, Hammer C, Delamarre L. Antigen presentation in cancer: insights into tumour immunogenicity and immune evasion. Nat Rev Cancer. 2021;21(5):298–312. doi:10.1038/S41568-021-00339-Z;SUBJMETA
12. Gutiérrez-Martínez E, Planès R, Anselmi G, Reynolds M, Menezes S, Adiko AC, Saveanu L, Guermonprez P. Cross-presentation of cell-associated antigens by MHC class I in dendritic cell subsets. Front Immunol. 2015;6(JUL):146579. doi:10.3389/FIMMU.2015.00363/FULL
13. Eiz-Vesper B, Schmetzer HM. Antigen-Presenting Cells: Potential of Proven und New Players in Immune Therapies. Transfusion Medicine and Hemotherapy. 2020;47(6):429–431. doi:10.1159/000512729
14. Murray PJ. Macrophage Polarization. Annu Rev Physiol. 2017;79(Volume 79, 2017):541–566. doi:10.1146/ANNUREV-PHYSIOL-022516-034339/CITE/REFWORKS
15. Pollard JW. Trophic macrophages in development and disease. Nature Reviews Immunology 2009 9:4. 2009;9(4):259–270. doi:10.1038/nri2528
16. Wynn TA, Chawla A, Pollard JW. Macrophage biology in development, homeostasis and disease. Nature 2013 496:7446. 2013;496(7446):445–455. doi:10.1038/nature12034
17. Chen W, Zhang Y, Zhai X, Xie L, Guo Y, Chen C, Li Y, Wang F, Zhu Z, Zheng L, et al. Microglial phagocytosis and regulatory mechanisms after stroke. Journal of Cerebral Blood Flow & Metabolism. 2022;42(9):1579–1596. doi:10.1177/0271678X221098841
18. Rodríguez-Pinto D. B cells as antigen presenting cells. Cell Immunol. 2005;238(2):67–75. doi:10.1016/J.CELLIMM.2006.02.005
19. Pearce EJ, Everts B. Dendritic cell metabolism. Nat Rev Immunol. 2015;15(1):18–29. doi:10.1038/NRI3771;SUBJMETA
20. O'Sullivan D, Pearce EL. Expanding the role of metabolism in T cells. Science (1979). 2015;348(6238):976–977. doi:10.1126/SCIENCE.AAC4997
21. Bielanin JP, Sun D. Significance of Microglial Energy Metabolism in Maintaining Brain Homeostasis. Transl Stroke Res. 2023;14(4):435–437. doi:10.1007/S12975-022-01069-6/FIGURES/1
22. Guak H, Al Habyan S, Ma EH, Aldossary H, Al-Masri M, Won SY, Ying T, Fixman ED, Jones RG, McCaffrey LM, et al. Glycolytic metabolism is essential for CCR7 oligomerization and dendritic cell migration. Nat Commun. 2018;9(1):2463. doi:10.1038/s41467-018-04804-6
23. Krawczyk CM, Holowka T, Sun J, Blagih J, Amiel E, DeBerardinis RJ, Cross JR, Jung E, Thompson CB, Jones RG, et al. Toll-like receptor–induced changes in glycolytic metabolism regulate dendritic cell activation. Blood. 2010;115(23):4742–4749. doi:10.1182/BLOOD-2009-10-249540

24. Geng Y, DeLay SL, Chen X, Miska J. It Is Not Just About Storing Energy: The Multifaceted Role of Creatine Metabolism on Cancer Biology and Immunology. International Journal of Molecular Sciences 2024, Vol. 25, Page 13273. 2024;25(24):13273. doi:10.3390/IJMS252413273
25. Waters LR, Ahsan FM, Wolf DM, Shirihai O, Teitell MA. Initial B Cell Activation Induces Metabolic Reprogramming and Mitochondrial Remodeling. iScience. 2018;5:99–109. doi:10.1016/j.isci.2018.07.005
26. Wang R, Green DR. Metabolic reprogramming and metabolic dependency in T cells. Immunol Rev. 2012;249(1):14–26. doi:10.1111/J.1600-065X.2012.01155.X;CSUBTYPE:STRING:SPECIAL;PAGE:STRING:ARTICLE/CHAPTER
27. Kalia V, Sarkar S, Gourley TS, Rouse BT, Ahmed R. Differentiation of memory B and T cells. Curr Opin Immunol. 2006;18(3):255–264. doi:10.1016/J.COI.2006.03.020
28. Pang J, Koh TJ. Proliferation of monocytes and macrophages in homeostasis, infection, injury, and disease. J Leukoc Biol. 2023;114(6):532–546. doi:10.1093/JLEUKO/QIAD093
29. O'Sullivan D. The metabolic spectrum of memory T cells. Immunol Cell Biol. 2019;97(7):636–646. doi:10.1111/IMCB.12274;ISSUE:ISSUE:DOI
30. Netea MG, Joosten LAB, Latz E, Mills KHG, Natoli G, Stunnenberg HG, O'Neill LAJ, Xavier RJ. Trained immunity: A program of innate immune memory in health and disease. Science (1979). 2016;352(6284):427. doi:10.1126/SCIENCE.AAF1098
31. Ziogas A, Bruno M, van der Meel R, Mulder WJM, Netea MG. Trained immunity: Target for prophylaxis and therapy. Cell Host Microbe. 2023;31(11):1776–1791. doi:10.1016/J.CHOM.2023.10.015
32. Netea MG, Domínguez-Andrés J, Barreiro LB, Chavakis T, Divangahi M, Fuchs E, Joosten LAB, van der Meer JWM, Mhlanga MM, Mulder WJM, et al. Defining trained immunity and its role in health and disease. Nat Rev Immunol. 2020;20(6):375–388. doi:10.1038/S41577-020-0285-6;SUBJMETA
33. Pham LN, Dionne MS, Shirasu-Hiza M, Schneider DS. A specific primed immune response in Drosophila is dependent on phagocytes. PLoS Pathog. 2007;3(3). doi:10.1371/JOURNAL.PPAT.0030026
34. Quintin J, Saeed S, Martens JHA, Giamarellos-Bourboulis EJ, Ifrim DC, Logie C, Jacobs L, Jansen T, Kullberg BJ, Wijmenga C, et al. Candida albicans infection affords protection against reinfection via functional reprogramming of monocytes. Cell Host Microbe. 2012;12(2):223–232. doi:10.1016/j.chom.2012.06.006

35. Arts RJW, Carvalho A, La Rocca C, Palma C, Rodrigues F, Silvestre R, Kleinnijenhuis J, Lachmandas E, Gonçalves LG, Belinha A, et al. Immunometabolic Pathways in BCG-Induced Trained Immunity. Cell Rep. 2016;17(10):2562–2571. doi:10.1016/j.celrep.2016.11.011
36. Reeves RK, Li H, Jost S, Blass E, Li H, Schafer JL, Varner V, Manickam C, Eslamizar L, Altfeld M, et al. Antigen-specific NK cell memory in rhesus macaques. Nature Immunology 2015 16:9. 2015;16(9):927–932. doi:10.1038/ni.3227
37. Raghav PK, Gangenahalli G. Hematopoietic Stem Cell Molecular Targets and Factors Essential for Hematopoiesis. J Stem Cell Res Ther. 2018;8(11). doi:10.4172/2157-7633.1000441
38. Rakshit S, Zhang Y, Manibog K, Shafraz O, Sivasankar S. Ideal, catch, and slip bonds in cadherin adhesion. Proc Natl Acad Sci U S A. 2012;109(46):18815–18820. doi:10.1073/PNAS.1208349109/-/DCSUPPLEMENTAL
39. Hyun Y-M, Chung H-L, McGrath JL, Waugh RE, Kim M. Activated integrin VLA-4 localizes to the lamellipodia and mediates T cell migration on VCAM-1. J Immunol. 2009;183(1):359–369. doi:10.4049/JIMMUNOL.0803388
40. Bednarczyk M, Stege H, Grabbe S, Bros M. β2 Integrins—Multi-Functional Leukocyte Receptors in Health and Disease. International Journal of Molecular Sciences 2020, Vol. 21, Page 1402. 2020;21(4):1402. doi:10.3390/IJMS21041402
41. Van der Flier A, Sonnenberg A. Function and interactions of integrins. Cell Tissue Res. 2001;305(3):285–298. doi:10.1007/S004410100417/METRICS
42. Varki A. Selectin ligands. Proceedings of the National Academy of Sciences. 1994;91(16):7390–7397. doi:10.1073/PNAS.91.16.7390
43. Ivetic A. A head-to-tail view of L-selectin and its impact on neutrophil behaviour. Cell and Tissue Research 2018 371:3. 2018;371(3):437–453. doi:10.1007/S00441-017-2774-X
44. Zarbock A, Ley K, McEver RP, Hidalgo A. Leukocyte ligands for endothelial selectins: specialized glycoconjugates that mediate rolling and signaling under flow. Blood. 2011;118(26):6743. doi:10.1182/BLOOD-2011-07-343566
45. Rosen SD. Ligands for L-selectin: Homing, inflammation, and beyond. Annu Rev Immunol. 2004;22(Volume 22, 2004):129–156. doi:10.1146/ANNUREV.IMMUNOL.21.090501.080131/CITE/REFWORKS
46. Whittard JD, Craig SE, Mould AP, Koch A, Pertz O, Engel J, Humphries MJ. E-cadherin is a ligand for integrin α2β1. Matrix Biology. 2002;21(6):525–532. doi:10.1016/S0945-053X(02)00037-9
47. Angst BD, Marcozzi C, Magee AI. The cadherin superfamily: diversity in form and function. J Cell Sci. 2001;114(4):629–641. doi:10.1242/JCS.114.4.629

48. Harrison OJ, Brasch J, Lasso G, Katsamba PS, Ahlsen G, Honig B, Shapiro L. Structural basis of adhesive binding by desmocollins and desmogleins. Proc Natl Acad Sci U S A. 2016;113(26):7160–7165. doi:10.1073/PNAS.1606272113/-/DCSUPPLEMENTAL
49. Binder C, Cvetkovski F, Sellberg F, Berg S, Paternina Visbal H, Sachs DH, Berglund E, Berglund D. CD2 Immunobiology. Front Immunol. 2020;11:533081. doi:10.3389/FIMMU.2020.01090/XML
50. Aricescu AR, Jones EY. Immunoglobulin superfamily cell adhesion molecules: zippers and signals. Curr Opin Cell Biol. 2007;19(5):543–550. doi:10.1016/J.CEB.2007.09.010
51. Tan RPA, Leshchyns'Ka I, Sytnyk V. Glycosylphosphatidylinositol-anchored immunoglobulin superfamily cell adhesion molecules and their role in neuronal development and synapse regulation. Front Mol Neurosci. 2017;10. doi:10.3389/FNMOL.2017.00378/FULL
52. Staunton DE, Marlin SD, Stratowa C, Dustin ML, Springer TA. Primary structure of ICAM-1 demonstrates interaction between members of the immunoglobulin and integrin supergene families. Cell. 1988;52(6):925–933. doi:10.1016/0092-8674(88)90434-5
53. Hermans D, van Beers L, Broux B. Nectin Family Ligands Trigger Immune Effector Functions in Health and Autoimmunity. Biology (Basel). 2023;12(3):452. doi:10.3390/BIOLOGY12030452
54. Murakami K, Ganguly S. The Nectin family ligands, PVRL2 and PVR, in cancer immunology and immunotherapy. Front Immunol. 2024;15:1441730. doi:10.3389/FIMMU.2024.1441730/FULL
55. Zhang Y, Lin Z, Fang Y, Wu J. Prediction of catch-slip bond transition of Kindlin2/β3 integrin via steered molecular dynamics simulation. J Chem Inf Model. 2020;60(10):5132–5141. doi:10.1021/ACS.JCIM.0C00837/SUPPL_FILE/CI0C00837_SI_006.AVI
56. Thomas W. Catch bonds in adhesion. Annu Rev Biomed Eng. 2008;10(Volume 10, 2008):39–57. doi:10.1146/ANNUREV.BIOENG.10.061807.160427/CITE/REFWORKS
57. Varki A. Selectin ligands. Proceedings of the National Academy of Sciences. 1994;91(16):7390–7397. doi:10.1073/PNAS.91.16.7390
58. Ley K. The role of selectins in inflammation and disease. Trends Mol Med. 2003;9(6):263–268. doi:10.1016/S1471-4914(03)00071-6/ASSET/B191F75B-BDD5-4BA3-A372-90AFC39B1B6A/MAIN.ASSETS/GR3.GIF
59. KANSAS GS. Structure and function of L-selectin. APMIS. 1992;100(1–6):287–293. doi:10.1111/J.1699-0463.1992.TB00874.X,
60. He M, Zhou X, Wang X. Glycosylation: mechanisms, biological functions and clinical implications. Signal Transduction and Targeted Therapy 2024 9:1. 2024;9(1):1–33. doi:10.1038/s41392-024-01886-1

61. Geng Y, Marshall JR, King MR. Glycomechanics of the metastatic cascade: Tumor cell-endothelial cell interactions in the circulation. Ann Biomed Eng. 2012;40(4):790–805. doi:10.1007/S10439-011-0463-6
62. Jin F, Wang F. The physiological and pathological roles and applications of sialyl Lewis x, a common carbohydrate ligand of the three selectins. Glycoconj J. 2020;37(2):277–291. doi:10.1007/S10719-020-09912-4/TABLES/4
63. Mehta-D'souza P, Klopocki AG, Oganesyan V, Terzyan S, Mather T, Li Z, Panicker SR, Zhu C, McEver RP. Glycan bound to the selectin low affinity state engages Glu-88 to stabilize the high affinity state under force. Journal of Biological Chemistry. 2017;292(6):2510–2518. doi:10.1074/jbc.M116.767186
64. Lawrence MB, Kansas GS, Kunkel EJ, Ley K. Threshold levels of fluid shear promote leukocyte adhesion through selectins (CD62L,P,E). Journal of Cell Biology. 1997;136(3):717–727. doi:10.1083/JCB.136.3.717
65. Dupas A, Goetz JG, Osmani N. Extravasation of immune and tumor cells from an endothelial perspective. J Cell Sci. 2024;137(21). doi:10.1242/JCS.262066/362938
66. Kang W, Li L, Wang J. Synergistic Regulation Mechanism of Selectin and Integrin on Leukocyte Adhesion Under Shear Flow. Journal of Applied Mechanics, Transactions ASME. 2022;89(1). doi:10.1115/1.4052367/1119445
67. Dong X, Peng S, Ling Y, Huang B, Tu W, Sun X, Li Q, Fang Y, Wu J. ATRA treatment slowed P-selectin-mediated rolling of flowing HL60 cells in a mechano-chemical-dependent manner. Front Immunol. 2023;14:1148543. doi:10.3389/FIMMU.2023.1148543/BIBTEX
68. Ebsen H, Schröder A, Kabelitz D, Janssen O. Differential Surface Expression of ADAM10 and ADAM17 on Human T Lymphocytes and Tumor Cells. PLoS One. 2013;8(10):e76853. doi:10.1371/JOURNAL.PONE.0076853
69. Lisi S, D'Amore M, Sisto M. ADAM17 at the interface between inflammation and autoimmunity. Immunol Lett. 2014;162(1):159–169. doi:10.1016/J.IMLET.2014.08.008
70. Killock DJ, Ivetić A. The cytoplasmic domains of TNFα-converting enzyme (TACE/ADAM17) and L-selectin are regulated differently by p38 MAPK and PKC to promote ectodomain shedding. Biochemical Journal. 2010;428(2):293–304. doi:10.1042/BJ20091611
71. Kahn J, Walcheck B, Migaki GI, Jutila MA, Kishimoto TK. Calmodulin regulates L-selectin adhesion molecule expression and function through a protease-dependent mechanism. Cell. 1998;92(6):809–818. doi:10.1016/S0092-8674(00)81408-7/ASSET/78E98B9E-7102-4511-813F-C5D0A479DD2E/MAIN.ASSETS/GR7.JPG

72. Gul IS, Hulpiau P, Saeys Y, van Roy F. Evolution and diversity of cadherins and catenins. Exp Cell Res. 2017;358(1):3–9. doi:10.1016/J.YEXCR.2017.03.001
73. Gul IS, Hulpiau P, Saeys Y, van Roy F. Evolution and diversity of cadherins and catenins. Exp Cell Res. 2017;358(1):3–9. doi:10.1016/J.YEXCR.2017.03.001
74. Rakshit S, Zhang Y, Manibog K, Shafraz O, Sivasankar S. Ideal, catch, and slip bonds in cadherin adhesion. Proc Natl Acad Sci U S A. 2012;109(46):18815–18820. doi:10.1073/PNAS.1208349109/-/DCSUPPLEMENTAL
75. Harrison OJ, Brasch J, Lasso G, Katsamba PS, Ahlsen G, Honig B, Shapiro L. Structural basis of adhesive binding by desmocollins and desmogleins. Proc Natl Acad Sci U S A. 2016;113(26):7160–7165. doi:10.1073/PNAS.1606272113/-/DCSUPPLEMENTAL
76. Bella J, Kolatkar PR, Marlor CW, Greve JM, Rossmann MG. The structure of the two amino-terminal domains of human ICAM-1 suggests how it functions as a rhinovirus receptor and as an LFA-1 integrin ligand. Proc Natl Acad Sci U S A. 1998;95(8):4140–4145. doi:10.1073/PNAS.95.8.4140/ASSET/B57CDFB8-E21F-42A7-AC54-4A0306E93099/ASSETS/GRAPHIC/PQ0680126005.JPEG
77. Holness CL, Simmons DL. Structural motifs for recognition and adhesion in members of the immunoglobulin superfamily. J Cell Sci. 1994;107(8):2065–2070. doi:10.1242/JCS.107.8.2065
78. Ogita H, Rikitake Y, Miyoshi J, Takai Y. Cell adhesion molecules nectins and associating proteins: Implications for physiology and pathology. Proc Jpn Acad Ser B Phys Biol Sci. 2010;86(6):621. doi:10.2183/PJAB.86.621
79. Samanta D, Almo SC. Nectin family of cell-adhesion molecules: structural and molecular aspects of function and specificity. Cell Mol Life Sci. 2014;72(4):645. doi:10.1007/S00018-014-1763-4
80. Samanta D, Almo SC. Nectin family of cell-adhesion molecules: Structural and molecular aspects of function and specificity. Cellular and Molecular Life Sciences. 2015;72(4):645–658. doi:10.1007/S00018-014-1763-4/FIGURES/8
81. Miyoshi J, Takai Y. Nectin and nectin-like molecules: biology and pathology. Am J Nephrol. 2007;27(6):590–604. doi:10.1159/000108103
82. Buckle I, Guillerey C. Inhibitory Receptors and Immune Checkpoints Regulating Natural Killer Cell Responses to Cancer. Cancers (Basel). 2021;13(17):4263. doi:10.3390/CANCERS13174263
83. Hynes RO. The emergence of integrins: a personal and historical perspective. Matrix Biol. 2004;23(6):333. doi:10.1016/J.MATBIO.2004.08.001
84. Humphries MJ. Integrin Structure. Biochem Soc Trans. 2000;28(4):311–340. doi:10.1042/BST0280311

85. Giancotti FG, Ruoslahti E. Integrin signaling. Science (1979). 1999;285(5430):1028–1032. doi:10.1126/SCIENCE.285.5430.1028/ASSET/DB7B6FCE-5D55-4DBF-8CD7-FACB4F1228FD/ASSETS/GRAPHIC/SE3097724004.JPEG
86. Campbell ID, Humphries MJ. Integrin Structure, Activation, and Interactions. Cold Spring Harb Perspect Biol. 2011;3(3):a004994. doi:10.1101/CSHPERSPECT.A004994
87. Mezu-Ndubuisi OJ, Maheshwari A. The role of integrins in inflammation and angiogenesis. Pediatr Res. 2021;89(7):1619–1626. doi:10.1038/S41390-020-01177-9;KWRD=MEDICINE
88. Arnaout MA, Mahalingam B, Xiong JP. Integrin structure, allostery, and bidirectional signaling. Annu Rev Cell Dev Biol. 2005;21(Volume 21, 2005):381–410. doi:10.1146/ANNUREV.CELLBIO.21.090704.151217/CITE/REFWORKS
89. Landis RC, McDowall A, Holness CLL, Littler AJ, Simmons DL, Hogg N. Involvement of the I domain of LFA-1 in selective binding to ligands ICAM-1 and ICAM-3. Journal of Cell Biology. 1994;126(2):529–537. doi:10.1083/JCB.126.2.529
90. Whittaker CA, Hynes RO. Distribution and Evolution of von Willebrand/Integrin A Domains: Widely Dispersed Domains with Roles in Cell Adhesion and Elsewhere. Mol Biol Cell. 2002;13(10):3369. doi:10.1091/MBC.E02-05-0259
91. Constantin G, Majeed M, Giagulli C, Piccio L, Kim JY, Butcher EC, Laudanna C. Chemokines Trigger Immediate β2 Integrin Affinity and Mobility Changes: Differential Regulation and Roles in Lymphocyte Arrest under Flow. Immunity. 2000;13(6):759–769. doi:10.1016/S1074-7613(00)00074-1
92. Berton G, Lowell CA. Integrin Signalling in Neutrophils and Macrophages. Cell Signal. 1999;11(9):621–635. doi:10.1016/S0898-6568(99)00003-0
93. Moser M, Legate KR, Zent R, Fässler R. The tail of integrins, talin, and kindlins. Science (1979). 2009;324(5929):895–899. doi:10.1126/SCIENCE.1163865
94. Barczyk M, Carracedo S, Gullberg D. Integrins. Cell Tissue Res. 2010;339(1):269–280. doi:10.1007/S00441-009-0834-6/TABLES/2
95. Hughes PE, Diaz-Gonzalez F, Leong L, Wu C, McDonald JA, Shattil SJ, Ginsberg MH. Breaking the Integrin Hinge. Journal of Biological Chemistry. 1996;271(12):6571–6574. doi:10.1074/jbc.271.12.6571
96. Li W, Metcalf DG, Gorelik R, Li R, Mitra N, Nanda V, Law PB, Lear JD, DeGrado WF, Bennett JS. A push-pull mechanism for regulating integrin function. Proc Natl Acad Sci U S A. 2005;102(5):1424–1429. doi:10.1073/PNAS.0409334102/SUPPL_FILE/09334FIG8.PDF
97. Sun Z, Costell M, Fässler R. Integrin activation by talin, kindlin and mechanical forces. Nature Cell Biology 2019 21:1. 2019;21(1):25–31. doi:10.1038/s41556-018-0234-9

98. Calderwood DA. Talin controls integrin activation. Biochem Soc Trans. 2004;32(3):434–437. doi:10.1042/BST0320434
99. Knezevic I, Leisner TM, Lam SCT. Direct Binding of the Platelet Integrin αIIbβ3 (GPIIb-IIIa) to Talin: EVIDENCE THAT INTERACTION IS MEDIATED THROUGH THE CYTOPLASMIC DOMAINS OF BOTH αIIb AND β3. Journal of Biological Chemistry. 1996;271(27):16416–16421. doi:10.1074/JBC.271.27.16416
100. Dahal N, Sharma S, Phan B, Eis A, Popa I. Mechanical regulation of talin through binding and history-dependent unfolding. Sci Adv. 2022;8(28):7719. doi:10.1126/SCIADV.ABL7719/SUPPL_FILE/SCIADV.ABL7719_SM.PDF
101. Kim C, Ye F, Hu X, Ginsberg MH. Talin activates integrins by altering the topology of the β transmembrane domain. Journal of Cell Biology. 2012;197(5):605–611. doi:10.1083/JCB.201112141
102. Xin H, Huang J, Song Z, Mao J, Xi X, Shi X. Structure, signal transduction, activation, and inhibition of integrin αIIbβ3. Thromb J. 2023;21(1):1–15. doi:10.1186/S12959-023-00463-W/TABLES/2
103. Yang J, Zhu L, Zhang H, Hirbawi J, Fukuda K, Dwivedi P, Liu J, Byzova T, Plow EF, Wu J, et al. Conformational activation of talin by RIAM triggers integrin-mediated cell adhesion. Nat Commun. 2014;5(1):5880. doi:10.1038/NCOMMS6880;TECHMETA
104. Ye F, Kim C, Ginsberg MH. Molecular mechanism of inside-out integrin regulation. Journal of Thrombosis and Haemostasis. 2011;9(1 S):20–25. doi:10.1111/J.1538-7836.2011.04355.X
105. Abram CL, Lowell CA. The ins and outs of leukocyte integrin signaling. Annu Rev Immunol. 2009;27(Volume 27, 2009):339–362. doi:10.1146/ANNUREV.IMMUNOL.021908.132554/CITE/REFWORKS
106. Yan B, Calderwood DA, Yaspan B, Ginsberg MH. Calpain Cleavage Promotes Talin Binding to the β3 Integrin Cytoplasmic Domain. Journal of Biological Chemistry. 2001;276(30):28164–28170. doi:10.1074/jbc.M104161200
107. Sun H, Lagarrigue F, Ginsberg MH. The Connection Between Rap1 and Talin1 in the Activation of Integrins in Blood Cells. Front Cell Dev Biol. 2022;10:908622. doi:10.3389/FCELL.2022.908622/FULL
108. Lagarrigue F, Tan B, Du Q, Fan Z, Lopez-Ramirez MA, Gingras AR, Wang H, Qi W, Sun H. Direct Binding of Rap1 to Talin1 and to MRL Proteins Promotes Integrin Activation in CD4+ T Cells. J Immunol. 2022;208(6):1378–1388. doi:10.4049/JIMMUNOL.2100843

109. Chang YC, Su W, Cho E ah, Zhang H, Huang Q, Philips MR, Wu J. Molecular basis for autoinhibition of RIAM regulated by FAK in integrin activation. Proceedings of the National Academy of Sciences. 2019;116(9):3524–3529. doi:10.1073/PNAS.1818880116
110. Kliche S, Worbs T, Wang X, Degen J, Patzak I, Meineke B, Togni M, Moser M, Reinhold A, Kiefer F, et al. CCR7-mediated LFA-1 functions in T cells are regulated by 2 independent ADAP/SKAP55 modules. Blood. 2012;119(3):777–785. doi:10.1182/BLOOD-2011-06-362269
111. Borowsky ML, Hynes RO. Layilin, A Novel Talin-binding Transmembrane Protein Homologous with C-type Lectins, is Localized in Membrane Ruffles. Journal of Cell Biology. 1998;143(2):429–442. doi:10.1083/JCB.143.2.429
112. Chen HC, Appeddu PA, Parsons JT, Hildebrand JD, Schaller MD, Guan JL. Interaction of Focal Adhesion Kinase with Cytoskeletal Protein Talin. Journal of Biological Chemistry. 1995;270(28):16995–16999. doi:10.1074/JBC.270.28.16995
113. Martel V, Racaud-Sultan C, Dupe S, Marie C, Paulhe F, Galmiche A, Block MR, Albiges-Rizo C. Conformation, Localization, and Integrin Binding of Talin Depend on Its Interaction with Phosphoinositides. Journal of Biological Chemistry. 2001;276(24):21217–21227. doi:10.1074/JBC.M102373200/ASSET/314AFEEC-FB5F-49C6-81F5-C80AF01B6A6F/MAIN.ASSETS/GR10.JPG
114. Calderwood DA, Zent R, Grant R, Rees DJG, Hynes RO, Ginsberg MH. The Talin Head Domain Binds to Integrin β Subunit Cytoplasmic Tails and Regulates Integrin Activation. Journal of Biological Chemistry. 1999;274(40):28071–28074. doi:10.1074/JBC.274.40.28071
115. Gao T, Maskalenko NA, Kabir S, Campbell KS, Wu J. Molecular basis of β2 integrin activation by talin unveils subunit-specific mechanisms of integrin signaling. Cell Rep. 2025;44(5):115607. doi:10.1016/J.CELREP.2025.115607
116. Yao M, Goult BT, Chen H, Cong P, Sheetz MP, Yan J. Mechanical activation of vinculin binding to talin locks talin in an unfolded conformation. Sci Rep. 2014;4(1):1–7. doi:10.1038/SREP04610;TECHMETA=9;SUBJMETA=2265,337,631,79,80;KWRD=CELL+ADHESION,SINGLE-MOLECULE+BIOPHYSICS
117. Hemmings L, Rees DJG, Ohanian V, Bolton SJ, Gilmore AP, Patel B, Priddle H, Trevithick JE, Hynes RO, Critchley DR. Talin contains three actin-binding sites each of which is adjacent to a vinculin-binding site. J Cell Sci. 1996;109(11):2715–2726. doi:10.1242/JCS.109.11.2715
118. Shimaoka M, Takagi J, Springer TA. Conformational regulation of integrin structure and function. Annu Rev Biophys Biomol Struct. 2002;31(Volume 31, 2002):485–516. doi:10.1146/ANNUREV.BIOPHYS.31.101101.140922/CITE/REFWORKS

119. Hughes PE, Pfaff M. Integrin affinity modulation. Trends Cell Biol. 1998;8(9):359–364. doi:10.1016/S0962-8924(98)01339-7
120. Shimaoka M, Xiao T, Liu JH, Yang Y, Dong Y, Jun CD, McCormack A, Zhang R, Joachimiak A, Takagi J, et al. Structures of the αL I Domain and Its Complex with ICAM-1 Reveal a Shape-Shifting Pathway for Integrin Regulation. Cell. 2003;112(1):99. doi:10.1016/S0092-8674(02)01257-6
121. Gaikwad HK, Jaswandkar S V., Katti KS, Haage A, Katti DR. Molecular basis of conformational changes and mechanics of integrins. Philosophical Transactions of the Royal Society A. 2023;381(2250). doi:10.1098/RSTA.2022.0243
122. Burbach BJ, Medeiros RB, Mueller KL, Shimizu Y. T-cell receptor signaling to integrins. Immunol Rev. 2007;218(1):65–81. doi:10.1111/J.1600-065X.2007.00527.X;REQUESTEDJOURNAL:JOURNAL:1600065X;PAGE:STRING:ARTICLE/CHAPTER
123. Cairo CW, Mirchev R, Golan DEE. Cytoskeletal Regulation Couples LFA-1 Conformational Changes to Receptor Lateral Mobility and Clustering. Immunity. 2006;25(2):297–308. doi:10.1016/J.IMMUNI.2006.06.012
124. Pribila JT, Quale AC, Mueller KL, Shimizu Y. Integrins and T cell-mediated immunity. Annu Rev Immunol. 2004;22:157–180. doi:10.1146/ANNUREV.IMMUNOL.22.012703.104649,
125. Bertoni A, Alabiso O, Galetto AS, Baldanzi G. Integrins in T Cell Physiology. International Journal of Molecular Sciences 2018, Vol. 19, Page 485. 2018;19(2):485. doi:10.3390/IJMS19020485
126. Vignoud L, Albigès-Rizo C, Frachet P, Block MR. NPXY motifs control the recruitment of the α5β1 integrin in focal adhesions independently of the association of talin with the β1 chain. J Cell Sci. 1997;110(12):1421–1430. doi:10.1242/JCS.110.12.1421
127. Durrant TN, Van Den Bosch MT, Hers I. Integrin αIIbβ3 outside-in signaling. Blood. 2017;130(14):1607. doi:10.1182/BLOOD-2017-03-773614
128. Stalker TJ, Newman DK, Ma P, Wannemacher KM, Brass LF. Platelet signaling. Handb Exp Pharmacol. 2012;210:59–85. doi:10.1007/978-3-642-29423-5_3/FIGURES/6
129. Elosegui-Artola A, Oria R, Chen Y, Kosmalska A, Pérez-González C, Castro N, Zhu C, Trepat X, Roca-Cusachs P. Mechanical regulation of a molecular clutch defines force transmission and transduction in response to matrix rigidity. Nature Cell Biology 2016 18:5. 2016;18(5):540–548. doi:10.1038/ncb3336
130. Nordenfelt P, Elliott HL, Springer TA. Coordinated integrin activation by actin-dependent force during T-cell migration. Nat Commun. 2016;7(1):1–15. doi:10.1038/NCOMMS13119;TECHMETA

131. Zhang H, Yang M, Kim SH, Li ITS. Integrin force loading rate in mechanobiology: From model to molecular measurement. QRB Discov. 2025;6. doi:10.1017/QRD.2024.28
132. Barcelona-Estaje E, Oliva MAG, Cunniffe F, Rodrigo-Navarro A, Genever P, Dalby MJ, Roca-Cusachs P, Cantini M, Salmeron-Sanchez M. N-cadherin crosstalk with integrin weakens the molecular clutch in response to surface viscosity. Nature Communications . 2024;15(1):1–12. doi:10.1038/S41467-024-53107-6;TECHMETA
133. Case LB, Waterman CM. Integration of actin dynamics and cell adhesion by a three-dimensional, mechanosensitive molecular clutch. Nat Cell Biol. 2015;17(8):955–963. doi:10.1038/NCB3191;SUBJMETA
134. Pfaff M, Du X, Ginsberg MH. Calpain cleavage of integrin β cytoplasmic domains. FEBS Lett. 1999;460(1):17–22. doi:10.1016/S0014-5793(99)01250-8
135. Bate N, Gingras AR, Bachir A, Horwitz R, Ye F, Patel B, Goult BT, Critchley DR. Talin Contains A C-Terminal Calpain2 Cleavage Site Important In Focal Adhesion Dynamics. PLoS One. 2012;7(4):e34461. doi:10.1371/JOURNAL.PONE.0034461
136. Zhao Y, Malinin NL, Meller J, Ma Y, West XZ, Bledzka K, Qin J, Podrez EA, Byzova T V. Regulation of cell adhesion and migration by Kindlin-3 cleavage by calpain. Journal of Biological Chemistry. 2012;287(47):40012–40020. doi:10.1074/jbc.M112.380469
137. Ji J, Su L, Liu Z. Critical role of calpain in inflammation. Biomed Rep. 2016;5(6):647–652. doi:10.3892/BR.2016.785/HTML
138. Deshpande R V., Goust J-M, Chakrabarti AK, Barbosa E, Hogan EL, Banik NL. Calpain Expression in Lymphoid Cells. Journal of Biological Chemistry. 1995;270(6):2497–2505. doi:10.1074/jbc.270.6.2497
139. Hirata H, Tatsumi H, Hayakawa K, Sokabe M. Non-channel mechanosensors working at focal adhesion-stress fiber complex. Pflugers Arch. 2015;467(1):141–155. doi:10.1007/S00424-014-1558-3
140. Huang J, Li X, Shi X, Zhu M, Wang J, Huang S, Huang X, Wang H, Li L, Deng H, et al. Platelet integrin αIIbβ3: Signal transduction, regulation, and its therapeutic targeting. J Hematol Oncol. 2019;12(1). doi:10.1186/S13045-019-0709-6
141. Goult BT, Zacharchenko T, Bate N, Tsang R, Hey F, Gingras AR, Elliott PR, Roberts GCK, Ballestrem C, Critchley DR, et al. RIAM and vinculin binding to talin are mutually exclusive and regulate adhesion assembly and turnover. Journal of Biological Chemistry. 2013;288(12):8238–8249. doi:10.1074/jbc.M112.438119
142. Malinin NL, Plow EF, Byzova T V. Kindlins in FERM adhesion. Blood. 2010;115(20):4011–4017. doi:10.1182/BLOOD-2009-10-239269

143. Bouaouina M, Calderwood DA. Kindlins. Current Biology. 2011;21(3):R99–R101. doi:10.1016/j.cub.2010.12.002
144. Bledzka K, Bialkowska K, Sossey-Alaoui K, Vaynberg J, Pluskota E, Qin J, Plow EF. Kindlin-2 directly binds actin and regulates integrin outside-in signaling. Journal of Cell Biology. 2016;213(1):97–108. doi:10.1083/JCB.201501006
145. Calderwood DA, Campbell ID, Critchley DR. Talins and kindlins; partners in integrin-mediated adhesion. Nat Rev Mol Cell Biol. 2013;14(8):503. doi:10.1038/NRM3624
146. Ithychanda SS, Das M, Ma YQ, Ding K, Wang X, Gupta S, Wu C, Plow EF, Qin J. Migfilin, a molecular switch in regulation of integrin activation. Journal of Biological Chemistry. 2009;284(7):4713–4722. doi:10.1074/JBC.M807719200/ATTACHMENT/AF669176-7D7A-422B-89AE-1610D5FA55F5/MMC1.PDF
147. Legate KR, Montañez E, Kudlacek O, Fässler R. ILK, PINCH and parvin: The tIPP of integrin signalling. Nat Rev Mol Cell Biol. 2006;7(1):20–31. doi:10.1038/NRM1789;KWRD=LIFE+SCIENCES
148. Górska A, Mazur AJ. Integrin-linked kinase (ILK): the known vs. the unknown and perspectives. Cellular and Molecular Life Sciences 2022 79:2. 2022;79(2):1–26. doi:10.1007/S00018-021-04104-1
149. Serrano I, McDonald PC, Lock F, Muller WJ, Dedhar S. Inactivation of the Hippo tumour suppressor pathway by integrin-linked kinase. Nat Commun. 2013;4. doi:10.1038/NCOMMS3976,
150. Hannigan GE, McDonald PC, Walsh MP, Dedhar S. Integrin-linked kinase: Not so pseudo after all. Oncogene. 2011;30(43):4375–4385. doi:10.1038/ONC.2011.177;SUBJMETA
151. Deng JT, Van Lierop JE, Sutherland C, Walsh MP. Ca2+-independent Smooth Muscle Contraction. Journal of Biological Chemistry. 2001;276(19):16365–16373. doi:10.1074/jbc.m011634200
152. Vachon PH. Integrin Signaling, Cell Survival, and Anoikis: Distinctions, Differences, and Differentiation. J Signal Transduct. 2011;2011(1):738137. doi:10.1155/2011/738137
153. de Sousa Mesquita AP, de Araújo Lopes S, Pernambuco Filho PCA, Nader HB, Lopes CC. Acquisition of anoikis resistance promotes alterations in the Ras/ERK and PI3K/Akt signaling pathways and matrix remodeling in endothelial cells. Apoptosis. 2017;22(9):1116–1137. doi:10.1007/S10495-017-1392-0/METRICS
154. Choi C, Kwon J, Lim S, Helfman DM. Integrin β1, myosin light chain kinase and myosin IIA are required for activation of PI3K-AKT signaling following MEK inhibition in metastatic triple negative breast cancer. Oncotarget. 2016;7(39):63466. doi:10.18632/ONCOTARGET.11525

155. Escate R, Padro T, Badimon L. LDL accelerates monocyte to macrophage differentiation: Effects on adhesion and anoikis. Atherosclerosis. 2016;246:177–186. doi:10.1016/J.ATHEROSCLEROSIS.2016.01.002
156. Munn DH, Beall AC, Song D, Wrenn RW, Throckmorton DC. Activation-induced apoptosis in human macrophages: developmental regulation of a novel cell death pathway by macrophage colony-stimulating factor and interferon gamma. Journal of Experimental Medicine. 1995;181(1):127–136. doi:10.1084/JEM.181.1.127
157. Oloumi A, McPhee T, Dedhar S. Regulation of E-cadherin expression and β-catenin/Tcf transcriptional activity by the integrin-linked kinase. Biochimica et Biophysica Acta (BBA) - Molecular Cell Research. 2004;1691(1):1–15. doi:10.1016/J.BBAMCR.2003.12.002
158. Aplin AE, Stewart SA, Assoian RK, Juliano RL. Integrin-Mediated Adhesion Regulates ERK Nuclear Translocation and Phosphorylation of Elk-1. J Cell Biol. 2001;153(2):273. doi:10.1083/JCB.153.2.273
159. Maik-Rachline G, Hacohen-Lev-Ran A, Seger R. Nuclear ERK: Mechanism of Translocation, Substrates, and Role in Cancer. Int J Mol Sci. 2019;20(5):1194. doi:10.3390/IJMS20051194
160. Weirich KL, Stam S, Munro E, Gardel ML. Actin bundle architecture and mechanics regulate myosin II force generation. Biophys J. 2021;120(10):1957. doi:10.1016/J.BPJ.2021.03.026
161. Xu Z, Zhou Y, Yu H, Chen X, Ma YQ. Myosin light chain 6 (Myl6) interacts with kindlin-3 and is required to support integrin αIIbβ3 activation in platelets in mice. Journal of Thrombosis and Haemostasis. 2024;22(7):2009–2017. doi:10.1016/J.JTHA.2024.01.007
162. Hong W, Guan KL. The YAP and TAZ transcription co-activators: Key downstream effectors of the mammalian Hippo pathway. Semin Cell Dev Biol. 2012;23(7):785–793. doi:10.1016/J.SEMCDB.2012.05.004
163. Panciera T, Azzolin L, Cordenonsi M, Piccolo S. Mechanobiology of YAP and TAZ in physiology and disease. Nat Rev Mol Cell Biol. 2017;18(12):758–770. doi:10.1038/NRM.2017.87;SUBJMETA
164. Meli VS, Veerasubramanian PK, Downing TL, Wang W, Liu WF. Mechanosensation to inflammation: Roles for YAP/TAZ in innate immune cells. Sci Signal. 2023;16(783). doi:10.1126/SCISIGNAL.ADC9656
165. Stein C, Bardet AF, Roma G, Bergling S, Clay I, Ruchti A, Agarinis C, Schmelzle T, Bouwmeester T, Schübeler D, et al. YAP1 Exerts Its Transcriptional Control via TEAD-Mediated Activation of Enhancers. PLoS Genet. 2015;11(8):e1005465. doi:10.1371/JOURNAL.PGEN.1005465
166. Zanconato F, Forcato M, Battilana G, Azzolin L, Quaranta E, Bodega B, Rosato A, Bicciato S, Cordenonsi M, Piccolo S. Genome-wide association between YAP/TAZ/TEAD and AP-1 at

enhancers drives oncogenic growth. Nat Cell Biol. 2015;17(9):1218–1227. doi:10.1038/NCB3216;TECHMETA

167. Hagenbeek TJ, Zbieg JR, Hafner M, Mroue R, Lacap JA, Sodir NM, Noland CL, Afghani S, Kishore A, Bhat KP, et al. An allosteric pan-TEAD inhibitor blocks oncogenic YAP/TAZ signaling and overcomes KRAS G12C inhibitor resistance. Nat Cancer. 2023;4(6):812–828. doi:10.1038/S43018-023-00577-0

168. Piccolo S, Dupont S, Cordenonsi M. The Biology of YAP/TAZ: Hippo Signaling and Beyond. https://doi.org/10.1152/physrev.00005.2014. 2014;94(4):1287–1312. doi:10.1152/PHYSREV.00005.2014

169. Zhao B, Wei X, Li W, Udan RS, Yang Q, Kim J, Xie J, Ikenoue T, Yu J, Li L, et al. Inactivation of YAP oncoprotein by the Hippo pathway is involved in cell contact inhibition and tissue growth control. Genes Dev. 2007;21(21):2747–2761. doi:10.1101/GAD.1602907

170. Zhao B, Li L, Tumaneng K, Wang CY, Guan KL. A coordinated phosphorylation by Lats and CK1 regulates YAP stability through SCFβ-TRCP. Genes Dev. 2010;24(1):72–85. doi:10.1101/GAD.1843810

171. Saucedo LJ, Edgar BA. Filling out the Hippo pathway. Nat Rev Mol Cell Biol. 2007;8(8):613–621. doi:10.1038/NRM2221

172. Liu CY, Zha ZY, Zhou X, Zhang H, Huang W, Zhao D, Li T, Chan SW, Lim CJ, Hong W, et al. The hippo tumor pathway promotes TAZ degradation by phosphorylating a phosphodegron and recruiting the SCFβ-TrCP E3 ligase. Journal of Biological Chemistry. 2010;285(48):37159–37169. doi:10.1074/jbc.M110.152942

173. Basu S, Totty NF, Irwin MS, Sudol M, Downward J. Akt phosphorylates the Yes-associated protein, YAP, to induce interaction with 14-3-3 and attenuation of p73-mediated apoptosis. Mol Cell. 2003;11(1):11–23. doi:10.1016/S1097-2765(02)00776-1

174. Danovi SA, Rossi M, Gudmundsdottir K, Yuan M, Melino G, Basu S. Yes-Associated Protein (YAP) is a critical mediator of c-Jun-dependent apoptosis [3]. Cell Death Differ. 2008;15(1):217–219. doi:10.1038/SJ.CDD.4402226;KWRD

175. Levy D, Adamovich Y, Reuven N, Shaul Y. Yap1 Phosphorylation by c-Abl Is a Critical Step in Selective Activation of Proapoptotic Genes in Response to DNA Damage. Mol Cell. 2008;29(3):350–361. doi:10.1016/j.molcel.2007.12.022

176. Rosenbluh J, Nijhawan D, Cox AG, Li X, Neal JT, Schafer EJ, Zack TI, Wang X, Tsherniak A, Schinzel AC, et al. β-Catenin-driven cancers require a YAP1 transcriptional complex for survival and tumorigenesis. Cell. 2012;151(7):1457–1473. doi:10.1016/j.cell.2012.11.026

177. Klaus A, Birchmeier W. Wnt signalling and its impact on development and cancer. Nat Rev Cancer. 2008;8(5):387–398. doi:10.1038/NRC2389
178. Yuan Y, Wu D, Hou Y, Zhang Y, Tan C, Nie X, Zhao Z, Hou J. Wnt signaling: Modulating tumor-associated macrophages and related immunotherapeutic insights. Biochem Pharmacol. 2024;223:116154. doi:10.1016/J.BCP.2024.116154
179. Stokowski RP, Cox DR. Functional analysis of the neurofibromatosis type 2 protein by means of disease-causing point mutations. Am J Hum Genet. 2000;66(3):873–891. doi:10.1086/302812
180. Yu J, Zheng Y, Dong J, Klusza S, Deng WM, Pan D. Kibra Functions as a Tumor Suppressor Protein that Regulates Hippo Signaling in Conjunction with Merlin and Expanded. Dev Cell. 2010;18(2):288–299. doi:10.1016/j.devcel.2009.12.012
181. Cordenonsi M, Zanconato F, Azzolin L, Forcato M, Rosato A, Frasson C, Inui M, Montagner M, Parenti AR, Poletti A, et al. The hippo transducer TAZ confers cancer stem cell-related traits on breast cancer cells. Cell. 2011;147(4):759–772. doi:10.1016/j.cell.2011.09.048
182. Palazzo AF, Eng CH, Schlaepfer DD, Marcantonio EE, Gundersen GG. Localized Stabilization of Microtubules by Integrin- and FAK-Facilitated Rho Signaling. Science (1979). 2004;303(5659):836–839. doi:10.1126/SCIENCE.1091325
183. Jakus Z, Fodor S, Abram CL, Lowell CA, Mócsai A. Immunoreceptor-like signaling by β2 and β3 integrins. Trends Cell Biol. 2007;17(10):493–501. doi:10.1016/J.TCB.2007.09.001
184. Dupont S, Morsut L, Aragona M, Enzo E, Giulitti S, Cordenonsi M, Zanconato F, Le Digabel J, Forcato M, Bicciato S, et al. Role of YAP/TAZ in mechanotransduction. Nature. 2011;474(7350):179–184. doi:10.1038/NATURE10137;SUBJMETA
185. Guan JL. Integrins, Rafts, Rac, and Rho. Science (1979). 2004;303(5659):773–774. doi:10.1126/SCIENCE.1094376
186. Hermann MR, Jakobson M, Colo GP, Rognoni E, Jakobson M, Kupatt C, Posern G, Fässler R. Integrins synergise to induce expression of the MRTF-A-SRF target gene ISG15 for promoting cancer cell invasion. J Cell Sci. 2016;129(7):1391–1403. doi:10.1242/JCS.177592/260034/AM/INTEGRINS-SYNERGIZE-TO-INDUCE-EXPRESSION-OF-THE
187. Taylor A, Halene S. The regulatory role of serum response factor pathway in neutrophil inflammatory response. Curr Opin Hematol. 2015;22(1):67–73. doi:10.1097/MOH.0000000000000099
188. Record J, Malinova D, Zenner HL, Plagnol V, Nowak K, Syed F, Bouma G, Curtis J, Gilmour K, Cale C, et al. Immunodeficiency and severe susceptibility to bacterial infection associated with a loss-of-function homozygous mutation of MKL1. Blood. 2015;126(13):1527–1535. doi:10.1182/BLOOD-2014-12-611012

189. Palazzo AF, Cook TA, Alberts AS, Gundersen GG. mDia mediates Rho-regulated formation and orientation of stable microtubules. Nat Cell Biol. 2001;3(8):723–729. doi:10.1038/35087035;KWRD
190. Lappalainen P, Kotila T, Jégou A, Romet-Lemonne G. Biochemical and mechanical regulation of actin dynamics. Nat Rev Mol Cell Biol. 2022;23(12):836–852. doi:10.1038/S41580-022-00508-4
191. Olson EN, Nordheim A. Linking actin dynamics and gene transcription to drive cellular motile functions. Nat Rev Mol Cell Biol. 2010;11(5):353–365. doi:10.1038/NRM2890;SUBJMETA
192. Zhu C, Chen W, Lou J, Rittase W, Li K. Mechanosensing through immunoreceptors. Nature Immunology 2019 20:10. 2019;20(10):1269–1278. doi:10.1038/s41590-019-0491-1
193. Zhang X, Kim TH, Thauland TJ, Li H, Majedi FS, Ly C, Gu Z, Butte MJ, Rowat AC, Li S. Unraveling the mechanobiology of immune cells. Curr Opin Biotechnol. 2020;66:236–245. doi:10.1016/J.COPBIO.2020.09.004
194. Driscoll TP, Bidone TC, Ahn SJ, Yu A, Groisman A, Voth GA, Schwartz MA. Integrin-based mechanosensing through conformational deformation. Biophys J. 2021;120(20):4349–4359. doi:10.1016/J.BPJ.2021.09.010/ATTACHMENT/64D8B37C-A685-42FA-BCF9-D8BFFDD3A585/MMC2.PDF
195. Choi Y, Kwon JE, Cho YK. Dendritic cell migration is tuned by mechanical stiffness of the confining space. Cells. 2021;10(12). doi:10.3390/CELLS10123362/S1
196. Lee M, Du H, Winer DA, Clemente-Casares X, Tsai S. Mechanosensing in macrophages and dendritic cells in steady-state and disease. Front Cell Dev Biol. 2022;10:1044729. doi:10.3389/FCELL.2022.1044729/FULL
197. Okamoto T, Takagi Y, Kawamoto E, Park EJ, Usuda H, Wada K, Shimaoka M. Reduced substrate stiffness promotes M2-like macrophage activation and enhances peroxisome proliferator-activated receptor γ expression. Exp Cell Res. 2018;367(2):264–273. doi:10.1016/J.YEXCR.2018.04.005
198. Chakraborty M, Chu K, Shrestha A, Revelo XS, Zhang X, Gold MJ, Khan S, Lee M, Huang C, Akbari M, et al. Mechanical Stiffness Controls Dendritic Cell Metabolism and Function. Cell Rep. 2021;34(2):108609. doi:10.1016/j.celrep.2020.108609
199. Haschak M, LoPresti S, Stahl E, Dash S, Popovich B, Brown BN. Macrophage phenotype and function are dependent upon the composition and biomechanics of the local cardiac tissue microenvironment. Aging (Albany NY). 2021;13(13):16938. doi:10.18632/AGING.203054
200. Scott RA, Kiick KL, Akins RE. Substrate stiffness directs the phenotype and polarization state of cord blood derived macrophages. Acta Biomater. 2021;122:220–235. doi:10.1016/J.ACTBIO.2020.12.040

201. Srivastava LK, Ehrlicher AJ. Sensing the squeeze: nuclear mechanotransduction in health and disease. Nucleus. 2024;15(1). doi:10.1080/19491034.2024.2374854;SUBPAGE:STRING:FULL
202. Koushki N, Ghagre A, Srivastava LK, Molter C, Ehrlicher AJ. Nuclear compression regulates YAP spatiotemporal fluctuations in living cells. Proc Natl Acad Sci U S A. 2023;120(28):e2301285120. doi:10.1073/PNAS.2301285120;WEBSITE:WEBSITE:PNAS-SITE;ISSUE:ISSUE:DOI
203. Pan S. Molecular Mechanisms Responsible for the Atheroprotective Effects of Laminar Shear Stress. https://home.liebertpub.com/ars. 2009;11(7):1669–1682. doi:10.1089/ARS.2009.2487
204. Chien S. Mechanotransduction and endothelial cell homeostasis: the wisdom of the cell. https://doi.org/10.1152/ajpheart.01047.2006. 2007;292(3):1209–1224. doi:10.1152/AJPHEART.01047.2006
205. Obi S, Masuda H, Shizuno T, Sato A, Yamamoto K, Ando J, Abe Y, Asahara T. Fluid shear stress induces differentiation of circulating phenotype endothelial progenitor cells. https://doi.org/10.1152/ajpcell.00133.2012. 2012;303(6):595–606. doi:10.1152/AJPCELL.00133.2012
206. Gonzalez-Molina J, Zhang X, Borghesan M, Mendonça da Silva J, Awan M, Fuller B, Gavara N, Selden C. Extracellular fluid viscosity enhances liver cancer cell mechanosensing and migration. Biomaterials. 2018;177:113–124. doi:10.1016/J.BIOMATERIALS.2018.05.058
207. Barcelona-Estaje E, Oliva MAG, Cunniffe F, Rodrigo-Navarro A, Genever P, Dalby MJ, Roca-Cusachs P, Cantini M, Salmeron-Sanchez M. N-cadherin crosstalk with integrin weakens the molecular clutch in response to surface viscosity. Nature Communications 2024 15:1. 2024;15(1):8824-. doi:10.1038/s41467-024-53107-6
208. Cao C, Xu Z, Liu Y, Cheng B, Xu F, Cao C, Xu Z, Liu Y, Cheng B, Xu F. Enhancement effects of extracellular fluid viscosity and matrix stiffness on cancer cell mechanosensing. Acta Mechanica Sinica 2023 39:11. 2023;39(11):223238-. doi:10.1007/S10409-023-23238-X
209. Di X, Gao X, Peng L, Ai J, Jin X, Qi S, Li H, Wang K, Luo D. Cellular mechanotransduction in health and diseases: from molecular mechanism to therapeutic targets. Signal Transduction and Targeted Therapy 2023 8:1. 2023;8(1):282-. doi:10.1038/s41392-023-01501-9
210. Shattil SJ, Newman PJ. Integrins: Dynamic scaffolds for adhesion and signaling in platelets. Blood. 2004;104(6):1606–1615. doi:10.1182/BLOOD-2004-04-1257,
211. Law DA, DeGuzman FR, Heiser P, Ministri-Madrid K, Killeen N, Phillips DR. Integrin cytoplasmic tyrosine motif is required for outside-in αIIbβ3 signalling and platelet function. Nature. 1999;401(6755):808–811. doi:10.1038/44599,

212. Law DA, Nannizzi-Alaimo L, Ministri K, Hughes PE, Forsyth J, Turner M, Shattil SJ, Ginsberg MH, Tybulewicz VLJ, Phillips DR. Genetic and Pharmacological Analyses of Syk Function in αIIbβ3 Signaling in Platelets. Blood. 1999;93(8):2645–2652. doi:10.1182/BLOOD.V93.8.2645
213. Boylan B, Gao C, Rathore V, Gill JC, Newman DK, Newman PJ. Identification of FcγRIIa as the ITAM-bearing receptor mediating αIIbβ3 outside-in integrin signaling in human platelets. Blood. 2008;112(7):2780–2786. doi:10.1182/BLOOD-2008-02-142125
214. Durrant TN, Van Den Bosch MT, Hers I. Integrin αIIbβ3 outside-in signaling. Blood. 2017;130(14):1607–1619. doi:10.1182/BLOOD-2017-03-773614
215. Shattil SJ, Kim C, Ginsberg MH. The final steps of integrin activation: the end game. Nature Reviews Molecular Cell Biology 2010 11:4. 2010;11(4):288–300. doi:10.1038/nrm2871
216. Buensuceso C, Virgilio M de, Chemistry SS-J of B, 2003 undefined. Detection of integrin αIIbβ3clustering in living cells. ElsevierC Buensuceso, M de Virgilio, SJ ShattilJournal of Biological Chemistry, 2003•Elsevier.
217. Fong K, Zhu H, Span L, Moore D, … KY-J of B, 2016 undefined. Directly activating the integrin αIIbβ3 initiates outside-in signaling by causing αIIbβ3 clustering. ElsevierKP Fong, H Zhu, LM Span, DT Moore, K Yoon, R Tamura, H Yin, WF DeGrado, JS BennettJournal of Biological Chemistry, 2016•Elsevier.
218. Li R, Mitra N, Gratkowski H, Vilaire G, Litvinov R, Nagasami C, Weisel JW, Lear JD, DeGrado WF, Bennett JS. Activation of integrin αIIbβ3 by modulation of transmembrane helix associations. Science (1979). 2003;300(5620):795–798. doi:10.1126/SCIENCE.1079441/SUPPL_FILE/LI.SOM.PDF
219. Hato T, Pampori N, Shattil SJ. Complementary Roles for Receptor Clustering and Conformational Change in the Adhesive and Signaling Functions of Integrin αIIbβ3. Journal of Cell Biology. 1998;141(7):1685–1695. doi:10.1083/JCB.141.7.1685
220. Kanner SB, Grosmaire LS, Ledbetter JA, Damlet NK. Beta 2-integrin LFA-1 signaling through phospholipase C-gamma 1 activation. Proceedings of the National Academy of Sciences. 1993;90(15):7099–7103. doi:10.1073/PNAS.90.15.7099
221. Van Seventer GA, Bonvini E, Yamada H, Conti A, Stringfellow S, June CH, Shaw S. Costimulation of T cell receptor/CD3-mediated activation of resting human CD4+ T cells by leukocyte function-associated antigen-1 ligand intercellular cell adhesion molecule-1 involves prolonged inositol phospholipid hydrolysis and sustained increase of intracellular Ca2+ levels. J Immunol. 1992;149(12):3872–3880. doi:10.4049/jimmunol.149.12.3872

222. Ni H-T, Deeths MJ, Mescher MF. LFA-1-mediated costimulation of CD8+ T cell proliferation requires phosphatidylinositol 3-kinase activity. J Immunol. 2001;166(11):6523–6529. doi:10.4049/JIMMUNOL.166.11.6523
223. Baker RG, Hsu CJ, Lee D, Jordan MS, Maltzman JS, Hammer DA, Baumgart T, Koretzky GA. The Adapter Protein SLP-76 Mediates "Outside-In" Integrin Signaling and Function in T Cells. Mol Cell Biol. 2009;29(20):5578–5589. doi:10.1128/MCB.00283-09
224. Hogg N, Laschinger M, Giles K, McDowall A. T-cell integrins: more than just sticking points. J Cell Sci. 2003;116(23):4695–4705. doi:10.1242/JCS.00876
225. Dupuy AG, Caron E. Integrin-dependent phagocytosis – spreading from microadhesion to new concepts. J Cell Sci. 2008;121(11):1773–1783. doi:10.1242/JCS.018036
226. Wiedemann A, Patel JC, Lim J, Tsun A, Van Kooyk Y, Caron E. Two distinct cytoplasmic regions of the β2 integrin chain regulate RhoA function during phagocytosis. Journal of Cell Biology. 2006;172(7):1069–1076. doi:10.1083/JCB.200508075
227. Hari A, Zhang Y, Tu Z, Detampel P, Stenner M, Ganguly A, Shi Y. Activation of NLRP3 inflammasome by crystalline structures via cell surface contact. Sci Rep. 2014;4(1):1–8. doi:10.1038/SREP07281;TECHMETA
228. Van Kooyk Y, Van De Wiel-van Kemenade E, Weder P, Huijbens RJF, Figdor CG. Lymphocyte function-associated antigen 1 dominates very late antigen 4 in binding of activated T cells to endothelium. Journal of Experimental Medicine. 1993;177(1):185–190. doi:10.1084/JEM.177.1.185
229. Sosa-Costa A, De Val SI, Sevilla-Movilla S, Borgman KJE, Manzo C, Teixidó J, Garcia-Parajo MF. Lateral mobility and nanoscale spatial arrangement of chemokine-activated α4β1 integrins on T cells. Journal of Biological Chemistry. 2016;291(40):21053–21062. doi:10.1074/jbc.M116.733709
230. Yakubenko VP, Lobb RR, Plow EF, Ugarova TP. Differential Induction of Gelatinase B (MMP-9) and Gelatinase A (MMP-2) in T Lymphocytes upon α4β1-Mediated Adhesion to VCAM-1 and the CS-1 Peptide of Fibronectin. Exp Cell Res. 2000;260(1):73–84. doi:10.1006/EXCR.2000.5002
231. Segarra M, Vilardell C, Matsumoto K, Esparza J, Lozano E, Serra-Pages C, Urbano-Márquez A, Yamada KM, Cid MC. Dual function of focal adhesion kinase in regulating integrin-induced MMP-2 and MMP-9 release by human T lymphoid cells. FASEB Journal. 2005;19(13):1875–1877. doi:10.1096/FJ.04-3574FJE
232. Shulman Z, Shinder V, Klein E, Grabovsky V, Yeger O, Geron E, Montresor A, Bolomini-Vittori M, Feigelson SW, Kirchhausen T, et al. Lymphocyte Crawling and Transendothelial Migration

Require Chemokine Triggering of High-Affinity LFA-1 Integrin. Immunity. 2009;30(3):384–396. doi:10.1016/j.immuni.2008.12.020
233. Aoudjit F, Potworowski EF, St-Pierre Y. Bi-Directional Induction of Matrix Metalloproteinase-9 and Tissue Inhibitor of Matrix Metalloproteinase-1 During T Lymphoma/Endothelial Cell Contact: Implication of ICAM-1. The Journal of Immunology. 1998;160(6):2967–2973. doi:10.4049/JIMMUNOL.160.6.2967
234. Čemerski S, Shaw A. Immune synapses in T-cell activation. Curr Opin Immunol. 2006;18(3):298–304. doi:10.1016/J.COI.2006.03.011
235. Dustin ML, Baldari CT. The Immune Synapse: Past, Present, and Future. Methods in Molecular Biology. 2017;1584:1–5. doi:10.1007/978-1-4939-6881-7_1
236. Tseng S-Y, Liu M, Dustin ML. CD80 cytoplasmic domain controls localization of CD28, CTLA-4, and protein kinase Ctheta in the immunological synapse. J Immunol. 2005;175(12):7829–7836. doi:10.4049/JIMMUNOL.175.12.7829
237. Pentcheva-Hoang T, Egen JG, Wojnoonski K, Allison JP. B7-1 and B7-2 selectively recruit CTLA-4 and CD28 to the immunological synapse. Immunity. 2004;21(3):401–413. doi:10.1016/j.immuni.2004.06.017
238. Schneider H, Rudd CE. Diverse Mechanisms Regulate the Surface Expression of Immunotherapeutic Target CTLA-4. Front Immunol. 2014;5(DEC):619. doi:10.3389/FIMMU.2014.00619
239. Valk E, Rudd CE, Schneider H. CTLA-4 trafficking and surface expression. Trends Immunol. 2008;29(6):272–279. doi:10.1016/j.it.2008.02.011
240. Huang W, Lin W, Chen B, Zhang J, Gao P, Fan Y, Lin Y, Wei P. NFAT and NF-κB dynamically co-regulate TCR and CAR signaling responses in human T cells. Cell Rep. 2023;42(7). doi:10.1016/j.celrep.2023.112663
241. Rush-Kittle J, Gámez-Díaz L, Grimbacher B. Inborn errors of immunity associated with defects of self-tolerance checkpoints: The CD28 family. Pediatric Allergy and Immunology. 2022;33(12). doi:10.1111/PAI.13886
242. Huse M, Lillemeier BF, Kuhns MS, Chen DS, Davis MM. T cells use two directionally distinct pathways for cytokine secretion. Nat Immunol. 2006;7(3):247–255. doi:10.1038/NI1304;KWRD
243. Dustin ML, Groves JT. Receptor signaling clusters in the immune synapse. Annu Rev Biophys. 2012;41(1):543–556. doi:10.1146/ANNUREV-BIOPHYS-042910-155238/CITE/REFWORKS
244. Dustin ML. Insights into Function of the Immunological Synapse from Studies with Supported Planar Bilayers. Curr Top Microbiol Immunol. 2010;340(1):1–24. doi:10.1007/978-3-642-03858-7_1

245. Scharffetter-Kochanek K, Lu H, Norman K, Van Nood N, Munoz F, Grabbe S, McArthur M, Lorenzo I, Kaplan S, Ley K, et al. Spontaneous Skin Ulceration and Defective T Cell Function in CD18 Null Mice. Journal of Experimental Medicine. 1998;188(1):119–131. doi:10.1084/JEM.188.1.119
246. Mestas J, Hughes CCW. Of Mice and Not Men: Differences between Mouse and Human Immunology. The Journal of Immunology. 2004;172(5):2731–2738. doi:10.4049/JIMMUNOL.172.5.2731
247. Bouti P, Webbers SDS, Fagerholm SC, Alon R, Moser M, Matlung HL, Kuijpers TW. β2 Integrin Signaling Cascade in Neutrophils: More Than a Single Function. Front Immunol. 2021;11:619925. doi:10.3389/FIMMU.2020.619925/FULL
248. Cappenberg A, Kardell M, Zarbock A. Selectin-Mediated Signaling—Shedding Light on the Regulation of Integrin Activity in Neutrophils. Cells 2022, Vol. 11, Page 1310. 2022;11(8):1310. doi:10.3390/CELLS11081310
249. Schnoor M, Vadillo E, Guerrero-Fonseca IM. The extravasation cascade revisited from a neutrophil perspective. Curr Opin Physiol. 2021;19:119–128. doi:10.1016/J.COPHYS.2020.09.014
250. Uzel G, Kleiner DE, Kuhns DB, Holland SM. Dysfunctional LAD-1 neutrophils and colitis. Gastroenterology. 2001;121(4):958–964. doi:10.1053/GAST.2001.28022
251. Kuijpers TW, Van Bruggen R, Kamerbeek N, Tool ATJ, Hicsonmez G, Gurgey A, Karow A, Verhoeven AJ, Seeger K, Sanal Ö, et al. Natural history and early diagnosis of LAD-1/variant syndrome. Blood. 2007;109(8):3529–3537. doi:10.1182/BLOOD-2006-05-021402
252. Brinkmann V, Reichard U, Goosmann C, Fauler B, Uhlemann Y, Weiss DS, Weinrauch Y, Zychlinsky A. Neutrophil Extracellular Traps Kill Bacteria. Science (1979). 2004;303(5663):1532–1535. doi:10.1126/SCIENCE.1092385/SUPPL_FILE/1092385S2.MOV
253. Liew PX, Kubes P. The Neutrophil's Role During Health and Disease. https://doi.org/10.1152/physrev.00012.2018. 2019;99(2):1223–1248. doi:10.1152/PHYSREV.00012.2018
254. Gresham HD, Graham IL, Anderson DC, Brown EJ. Leukocyte adhesion-deficient neutrophils fail to amplify phagocytic function in response to stimulation. Evidence for CD11b/CD18-dependent and -independent mechanisms of phagocytosis. J Clin Invest. 1991;88(2):588–597. doi:10.1172/JCI115343
255. Steblyanko M, Anikeeva N, Campbell KS, Keen JH, Sykulev Y. Integrins Influence the Size and Dynamics of Signaling Microclusters in a Pyk2-dependent Manner. Journal of Biological Chemistry. 2015;290(19):11833–11842. doi:10.1074/JBC.M114.614719

256. Liu D, Bryceson YT, Meckel T, Vasiliver-Shamis G, Dustin ML, Long EO. Integrin-Dependent Organization and Bidirectional Vesicular Traffic at Cytotoxic Immune Synapses. Immunity. 2009;31(1):99–109. doi:10.1016/j.immuni.2009.05.009
257. Boras M, Volmering S, Bokemeyer A, Rossaint J, Block H, Bardel B, Van Marck V, Heitplatz B, Kliche S, Reinhold A, et al. Skap2 is required for β2 integrin-mediated neutrophil recruitment and functions. J Exp Med. 2017;214(3):851–874. doi:10.1084/JEM.20160647/VIDEO-4
258. Husemann J, Obstfeld A, Febbraio M, Kodama T, Silverstein SC. CD11b/CD18 mediates production of reactive oxygen species by mouse and human macrophages adherent to matrixes containing oxidized LDL. Arterioscler Thromb Vasc Biol. 2001;21(8):1301–1305. doi:10.1161/HQ0801.095150/ASSET/4A34677C-3F5C-4BF6-B206-01FB7CE49708/ASSETS/GRAPHIC/G1784F2.JPEG
259. Schetters STT, Gomez-Nicola D, Garcia-Vallejo JJ, Van Kooyk Y. Neuroinflammation: Microglia and T Cells Get Ready to Tango. Front Immunol. 2018;8(JAN):1905. doi:10.3389/FIMMU.2017.01905
260. Locati M, Curtale G, Mantovani A. Diversity, Mechanisms, and Significance of Macrophage Plasticity. Annual Review of Pathology: Mechanisms of Disease. 2020;15(Volume 15, 2020):123–147. doi:10.1146/ANNUREV-PATHMECHDIS-012418-012718/CITE/REFWORKS
261. Jeon YJ, Won HY, Moon MY, Choi WH, Chang CH, Lee JY, Kim J, Kim SC, Kim YS, Park JB. Interaction of microglia and amyloid-β through β2-integrin is regulated by RhoA. Neuroreport. 2008;19(17):1661–1665. doi:10.1097/WNR.0B013E3283140F10
262. Gilbert NG, Elaine MTC, Shi Y. Recent developments in immune activation by uric acid crystals. Arch Immunol Ther Exp (Warsz). 2010;58(4):273–277. doi:10.1007/S00005-010-0082-1/METRICS
263. Brose N, Rosemund C. Move over protein kinase C, you've got company: alternative cellular effectors of diacylglycerol and phorbol esters. J Cell Sci. 2002;115(23):4399–4411. doi:10.1242/JCS.00122
264. Herb M, Schramm M. Functions of ROS in Macrophages and Antimicrobial Immunity. Antioxidants 2021, Vol. 10, Page 313. 2021;10(2):313. doi:10.3390/ANTIOX10020313
265. Hatscher L, Amon L, Heger L, Dudziak D. Inflammasomes in dendritic cells: Friend or foe? Immunol Lett. 2021;234:16–32. doi:10.1016/J.IMLET.2021.04.002
266. Paik S, Kim JK, Silwal P, Sasakawa C, Jo EK. An update on the regulatory mechanisms of NLRP3 inflammasome activation. Cell Mol Immunol. 2021;18(5):1141–1160. doi:10.1038/S41423-021-00670-3;SUBJMETA=2177,250,254,256,38,631;KWRD=AUTOIMMUNITY,INFECTION,INFLAMMASOME

267. Gupta N, Sahu A, Prabhakar A, Chatterjee T, Tyagi T, Kumari B, Khan N, Nair V, Bajaj N, Sharma M, et al. Activation of NLRP3 inflammasome complex potentiates venous thrombosis in response to hypoxia. Proc Natl Acad Sci U S A. 2017;114(18):4763–4768. doi:10.1073/PNAS.1620458114/SUPPL_FILE/PNAS.1620458114.SD01.PDF
268. Ma Q, Lim CS. Molecular Activation of NLRP3 Inflammasome by Particles and Crystals: A Continuing Challenge of Immunology and Toxicology. Annu Rev Pharmacol Toxicol. 2024;64(Volume 64, 2024):417–433. doi:10.1146/ANNUREV-PHARMTOX-031023-125300/CITE/REFWORKS
269. Jung ES, Suh K, Han J, Kim H, Kang HS, Choi WS, Mook-Jung I. Amyloid-β activates NLRP3 inflammasomes by affecting microglial immunometabolism through the Syk-AMPK pathway. Aging Cell. 2022;21(5). doi:10.1111/ACEL.13623,
270. Tannahill GM, Curtis AM, Adamik J, Palsson-Mcdermott EM, McGettrick AF, Goel G, Frezza C, Bernard NJ, Kelly B, Foley NH, et al. Succinate is an inflammatory signal that induces IL-1β through HIF-1α. Nature. 2013;496(7444):238–242. doi:10.1038/NATURE11986;SUBJMETA
271. Krawczyk CM, Holowka T, Sun J, Blagih J, Amiel E, DeBerardinis RJ, Cross JR, Jung E, Thompson CB, Jones RG, et al. Toll-like receptor-induced changes in glycolytic metabolism regulate dendritic cell activation. Blood. 2010;115(23):4742–4749. doi:10.1182/blood-2009-10-249540
272. Zhang Y, Liu W, Zhong Y, Li Q, Wu M, Yang L, Liu X, Zou L. Metformin Corrects Glucose Metabolism Reprogramming and NLRP3 Inflammasome-Induced Pyroptosis via Inhibiting the TLR4/NF-κB/PFKFB3 Signaling in Trophoblasts: Implication for a Potential Therapy of Preeclampsia. Oxid Med Cell Longev. 2021;2021(1):1806344. doi:10.1155/2021/1806344
273. Kanayama M, Morimoto J, Matsui Y, Ikesue M, Danzaki K, Kurotaki D, Ito K, Yoshida T, Uede T. α9β1 integrin-mediated signaling serves as an intrinsic regulator of pathogenic Th17 cell generation. J Immunol. 2011;187(11):5851–5864. doi:10.4049/JIMMUNOL.1101524
274. Zheng C, Chen J, Chu F, Zhu J, Jin T. Inflammatory Role of TLR-MyD88 Signaling in Multiple Sclerosis. Front Mol Neurosci. 2020;12:508409. doi:10.3389/FNMOL.2019.00314/FULL
275. Alhamdan F, Bayarsaikhan G, Yuki K. Toll-like receptors and integrins crosstalk. Front Immunol. 2024;15:1403764. doi:10.3389/FIMMU.2024.1403764
276. Cui Y, Rolova T, Fagerholm SC. The role of integrins in brain health and neurodegenerative diseases. Eur J Cell Biol. 2024;103(3). doi:10.1016/j.ejcb.2024.151441
277. Ling GS, Bennett J, Woollard KJ, Szajna M, Fossati-Jimack L, Taylor PR, Scott D, Franzoso G, Cook HT, Botto M. Integrin CD11b positively regulates TLR4-induced signalling pathways in

dendritic cells but not in macrophages. Nature Communications 2014 5:1. 2014;5(1):1–12. doi:10.1038/ncomms4039
278. Murray PJ, Allen JE, Biswas SK, Fisher EA, Gilroy DW, Goerdt S, Gordon S, Hamilton JA, Ivashkiv LB, Lawrence T, et al. Macrophage Activation and Polarization: Nomenclature and Experimental Guidelines. Immunity. 2014;41(1):14–20. doi:10.1016/J.IMMUNI.2014.06.008
279. Yunna C, Mengru H, Lei W, Weidong C. Macrophage M1/M2 polarization. Eur J Pharmacol. 2020;877:173090. doi:10.1016/J.EJPHAR.2020.173090
280. Ginhoux F, Lim S, Hoeffel G, Low D, Huber T. Origin and differentiation of microglia. Front Cell Neurosci. 2013;7(MAR):46040. doi:10.3389/FNCEL.2013.00045/FULL
281. Kierdorf K, Erny D, Goldmann T, Sander V, Schulz C, Perdiguero EG, Wieghofer P, Heinrich A, Riemke P, Hölscher C, et al. Microglia emerge from erythromyeloid precursors via Pu.1- and Irf8-dependent pathways. Nature Neuroscience 2013 16:3. 2013;16(3):273–280. doi:10.1038/nn.3318
282. Chitu V, Gokhan Ş, Nandi S, Mehler MF, Stanley ER. Emerging Roles for CSF-1 Receptor and its Ligands in the Nervous System. Trends Neurosci. 2016;39(6):378–393. doi:10.1016/j.tins.2016.03.005
283. Paolicelli RC, Sierra A, Stevens B, Tremblay ME, Aguzzi A, Ajami B, Amit I, Audinat E, Bechmann I, Bennett M, et al. Microglia states and nomenclature: A field at its crossroads. Neuron. 2022;110(21):3458–3483. doi:10.1016/J.NEURON.2022.10.020
284. Paolicelli RC, Sierra A, Stevens B, Tremblay ME, Aguzzi A, Ajami B, Amit I, Audinat E, Bechmann I, Bennett M, et al. Microglia states and nomenclature: A field at its crossroads. Neuron. 2022;110(21):3458–3483. doi:10.1016/J.NEURON.2022.10.020
285. Srinivasan K, Friedman BA, Etxeberria A, Huntley MA, van der Brug MP, Foreman O, Paw JS, Modrusan Z, Beach TG, Serrano GE, et al. Alzheimer's Patient Microglia Exhibit Enhanced Aging and Unique Transcriptional Activation. Cell Rep. 2020;31(13). doi:10.1016/j.celrep.2020.107843
286. Qin C, Zhou LQ, Ma XT, Hu ZW, Yang S, Chen M, Bosco DB, Wu LJ, Tian DS. Dual Functions of Microglia in Ischemic Stroke. Neuroscience Bulletin 2019 35:5. 2019;35(5):921–933. doi:10.1007/S12264-019-00388-3
287. Planas AM. Role of microglia in stroke. Glia. 2024;72(6):1016–1053. doi:10.1002/GLIA.24501;REQUESTEDJOURNAL:JOURNAL:10981136;PAGE:STRING:ARTICLE/CHAPTER
288. Ekdahl CT, Kokaia Z, Lindvall O. Brain inflammation and adult neurogenesis: The dual role of microglia. Neuroscience. 2009;158(3):1021–1029. doi:10.1016/j.neuroscience.2008.06.052
289. Graeber MB, Streit WJ. Microglia: biology and pathology. Acta Neuropathologica 2009 119:1. 2009;119(1):89–105. doi:10.1007/S00401-009-0622-0

290. Yu F, Huang T, Ran Y, Li D, Ye L, Tian G, Xi J, Liu Z. New Insights Into the Roles of Microglial Regulation in Brain Plasticity-Dependent Stroke Recovery. Front Cell Neurosci. 2021;15:727899. doi:10.3389/FNCEL.2021.727899/FULL
291. Walton NM, Sutter BM, Laywell ED, Levkoff LH, Kearns SM, Marshall GP, Scheffler B, Steindler DA. Microglia instruct subventricular zone neurogenesis. Glia. 2006;54(8):815–825. doi:10.1002/GLIA.20419;JOURNAL:JOURNAL:10981136;ISSUE:ISSUE:DOI
292. Jiménez-Cortegana C, Palomares F, Alba G, Santa-María C, de la Cruz-Merino L, Sánchez-Margalet V, López-Enríquez S. Dendritic cells: the yin and yang in disease progression. Front Immunol. 2023;14:1321051. doi:10.3389/FIMMU.2023.1321051/FULL
293. Eisenbarth SC. Dendritic cell subsets in T cell programming: location dictates function. Nat Rev Immunol. 2019;19(2):89–103. doi:10.1038/S41577-018-0088-1;SUBJMETA
294. Musumeci A, Lutz K, Winheim E, Krug AB. What Makes a pDC: Recent Advances in Understanding Plasmacytoid DC Development and Heterogeneity. Front Immunol. 2019;10(MAY):1222. doi:10.3389/FIMMU.2019.01222
295. Swiecki M, Colonna M. The multifaceted biology of plasmacytoid dendritic cells. Nat Rev Immunol. 2015;15(8):471–485. doi:10.1038/NRI3865;SUBJMETA
296. Backer RA, Probst HC, Clausen BE. Classical DC2 subsets and monocyte-derived DC: Delineating the developmental and functional relationship. Eur J Immunol. 2023;53(3):2149548. doi:10.1002/EJI.202149548;ISSUE:ISSUE:DOI
297. Mildner A, Yona S, Jung S. A close encounter of the third kind: monocyte-derived cells. Adv Immunol. 2013;120:69–103. doi:10.1016/B978-0-12-417028-5.00003-X
298. Serbina N V., Salazar-Mather TP, Biron CA, Kuziel WA, Pamer EG. TNF/iNOS-producing dendritic cells mediate innate immune defense against bacterial infection. Immunity. 2003;19(1):59–70. doi:10.1016/S1074-7613(03)00171-7
299. Helft J, Böttcher J, Chakravarty P, Zelenay S, Huotari J, Schraml BU, Goubau D, Reis e Sousa C. GM-CSF Mouse Bone Marrow Cultures Comprise a Heterogeneous Population of CD11c+MHCII+ Macrophages and Dendritic Cells. Immunity. 2015;42(6):1197–1211. doi:10.1016/j.immuni.2015.05.018
300. Kuokkanen E, Šuštar V, Mattila PK. Molecular control of B cell activation and immunological synapse formation. Traffic. 2015;16(4):311–326. doi:10.1111/TRA.12257
301. Ma S, Ming Y, Wu J, Cui G. Cellular metabolism regulates the differentiation and function of T-cell subsets. Cell Mol Immunol. 2024;21(5):419–435. doi:10.1038/S41423-024-01148-8
302. Wilfahrt D, Delgoffe GM. Metabolic waypoints during T cell differentiation. Nat Immunol. 2024;25(2):206–217. doi:10.1038/S41590-023-01733-5

303. Shi Y, Zhang H, Miao C. Metabolic reprogram and T cell differentiation in inflammation: current evidence and future perspectives. Cell Death Discov. 2025;11(1):1–12. doi:10.1038/S41420-025-02403-1;SUBJMETA
304. Ma XM, Blenis J. Molecular mechanisms of mTOR-mediated translational control. Nat. Rev. Mol. Cell Biol. 2009;10(5):307–318. doi:10.1038/nrm2672
305. He L, Cho S, Blenis J. mTORC1, the maestro of cell metabolism and growth. Genes Dev. 2025;39(1–2):109–131. doi:10.1101/GAD.352084.124
306. Delgoffe GM, Kole TP, Zheng Y, Zarek PE, Matthews KL, Xiao B, Worley PF, Kozma SC, Powell JD. The mTOR Kinase Differentially Regulates Effector and Regulatory T Cell Lineage Commitment. Immunity. 2009;30(6):832–844. doi:10.1016/j.immuni.2009.04.014
307. Chi H. Regulation and function of mTOR signalling in T cell fate decisions. Nature Reviews Immunology 2012 12:5. 2012;12(5):325–338. doi:10.1038/nri3198
308. Martin-Cofreces NB, Valpuesta JM, Sánchez-Madrid F. T cell asymmetry and metabolic crosstalk can fine-tune immunological synapses. Trends Immunol. 2021;42(8):649–653. doi:10.1016/j.it.2021.06.007
309. Sun L, Yang X, Yuan Z, Wang H. Metabolic Reprogramming in Immune Response and Tissue Inflammation. Arterioscler Thromb Vasc Biol. 2020;40(9):1990–2001. doi:10.1161/ATVBAHA.120.314037;ISSUE:ISSUE:DOI
310. He Z, Zhu X, Shi Z, Wu T, Wu L. Metabolic regulation of dendritic cell differentiation. Front Immunol. 2019;10(MAR):425127. doi:10.3389/FIMMU.2019.00410/REFERENCE
311. Wculek SK, Khouili SC, Priego E, Heras-Murillo I, Sancho D. Metabolic Control of Dendritic Cell Functions: Digesting Information. Front Immunol. 2019;10:775. doi:10.3389/FIMMU.2019.00775/BIBTEX
312. Møller SH, Wang L, Ho PC. Metabolic programming in dendritic cells tailors immune responses and homeostasis. Cell Mol Immunol. 2022;19(3):370–383. doi:10.1038/S41423-021-00753-1;SUBJMETA
313. Ballesteros-Álvarez J, Andersen JK. mTORC2: The other mTOR in autophagy regulation. Aging Cell. 2021;20(8):e13431. doi:10.1111/ACEL.13431
314. Amiel E, Everts B, Freitas TC, King IL, Curtis JD, Pearce EL, Pearce EJ. Inhibition of mTOR promotes dendritic cell activation and enhances therapeutic autologous vaccination in mice. J Immunol. 2012;189(5):2151. doi:10.4049/JIMMUNOL.1103741
315. Dibble CC, Asara JM, Manning BD. Characterization of Rictor Phosphorylation Sites Reveals Direct Regulation of mTOR Complex 2 by S6K1. Mol Cell Biol. 2009;29(21):5657. doi:10.1128/MCB.00735-09

316. Bahrambeigi S, Shafiei-Irannejad V. Immune-mediated anti-tumor effects of metformin; targeting metabolic reprogramming of T cells as a new possible mechanism for anti-cancer effects of metformin. Biochem Pharmacol. 2020;174:113787. doi:10.1016/J.BCP.2019.113787
317. Jia J, Cheng J, Ni J, Zhen X. Neuropharmacological Actions of Metformin in Stroke. Curr Neuropharmacol. 2015;13(3):389–394. doi:10.2174/1570159X13666150205143555/CITE/REFWORKS
318. Liu X, Yu P, Xu Y, Wang Y, Chen J, Tang F, Hu Z, Zhou J, Liu L, Qiu W, et al. Metformin induces tolerogenicity of dendritic cells by promoting metabolic reprogramming. Cellular and Molecular Life Sciences. 2023;80(10):1–19. doi:10.1007/S00018-023-04932-3/FIGURES/7
319. van Eijck CWF, Vadgama D, van Eijck CHJ, Wilmink JW, (DPCG) for the DPCG, Lips DJ, van der Harst E, Kazemier G, Patijn GA, de Hingh IH, et al. Metformin boosts antitumor immunity and improves prognosis in upfront resected pancreatic cancer: an observational study. JNCI: Journal of the National Cancer Institute. 2024;116(8):1374–1383. doi:10.1093/JNCI/DJAE070
320. Qing L, Fu J, Wu P, Zhou Z, Yu F, Tang J. Metformin induces the M2 macrophage polarization to accelerate the wound healing via regulating AMPK/mTOR/NLRP3 inflammasome singling pathway. Am J Transl Res. 2019;11(2):655.
321. Longo VD, Mattson MP. Fasting: Molecular Mechanisms and Clinical Applications. Cell Metab. 2014;19(2):181–192. doi:10.1016/J.CMET.2013.12.008
322. Abedi V, Farahani SS, Bragazzi NL, Adawi M, Watad A, Brown S, Aazza K, Aazza H, Zouhir M, Sharif K, et al. Ramadan Fasting exerts immunomodulatory effects: insights from a Systematic Review. Ramadan Fasting Exerts Immunomodulatory Effects: Insights from a Systematic Review. Front. Immunol. 2017;8:1144. doi:10.3389/fimmu.2017.01144
323. Tiwari S, Sapkota N, Han Z. Effect of fasting on cancer: A narrative review of scientific evidence. Cancer Sci. 2022;113(10):3291–3302. doi:10.1111/CAS.15492
324. Islam MA, Khandker SS, Kotyla PJ, Hassan R. Immunomodulatory Effects of Diet and Nutrients in Systemic Lupus Erythematosus (SLE): A Systematic Review. Front Immunol. 2020;11:480790. doi:10.3389/FIMMU.2020.01477/FULL
325. Verduci E, Köglmeier J. Immunomodulation in Children: The Role of the Diet. J Pediatr Gastroenterol Nutr. 2021;73(3):293–298. doi:10.1097/MPG.0000000000003152;SUBPAGE:STRING:FULL
326. West CE, D'Vaz N, Prescott SL. Dietary immunomodulatory factors in the development of immune tolerance. Curr Allergy Asthma Rep. 2011;11(4):325–333. doi:10.1007/S11882-011-0200-0/FIGURES/1

327. Lawrence MB, Springer TA. Leukocytes roll on a selectin at physiologic flow rates: Distinction from and prerequisite for adhesion through integrins. Cell. 1991;65(5):859–873. doi:10.1016/0092-8674(91)90393-D
328. McEver RP. Selectins: lectins that initiate cell adhesion under flow. Curr Opin Cell Biol. 2002;14(5):581–586. doi:10.1016/S0955-0674(02)00367-8
329. Dewitt S, Hallett M. Leukocyte membrane "expansion": a central mechanism for leukocyte extravasation. J Leukoc Biol. 2007;81(5):1160–1164. doi:10.1189/JLB.1106710
330. Phillips ML, Schwartz BR, Etzioni A, Bayer R, Ochs HD, Paulson JC, Harlan JM. Neutrophil adhesion in leukocyte adhesion deficiency syndrome type 2. Journal of Clinical Investigation. 1995;96(6):2898. doi:10.1172/JCI118361
331. Abram CL, Lowell CA. The ins and outs of leukocyte integrin signaling. Annu Rev Immunol. 2009;27(Volume 27, 2009):339–362. doi:10.1146/ANNUREV.IMMUNOL.021908.132554/CITE/REFWORKS
332. Alon R, Etzioni A. LAD-III, a novel group of leukocyte integrin activation deficiencies. Trends Immunol. 2003;24(10):561–566. doi:10.1016/J.IT.2003.08.001
333. Rutledge NS, Muller WA. Understanding Molecules that Mediate Leukocyte Extravasation. Curr Pathobiol Rep. 2020;8(2):25–35. doi:10.1007/S40139-020-00207-9/TABLES/2
334. Middleton J, Patterson AM, Gardner L, Schmutz C, Ashton BA. Leukocyte extravasation: chemokine transport and presentation by the endothelium. Blood. 2002;100(12):3853–3860. doi:10.1182/BLOOD.V100.12.3853
335. Schnoor M, Alcaide P, Voisin MB, Van Buul JD. Crossing the Vascular Wall: Common and Unique Mechanisms Exploited by Different Leukocyte Subsets during Extravasation. Mediators Inflamm. 2015;2015:946509. doi:10.1155/2015/946509
336. Schmidt S, Moser M, Sperandio M. The molecular basis of leukocyte recruitment and its deficiencies. Mol Immunol. 2013;55(1):49–58. doi:10.1016/J.MOLIMM.2012.11.006
337. Kuijpers TW, Van Lier RAW, Hamann D, De Boer M, Thung LY, Weening RS, Verhoeven AJ, Roos D. Leukocyte adhesion deficiency type 1 (LAD-1)/variant. A novel immunodeficiency syndrome characterized by dysfunctional β2 integrins. Journal of Clinical Investigation. 1997;100(7):1725–1733. doi:10.1172/JCI119697
338. Nourshargh S, Renshaw SA, Imhof BA. Reverse Migration of Neutrophils: Where, When, How, and Why? Trends Immunol. 2016;37(5):273–286. doi:10.1016/j.it.2016.03.006
339. Muller WA. Mechanisms of leukocyte transendothelial migration. Annual Review of Pathology: Mechanisms of Disease. 2011;6(Volume 6, 2011):323–344. doi:10.1146/ANNUREV-PATHOL-011110-130224/CITE/REFWORKS

340. Majno G, Palade GE. STUDIES ON INFLAMMATION I. The Effect of Histamine and Serotonin on Vascular Permeability: An Electron Microscopic Study. J Biophys Biochem Cytol. 1961;11(3):571–605. doi:10.1083/JCB.11.3.571
341. Nan W, He Y, Wang S, Zhang Y. Molecular mechanism of VE-cadherin in regulating endothelial cell behaviour during angiogenesis. Front Physiol. 2023;14:1234104. doi:10.3389/FPHYS.2023.1234104/BIBTEX
342. Muller WA. Transendothelial migration: unifying principles from the endothelial perspective. Immunol Rev. 2016;273(1):61–75. doi:10.1111/IMR.12443
343. Sage PT, Carman C V. Settings and mechanisms for trans-cellular diapedesis. Front Biosci. 2009;14(13):5066. doi:10.2741/3587
344. Evans E, Leung A, Zhelev D. Synchrony of cell spreading and contraction force as phagocytes engulf large pathogens. Journal of Cell Biology. 1993;122(6):1295–1300. doi:10.1083/JCB.122.6.1295
345. Herant M, Heinrich V, Dembo M. Mechanics of neutrophil phagocytosis: behavior of the cortical tension. J Cell Sci. 2005;118(9):1789–1797. doi:10.1242/JCS.02275
346. Herant M, Heinrich V, Dembo M. Mechanics of neutrophil phagocytosis: experiments and quantitative models. J Cell Sci. 2006;119(9):1903–1913. doi:10.1242/JCS.02876
347. Erlandsen SL, Hasslen SR, Nelson RD. Detection and spatial distribution of the β2 integrin (Mac-1) and L- selectin (LECAM-1) adherence receptors on human neutrophils by high- resolution field emission SEM. Journal of Histochemistry and Cytochemistry. 1993;41(3):327–333. doi:10.1177/41.3.7679125;WEBSITE:WEBSITE:SAGE;WGROUP:STRING:PUBLICATION
348. Jung Y, Riven I, Feigelson SW, Kartvelishvily E, Tohya K, Miyasaka M, Alon R, Haran G. Three-dimensional localization of T-cell receptors in relation to microvilli using a combination of superresolution microscopies. Proc Natl Acad Sci U S A. 2016;113(40):E5916–E5924. doi:10.1073/PNAS.1605399113;SUBPAGE:STRING:FULL
349. Hanna S, Etzioni A. Leukocyte adhesion deficiencies. Ann N Y Acad Sci. 2012;1250(1):50–55. doi:10.1111/J.1749-6632.2011.06389.X
350. Leukocyte Adhesion Deficiency Treatment & Management: Approach Considerations, Medical Care, Surgical Care. [accessed September 12, 2025]. https://emedicine.medscape.com/article/887236-treatment?form=fpf
351. Almarza Novoa E, Kasbekar S, Thrasher AJ, Kohn DB, Sevilla J, Nguyen T, Schwartz JD, Bueren JA. Leukocyte adhesion deficiency-I: A comprehensive review of all published cases. J Allergy Clin Immunol Pract. 2018;6(4):1418-1420.e10. doi:10.1016/J.JAIP.2017.12.008

352. Schmidt S, Moser M, Sperandio M. The molecular basis of leukocyte recruitment and its deficiencies. Mol Immunol. 2013;55(1):49–58. doi:10.1016/J.MOLIMM.2012.11.006
353. Ehirchiou D, Xiong Y, Xu G, Chen W, Shi Y, Zhang L. CD11b facilitates the development of peripheral tolerance by suppressing Th17 differentiation. J Exp Med. 2007;204(7):1519–1524. doi:10.1084/jem.20062292
354. Moutsopoulos NM, Konkel J, Sarmadi M, Eskan MA, Wild T, Dutzan N, Abusleme L, Zenobia C, Hosur KB, Abe T, et al. Defective Neutrophil Recruitment in Leukocyte Adhesion Deficiency Type I Disease Causes Local IL-17-driven Inflammatory Bone Loss. Sci Transl Med. 2014;6(229):229ra40. doi:10.1126/SCITRANSLMED.3007696
355. Moutsopoulos NM, Konkel J, Sarmadi M, Eskan MA, Wild T, Dutzan N, Abusleme L, Zenobia C, Hosur KB, Abe T, et al. Defective neutrophil recruitment in leukocyte adhesion deficiency type I disease causes local IL-17-driven inflammatory bone loss. Sci Transl Med. 2014;6(229). doi:10.1126/SCITRANSLMED.3007696/SUPPL_FILE/6-229RA40_SM.PDF
356. Scharffetter-Kochanek K, Lu H, Norman K, Van Nood N, Munoz F, Grabbe S, McArthur M, Lorenzo I, Kaplan S, Ley K, et al. Spontaneous Skin Ulceration and Defective T Cell Function in CD18 Null Mice. Journal of Experimental Medicine. 1998;188(1):119–131. doi:10.1084/JEM.188.1.119
357. Geroldinger-Simić M, Lehner K, Klein G, Sepp N, Jabkowski J. An adult with severe leukocyte adhesion deficiency type 1. JAAD Case Rep. 2022;19:1–3. doi:10.1016/J.JDCR.2021.10.031
358. Yakubenia S, Wild MK. Leukocyte adhesion deficiency II. FEBS J. 2006;273(19):4390–4398. doi:10.1111/J.1742-4658.2006.05438.X
359. Marquardt T, Lühn K, Srikrishna G, Freeze HH, Harms E, Vestweber D. Correction of Leukocyte Adhesion Deficiency Type II With Oral Fucose. Blood. 1999;94(12):3976–3985. doi:10.1182/BLOOD.V94.12.3976
360. Yakubenia S, Wild MK. Leukocyte adhesion deficiency II. FEBS J. 2006;273(19):4390–4398. doi:10.1111/J.1742-4658.2006.05438.X
361. Tahata S, Raymond K, Quade M, Barnes S, Boyer S, League S, Kumanovics A, Abraham R, Jacob E, Menon P, et al. Defining the mild variant of leukocyte adhesion deficiency type II (SLC35C1-congenital disorder of glycosylation) and response to l-fucose therapy: Insights from two new families and review of the literature. Am J Med Genet A. 2022;188(7):2005–2018. doi:10.1002/AJMG.A.62737
362. Moser M, Nieswandt B, Ussar S, Pozgajova M, Fässler R. Kindlin-3 is essential for integrin activation and platelet aggregation. Nature Medicine 2008 14:3. 2008;14(3):325–330. doi:10.1038/nm1722

363. Bergmeier W, Goerge T, Wang HW, Crittenden JR, Baldwin ACW, Cifuni SM, Housman DE, Graybiel AM, Wagner DD. Mice lacking the signaling molecule CalDAG-GEFI represent a model for leukocyte adhesion deficiency type III. J Clin Invest. 2007;117(6):1699–1707. doi:10.1172/JCI30575
364. Kilic SS, Etzioni A. The clinical spectrum of leukocyte adhesion deficiency (LAD) III due to defective CalDAG-GEF1. J Clin Immunol. 2009;29(1):117–122. doi:10.1007/S10875-008-9226-Z/TABLES/2
365. Hanna S, Etzioni A. Leukocyte adhesion deficiencies. Ann N Y Acad Sci. 2012;1250(1):50–55. doi:10.1111/J.1749-6632.2011.06389.X
366. Alon R, Etzioni A. LAD-III, a novel group of leukocyte integrin activation deficiencies. Trends Immunol. 2003;24(10):561–566. doi:10.1016/J.IT.2003.08.001
367. MELLER J, MALININ NL, PANIGRAHI S, KERR BA, PATIL A, MA Y, VENKATESWARAN L, ROGOZIN IB, MOHANDAS N, EHLAYEL MS, et al. Novel aspects of Kindlin-3 function in humans based on a new case of leukocyte adhesion deficiency III. Journal of Thrombosis and Haemostasis. 2012;10(7):1397–1408. doi:10.1111/J.1538-7836.2012.04768.X'))
368. Klapproth S, Moretti FA, Zeiler M, Ruppert R, Breithaupt U, Mueller S, Haas R, Mann M, Sperandio M, Fässler R, et al. Minimal amounts of kindlin-3 suffice for basal platelet and leukocyte functions in mice. Blood. 2015;126(24):2592–2600. doi:10.1182/BLOOD-2015-04-639310
369. Moser M, Nieswandt B, Ussar S, Pozgajova M, Fässler R. Kindlin-3 is essential for integrin activation and platelet aggregation. Nature Medicine 2008 14:3. 2008;14(3):325–330. doi:10.1038/nm1722
370. Xu Z, Chen X, Zhi H, Gao J, Bialkowska K, Byzova T V., Pluskota E, White GC, Liu J, Plow EF, et al. Direct interaction of kindlin-3 with integrin αiibβ3 in platelets is required for supporting arterial thrombosis in mice. Arterioscler Thromb Vasc Biol. 2014;34(9):1961–1967. doi:10.1161/ATVBAHA.114.303851/-/DC1
371. Klapproth S, Moretti FA, Zeiler M, Ruppert R, Breithaupt U, Mueller S, Haas R, Mann M, Sperandio M, Fässler R, et al. Minimal amounts of kindlin-3 suffice for basal platelet and leukocyte functions in mice. Blood. 2015;126(24):2592–2600. doi:10.1182/BLOOD-2015-04-639310
372. Thomas C, Le Deist F, Cavazzana-Calvo M, Benkerrou M, Haddad E, Blanche S, Hartmann W, Friedrich W, Fischer A. Results of Allogeneic Bone Marrow Transplantation in Patients With Leukocyte Adhesion Deficiency. Blood. 1995;86(4):1629–1635. doi:10.1182/BLOOD.V86.4.1629.BLOODJOURNAL8641629

373. Jabado N, Le Deist F, Cant A, De Graeff-Meeders ER, Fasth A, Morgan G, Vellodi A, Hale G, Bujan W, Thomas C, et al. Bone marrow transplantation from genetically HLA-nonidentical donors in children with fatal inherited disorders excluding severe combined immunodeficiencies: Use of two monoclonal antibodies to prevent graft rejection. Pediatrics. 1996;98(3):420–428. doi:10.1542/peds.98.3.420
374. Saultier P, Szepetowski S, Canault M, Falaise C, Poggi M, Suchon P, Barlogis V, Michel G, Loyau S, Jandrot-Perrus M, et al. Long-term management of leukocyte adhesion deficiency type III without hematopoietic stem cell transplantation. Haematologica. 2018;103(6):e264–e267. doi:10.3324/HAEMATOL.2017.186304
375. Stepensky PY, Wolach B, Gavrieli R, Rousso S, Ami T Ben, Goldman V, Rozovsky K, Hanna S, Etzioni A, Weintraub M. Leukocyte Adhesion Deficiency Type III: Clinical Features and Treatment with Stem Cell Transplantation. J Pediatr Hematol Oncol. 2015;37(4):264–268. doi:10.1097/MPH.0000000000000228
376. Morrison VL, MacPherson M, Savinko T, Lek HS, Prescott A, Fagerholm SC. The β2 integrin–kindlin-3 interaction is essential for T-cell homing but dispensable for T-cell activation in vivo. Blood. 2013;122(8):1428–1436. doi:10.1182/BLOOD-2013-02-484998
377. Morrison VL, James MJ, Grzes K, Cook P, Glass DG, Savinko T, Lek HS, Gawden-Bone C, Watts C, Millington OR, et al. Loss of beta2-integrin-mediated cytoskeletal linkage reprogrammes dendritic cells to a mature migratory phenotype. Nat Commun. 2014;5:5359. doi:10.1038/ncomms6359
378. Guenther C, Faisal I, Fusciello M, Sokolova M, Harjunpää H, Ilander M, Tallberg R, Vartiainen MK, Alon R, Gonzalez-Granado JM, et al. β2-integrin adhesion regulates dendritic cell epigenetic and transcriptional landscapes to restrict dendritic cell maturation and tumor rejection. Cancer Immunol Res. 2021;9(11):1354–1369. doi:10.1158/2326-6066.CIR-21-0094
379. Schmidt CA, Fisher-Wellman KH, Darrell Neufer P. From OCR and ECAR to energy: Perspectives on the design and interpretation of bioenergetics studies. Journal of Biological Chemistry. 2021;297(4):101140. doi:10.1016/J.JBC.2021.101140
380. Zhang J, Zhang Q. Using seahorse machine to measure OCR and ECAR in cancer cells. Methods in Molecular Biology. 2019;1928:353–363. doi:10.1007/978-1-4939-9027-6_18/FIGURES/5
381. Argüello RJ, Combes AJ, Char R, Gigan JP, Baaziz AI, Bousiquot E, Camosseto V, Samad B, Tsui J, Yan P, et al. SCENITH: A Flow Cytometry-Based Method to Functionally Profile Energy Metabolism with Single-Cell Resolution. Cell Metab. 2020;32(6):1063-1075.e7. doi:10.1016/J.CMET.2020.11.007

382. Møller SH, Wang L, Ho PC. Metabolic programming in dendritic cells tailors immune responses and homeostasis. Cellular & Molecular Immunology 2021 19:3. 2021;19(3):370–383. doi:10.1038/s41423-021-00753-1
383. Hindupur SK, González A, Hall MN. The Opposing Actions of Target of Rapamycin and AMP-Activated Protein Kinase in Cell Growth Control. Cold Spring Harb Perspect Biol. 2015;7(8):a019141. doi:10.1101/CSHPERSPECT.A019141
384. Pezze PD, Ruf S, Sonntag AG, Langelaar-Makkinje M, Hall P, Heberle AM, Navas PR, Van Eunen K, Tölle RC, Schwarz JJ, et al. A systems study reveals concurrent activation of AMPK and mTOR by amino acids. Nat Commun. 2016;7(1):1–19. doi:10.1038/NCOMMS13254;TECHMETA
385. Oh K-S, Gottschalk RA, Lounsbury NW, Sun J, Dorrington MG, Baek S, Sun G, Wang Z, Krauss KS, Milner JD, et al. Dual Roles for Ikaros in Regulation of Macrophage Chromatin State and Inflammatory Gene Expression. J Immunol. 2018;201(2):757–771. doi:10.4049/jimmunol.1800158
386. Joshi I, Yoshida T, Jena N, Qi X, Zhang J, Van Etten RA, Georgopoulos K. Loss of Ikaros DNA-binding function confers integrin-dependent survival on pre-B cells and progression to acute lymphoblastic leukemia. Nat Immunol. 2014;15(3):294–304. doi:10.1038/ni.2821
387. Cytlak U, Resteu A, Bogaert D, Kuehn HS, Altmann T, Gennery A, Jackson G, Kumanovics A, Voelkerding K V, Prader S, et al. Ikaros family zinc finger 1 regulates dendritic cell development and function in humans. Nat Commun. 2018;9(1):1239. doi:10.1038/s41467-018-02977-8
388. Jantsch J, Chakravortty D, Turza N, Prechtel AT, Buchholz B, Gerlach RG, Volke M, Gläsner J, Warnecke C, Wiesener MS, et al. Hypoxia and hypoxia-inducible factor-1 alpha modulate lipopolysaccharide-induced dendritic cell activation and function. J Immunol. 2008;180(7):4697–4705. doi:10.4049/JIMMUNOL.180.7.4697
389. Wang F, Zhang S, Vuckovic I, Jeon R, Lerman A, Folmes CD, Dzeja PP, Herrmann J. Glycolytic Stimulation Is Not a Requirement for M2 Macrophage Differentiation. Cell Metab. 2018;28(3):463-475.e4. doi:10.1016/j.cmet.2018.08.012
390. Guenther C, Faisal I, Uotila LM, Asens ML, Harjunpää H, Savinko T, Öhman T, Yao S, Moser M, Morris SW, et al. A β2-Integrin/MRTF-A/SRF Pathway Regulates Dendritic Cell Gene Expression, Adhesion, and Traction Force Generation. Front Immunol. 2019;10:1138. doi:10.3389/fimmu.2019.01138
391. Tseng KY, Stratoulias V, Hu WF, Wu JS, Wang V, Chen YH, Seelbach A, Huttunen HJ, Kulesskaya N, Pang CY, et al. Augmenting hematoma-scavenging capacity of innate immune cells by CDNF reduces brain injury and promotes functional recovery after intracerebral hemorrhage. Cell Death & Disease 2023 14:2. 2023;14(2):1–20. doi:10.1038/s41419-022-05520-2

392. Chopp M, Zhang RL, Chen H, Li Y, Jiang N, Rusche JR. Postischemic administration of an anti-Mac-1 antibody reduces ischemic cell damage after transient middle cerebral artery occlusion in rats. Stroke. 1994;25(4):869–875. doi:10.1161/01.STR.25.4.869
393. Soriano SG, Coxon A, Wang YF, Frosch MP, Lipton SA, Hickey PR, Mayadas TN. Mice Deficient in Mac-1 (CD11b/CD18) Are Less Susceptible to Cerebral Ischemia/Reperfusion Injury. Stroke. 1999;30(1):134–139. doi:10.1161/01.STR.30.1.134
394. Chen H, Chopp M, Zhang RL, Bodzin G, Chen Q, Rusche JR, Todd RF. Anti-CD11b monoclonal antibody reduces ischemic cell damage after transient focal cerebral ischemia in rat. Ann Neurol. 1994;35(4):458–463. doi:10.1002/ANA.410350414
395. Arumugam T V., Salter JW, Chidlow JH, Ballantyne CM, Kevil CG, Granger DN. Contributions of LFA-1 and Mac-1 to brain injury and microvascular dysfunction induced by transient middle cerebral artery occlusion. https://doi.org/10.1152/ajpheart.00588.2004. 2004;287(6 56-6). doi:10.1152/AJPHEART.00588.2004
396. Matsuo Y, Onodera H, Shiga Y, Shozuhara H, Ninomiya M, Kihara T, Tamatani T, Miyasaka M, Kogure K. Role of cell adhesion molecules in brain injury after transient middle cerebral artery occlusion in the rat. Brain Res. 1994;656(2):344–352. doi:10.1016/0006-8993(94)91478-8
397. Wang Y, Tian M, Tan J, Pei X, Lu C, Xin Y, Deng S, Zhao F, Gao Y, Gong Y. Irisin ameliorates neuroinflammation and neuronal apoptosis through integrin αVβ5/AMPK signaling pathway after intracerebral hemorrhage in mice. J Neuroinflammation. 2022;19(1):1–20. doi:10.1186/S12974-022-02438-6/FIGURES/8
398. Gao YY, Tao T, Wu D, Zhuang Z, Lu Y, Wu LY, Liu GJ, Zhou Y, Zhang DD, Wang H, et al. MFG-E8 attenuates inflammation in subarachnoid hemorrhage by driving microglial M2 polarization. Exp Neurol. 2021;336:113532. doi:10.1016/J.EXPNEUROL.2020.113532
399. Ungai-Salánki R, Peter B, Gerecsei T, Orgovan N, Horvath R, Szabó B. A practical review on the measurement tools for cellular adhesion force. Adv Colloid Interface Sci. 2019;269:309–333. doi:10.1016/J.CIS.2019.05.005
400. Beemiller P, Krummel MF. Mediation of T-cell activation by actin meshworks. Cold Spring Harb Perspect Biol. 2010;2(9). doi:10.1101/CSHPERSPECT.A002444
401. Hu KH, Butte MJ. T cell activation requires force generation. Journal of Cell Biology. 2016;213(5):535–542. doi:10.1083/JCB.201511053
402. Sabatos CA, Doh J, Chakravarti S, Friedman RS, Pandurangi PG, Tooley AJ, Krummel MF. A Synaptic Basis for Paracrine Interleukin-2 Signaling during Homotypic T Cell Interaction. Immunity. 2008;29(2):238–248. doi:10.1016/j.immuni.2008.05.017

403. Li D, Molldrem JJ, Ma Q. LFA-1 regulates CD8+ T cell activation via T cell receptor-mediated and LFA-1-mediated Erk1/2 signal pathways. Journal of Biological Chemistry. 2009;284(31):21001–21010. doi:10.1074/jbc.M109.002865

404. Pui-Yan Ma V, Hu Y, Kellner A V, Brockman JM, Velusamy A, Blanchard AT, Evavold BD, Alon R, Salaita K. The magnitude of LFA-1/ICAM-1 forces fine-tune TCR-triggered T cell activation. Sci. Adv. 2022;8:4485.

405. San Lek H, Morrison VL, Conneely M, Campbell PA, McGloin D, Kliche S, Watts C, Prescott A, Fagerholm SC. The Spontaneously Adhesive Leukocyte Function-associated Antigen-1 (LFA-1) Integrin in Effector T Cells Mediates Rapid Actin- and Calmodulin-dependent Adhesion Strengthening to Ligand under Shear Flow. Journal of Biological Chemistry. 2013;288(21):14698–14708. doi:10.1074/JBC.M112.430918

406. Rabets Y, Backholm M, Dalnoki-Veress K, Ryu WS. Direct measurements of drag forces in c. elegans crawling locomotion. Biophys J. 2014;107(8):1980–1987. doi:10.1016/j.bpj.2014.09.006

407. Backholm M, Bäumchen O. Micropipette force sensors for in vivo force measurements on single cells and multicellular microorganisms. Nat Protoc. 2019;14(2):594–615. doi:10.1038/S41596-018-0110-X;SUBJMETA

408. Chen W, Lou J, Zhu C. Forcing switch from short- to intermediate- and long-lived states of the αA domain generates LFA-1/ICAM-1 catch bonds. Journal of Biological Chemistry. 2011;286(20):18344. doi:10.1074/JBC.A110.155770

409. Majowicz A, van der Marel S, te Velde AA, Meijer SL, Petry H, van Deventer SJ, Ferreira V. Murine CD4+CD25- cells activated in vitro with PMA/ionomycin and anti-CD3 acquire regulatory function and ameliorate experimental colitis in vivo. BMC Gastroenterol. 2012;12(1):1–9. doi:10.1186/1471-230X-12-172/FIGURES/5

410. Kokate SB, Ciuba K, Tran VD, Kumari R, Tojkander S, Engel U, Kogan K, Kumar S, Lappalainen P. Caldesmon controls stress fiber force-balance through dynamic cross-linking of myosin II and actin-tropomyosin filaments. Nature Communications 2022 13:1. 2022;13(1):1–20. doi:10.1038/s41467-022-33688-w

411. Du M, Kalia N, Frumento G, Chen F, Zhang Z. Biomechanical properties of human T cells in the process of activation based on diametric compression by micromanipulation. Med Eng Phys. 2017;40:20–27. doi:10.1016/J.MEDENGPHY.2016.11.011

412. Kim J. Regulation of Immune Cell Functions by Metabolic Reprogramming. J Immunol Res. 2018;2018(1):8605471. doi:10.1155/2018/8605471

413. Kelly B, O'Neill LAJ. Metabolic reprogramming in macrophages and dendritic cells in innate immunity. Cell Research 2015 25:7. 2015;25(7):771–784. doi:10.1038/cr.2015.68

414. Hato L, Vizcay A, Eguren I, Pérez-Gracia JL, Rodríguez J, Gállego Pérez-Larraya J, Sarobe P, Inogés S, Díaz de Cerio AL, Santisteban M. Dendritic Cells in Cancer Immunology and Immunotherapy. Cancers 2024, Vol. 16, Page 981. 2024;16(5):981. doi:10.3390/CANCERS16050981
415. Anguille S, Smits EL, Lion E, Van Tendeloo VF, Berneman ZN. Clinical use of dendritic cells for cancer therapy. Lancet Oncol. 2014;15(7):e257–e267. doi:10.1016/S1470-2045(13)70585-0
416. Palucka K, Banchereau J. Dendritic-Cell-Based Therapeutic Cancer Vaccines. Immunity. 2013;39(1):38–48. doi:10.1016/J.IMMUNI.2013.07.004
417. Zanotta S, Galati D, De Filippi R, Pinto A. Enhancing Dendritic Cell Cancer Vaccination: The Synergy of Immune Checkpoint Inhibitors in Combined Therapies. International Journal of Molecular Sciences 2024, Vol. 25, Page 7509. 2024;25(14):7509. doi:10.3390/IJMS25147509
418. Schaller TH, Sampson JH. Advances and challenges: dendritic cell vaccination strategies for glioblastoma. Expert Rev Vaccines. 2016;16(1):27. doi:10.1080/14760584.2016.1218762
419. Niveau C, Cettour-Cave M, Mouret S, Sosa Cuevas E, Pezet M, Roubinet B, Gil H, De Fraipont F, Landemarre L, Charles J, et al. MCT1 lactate transporter blockade re-invigorates anti-tumor immunity through metabolic rewiring of dendritic cells in melanoma. Nature Communications . 2025;16(1):1–24. doi:10.1038/S41467-025-56392-X;TECHMETA
420. Zhou Y, Xie Y, Qi J, Hu J, Yang Y, Deng F, Zhu Y, Deng W, Mei L, Goldys EM, et al. A leucine derivate-adjuvanted LNP vaccine enhances antitumor immunity through mTOR activation and metabolic reprograming in dendritic cells. Biomaterials. 2026;325:123539. doi:10.1016/J.BIOMATERIALS.2025.123539
421. Watson AR, Dai H, Zheng Y, Nakano R, Giannou AD, Menk A V., Stolz DB, Delgoffe GM, Thomson AW. MTORC2 deficiency alters the metabolic profile of conventional dendritic cells. Front Immunol. 2019;10(JUL):443636. doi:10.3389/FIMMU.2019.01451/BIBTEX
422. Hannigan G, Troussard AA, Dedhar S. Integrin-linked kinase: A cancer therapeutic target unique among its ILK. Nat Rev Cancer. 2005;5(1):51–63. doi:10.1038/NRC1524;KWRD
423. Zhong D, Xiong L, Liu T, Liu X, Liu X, Chen J, Sun SY, Khuri FR, Zong Y, Zhou Q, et al. The glycolytic inhibitor 2-deoxyglucose activates multiple prosurvival pathways through IGF1R. Journal of Biological Chemistry. 2009;284(35):23225–23233. doi:10.1074/jbc.M109.005280
424. Larrue C, Saland E, Vergez F, Serhan N, Delabesse E, Mas VM De, Hospital MA, Tamburini J, Manenti S, Sarry JE, et al. Antileukemic activity of 2-deoxy-D-glucose through inhibition of N-linked glycosylation in acute myeloid leukemia with FLT3-ITD or c-KIT mutations. Mol Cancer Ther. 2015;14(10):2364–2373. doi:10.1158/1535-7163.MCT-15-0163/85460/AM/ANTI-LEUKEMIC-ACTIVITY-OF-2-DEOXY-D-GLUCOSE

425. Atwood D, He Z, Miyazaki M, Hailu F, Klawitter J, Edelstein CL. Early treatment with 2-deoxy-d-glucose reduces proliferative proteins in the kidney and slows cyst growth in a hypomorphic Pkd1 mouse model of autosomal dominant polycystic kidney disease (PKD). Cell Signal. 2024;123:111351. doi:10.1016/J.CELLSIG.2024.111351
426. Herzig S, Shaw RJ. AMPK: Guardian of metabolism and mitochondrial homeostasis. Nat Rev Mol Cell Biol. 2018;19(2):121–135. doi:10.1038/NRM.2017.95;SUBJMETA
427. Ehm P, Jücker M. The Inositol-5-Phosphatase SHIP1: Expression, Regulation and Role in Acute Lymphoblastic Leukemia. Int J Mol Sci. 2025;26(14). doi:10.3390/IJMS26146935
428. Chan LN, Chen Z, Braas D, Lee JW, Xiao G, Geng H, Cosgun KN, Hurtz C, Shojaee S, Cazzaniga V, et al. Metabolic gatekeeper function of B-lymphoid transcription factors. Nature. 2017;542(7642):479–483. doi:10.1038/NATURE21076;SUBJMETA
429. Martín-Lorenzo A, Auer F, Chan LN, García-Ramírez I, Gonzalez-Herrero I, Rodríguez-Hernandez G, Bartenhagen C, Dugas M, Gombert M, Ginzel S, et al. Loss of Pax5 exploits sca1-BCR-ABLp190 susceptibility to confer the metabolic shift essential for pB-ALL. Cancer Res. 2018;78(10):2669–2679. doi:10.1158/0008-5472.CAN-17-3262/653153/AM/LOSS-OF-PAX5-EXPLOITS-SCA1-BCR-ABLP190
430. Cazzaniga G, Van Delft FW, Lo Nigro L, Ford AM, Score J, Iacobucci I, Mirabile E, Taj M, Colman SM, Biondi A, et al. Developmental origins and impact of BCR-ABL1 fusion and IKZF1 deletions in monozygotic twins with Ph+ acute lymphoblastic leukemia. Blood. 2011;118(20):5559–5564. doi:10.1182/BLOOD-2011-07-366542
431. Heizmann B, Kastner P, Chan S. The Ikaros family in lymphocyte development. Curr Opin Immunol. 2018;51:14–23. doi:10.1016/J.COI.2017.11.005
432. Jiang G-N, Lin Q-Y, An X-B, Yu W-J, Bai J, Yu X, Wang F, Li H-H. Integrin CD11b Alleviates Cerebral Ischemia/Reperfusion Injury via a Mechanism Involving Microglia/Macrophage Polarization. Journal of Molecular Neuroscience 2025 75:4. 2025;75(4):1–18. doi:10.1007/S12031-025-02414-8
433. Lv J, Jiao Y, Zhao X, Kong X, Chen Y, Li L, Chen X, Tao X, Dong D. Examining the Impact of Microglia on Ischemic Stroke With an Emphasis on the Metabolism of Immune Cells. CNS Neurosci Ther. 2025;31(2):e70229. doi:10.1111/CNS.70229
434. Bernier LP, York EM, MacVicar BA. Immunometabolism in the Brain: How Metabolism Shapes Microglial Function. Trends Neurosci. 2020;43(11):854–869. doi:10.1016/J.TINS.2020.08.008

435. Cheng J, Zhang R, Xu Z, Ke Y, Sun R, Yang H, Zhang X, Zhen X, Zheng LT. Early glycolytic reprogramming controls microglial inflammatory activation. J Neuroinflammation. 2021;18(1):1–18. doi:10.1186/S12974-021-02187-Y/FIGURES/9
436. Sukumar M, Liu J, Ji Y, Subramanian M, Crompton JG, Yu Z, Roychoudhuri R, Palmer DC, Muranski P, Karoly ED, et al. Inhibiting glycolytic metabolism enhances CD8+ T cell memory and antitumor function. J Clin Invest. 2013;123(10):4479–4488. doi:10.1172/JCI69589
437. Ghosh S, Castillo E, Frias ES, Swanson RA. Bioenergetic regulation of microglia. Glia. 2018;66(6):1200–1212. doi:10.1002/GLIA.23271
438. Appelberg KS, Hovda DA, Prins ML. The effects of a ketogenic diet on behavioral outcome after controlled cortical impact injury in the juvenile and adult rat. J Neurotrauma. 2009;26(4):497–506. doi:10.1089/NEU.2008.0664
439. Jin Q, Cheng J, Liu Y, Wu J, Wang X, Wei S, Zhou X, Qin Z, Jia J, Zhen X. Improvement of functional recovery by chronic metformin treatment is associated with enhanced alternative activation of microglia/macrophages and increased angiogenesis and neurogenesis following experimental stroke. Brain Behav Immun. 2014;40:131–142. doi:10.1016/J.BBI.2014.03.003
440. Bourget C, Adams K V., Morshead CM. Reduced microglia activation following metformin administration or microglia ablation is sufficient to prevent functional deficits in a mouse model of neonatal stroke. J Neuroinflammation. 2022;19(1):1–21. doi:10.1186/S12974-022-02487-X/FIGURES/5
441. Fritzsche M, Kruse K. Mechanical force matters in early T cell activation. Proceedings of the National Academy of Sciences. 2024;121(37):e2404748121. doi:10.1073/PNAS.2404748121

Publication I

ONCOIMMUNOLOGY
2024, VOL. 13, NO. 1, 2369373
https://doi.org/10.1080/2162402X.2024.2369373

Taylor & Francis
Taylor & Francis Group

ORIGINAL RESEARCH

OPEN ACCESS Check for updates

Loss of β2-integrin function results in metabolic reprogramming of dendritic cells, leading to increased dendritic cell functionality and anti-tumor responses

Heidi Harjunpää[a], Riku Somermäki[a*], Guillem Saldo Rubio[a*], Manlio Fusciello[b], Sara Feola[b], Imrul Faisal[a], Anni I Nieminen[c], Liang Wang[a], Marc Llort Asens[a], Hongxia Zhao[a], Ove Eriksson[d], Vincenzo Cerullo[b], and Susanna C Fagerholm[a]

[a]Molecular and Integrative Biosciences Research Programme, Faculty of Biological and Environmental Sciences, University of Helsinki, Helsinki, Finland; [b]Faculty of Pharmacy, University of Helsinki, Helsinki, Finland; [c]Institute for Molecular Medicine Finland (FIMM), University of Helsinki, Helsinki, Finland; [d]Biochemistry and Developmental biology, Medicum, Faculty of Medicine, University of Helsinki, Helsinki, Finland

ABSTRACT

Dendritic cells (DCs) are the main antigen presenting cells of the immune system and are essential for anti-tumor responses. DC-based immunotherapies are used in cancer treatment, but their functionality is not optimized and their clinical efficacy is currently limited. Approaches to improve DC functionality in anti-tumor immunity are therefore required. We have previously shown that the loss of β2-integrin-mediated adhesion leads to epigenetic reprogramming of bone marrow-derived DCs (BM-DCs), resulting in an increased expression of costimulatory markers (CD86, CD80, and CD40), cytokines (IL-12) and the chemokine receptor CCR7. We now show that the loss of β2-integrin-mediated adhesion of BM-DCs also leads to a generally suppressed metabolic profile, with reduced metabolic rate, decreased ROS production, and lowered glucose uptake in cells. The mRNA levels of glycolytic enzymes and glucose transporters were reduced, indicating transcriptional regulation of the metabolic phenotype. Surprisingly, although signaling through a central regulator of immune cell metabolisms, the mechanistic target of rapamycin (mTOR), was increased in BM-DCs with dysfunctional integrins, rapamycin treatment revealed that mTOR signaling was not involved in suppressing DC metabolism. Instead, bioinformatics and functional analyses showed that the Ikaros transcription factor may be involved in regulating the metabolic profile of non-adhesive DCs. Inversely, we found that induction of metabolic stress through treatment of cells with low levels of an inhibitor of glycolysis, 2-deoxyglucose (2DG), led to increased BM-DC activation. Specifically, 2DG treatment led to increased levels of *Il-12* and *Ccr7* mRNA, increased production of IL-12, increased levels of cell surface CCR7 and increased *in vitro* migration and T cell activation potential. Furthermore, 2DG treatment led to increased histone methylation in cells (H3K4me3, H3K27me3), indicating metabolic reprogramming. Finally, metabolic stress induced by 2DG treatment led to improved BM-DC-mediated anti-tumor responses *in vivo* in a melanoma cancer model, B16-OVA. In conclusion, our results indicate a role for β2-integrin-mediated adhesion in regulating a novel type of metabolic reprogramming of DCs and DC-mediated anti-tumor responses, which may be targeted to enhance DC-mediated anti-tumor responses in cancer immunotherapy.

ARTICLE HISTORY
Received 3 November 2023
Revised 13 June 2024
Accepted 13 June 2024

KEYWORDS
Integrin; dendritic cell; cancer immunotherapy; cell metabolism; cell adhesion; CCR7; glycolysis; 2-deoxyglucose; Ikaros; mTOR

Introduction

DCs are the main antigen presenting cells of the immune system and play major roles in activating and polarizing the immune response. In peripheral tissues, DCs first take up antigens followed by activation (maturation and reprogramming) in response to associated pathogen and danger signals and then migrate to lymph nodes where they activate and polarize T cell responses.[1] Because of their essential role in T cell activation, DCs are also used in immunotherapeutic approaches to treat cancer. Currently, the only FDA-approved DC-based vaccine (for prostate cancer) is Provenge, which consists of monocyte-derived DCs which are expanded from patients' peripheral blood, loaded with tumor antigens and injected back into patients. However, although they are safe and well tolerated, the clinical efficacy of dendritic cell vaccines is limited, at least in part due to poor DC migration to lymph nodes and/or due to limited T cell activation/polarization capacity.[2,3] Therefore, understanding how to improve DC functionality *in vitro* and *in vivo* could offer new approaches to enhance immunotherapy for cancer, either alone or in combination with other therapies.

DC activation is associated with large changes in gene expression as well as epigenetic changes (reprogramming).[4] Simultaneously, the cells undergo fundamental changes in integrin-mediated adhesiveness and phagocytic capacity, which are both downregulated when the cells acquire the migratory phenotype.[5–7] DC activation is also associated with metabolic changes such as reduced oxidative phosphorylation,

CONTACT Susanna C Fagerholm susanna.fagerholm@helsinki.fi Molecular and Integrative Biosciences Research Programme, Faculty of Biological and Environmental Sciences, University of Helsinki, P.B. 56, Helsinki 00014, Finland

*Equal contribution.

Supplemental data for this article can be accessed online at https://doi.org/10.1080/2162402X.2024.2369373.

increased aerobic glycolysis, and changes in lipid metabolism.[8,9] The mechanistic target of rapamycin (mTOR) signaling pathway is often involved in metabolic reprogramming of immune cells and has previously been reported to be important also for TLR-induced DC metabolic reprogramming.[10] In particular, mTOR/HIF-1α/iNOS signaling is required for sustained glycolytic reprogramming at later time points after activation, which is required for DC survival.[8]

Integrins are pivotal adhesion and mechanoreceptors in cells, which play a central role in immune cell trafficking and effector functions. β2-integrins are leukocyte-specific molecules that play diverse roles in DCs, including cDC2 positioning in spleen[11] and trafficking of DCs to lymph nodes in inflammatory but not homeostatic conditions.[1] Interestingly, β2-integrins can also restrict immune cell responses by, e.g., inhibiting toll-like receptor signaling in macrophages and DCs, promoting tolerance, and suppressing colitis and dermatitis.[12–17] Thus, β2-integrins can also play homeostatic and regulatory roles in immunity and inflammation. We have previously shown that β2-integrins inhibit bone marrow-derived DC (BM-DC) activation/reprogramming *in vitro* and BM-DC-mediated Th1 polarization and anti-tumor responses *in vivo*.[6,14,18] In TTT/AAA-β2-integrin knock-in mice (β2-integrin KI), where β2-integrins are expressed but dysfunctional due to reduced binding to kindlin-3, an important cytoplasmic regulator of integrins, there are increased numbers of migratory DCs (migDCs) in lymph nodes and spleen. In addition, endogenous β2-integrin KI DCs display increased trafficking to lymph nodes and increased maturation with elevated expression of CD86 *in vivo*.[7] Increased BM-DC activation in response to loss of integrin-mediated adhesion occurs through changes in epigenetic (e.g. histone methylation, H3K4me3, and H3K27me3) and chromatin landscapes, large changes in gene expression (increased expression of, e.g., *Cd86*, *Cd40*, *Ccr7*, *Fscn1*, and *Il12*), and fundamental changes in transcription factors of Ikaros and RelA-mediated gene expression.[18,19] Integrins thus mediate interactions between the DC and its microenvironment, hence suppressing DC reprogramming and maturation both *in vitro* and *in vivo* settings, contributing to immune homeostasis.

As myeloid cell reprogramming is well known to be associated both with epigenetic and with metabolic changes,[8,9,20] here, we investigated whether integrin dysfunction is also associated with metabolic changes in DCs, using BM-DCs as a model system. Our results reveal major metabolic reprogramming in BM-DCs expressing dysfunctional β2-integrins with reduced metabolism, and production of reactive oxygen species (ROS). The expression of glycolytic enzymes and glucose transporters was downregulated, and the metabolic reprogramming was shown to be partially driven by the transcription factor Ikaros. We also show that mimicking such metabolic stress in wild-type (WT) BM-DCs by treating cells with low concentration of glycolysis inhibitor, 2-deoxyglucose (2DG), drives increased DC activation (increased expression of IL-12 and CCR7, *in vitro* migration and T cell activation potential), increased H3K4me3 and H3K27me3 histone methylation, and enhanced anti-tumor responses *in vivo*. In conclusion, integrin-mediated cell adhesion regulates the metabolic and epigenetic phenotypes of BM-DCs, showing that the β2-integrin-mediated regulation of metabolic profile of DCs plays a pivotal role in their activation, which may be targeted to optimize anti-tumor responses of these cells.

Results

Inactivating β2-integrins leads to an altered metabolic profile of BM-DCs

As immune cell reprogramming often goes hand-in-hand with metabolic changes, we decided to investigate a putative relationship between integrin adhesion and cellular metabolism in DCs. We first investigated publicly available transcriptomics data of migDCs isolated from murine lymphoid organs for their expression levels of migratory, adhesion, and metabolic genes.[6] Compared to tissue resident DCs, migDCs express higher mRNA levels of migratory genes such as those encoding for chemokine receptors *(Ccr7)* and actin-binding proteins associated with cell migration (*Fscn1*) (Figure 1a). In contrast, pathways such as "cell–cell adhesion" and "integrin signaling" were downregulated, including expression of *Itgax*, *Itgb2*, and *Itgb7* genes, encoding for αX-integrin, β2-integrin, and β7-integrin, respectively (Figure 1a). Interestingly, also changes in the expression of metabolic genes were detected. In particular, the cells express very low levels of *Hk2*, encoding for the rate-limiting enzyme of glycolysis (hexokinase 2). Instead, *Eno2*, *Eno3* (enolase, involved in glycolysis), and *Gyg* (glycogenin, involved in the synthesis of glycogen) genes were upregulated (Figure 1a). MigDCs *in vivo* therefore display changes in the expression of genes associated with both cell adhesion and glucose metabolism.

Based on their transcriptional profile, granulocyte-macrophage colony-stimulating factor (GM-CSF)-cultured murine BM-DCs resemble *in vivo* migDCs, making them a useful *in vitro* tool to investigate migDC function.[21] We have previously shown that BM-DCs expressing dysfunctional β2-integrins display increased activation and migration and have extensively reported the phenotype of these cells (increased expression of CD80, CD86, CD40, CCR7, increased IL-12 production, increased 3D migration).[7,18] Representative histograms of expression of DC markers in WT and KI BM-DCs are also shown in Supplementary SFig 1a. We here turned to investigate the metabolic status of BM-DCs expressing dysfunctional β2-integrins. Analysis of our previously published RNA-Seq data from WT and β2-integrin KI BM-DCs[7] indeed indicated that several metabolic pathways were downregulated in the β2-integrin KI cells, including "glycolysis and gluconeogenesis", "biosynthesis of amino acids" and "lipid biosynthesis" (Figure 1b), indicating a changed metabolic profile of BM-DCs expressing dysfunctional integrins. Thus, we further analyzed the metabolomes of WT and β2-integrin KI BM-DCs by targeted mass spectrometry metabolomics profiling analysis (Figure 1c). This analysis revealed changes in several metabolites in BM-DCs expressing dysfunctional integrins, including several metabolites in pathways such as "arginine and proline metabolism", "urea cycle", "glycine and serine metabolism", and "mitochondrial electron transport" (Figure 1c–e). For example, the arginine levels were significantly increased, whilst itaconate, ornithine, orotate, and guanidinoacetate were decreased (Figure 1c). Analysis of RNA-Seq data confirmed

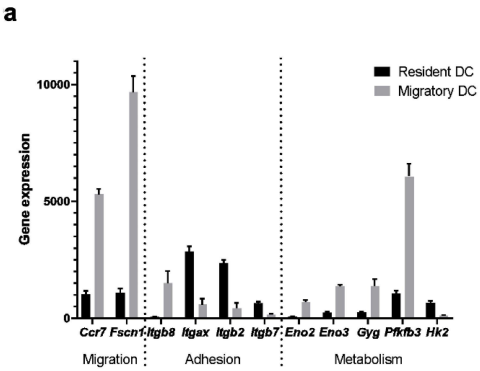

b

Gene Ontology (GO) term	Term name	P-value	Genes
KEGG_PATHWAY	Glycolysis and gluconeogenesis	1,7E-8	*Acss2, Aldh1b1, Aldh2, Aldh3b1, Akr1a1, Aldoa, Aldoc, Eno1, Gpi1, Gapdh, Hk2, Hk3, Minpp1, Pck2, Pfkl, Pfkm, Pgm1, Pgm2, Pgk1, Pgam1, Pkm, Tpi1*
GOTERM_BP_DIRECT	Glycolytic process	5,1E-7	*Htr2a, Aldoa, Aldoc, Eno1, Gpi1, Gapdh, Hk2, Hk3, Pfkl, Pfkm, Pgk1, Pgam1, Pkm, Tpi1*
KEGG_PATHWAY	Galactose metabolism	3,0E-7	*B4galt1, Ugp2, Akr1b8, Galk1, Gale, Gla, Glb1, Gaa, Hk2, Hk3, Pfkl, Pfkm, Pgm1, Pgm2*
KEGG_PATHWAY	Biosynthesis of amino acids	1,7E-6	*Phgdh, Nags, Aldoa, Aldoc, Acy1, Arg1, Asns, Bact1, Eno1, Gapdh, Idh1, Idh2, Pfkl, Pfkm, Pgk1, Pgam1, Prps2, Psat1, Pkm, Tkt, Tpi1*
UP_KW_BIOLOGICAL_PROCESS	Lipid biosynthesis	3,0E-5	*Agpat3, Hmgcs1, Hacd4, Dhcr7, Acly, Cds2, Elov7, Mid1ip1, Abhd5, Cers6, Cyp51, Cyb5r3, Fdft1, Fads2, Hsd17b7, Lss, Mboat7, Msmo1, Mvd, Pcyt1b, Pla2g4a, Pmvk, Ptges, Ptgs1, Scd1, Scd2, Sc5d, Tbxas1*
GOTERM_BP_DIRECT	Cholesterol biosynthetic process	2,0E-4	*Hmgcs1, Dhcr7, Cyp51, Cyb5r3, Fdft1, Hsd17b7, Insig1, Lss, Msmo1, Mvd, Pmvk*
KEGG_PATHWAY	Amino sugar and nucleotide sugar metabolism	1,0E-4	*Ugdh, Ugp2, Cmah, Cmas, Cyb5r3, Galk1, Gale, Gpi1, Hk2, Hk3, Hexa, Hexb, Pgm1, Pgm2*
KEGG_PATHWAY	TCA Cycle	9,9E-2	*Acly, Idh1, Idh2, Mdh2, Pck2, Sdhc*
UP_KW_BIOLOGICAL_PROCESS	Respiratory chain	6,3E-1	*Hlfd1a, Ndufb3, Ndufb6, Ndufc1, Cycs*

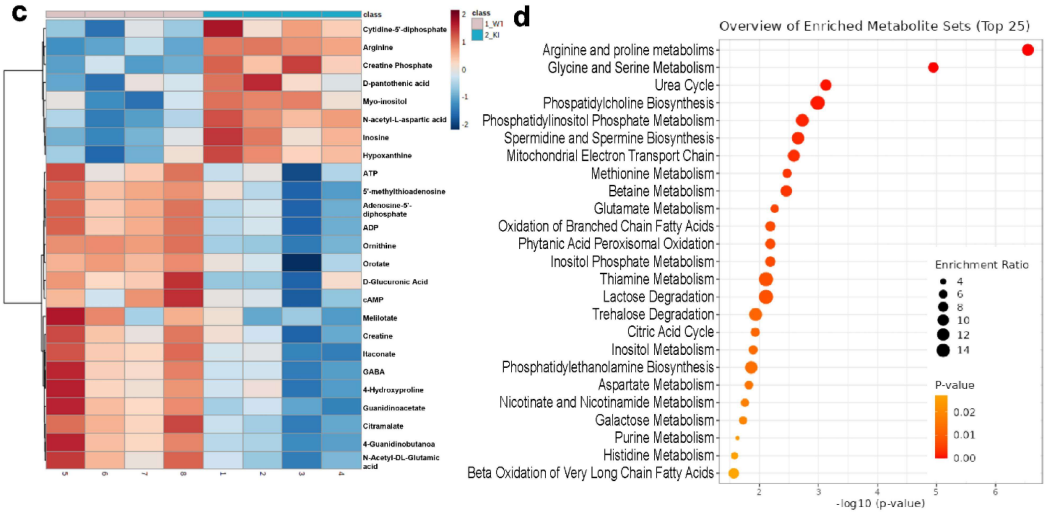

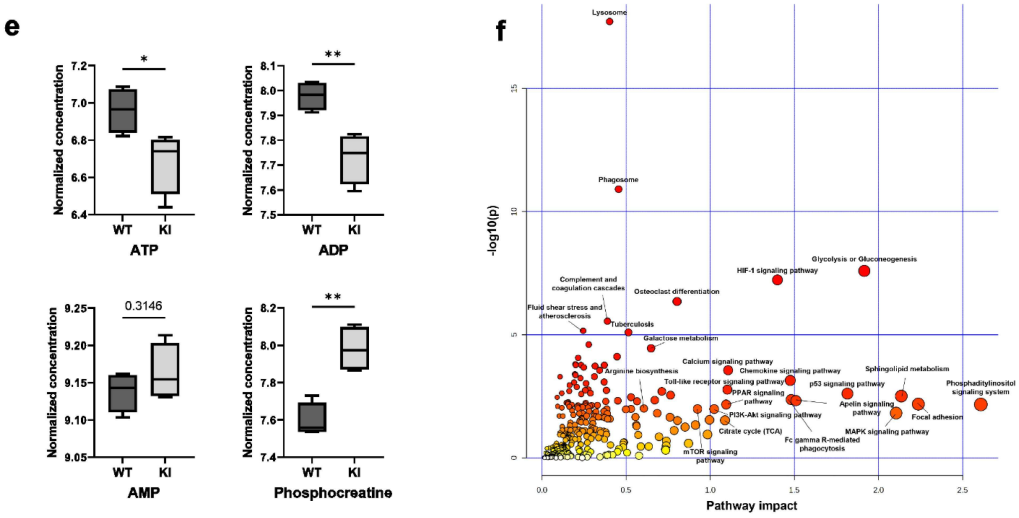

Figure 1. Multiomics analysis reveals an altered metabolic profile in BM-DCs expressing dysfunctional β2-integrins (a) Analysis of publicly available gene expression data of resident and migDCs[6] for genes involved in cell migration, adhesion and cellular metabolism. (b) Analysis of downregulated pathways in previously published RNA-Seq data from β2-integrin KI BM-DCs[7] using the DAVID bioinformatics tool. (c) Targeted mass spectrometry-based analysis of metabolites in WT and β2-integrin KI BM-DCs was performed as described in the Materials and methods section (n=4). (d) Metabolite set enrichment analysis (MSEA) of metabolites identified in WT and

significant downregulation of *Arg1*, the first enzyme in the arginine metabolic pathway, putatively explaining why especially arginine metabolism and the urea cycle were severely affected in these cells.[7] Mass spectrometry analysis also revealed differences in ATP, ADP (but not AMP), and phosphocreatine (a metabolic energy store) levels between WT and β2-integrin KI cells, indicating a significant change in metabolic status as a result of integrin dysfunction (Figure 1e). Indeed, integrating metabolomics and RNA-Seq data indicated "glycolysis or gluconeogenesis" to be the pathway showing the highest impact and significance by the integrin mutation in BM-DCs (Figure 1f). Other pathways that may be affected include the HIF1 pathway and the phosphatidyl inositol signaling system, which are pathways previously implicated in the regulation of metabolic reprogramming of DCs.[22] Therefore, our multi-omics data suggested changes in several metabolic pathways and in the metabolic status of BM-DCs expressing dysfunctional integrins.

Reduced metabolic rate and altered mitochondrial function in BM-DCs expressing inactive β2-integrins

Total cellular ATP is mainly generated by glycolysis and oxidative phosphorylation in mammalian cells. We found that the expression of glycolytic enzymes and ATP and ADP levels were reduced in β2-integrin KI BM-DCs (Figure 1e). In addition, glycolysis was heavily implicated as being regulated by integrins in the integrated multi-omics analysis (Figure 1f). To directly investigate the effect of integrin dysfunction on cellular metabolism, we turned to Seahorse Extracellular Flux analysis, capable of measuring extracellular acidification rate (ECAR) and oxygen consumption rate (OCR), thus indicating levels of glycolysis and oxidative phosphorylation, respectively, in cells in real time. Interestingly, we found differences in both ECAR (Figure 2a) and OCR (Figure 2b) between β2-integrin KI and WT BM-DCs. The basal rate of glycolysis (ECAR before injection of any cellular respiratory modulators) was not reduced in β2-integrin KI BM-DCs (Figure 2a). However, driving mitochondrial uncoupling with FCCP (which uncouples oxidative phosphorylation from ATP production, thereby driving increased aerobic glycolysis to compensate for the loss of ATP production; reflects cellular response to conditions of increased energy demand or stress) led to lower ECAR in integrin deficiency compared to WT cells (Figure 2a). In addition, BM-DCs expressing dysfunctional integrins displayed reduced maximal respiration, as well as spare respiratory capacity (which reflects the cell's ability to respond to increased energy demand) (Figure 2b–c and Supplementary Fig S1b). However, basal respiration, proton leak, mitochondrial ATP production, or coupling efficiency were not affected (Figure 2b–c, Supplementary Fig S1b). In addition, although our mass spectrometry analysis indicated that ATP and ADP levels were reduced in BM-DCs expressing dysfunctional integrins (Figure 1c), the ATP/ADP ratio in cells was not affected by integrin dysfunction (Figure 2d, Supplementary SFig 1c).

The reduced metabolic rate of the β2-integrin KI BM-DCs compared to WT was confirmed by measuring protein translation as a proxy for available cellular energy. Protein translation has previously been shown to correlate with metabolic activity in lymphocytes.[23] Indeed, the β2-integrin KI BM-DCs exhibited markedly reduced translation (puromycin incorporation) compared to WT BM-DCs (Figure 2e), confirming the lower metabolic rate in these cells.

Given that the overall metabolic status was decreased (lower level of protein translation and ATP) in β2-integrin KI compared to WT BM-DCs, we first assessed whether there was a difference in viability. No differences were observed between β2-integrin KI and WT BM-DCs even after 17 d in culture (Figure 2f). Next, we turned to investigate mitochondrial function in more detail. Firstly, we found that mitochondrial numbers were not affected (Figure 2g) in BM-DCs expressing dysfunctional β2-integrins. However, the mitochondrial membrane potential was slightly increased in β2-integrin KI BM-DCs (Figure 2h). In contrast, ROS levels were markedly reduced in cells with dysfunctional integrins (Figure 2i). Together with a reduced metabolism (Figure 2a–c) and lower translation rates (Figure 2e), these data indicated reduced glucose metabolism and mitochondrial function in β2-integrin KI BM-DCs.

Suppressed metabolism is regulated on the transcriptional level in BM-DCs expressing dysfunctional integrins

RNA-Seq analysis indicated that several glycolytic and glucose transporter genes were downregulated in BM-DCs expressing dysfunctional β2-integrins (Figure 1b). In addition, as there were differences in OCR rates under conditions of cellular stress, we next investigated the expression of genes involved in the pathways in WT and β2-integrin KI BM-DCs by qRT-PCR. Indeed, we found that the expression of glycolytic enzymes *Pfkl* and *Pkm* was significantly reduced in β2-integrin KI cells (Figure 3a). In contrast, there was no difference in the expression of genes such as *Hif1α* or *Phd3* (Figure 3a). In addition, we found that Glut1 was significantly downregulated at the protein level in these cells (Figure 3b). We therefore investigated glucose uptake in β2-integrin KI cells and found a significant downregulation of glucose uptake in these cells (Figure 3c). Together, these integrated multiomics data (Figures 1–3) showed a significant suppression of glycolytic metabolism of BM-DCs expressing dysfunctional β2-integrins. Furthermore, the data indicated that the altered metabolic profile is regulated, at least in part, on the transcriptional level.

β2-integrin KI BM-DCs using the publicly available MetaboAnalyst platform. e) Levels of central metabolites identified by mass spectrometry (normalized concentration e.g. log10). (f) Integrated RNA-Seq and metabolomics data analysis to identify most highly affected metabolic pathways was performed using the MetaboAnalyst platform. P-values are shown as <0.05*, <0.01**.

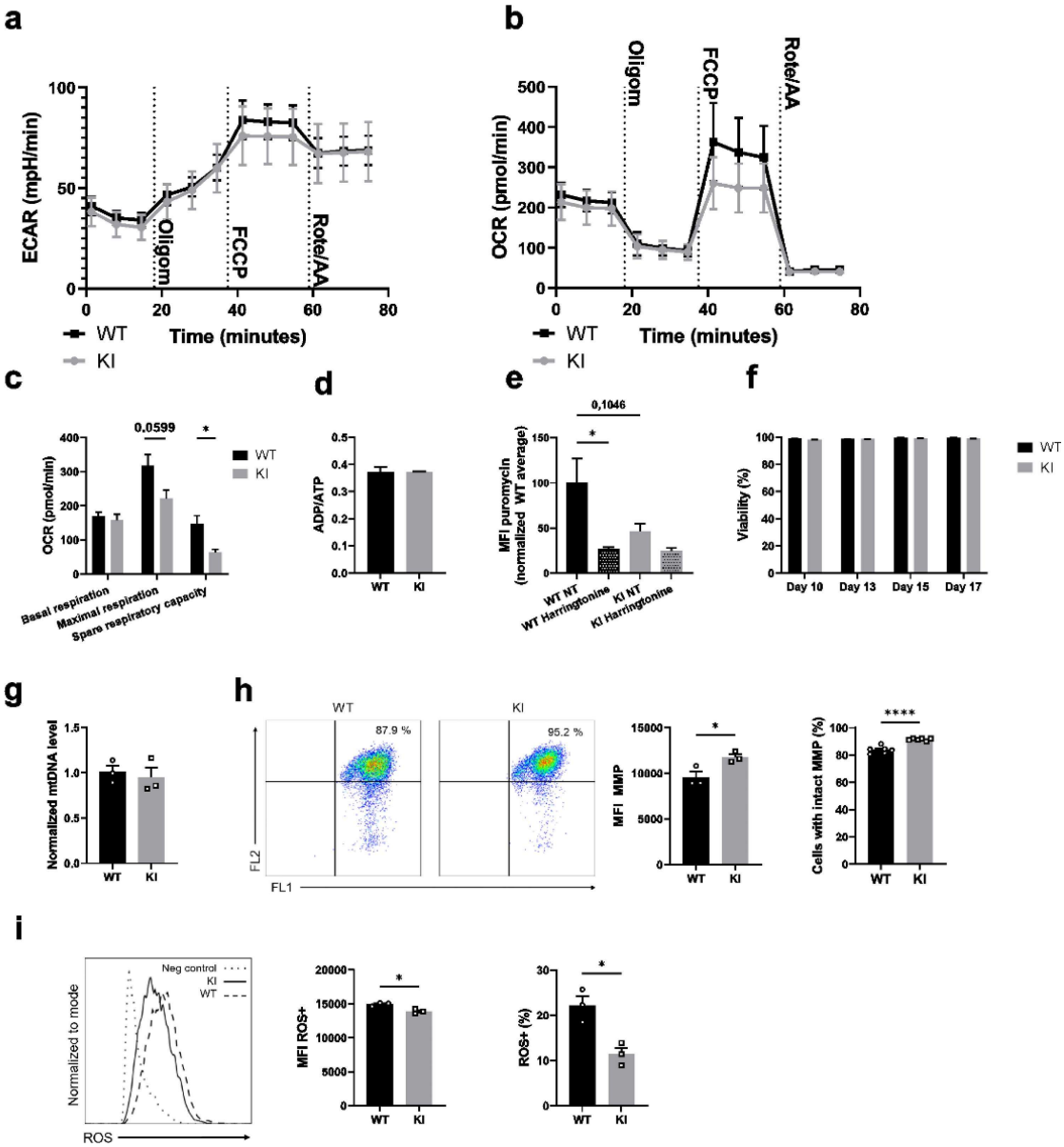

Figure 2. β2-integrin deficient BM-DCs display altered metabolic profile compared to BM-DCs with functional integrins. (a) Extracellular acidification rate (ECAR) and (b) oxygen consumption rate (OCR) of WT and β2-integrin KI BM-DCs were measured real time by utilizing Seahorse Extracellular Analyser and Mito Stress Test Kit (n=4). (c) Parameters indicating mitochondrial function in WT and β2-integrin KI BM-DCs were calculated based on OCR data shown in B). (d) ATP/ADP ratio in WT and β2-integrin KI BM-DCs was determined with luminescence-based ADP/ATP Ratio Assay Kit (n=3). (e) Metabolic activity of both WT and β2-integrin KI BM-DCs was assessed flow cytometrically by determining the level of puromycin incorporation. Harringtonine (translation inhibitor)-treated cells were used as a negative control and the result is normalized to the metabolic activity of WT cells. (n=3). Cell viability was assessed flow cytometrically (n=3). (g) Level of mitochondrial DNA (mtDNA) in WT and β2-integrin KI BM-DCs was assessed by qRT-PCR (n=3). (h) Mitochondrial membrane potential (MMP) and H) the level of reactive oxygen species (ROS) in WT and β2-integrin KI BM-DCs were assessed by flow cytometer with representative dot plots (h) or histograms (i), MFIs and proportions of positive cells shown (n=3). Data in a) and b) is representative of two independent experiments. Data in h) is either shown as representative of two independent experiments (dot plots and MFI) or pooled from the two independent experiments (proportions of positive cells). P-values are shown as <0.05*, <0.0001****.

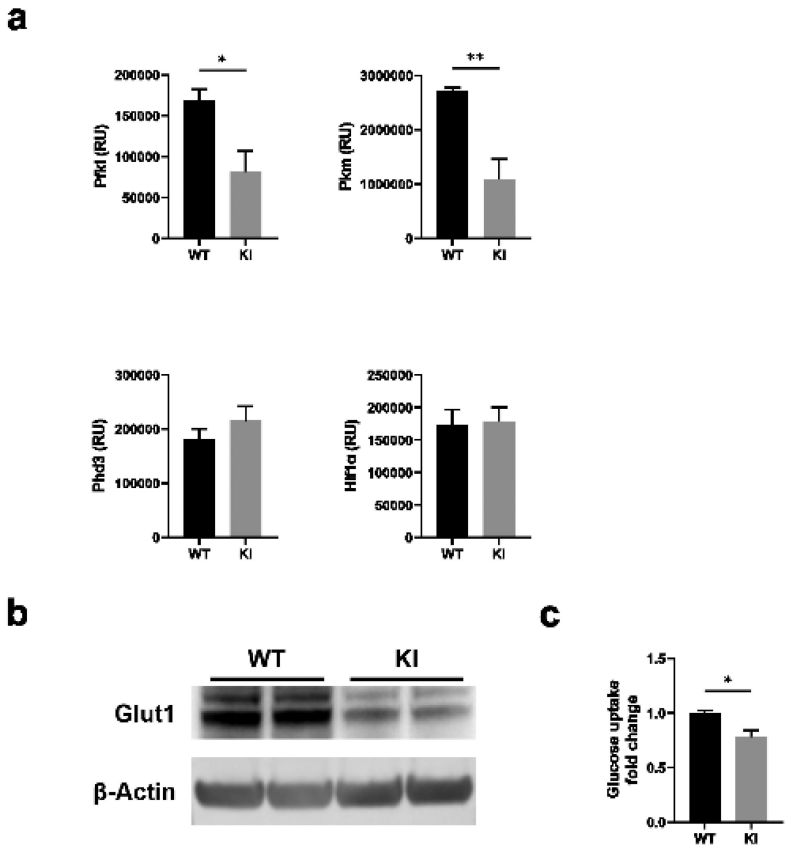

Figure 3. β2-integrin-deficient BM-DCs display reduced expression of glycolytic enzymes and glucose transporters as well as reduced glucose uptake. (a) Expression of Pfkl, Pkm, Hif1α and Phd3, b) protein level of Glut1 and c) glucose uptake in WT and β2-integrin KI BM-DC were determined by using a) qRT-PCR (n=3–5), (b) Western blotting (n=5) or (c) luminescence-based Glucose Uptake-Glo™ Assay kit (n=4) as described in the Materials and Methods. P-values are shown as <0.05*, <0.01**.

The mTOR pathway is not responsible for downregulation of glycolysis or oxidative phosphorylation in β2-integrin-deficient BM-DCs

We next turned to investigate putative pathways that may regulate the metabolic phenotype of BM-DCs where integrins are dysfunctional. Here, we found that Akt and mTOR signaling were upregulated in cells expressing dysfunctional β2-integrins (Figure 4a), and there was a trend toward increased iNOS expression in these cells, although the results did not reach statistical significance (Figure 4c). The AMPK (AMP-activated protein kinase) pathway opposes mTOR, and responds to energy stress in cells (high AMP/ATP ratio, high creatine/phosphocreatine ratio).[24] The activity of AMPK was slightly downregulated in β2-integrin KI cells (Figure 4b), possibly reflecting the high phosphocreatine levels in these cells (Figure 1b). Furthermore, the expression of iNOS was suppressed in β2-integrin KI cells by treatment with mTOR inhibitor, rapamycin (Figure 4c). However, we found that mTOR was not responsible for the differences in metabolism between WT and β2-integrin KI BM-DC, as treatment of β2-integrin KI cells with rapamycin did not reverse their metabolic phenotype (Figure 4d,e). Rather, rapamycin treatment further reduced ECAR and OCR rates and thus the overall metabolic rate in cells expressing dysfunctional integrins (Figure 4d–f, Supplementary Fig S1d). Both basal and maximal respiration were further reduced by rapamycin treatment, which also affected ATP production and spare respiratory capacity in β2-integrin KI BM-DCs (Figure 4f). In addition, as previously reported,[7] as part of their activated phenotype, IL-12 production was increased in β2-integrin KI cells (Figure 4g). However, treatment of β2-integrin KI cells with rapamycin did not reduce IL-12 production in these cells (Figure 4g). Together, our data suggest that although mTOR signaling is upregulated in BM-DCs expressing dysfunctional integrins, mTOR signaling is not responsible for their suppressed metabolic state or their increased activation.

Transcription factor Ikaros plays an important role in mediating the β2-integrin-regulated metabolic phenotype of BM-DCs

We have previously identified the transcription factor Ikaros (Ikzf1) as a major integrin-regulated factor involved in DC activation.[18] Ikaros has been reported to function both as

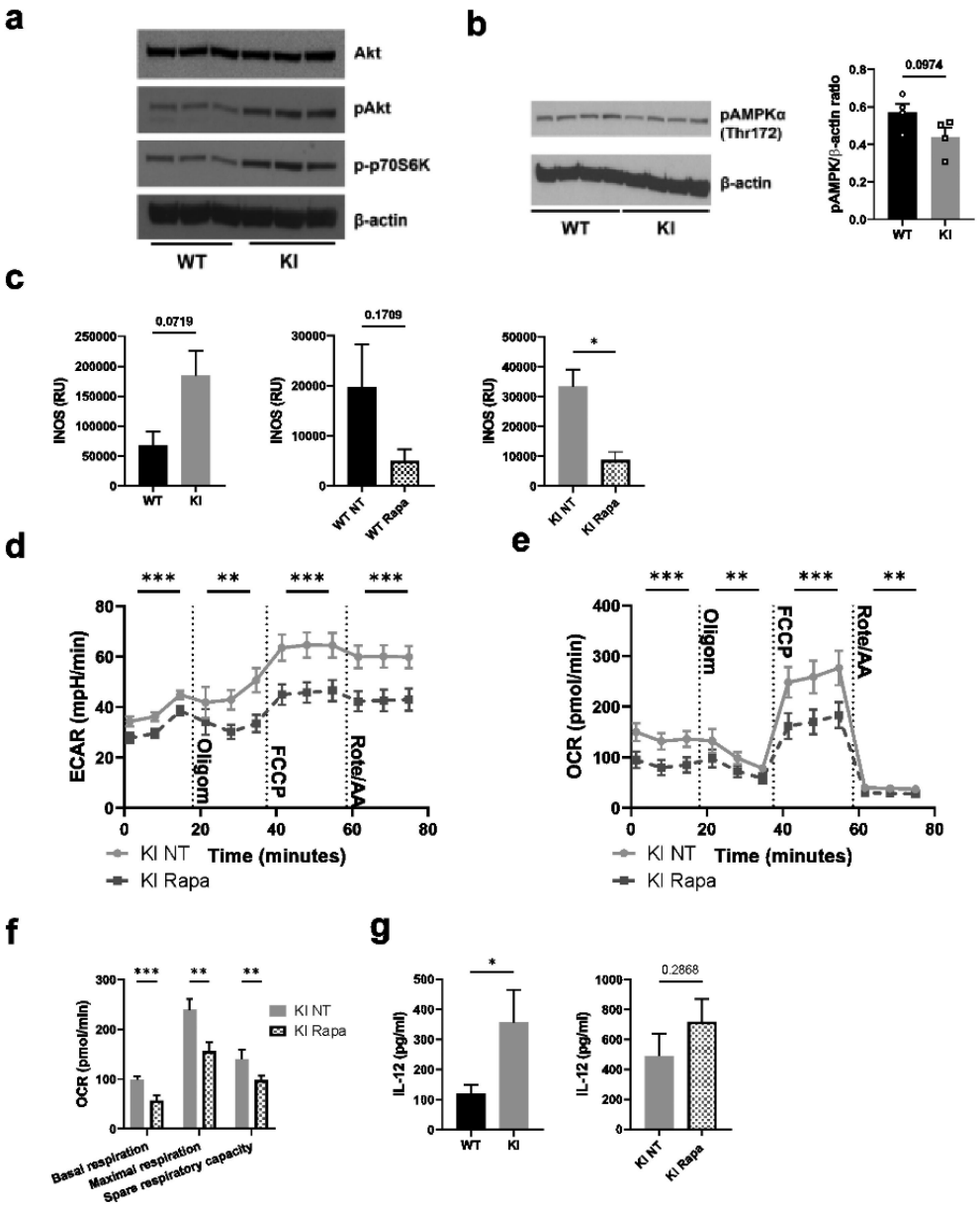

Figure 4. mTOR pathway is not responsible for the altered metabolic profile of β2-integrin KI BM-DCs. The activity of a) mTOR and b) AMPK pathways in WT and β2-integrin KI BM-DCs were assessed by Western blotting of (a) pAkt, phopho-p70S6K and b) pAMPKα (Thr172) (n=3–4). (b) for pAMPKα (Thr172), both the blot and quantification of the result are shown. (c) iNOS expression in WT and β2-integrin KI BM-DCs was determined by qRT-PCR in the presence or absence of rapamycin (n=3). (d) ECAR and e) OCR in β2-integrin KI BM-DCs, in the presence or absence of rapamycin, were analysed by Seahorse Extracellular analyser with a Mito Stress Test Kit (n=4) and (f) parameters of mitochondrial respiration were calculated from rates of oxygen consumption shown in (e). (g) ELISA was used to assess IL-12 production in WT and β2-integrin KI BM-DCs in the presence or absence of rapamycin. Data in g) is pooled from six (WT vs. KI) or four (KI vs. KI rapa) independent experiments. p-values are shown as <0.05*, <0.01**, <0.005***.

a transcriptional activator and a repressor, and to play a major role in DC development and function.[25,26] Furthermore, our published data show that Ikaros plays a pivotal role in regulating a transcriptional network governing DC activation and migration in integrin-deficient cells.[18] Therefore, to explore a putative role of Ikaros in regulating the metabolic phenotype of integrin-deficient DCs, we investigated the gene expression profile of

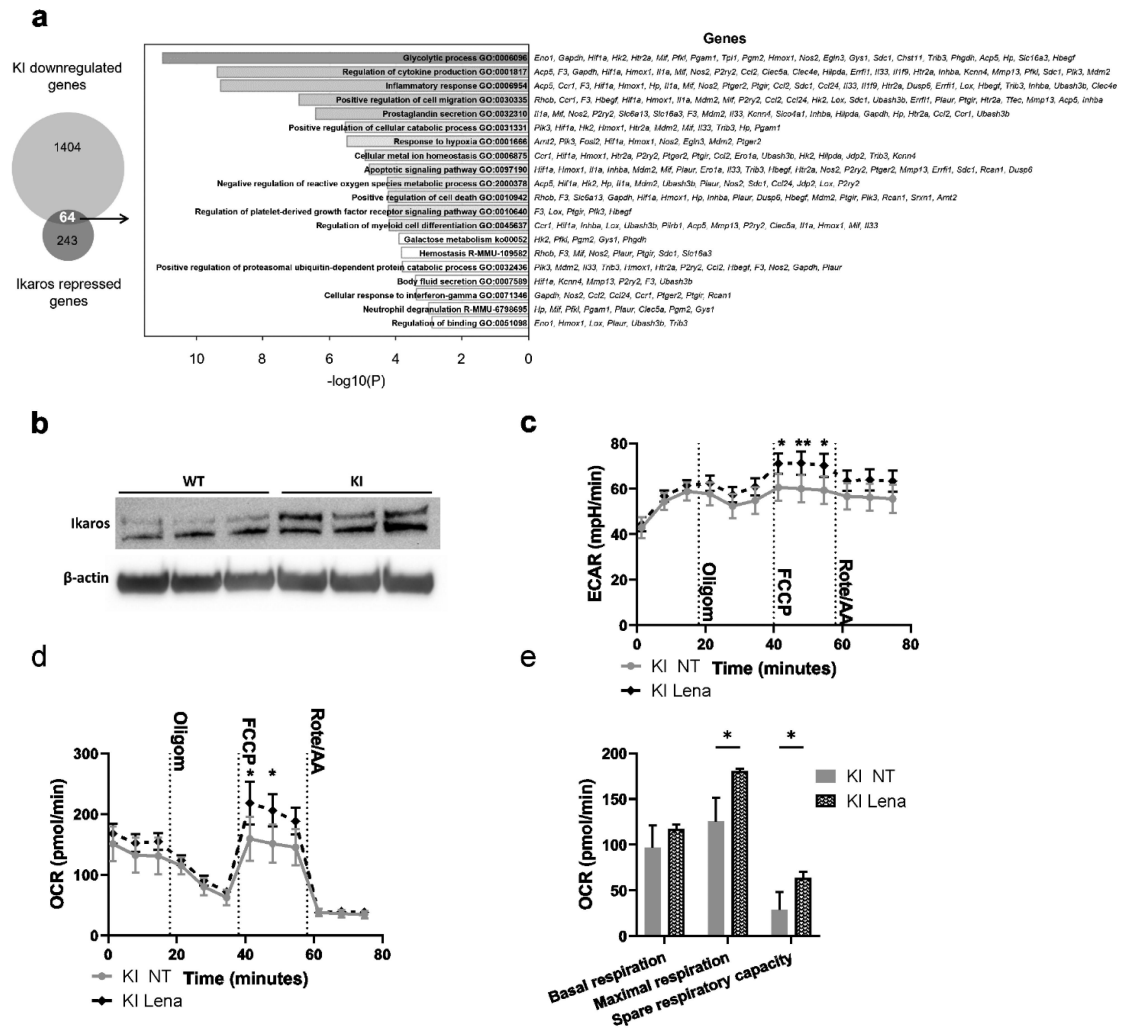

Figure 5. Transcription factor Ikaros has a key role in regulating β2-integrin-deficient BM-DC metabolism. (a) Comparison of genes repressed by Ikaros and genes being downregulated in β2-integrin KI BM-DCs. Here, the Ikaros-regulated genes are taken from[27] and the genes being downregulated in β2-integrin KI cells are based on RNA-Seq expression data.[18] GO-analysis result of the 64 intersect genes are also listed in a). (b) Ikaros levels in WT and β2-integrin KI BM-DCs was assessed by Western blotting (n=3). (c) ECAR and d) OCR in β2-integrin KI BM-DCs in the presence or absence of lenalidomide was assessed by Seahorse Extracellular Analyser with Mito Stress Test Kit as described in Materials and Methods (n=3). (e) Parameters of mitochondrial respiration were calculated based on OCR data shown in d). P-values are shown as <0.05*, <0.01**.

β2-integrin KI BM-DCs and compared that to Ikaros repressed genes.[27] Our bioinformatics analysis indicated an overlap between Ikaros-repressed genes[27] and genes downregulated in β2-integrin KI BM-DCs (64 genes; Figure 5a). Interestingly, based on pathway analysis, genes involved in the glycolytic process scored the highest among the overlapping genes (Figure 5a). In addition, we found that the Ikaros levels were increased in β2-integrin KI BM-DCs compared to WT cells (Figure 5b). Therefore, to explore the functional role of Ikaros in mediating the integrin-regulated suppressed metabolic phenotype of BM-DCs, we utilized lenalidomide, an inhibitor of the Ikaros family transcription factors that leads to their selective proteasome-induced degradation.[28] Indeed, the treatment of β2-integrin KI BM-DCs with lenalidomide increased the rates of both ECAR and OCR and thus reversed their metabolic phenotype (Figure 5c–e) but did not affect metabolism in WT cells (Supplementary SFig 1e). In particular, lenalidomide treatment led to upregulation of ECAR rates under conditions of metabolic stress (e.g. after FCCP treatment) in β2-integrin KI BM-DCs (Figure 5c). In addition, lenalidomide treatment led to increased oxidative phosphorylation, in particular, upregulation of maximal respiration and spare respiratory capacity in β2-integrin KI BM-DCs (Figure 5d–e, Supplementary

Fig S1f). In contrast, lenalidomide did not significantly alter Glut1 expression or glucose uptake in KI cells (Supplementary Fig S1g-h), indicating that glucose uptake alone is not responsible for the Ikaros-regulated metabolic phenotype. Together, these results indicate a key role of this transcription factor in repressing the metabolic phenotype of integrin-deficient BM-DCs.

Mimicking integrin-regulated metabolic suppression with low-dose 2DG activates BM-DCs through an epigenetic mechanism

Here, we show that BM-DCs expressing dysfunctional integrins display a suppressed metabolic phenotype. To explore whether such integrin-regulated metabolic suppression may contribute to DC activation, we investigated the consequences of WT BM-DCs treatment with various concentrations of 2-deoxy glucose (2DG), an inhibitor of glycolysis

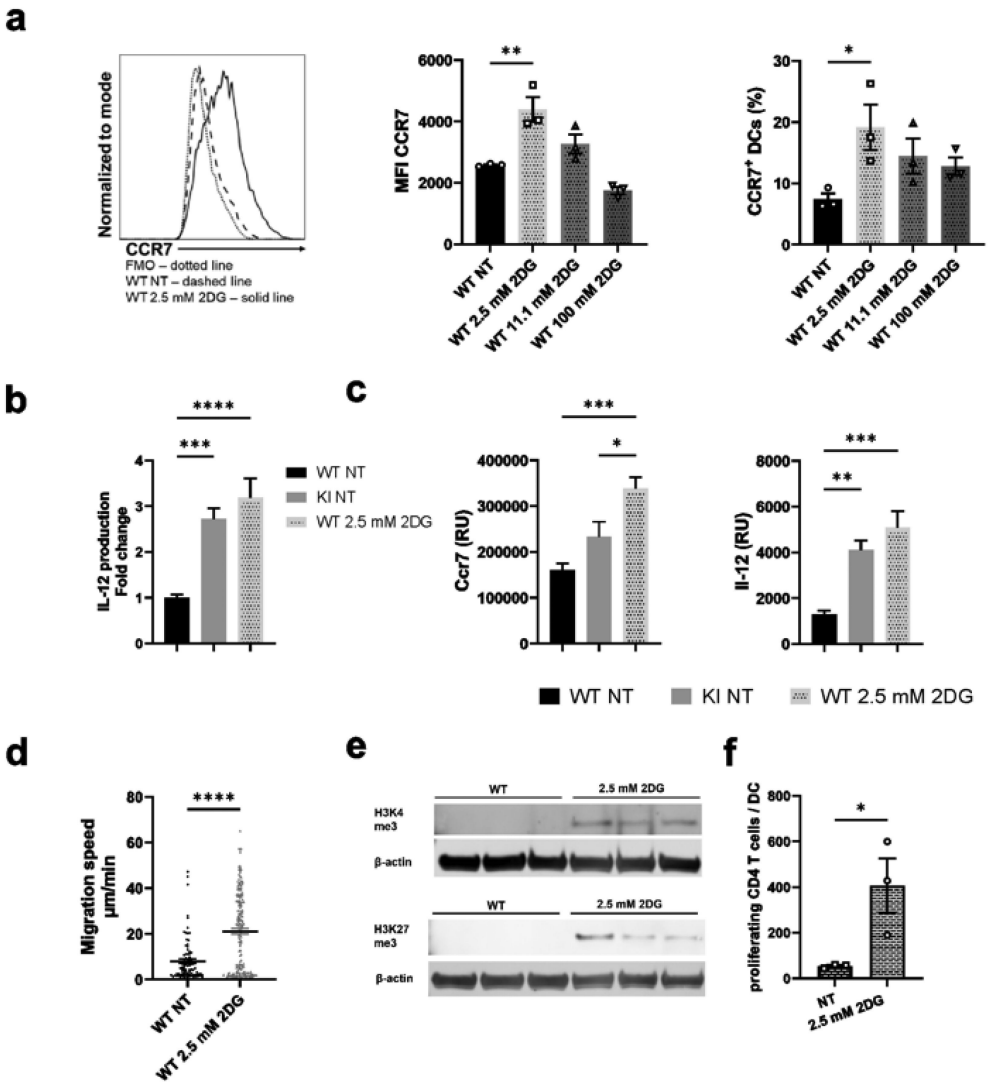

Figure 6. Inducing metabolic stress with low-dose 2DG activates BM-DCs. a) WT BM-DCs were treated with different amounts of 2DG, after which CCR7 expression was assessed by flow cytometry. Representative histograms for NT WT and 2.5 mM 2DG-treated WT BM-DCs, MFIs and proportion of CCR7 expressing cells are shown (n=3). b) Production of IL-12 by NT WT, NT β2-integrin KI or 2.5 mM 2DG-treated WT BM-DCs was assessed by ELISA (n=15–16). Data is pooled from five independent experiments. c) mRNA expression of CCR7 and IL-12 in NT WT, NT β2-integrin KI and 2.5 mM 2DG-treated WT BM-DCs, was assessed by qRT-PCR (n=5). d) Migration speed of WT BM-DCs with or without 2.5 mM 2DG-treatment in a 3D collagen matrix in response to a CCL19 gradient was assessed as described in the Materials and Methods (n=3 mice, a total of 267 WT and 346 2DG-treated WT cells were tracked). e) Histone methylation of H3K4me3 and H3K27me3 in NT WT and 2DG-treated WT BM-DCs was assessed by Western blotting (n=3). f) T cell proliferation was assessed by MLR by culturing CD4 T cells with NT or 2.5mM 2DG-treated BM-DCs. p-values are shown as <0.05*, <0.01**, <0.005***, <0.0001****.

(Figure 6). 2DG is a glucose analog that competes with glucose by binding to hexokinase, the rate-limiting enzyme of glycolysis, but it also reduces oxidative phosphorylation in cells by affecting pyruvate levels that feed into the TCA cycle, fueling oxidative phosphorylation.[29] Interestingly, metabolic suppression induced by treatment of WT BM-DCs with a low-dose of 2DG (2.5 mM) (in the presence of 11.1 mM glucose in the media) indeed led to their activation. Specifically, a low-dose 2DG treatment led to increased expression of the chemokine receptor CCR7 and production of the cytokine IL-12, both on the protein and mRNA levels (Figure 6a–c), whilst a higher dose of 2DG (11.1 mM), which blocks glycolysis and reduces oxidative phosphorylation in cells[29] did not have this effect (Figure 6a). In addition, other low doses of 2DG, 1 mM and 5 mM, resulted in lower CCR7 expression and/or IL-12 production in WT BM-DCs compared to 2.5 mM 2DG-treatment, suggesting 2,5 mM being the optimal 2DG dose to activate BM-DCs (Supplementary Fig S2a). Low-dose (2,5 mM) 2DG-treatment also led to significantly increased BM-DC migration speed in a 3D collagen matrix in response to the chemokine CCL19 (Figure 6d). In contrast, 2.5 mM 2DG treatment did not affect the expression of CD40, CD86, CD80, or MHC-II in WT cells (Supplementary Fig S2b), indicating that all aspects of the activated DC phenotype are not affected by suppressed cell metabolism. 2.5 mM 2DG treatment led to a further increase in CCR7 expression and IL-12 production also in β2-integrin KI cells (Supplementary Fig S2c), showing that further suppression of metabolism can also activate KI cells. However, compared to WT cells, 2.5 mM 2DG-treatment did not significantly increase the proportion of cells expressing CCR7 in the β2-integrin KI population, whilst in WT cells the proportion was significantly increased (Supplementary Fig S2d). Together with the experiments showing that metabolism is significantly reduced in β2-integrin KI cells, this experiment shows that reduced metabolism downstream of integrins in DCs may contribute to their activation.

Interestingly, 2.5 mM 2DG-treatment also increased CCR7 expression in LPS-activated BM-DCs (Supplementary Fig S3a) and in LPS or CpG activated Flt3L-induced BM-DCs (Supplementary Fig S3b-c). Notably, in Flt3L-induced BM-DCs, CCR7 expression significantly increased in CpG-activated conventional DC type 1 (cDC1) population and also in CpG or LPS-activated conventional DC type 2 (cDC2) population following 2.5 mM 2DG-treatment (Supplementary Fig S3c). In addition, 2.5 mM 2DG-treatment also increased CCR7 expression in a recently characterized human DC cell line (CAL-1) (Supplementary Fig S3d), thereby expanding a potential role for metabolic suppression in DC activation also to other murine DC populations and to human cells. However, changing the metabolic rate of WT BM-DCs in other ways, such as by excluding glucose or glutamine from the medium (thereby reducing glycolysis and glutaminolysis), did not significantly change BM-DC CCR7 or IL-12 expression (Supplementary Fig S4a). Similarly, treating cells with varying concentrations of rotenone (to inhibit oxidative phosphorylation) did not lead to a significant increase in IL-12 production (Supplementary Fig S4b). Interestingly, treating WT BM-DCs with benserazide, an inhibitor of Hk2 (a rate limiting enzyme of the glycolytic pathway), led to increased proportion of cells expressing CCR7 but did not affect CCR7 MFI or IL-12 production (Supplementary Fig S4c). These results indicate that blocking glycolysis or oxidative phosphorylation alone did not result in BM-DC activation; rather, partial metabolic suppression (of both glycolysis and oxidative phosphorylation, by using low-dose 2DG) was required to achieve BM-DC activation.

We have previously shown that β2-integrins regulate BM-DC activation through an epigenetic mechanism (H3K4me3 and H3K27me3 on specific genes).[18] Interestingly, low-dose 2DG-treatment of BM-DCs also increased both H3K4me3 and H3K27me3 levels in WT BM-DCs, indicating that suppressing glycolytic metabolism increases DC activation through an epigenetic effect (Figure 6e).

To investigate whether the low dose 2DG-induced increase in DC activation also correlates with T cell responses, we performed mixed lymphocyte reactions (MLR) of either non-treated (NT) or low dose 2DG-treated BM-DCs with T cells. Interestingly, T cell proliferation was significantly increased with 2.5 mM 2DG-treated DCs compared to NT DCs, showing the functional significance of metabolic suppression in DC phenotype (Figure 6f). In conclusion, metabolic suppression induced by low-dose 2DG-treatment activates BM-DCs in a similar way as integrin deficiency.

Metabolic suppression of BM-DCs with low dose 2DG-treatment ex vivo improves their anti-tumor responses in vivo

Our data indicate that metabolic suppression contributes to BM-DC reprogramming to an active, migratory phenotype. We have previously shown that integrins and integrin-regulated BM-DC epigenetic reprogramming regulate BM-DC anti-tumor responses through a CCR7-dependent mechanism.[18] As we show here that partially suppressing BM-DC glycolytic metabolism leads to BM-DC activation (increased cytokine responses, CCR7 expression, migration speed, and T cell activation potential), we decided to explore the effect of 2DG-induced metabolic stress in BM-DCs on tumor growth *in vivo*. For this, we used a well-established immunogenic mouse melanoma tumor model (B16-OVA). Following tumor establishment, WT mice were injected peritumorally either with PBS (Mock), with NT WT BM-DCs or with low-dose 2DG-treated WT BM-DCs, after which tumor growth was followed (Figure 7a). Interestingly, the treatment of tumor-bearing mice with 2DG-treated WT BM-DCs led to significantly reduced tumor growth compared to mice treated with non-treated WT BM-DCs (Figure 7b,d). Further, treatment with 2DG-treated WT BM-DCs also led to the elimination of tumors in a notable percentage of the mice (Figure 7c). Finally, even though the low-dose 2DG-treatment caused some decrease in BM-DC viability (Supplementary Fig S4d), 2DG-treated WT BM-DCs were still able to induce stronger anti-tumor response *in vivo* compared to NT WT BM-DCs.

Next, we performed immunophenotyping to the B16-OVA tumors harvested at the end of the experiment, to assess tumor

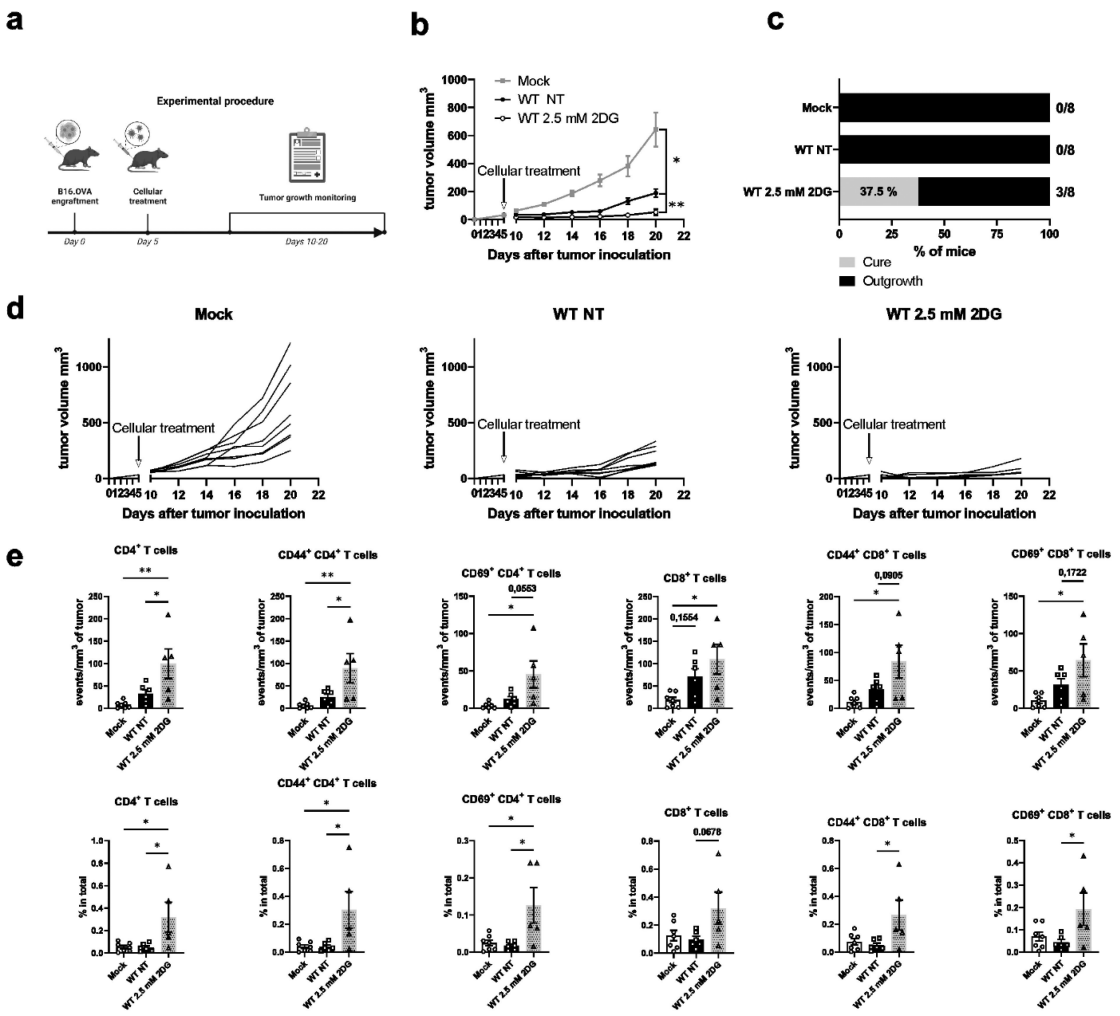

Figure 7. Metabolic suppression improves BM-DC-mediated anti-tumor responses in vivo. a) Experimental design of the tumor experiment. b) Growth of B16-OVA melanoma tumors before and after peritumoral injection of PBS (Mock), non-treated (NT) WT BM-DCs or WT BM-DCs treated with 2.5mM 2DG (n=8 mice per group). Tumor growth was measured every 2 d. c) the fractions of mice with tumor biomass (outgrowth) and no tumor biomass (cure) 20 d after tumor inoculation. d) Individual growth curves of B16-OVA melanoma tumors before and after peritumoral injection of PBS (Mock) (left panel), non-treated WT BM-DCs (middle panel) or WT BM-DCs treated with 2.5mM 2DG (right pane). e) Numbers and proportions of CD4 T cells, $CD44^+$(memory) CD4 T cells, $CD69^+$ (activated) CD4 T cells, CD8 T cells, $CD44^+$ (memory) CD8 T cells and CD69+ (activated) CD8 T cells in tumors, relative to tumor volume were determined flow cytometrically. P-values are shown as <0.05 *, <0.01 **.

infiltrating T cell populations. Overall, 2.5 mM 2DG BM-DC-treated tumors were more heavily infiltrated by $CD45^+$ leukocytes compared to the NT DC-treated or Mock-treated tumors (Figure 7e, Supplementary Fig S4e). There was an increase in CD4 T cell numbers as well as their proportions in tumors treated with 2DG BM-DCs compared to NT BM-DCs (Figure 7e). There were also more CD4 cells expressing CD44 (a memory T cell marker) in the tumors treated with 2DG-BM-DCs compared to NT DCs (Figure 7e). In addition, the proportion of activated (CD69-expressing) CD4 and CD8 T cells in the tumors (of total cells) were both increased, compared to tumors from NT DC-treated mice (Figure 7e). In conclusion, metabolic suppression with low-dose 2DG leads to BM-DC activation and increased anti-tumor responses mimicking loss of integrin-mediated adhesion, thus indicating a functional role for metabolic suppression in BM-DCs.

Discussion

Integrins are adhesion and mechanoreceptors that interact with the extracellular matrix, soluble proteins, or receptors on other cells using their extracellular domains and with cytoskeletal and signaling proteins on the intracellular side. Integrins allow cells to "read" the mechanical properties of

the microenvironments they reside in, leading to the activation of mechano-signaling pathways, which can also affect gene expression.[30] DCs downregulate integrin adhesion when they become activated by infectious signals and need to become migratory,[5,7,31,32] and thus, migDCs *in vivo* express low levels of β2-integrins.[6] We have previously shown that BM-DCs expressing dysfunctional β2-integrins display increased activation *in vitro* and *in vivo*, increased T-cell stimulation capabilities, and increased anti-tumor responses *in vivo*. This integrin-regulated elevated activation of BM-DCs was shown to involve epigenetic regulation (increased H3K4me3 and H3K27me3-levels) of a large number of genes, including those encoding for maturation markers (CD40, CD80, and CD86), cytokines (IL-12), and chemokine receptors (CCR7).

Here, we show that β2-integrin-mediated adhesion also extensively regulates BM-DC metabolic profile. Loss of adhesion leads to a significant downregulation of metabolic rate in BM-DCs. We show that this is associated with lower protein translation, reduced levels of cellular ATP (and ADP but not AMP), reduction in many glycolytic enzymes and glucose transporters, reduced glucose uptake, and ROS production. Cells therefore acquire a metabolically repressed state as a consequence of loss of cell adhesion. In addition to glycolysis and mitochondrial function, metabolomics studies revealed that several other pathways are also dysregulated, such as amino acid metabolism. Interestingly, we show that this integrin-regulated metabolic suppression is not regulated by the master metabolic regulator, mTOR but is at least partly controlled by the transcription factor Ikaros (Ikzf1), which we have previously shown to control integrin-regulated BM-DC activation.[18] Indeed, loss of Ikaros has been reported to lead to increased integrin activity, cell adhesion, and signaling in B cells.[33] Ikaros has also been reported to restrict glycolytic metabolism in B cells, by regulating glucose uptake and glycolytic signaling.[34] Together, these and our studies therefore show that Ikaros plays a major role as a "metabolic gatekeeper" in immune cells, restricting glycolytic processes in these cells leading to major consequences for immune cell function.

What we show here is profoundly different to what has been reported to take place during DC activation through pattern recognition receptors (PRRs), leading to significantly increased aerobic glycolysis but suppressed oxidative phosphorylation through HIF-1α and iNOS/nitric oxide (NO) production (NO inhibiting oxidative phosphorylation).[9] The cell activation-associated increase in glycolysis has been shown to support fatty acid synthesis required for endoplasmic reticulum growth and synthesis of costimulatory molecules, cytokines, and chemokines[9] and for the generation of ATP when oxidative phosphorylation is downregulated. In addition, inhibiting glycolysis by using high levels of 2DG has previously been shown to block LPS-induced BM-DC activation and DC-mediated T cell activation.[35] Further, glucose and glycolysis have also been shown to be important for CCR7 oligomerization in DCs and for DC migration.[36] In contrast, in integrin-deficient cells, decreased cell adhesion leads to increased BM-DC activation and epigenetic changes, resulting in increased expression of DC activation markers, cytokines, and chemokine receptors,[7,18] but also to reduced metabolic rates (this study). It is important to note that in our system, there is no PRR stimulation of the cells, only loss of adhesion leading to loss of interaction of the cells with their extracellular microenvironment.

We further show that restriction of glycolysis in WT BM-DCs by low-dose (2.5 mM) 2DG-treatment leads to a similar response as integrin deficiency. A low dose of 2DG is expected to reduce both the rates of glycolysis and oxidative phosphorylation in BM-DCs,[29] but not to block these pathways completely. Thereby, low-dose 2DG induces a suppressed metabolic phenotype similar to that seen in integrin-deficient cells, whilst complete blocking of glycolysis or oxidative phosphorylation did not have the same effect. We show that the treatment of BM-DCs with low concentration of 2DG leads to increased expression of CCR7 and IL-12, increased 3D migration *in vitro*, enhanced T cell activation potential *in vitro*, and induced epigenetic changes (changes in histone methylation) in the cells. Importantly, low-dose 2DG-treated BM-DCs also induce enhanced anti-tumor responses *in vivo* leading to reduced tumor growth, increased number of cures, and increased T cell infiltration into tumors in a mouse melanoma model. These results indicate that (integrin-mediated) metabolic control of DCs is also functionally important.

Glucose has previously been shown to limit BM-DC responses but in the context of TLR activation (by LPS).[22] After the initial high need of glucose, at later time points, glucose seems to restrict LPS-induced BM-DC responses and T cell activation, as replacement of glucose with galactose actually stimulates BM-DCs.[22] These results indicate that sustained high glycolysis also represses TLR-induced BM-DC activation. We show here that 2.5 mM 2DG treatment also enhances CCR7 expression in LPS treated DCs, in line with these previously published results.

Trained immunity or innate immune memory refers to a process in which innate immune cells, including DCs, display long-term epigenetic and metabolic reprogramming upon several types of stimuli, such as PRRs. In addition, as a consequence of this reprogramming, innate immune cells display altered responses toward a secondary challenge. Hence, the term "innate immune memory" has been coined to describe these alterations.[20] Interestingly, loss of adhesion results in epigenetic changes in BM-DCs (changes in H3K4me3 and H3K27me3 status).[18] The cells also display increased responses to secondary challenges such as LPS.[7] Here, we show that loss of adhesion also leads to a repressed metabolic phenotype of BM-DCs, which is functionally important. Our results therefore indicate that innate immune cells such as DCs display epigenetic and metabolic reprogramming upon loss of adhesion. We call this process "mechanical immune memory". Loss of adhesion may be a "danger signal" which activates DCs and leads to reprogramming and altered responses to a secondary challenge. Mechanical disruption of DC cellular interactions has indeed previously been found to lead to profound DC activation, but the underlying mechanisms have remained poorly understood.[37] We thus propose that mechanical interactions between tissue innate immune cells with their microenvironment have a bigger impact on immune responses than previously thought.

It is striking that treatment with low dose of 2DG, an inhibitor of glycolysis and oxidative phosphorylation, induces metabolic reprogramming of BM-DCs in a similar manner as integrin deficiency.[18] Importantly, this DC activation caused by metabolic restriction is reflected in increased DC-mediated tumor growth inhibition *in vivo*, presumably by affecting CCR7-dependent DC migration to lymph nodes and/or T cell activation, where IL-12 production plays a major role, or a combination of these effects. We show here that 2.5 mM 2DG-treatment increases CCR7 expression also in Flt3L-induced BM-DCs (which more closely resemble *in vivo* cDCs compared to GM-CSF-induced DCs) and in a human DC cell line. In the future, it will be essential to investigate the effect of low-dose 2DG treatment (or similar) on human primary DCs. DC-based immunotherapies are promising as they are already in clinical use, considered to be safe and induce immune responses in at least half of the treated patients.[2] However, their clinical efficacy is less impressive, and these therapies clearly need to be further optimized.[2] For example, the migratory and T cell activation capabilities of current DC vaccines are still relatively poor.[2] Based on the results presented here and previously,[18] targeting integrins or integrin-regulated epigenetic or metabolic pathways may therefore be a useful way to optimize DC-based immunotherapeutic approaches to tumors in the future and could also be combinable with other immunotherapeutic approaches such as immune checkpoint inhibitors.

Materials and methods

Mice and bone marrow collection

Integrin TTT/AAA β2-integrin knock-in mice (β2-integrin KI) have been previously described.[38] C57BL/6N WT littermates were purchased from Charles River and were used as controls for β2-integrin KI mice. Experiments were performed using male and female mice between ages 8 and 39 weeks. Animals were housed under conventional conditions in groups of up to five animals per cage with free access to food and water. Bone marrow was collected from euthanized animals and used for BM-DC cultures immediately. For the tumor experiment, C57BL/6J female mice were purchased from Charles River. Mice were 24 weeks old when the experiment started. All the experiments were performed according to the Finnish Act on the Protection of Animals Used for Scientific or Educational Purposes (497/2013) and to the Directive 2010/63/EU of the European Parliament and of the Council of 22 September 2010 on the protection of animals used for scientific purposes and approved by the Finnish National Animal Experiment Board (Hankelupalautakunta – ELLA).

BM-DC culture

BM-DCs were generated by culturing bone marrow cells for 9–10 d in DC media: 10 ng/ml GM-CSF (Peprotech, cat. # AF-315-03) in RPMI (Lonza, cat. # 12-167F/EuroClone, cat. # ECB9006L) supplemented with 10% FCS (Gibco, cat # 10500–064), 100 U/ml penicillin–streptomycin (penicillin, Orion, cat. # 465161; streptomycin Thermo Fisher Scientific, cat. # D7253-100 g) and 2 mM L-glutamine (Thermo Fisher Scientific, cat. # BP379–100), at 37°C in a humidified atmosphere of 5% CO_2. Media were added/changed on days 3, 6, and 8. In some experiments, cells were treated overnight with 20 nM rapamycin (Sigma-Aldrich, cat. # R8781-200UL), 10 μM Lenalidomide (Sigma-Aldrich, cat. # SML2283), 2DG (various concentrations) (Sigma-Aldrich, cat. # D8375), rotenone (various concentrations) (Sigma-Aldrich, cat. # R8875), glucose (various concentrations) (Sigma-Aldrich, cat. # G7021), L-glutamine (Thermo Fisher Scientific, cat. # BP379–100), benserazide (various concentrations) (Sigma-Aldrich, cat. # B7283) or 100 ng/ml LPS (Sigma-Aldrich, cat. # L6529). In glucose and glutamine exclusion experiments, cells were grown as above but overnight in RPMI media without glucose (MP Biomedicals, cat. # 091646854). To generate Fl3L-induced BM-DCs, bone marrow cells were cultured in 200 ng/ml Flt3L (Peprotech, cat. # 250-31 L) for 9 days, with feeding on days 3 and 6. On day 9, cells were stimulated overnight with 200 ng/ml Flt3L and either 1 μM CpG (InvivoGen, cat. # tlrl-1826) or 100 ng/ml LPS with or without 2.5 mM 2DG.

Tumor models and cell lines

The ovalbumin-expressing murine melanoma cell line B16-OVA was provided by Prof. Richard Vile (Mayo Clinic, Rochester, MN, USA). Mycoplasma test was routinely done one-week post-culture by analyzing the supernatant of the cells with MycoAlertTM Mycoplasma Detection Kit (Lonza, cat. #: LT07). The cell line was cultured in RPMI medium (Lonza, cat. # 12-167F) supplemented with 10% FBS (Thermo Fisher Scientific, cat. # 10500–064), 2 mM L-glutamine (Thermo Fisher Scientific, cat. # BP379–100), 1% penicillin/streptomycin (penicillin, Orion cat. # 465161; streptomycin Thermo Fisher Scientific, cat. # D7253-100 g). B16-OVA was cultured under Geneticin (Thermo Fisher Scientific, cat. # 10131035) selection at 37°C in a humidified atmosphere of 5% CO_2. The human DC cell line CAL-1[39] was obtained from Leibniz-Institut Deutsche Sammlung von Mikroorganismen und Zellkulturen (DSMZ, #ACC923). Cells were cultured in a complete growth medium (RPMI 1640 supplemented with 10% FCS, 100 U/ml penicillin–streptomycin (penicillin, Orion, cat. # 465161; streptomycin Thermo Fisher Scientific, cat. # D7253-100 g) and 2 mM L-glutamine (Thermo Fisher Scientific, cat. # BP379–100)), at 37°C in a humidified atmosphere of 5% CO_2. Cells were treated with 10 ng/ml human GM-CSF (Peprotech, cat. # 300–03) for 3 d and then cultured overnight without GM-CSF but with or without 2.5 mM 2DG.

Seahorse analysis

Oxygen consumption rate (OCR) and extracellular acidification rate (ECAR) were measured with Seahorse XF96 extracellular analyzer (Agilent) by using Seahorse XF Cell Mito Stress Test Kit (Agilent, cat. # 103015–100). Briefly, BM-DCs were detached with 5 mM EDTA in PBS and 100 000 cells/well plated in DC media on Seahorse XF96 cell culture microplates (Agilent, cat. # 101085–004). Following an o/n incubation at 37°C, 5% CO_2, the plates were centrifuged 300 G for 3 min at +4°C and DC media was

replaced by pre-warmed Seahorse media (Seahorse XF RPMI [Agilent, cat. # 103576–100], supplemented with 10 mM glucose [Sigma-Aldrich, cat. # D9434], 5 mM pyruvate [Sigma-Aldrich, cat. # P8574] and 5 mM glutamine [Sigma-Aldrich, cat. # G3126] and adjusted to pH 7.4). After 1 h incubation at 37°C, avoid from CO_2, the basal OCR and ECAR were measured, followed by sequential injection of oligomycin (1 µM) (Sigma-Aldrich, cat. # O4876), FCCP (1 µM) (Sigma-Aldrich, cat. # C2920), and rotenone/antimycin A (1 µM) (Sigma-Aldrich, cat. # R8875, A8678) at the indicated time points. Parameters such as basal respiration, maximal respiration, and ATP production were calculated according to manufacturer's instructions (Agilent). Data analysis was done by using Wave software (Agilent) and finalized in Excel and GraphPad Prism. All experiments had ten technical replicates, and in some experiments, the inhibitor treatments were added for o/n incubation.

Targeted LC-MS metabolomics profiling

BM-DCs were collected from petri dishes by scraping into ice-cold PBS and pelleted. Metabolites were extracted from cell pellets using 400 µl of ice-cold extraction solvent (Acetonitrile:Methanol:MQ; 40:40:20; Thermo Fisher Scientific, ACN cat. # A955–212, MeOH cat. # A456–212) and subsequently, samples were vortexed for 2 min, sonicated for 1 min followed by centrifugation at 14000 rpm at 4°C for 5 min. Supernatants were transferred into HPLC glass auto sampler vials (Thermo Fisher Scientific cat. # 11575894) and 2 µl of samples were injected into the Thermo Vanquish UHPLC coupled with Q-Exactive Orbitrap quadrupole mass spectrometer equipped with a heated electrospray ionization (H-ESI) source probe (Thermo Fisher Scientific) for analysis. The gradient elution was carried out with the following settings: flow rate of 0.100 ml/min using 20 mM ammonium hydrogen carbonate, adjusted to pH 9.4 with ammonium solution (25%) as mobile phase A and acetonitrile as mobile phase B. The gradient elution was initiated from 20% of mobile phase A and 80% of mobile phase B and maintained till 2 min, followed by 20% of mobile phase A gradually increasing up to 80% till 17 min, then 80% to 20% Mobile phase A decrease in 17.1 min and maintained up to 24 min. The column oven and auto-sampler temperatures were set to 40 ± 3°C and 5 ± 3°C, respectively. MS had the following settings: polarity switching, resolution of 35,000, the spray voltages of 4250 V for positive and 3250 V for negative mode, the sheath gas: 25 arbitrary units (AU), and the auxiliary gas: 15 AU, sweep gas flow 0, Capillary temperature: 275°C, S-lens RF level: 50.0. Instrument control was operated with the Xcalibur 4.1.31.9 software (Thermo Fisher Scientific), and the peak integration was done with the TraceFinder 4.1 software (Thermo Fisher Scientific) using confirmed retention times standardized with library kit (Merck, cat. # MSMLS-1EA). The data quality was monitored throughout the run using an in-house serum QC sample and interspersed throughout the run as every 10th sample. The metabolite data were checked for peak quality (poor chromatograph), % RSD, and carryover. The intensity peak area data was provided as an Excel spread sheet and further analyzed with the publicly available MetaboAnalyst platform.

Glucose uptake

Glucose uptake was measured using Glucose Uptake-Glo™ Assay kit (Promega, cat. # J1341) following manufacturer's protocol. Briefly, following BM-DC generation, the cells were detached and seeded on 96-well tissue culture treated with sterile ViewPlate microplate (PerkinElmer, cat. # 6005181) at 1×10^6/ml concentration. Following an overnight incubation at 37°C in a humidified atmosphere of 5% CO_2, the cells were washed with PBS (Lonza, cat. # 17-516F) and 1 mM 2DG (Sigma-Aldrich, cat. # D9761-100 MG) was added for 10 min. After stopping and neutralizing the 2DG uptake, 2-deoxyglucose-6-phosphate detection reagent was added for 2 h in dark RT. Luminescence was measured using Enspire™ Multimode plate reader and data analysis was done with GraphPad Prism. All reagents were included in the kit J1341 unless otherwise specified.

Translation rate analysis

The translation rate of BM-DCs was measured through covalent incorporation of Puromycin (Gibco, cat. # A11138–03) into nascent proteins and assayed through flow cytometry using an anti-Puromycin PE conjugated antibody (BioLegend, cat. # 381503) after fixing and permeabilizing the cells using the Foxp3 permeabilization kit (eBiocience, cat. # 00-5523-00). As a negative control, translation was blocked by treating the cells with Harringtonine (Sigma-Aldrich, cat. # SML1091-10 MG) at 2 µg/ml for 30 min before the addition of Puromycin. Puromycin was added at 10 ug/ml for 45 min after 30 min of incubation with the inhibitor. The incorporation of puromycin was then assayed via flow cytometry.

ROS measurements

The level of ROS was assessed with ROS-ID Total ROS/Superoxide Detection Kit (Enzo, cat. # ENZ-51010) according to the manufacturer's protocol. Briefly, BM-DCs were first washed with a wash buffer and then resuspended in a wash buffer with a concentration of 2×10^6 cells/ml. 5×10^5 cells were transferred in flow cytometry tubes, mixed with equal amount of 2× staining solution and incubated coverage from light at +37°C for 30 min. Data were collected using an LSR Fortessa flow cytometer (Becton Dickinson) and analyzed with FlowJo (Tree Star).

Mitochondrial membrane potential

The level of mitochondrial membrane potential was assessed by using MITO-ID Membrane Potential Detection Kit (Enzo, cat. # 51018) according to the manufacturer's instructions. Briefly, 5×10^5 BM-DCs per sample were first washed with an assay solution and then resuspended in a detection reagent and incubated coverage from light at RT for 15 min. Data were immediately collected following incubation using an LSR

Fortessa flow cytometer (Becton Dickinson) and later analyzed with FlowJo (Tree Star).

ADP/ATP ratio

ADP, ATP, and ADP/ATP ratios were determined with ADP/ATP Ratio Assay Kit (Sigma-Aldrich, cat. # MAK135) by following the manufacturer´s protocol. Shortly, BM-DCs were detached and transferred onto the assay microplate, sterile 96-well tissue culture-treated ViewPlate microplate (PerkinElmer cat. # 6005181) with 10 000 cells/well. Following an o/n incubation at 37°C, 5% CO_2, culture medium was replaced with ATP reagent and luminescence read with luminometer (Enspire™ Multimode plate reader) after 1-min incubation at RT (RLU_A). The microplate was then incubated at RT for 10 min followed by another luminescence read to determine the level of background (RLU_B). ADP reagent was then added to the wells, and the luminescence was again read after 1-min incubation at RT (RLU_C). ADP/ATP ratio was calculated using the formula: ADP/ATP ratio = (RLU_C-RLU_B) /RLU_A.

Flow cytometry

The following conjugated antibodies were used for flow cytometric analysis of BM-DCs (company, catalog number, and clones given in brackets): CCR7-PE (BioLegend, cat. # 120105, clone 4B12), MHCII-APC-eFluor780 (eBioscience, cat. # 47-5321-82, clone M5/114.15.2), CD80-APC (cat. # 17-0801-81, eBioscience, clone 16-10A1), CD40-PE (cat. # 124609, BioLegend, clone 3/23), CD86-FITC (cat. # 11-0862-85, BD Biosciences, clone GL1), Puromycin-PE (BioLegend, cat. # 381503, clone 2A4). The following conjugated antibodies were used for flow cytometric analysis to determine T cells and DCs in MLR: CD3-AF488 (Invitrogen, cat. # 53-0031-82, clone 145-2C11), CD4-PE-Cy7 (BioLegend, cat. # 100528, clone RM4–5), CD11c-APC-ef780 (BioLegend, cat. # 117310, clone: N418). The following conjugated antibodies were used in tumor immunophenotyping: CD3-Biotin (eBioscience, cat. #13-0031-82, clone 145-2C11), CD69-FITC (BioLegend, cat. # 104506, clone H1.2F3), NK1.1-FITC (Invitrogen, cat. # 48-5941-82, clone PK136), Streptavidin-V500 (BD Bioscience, cat. # 561419), CD45-BV650 (BD Bioscience, cat. # 563410, clone 30-F11), CD8a-APC-Cy7 (BioLegend, cat. # 100714, clone 53–6.7), CD44-PE (BD Bioscience, cat. # 553134, clone IM7), CD4-PE-Cy7 (BioLegend, cat. # 100528, clone RM4–5). The following conjugated antibodies were used for flow cytometric analysis of Flt3L-induced BM-DCs: CCR7-PE (BioLegend, cat. # 120105, clone 4B12), MHCII-APC-eFluor780 (eBioscience, cat. # 47-5321-82, clone M5/114.15.2), CD11b-APC (eBioscience, cat. # 17-0112-82, clone M1/70), CD11c-PE-Cy7 (eBioscience, cat. # 25-0114-81, clone N418), B220-FITC (Southern Biotech, cat. # 1665-02S, clone RA3-6B2). The following conjugated antibody was used to flow cytometrically assess CCR7 expression in CAL-1 cell line: CCR7-PE (eBioscience, cat. # 12-1979-42, clone 3D12). Fc-receptor block (BD Pharmingen, cat. # 553142 clone 2.4G2) was used in all experiments assessing mouse cells, and unstained and FMO controls were included in all panels. Propidium iodide (Sigma-Aldrich, cat. # P4864) or 7-AAD (eBioscience, cat. # 00-6993-50) was used to detect dead cells. Acquisition was performed on an LSR Fortessa flow cytometer (Becton Dickinson), and data were analyzed using FlowJo software (Tree Star).

ELISA

The level of IL-12 from WT and β2-integrin KI BM-DC supernatants was assessed with Mouse IL-12/IL-23 p40 Allele-specific DuoSet ELISA kit according to the manufacturer's instructions (R&D, cat. # DY499). Briefly, a 96-well maxisorp microplate (Thermo Fisher Scientific, cat. # 442404) was first coated with capture antibody o/n. The next day, the wells were washed and blocked with a reagent diluent (1% BSA [Biowest, cat. # P6154] in PBS [Lonza, cat. # 17-516F]) for a minimum of 1 h. The plate was then washed, and standards and samples were added. Following a 2 h incubation, the plate was washed and the detection antibody was added to the wells. After 2 h, the plate was washed, and Streptavidin-HRP (R&D, cat # DY998) was added for 20 min. After washing, the substrate solution (R&D, cat. # DY499) was added in the wells. Following visible color development (or latest after 20 min), sulfuric acid (Acros Organics, cat. # 124645001; diluted 1:4 in water) was added to stop the reaction. The optical density was immediately determined at 450 nm and background at 540 nm wavelength using Multiskan GO spectrophotometer (Thermo Fisher Scientific). IL-12 concentration was determined based on the standard curve, and data analysis was done using Excel and GraphPad Prism. All washing steps were performed by washing the plate first three times with 0.05% Tween (Fisher BioReagents, cat. # BP337) in PBS and then once with PBS only. All reagents were included in the kit DY499 unless stated otherwise.

Western blotting

Cells were lysed in a cold M-PER lysis buffer (Thermo Fisher Scientific, cat. # 78501) in the presence of phosphatase and protease inhibitors (Thermo Fisher Scientific, cat. # A32961), and lysates were analyzed by standard Western blotting protocol using commercial gels (Invitrogen, cat. # NW04120) and nitrocellulose membrane (GE Healthcare, cat. # 10600004). Primary antibodies used were against H3K4me3 (Cell Signaling Technology, cat. #9751S), H3K27me3 (Cell Signaling Technology, cat. #9733S), GLUT1 (Millipore, cat. # 07–1401), p-AMPK (Cell signaling, cat. # 2535S), p-Akt (Cell signaling, cat. # 9275S), p-p70S6K (Cell signaling, cat. # 9234S), Akt (Cell signaling, cat. # 9272S), Ikaros (Santa Cruz, cat. # sc-398,265), and β-Actin (Cell signaling, cat. # 4970S). Quantification of the pAMPK blot was done by using Image Studio Lite (LI-COR).

qRT-PCR

Total RNA was isolated from BM-DCs with Nucleospin RNA kit (Macherey-Nagel, cat. # 740955) and converted into cDNA by using High-Capacity cDNA Reverse Transcription kit (Thermo Fisher Scientific, cat. # 4368814) according to the manufacturer's

protocols. The qRT-PCR was performed by using TaqMan chemistry. Briefly, the cDNA was amplified in 11 µl volume containing TaqMan Fast Advanced Master Mix (Thermo Fisher Scientific, cat. # 4444557) and TaqMan primers/probes (Thermo Fisher Scientific cat. #;; Pfkl Mm00435587_m1; Pkm Mm00834102_gh; HIF1a Mm00468869_m1; Phd3 Mm00472200_m1; NOS2 Mm00440502_m1; CCR7 Mm01301785_m1; IL12 Mm00434174_m1). Each sample was run in triplicate, 18S rRNA (Thermo Fisher Scientific, cat. # 4333760T) was used as a reference gene, and no template control (NTC) was included in the assay. Reactions were run with CFX96 Touch Real-Time PCR Detection System (Bio-Rad) and data analyzed with CFX Maestro (Bio-Rad) and finalized with Excel (Microsoft) and Graph Pad Prism. Relative units were calculated by using the comparative CT ($2^{-\Delta\Delta Ct}$) method.

Mitochondrial DNA assay

Total DNA was extracted from BM-DCs using Nucleospin Triprep, Mini kit for RNA, DNA, and protein purification kit (Macherey-Nagel, cat. # 740966) according to the manufacturer's instructions. The copy number of mitochondrial DNA was assessed using qRT-PCR. qRT-PCR reactions were run with CFX96 Touch Real-Time PCR Detection System (Bio-Rad) using Maxima SYBR Green/ROX qPCR Master Mix (Thermo Fisher Scientific, cat. # K0221). Each sample was run in duplicate, and *human β-globin* was used as a reference gene. Primers used in this study were as follows: mtDNA F: 5'-ACCACAGTTTCATGCCCATCGT-3', mtDNA R: 5'-TTTATGGGCTTTGGTGAGGGAGGT-3', β-globin F: 5'-GGTGAAGGCTCATGGCAAGAAAG-3', and β-globin R: 5'-GTCACAGTGCAGCTCACTCAGT-3'. Data were analyzed with CFX Maestro (Bio-Rad) and finalized with Excel (Microsoft) and GraphPad Prism. Relative units were calculated by using the comparative CT ($2^{-\Delta\Delta Ct}$) method.

Cell migration assays

3D migration assays were performed with µ-Slide Chemotaxis 3D (Ibidi, cat. # 80326) imaging slides according to the manufacturer's protocol. Briefly, WT BM-DCs were left untreated or treated with 2.5 mM 2DG overnight. Cells were mixed into a bovine collagen I (Advanced BioMatrix, cat. # 5005-B) and injected into the slide's thin-imaging strip. After 45 min of collagen polymerization, one of the two chambers flanking the imaging strip was filled with media, the other with media containing mCCL19 (R&D systems, cat. # 361-MI-025) to a final concentration of 0.63 µg/µL. BM-DCs were imaged using the 3I Marianas imaging system (3I intelligent Imaging Innovations, Germany) by utilizing multipoint imaging. A 10×/0.30 EC Plan-Neofluar Ph1 WD = 5.2 M27 objective was used, and the dish was placed in a heated sample chamber (+37°C), in controlled 5% CO_2 atmosphere. Cells were imaged using bright field microscopy. BM-DC migration was compared for 4 h by cell imaging every 1 min. Cells were tracked using the Manual Tracking (Fabrice Cordelières, Institut Curie, Orsay) plugin for ImageJ. All cells that started the timelapse in-frame were tracked for the duration of the timelapse or until they moved out of bounds of the image. The raw tracking data was fed into the Chemotaxis and Migration Tool (Ibidi) plugin for ImageJ. From there, we calculated the average speed of migration of each track and defined any track which moved faster than 1 µm/min over 4 h as a migrating BM-DC and used the speed of those tracks for further comparative analysis.

Tumor experiment

B16-OVA cells were injected subcutaneously in the right flank (3×10^5 cells/mouse), and the tumors were grown until palpable. Mice were then injected peritumorally with either 1 million untreated WT BM-DCs, 2DG-treated WT BM-DCs or PBS (MOCK). Eight mice per condition were used. Tumor growth was followed until the tumors reached the ethical size limit with a caliper every second day. Caliper measurements were done on both sides of the tumor and the volume was calculated by the following formula: V= (W × 2 × L), where W is the tumor width and L is the tumor length. At the end point, tumors were harvested and frozen at −80°C before assessing immune cell content by flow cytometry.

Mixed lymphocyte reaction

CD4 T cells were isolated from the spleens of BALB/C mice with a CD4 T cell isolation kit (Miltenyi, cat. # 130-104-454) and labeled with cell-trace violet (Thermo Fisher Scientific, cat. # C34557) as per the manufacturer's instructions. BM-DCs were pretreated with 2.5 mM 2-Deoxy-D-Glucose (Sigma-Aldrich, cat. # D8375-5 G) overnight or left untreated. For mixed lymphocyte reactions (MLRs), T cells and BM-DCs were resuspended in a complete medium (RPMI) supplemented with 10% FCS (Gibco, cat # 10500–064), 100 U/ml penicillin–streptomycin (penicillin, Orion, cat. # 465161; streptomycin Thermo Fisher Scientific, cat. # D7253-100 g), 2 mM L-glutamine (Thermo Fisher Scientific, cat. # BP379–100) and 50 µM 2-mercaptoethanol (Fluka biochemika, cat. # 63690). T cells (7.7×10^5) were plated into 24-well tissue culture plate, and BM-DCs were added at 1:4 ratio. Cells were incubated for 5 d at 37°C and 5% CO_2. T cell proliferation was measured by flow cytometry, by analyzing the number of T cells where cell trace violet was reduced as compared to the starting situation.

Statistical analysis

Statistical significance between groups was assessed using t-tests or ANOVA followed by Tukey post-hoc. Mann–Whitney U-test was used for migration assay. All data represent mean ± SEM. All p values are shown as *, <0.05; **, <0.01; ***, <0.001; **** <0.0001.

Acknowledgments

The work in the author laboratories was supported by S.C.F. grants from Academy of Finland, E-RARE, Liv och Hälsa, Svenska Kulturfonden, Magnus Ehrnrooth foundation, HIPOC (HiLIFE), and a postdoctoral fellowship to H.H. grant (Academy of Finland). H.Z. was supported by the Academy of Finland (decision No.266846), Jane and Aatos Erkko Foundation, and V.C. by the European Research Council under the European Union's Horizon 2020 Framework programme (H2020)/ERC-

CoG-2015 Grant Agreement No. 681219, the Helsinki Institute of Life Science (HiLIFE), the Jane and Aatos Erkko Foundation, and the Cancer Society of Finland (Syöpäjärjestöt). We thank Merle Kampura, Taru Kostiainen, and Andrea Walander for their technical assistance.

Targeted mass spectrometry was performed at the metabolomics unit of the Institute of Molecular Medicine Finland that is supported by HiLIFE and Biocenter Finland. Animals were kept at the Laboratory Animal Centre of the University of Helsinki. Imaging was performed at the Light Microscopy Unit, Institute of Biotechnology, supported by HiLIFE and Biocenter Finland. Flow cytometry was performed at the Viikki HiLIFE Flow Cytometry Unit, University of Helsinki.

Disclosure statement

A provisional patent application has been filed in relation to this study (ID1374, Low dose 2DG treatment of dendritic cells improves their anti-tumor responses).

Funding

The work was supported by the Academy of Finland E-Rare HORIZON EUROPE European Research Council Helsinki Institute of Life Science, Helsingin Yliopisto Jane ja Aatos Erkon Säätiö Magnus Ehrnroothin Säätiö Medicinska Understödsföreningen Liv och Hälsa HIPOC (HiLIFE) Svenska Kulturfonden Syöpäjärjestöt .

Data availability statement

Metabolomics data for this study were generated at the Institute for Molecular Medicine Finland (FIMM), University of Helsinki, Finland, and are available from the corresponding author upon request. All other data generated in this study are also available upon request from the corresponding author.

References

1. Bošnjak B, Kth D, Förster R, Hammerschmidt SI. Imaging dendritic cell functions*. Immunol Rev. 2021;306(1):137–163. doi:10.1111/imr.13050.
2. Anguille S, Smits EL, Lion E, van Tendeloo VF, Berneman ZN. Clinical use of dendritic cells for cancer therapy. Lancet Oncol. 2014;15(7):e257–e267. doi:10.1016/s1470-2045(13)70585-0.
3. Gardner A, de Mingo Pulido Á, Ruffell B. Dendritic Cells and Their Role in Immunotherapy. Front Immunol. 2020;11:924. doi:10.3389/fimmu.2020.00924.
4. Liu J, Zhang X, Cheng Y, Cao X. Dendritic cell migration in inflammation and immunity. Cell Mol Immunol. 2021;18(11):2461–2471. doi:10.1038/s41423-021-00726-4.
5. Winzler C, Rovere P, Rescigno M, Granucci F, Penna G, Adorini L, Zimmermann VS, Davoust J, Ricciardi-Castagnoli P. Maturation stages of mouse dendritic cells in growth factor-dependent long-term cultures. J Exp Med. 1997;185(2):317–328. doi:10.1084/jem.185.2.317.
6. Miller JC, Brown BD, Shay T, Gautier EL, Jojic V, Cohain A, Pandey G, Leboeuf M, Elpek KG, Helft J. et al. Deciphering the transcriptional network of the dendritic cell lineage. Nat Immunol. 2012;13(9):888–899. doi:10.1038/ni.2370.
7. Morrison VL, James MJ, Grzes K, Cook P, Glass DG, Savinko T, Lek HS, Gawden-Bone C, Watts C, Millington OR. et al. Loss of beta2-integrin-mediated cytoskeletal linkage reprogrammes dendritic cells to a mature migratory phenotype. Nat Commun. 2014;5(1). doi:10.1038/ncomms6359.
8. Everts B, Amiel E, van der Windt GJW, Freitas TC, Chott R, Yarasheski KE, Pearce EL, Pearce EJ. Commitment to glycolysis sustains survival of NO-producing inflammatory dendritic cells. Blood. 2012;120(7):1422–1431. doi:10.1182/blood-2012-03-419747.
9. Everts B, Amiel E, Huang S-C, Smith AM, Chang C-H, Lam WY, Redmann V, Freitas TC, Blagih J, van der Windt GJW. et al. TLR-driven early glycolytic reprogramming via the kinases TBK1-IKKε supports the anabolic demands of dendritic cell activation. Nat Immunol. 2014;15(4):323–332. doi:10.1038/ni.2833.
10. O'Neill LAJ, Pearce EJ. Immunometabolism governs dendritic cell and macrophage function. J Exp Med. 2016;213(1):15–23. doi:10.1084/jem.20151570.
11. Liu D, Wu J, An J, Cyster JG. Requirements for cDC2 positioning in blood-exposed regions of the neonatal and adult spleen. J Exp Med. 2020;217(11):e20192300. doi:10.1084/jem.20192300.
12. Varga G, Balkow S, Wild MK, Stadtbaeumer A, Krummen M, Rothoeft T, Higuchi T, Beissert S, Wethmar K, Scharffetter-Kochanek K. et al. Active MAC-1 (CD11b/CD18) on DCs inhibits full T-cell activation. Blood. 2006;109(2):661–669. doi:10.1182/blood-2005-12-023044.
13. Ehirchiou D, Xiong Y, Xu G, Chen W, Shi Y, Zhang L. CD11b facilitates the development of peripheral tolerance by suppressing Th17 differentiation. J Exp Med. 2007;204(7):1519–1524. doi:10.1084/jem.20062292.
14. Savinko TS, Morrison VL, Uotila LM, Wolff CHJ, Alenius HT, Fagerholm SC. Functional Beta2-Integrins Restrict Skin Inflammation in vivo. J Invest Dermatol. 2015;135(9):2249–2257. doi:10.1038/jid.2015.164.
15. Han C, Jin J, Xu S, Liu H, Li N, Cao X. Integrin CD11b negatively regulates TLR-triggered inflammatory responses by activating syk and promoting degradation of MyD88 and TRIF via cbl-b. Nat Immunol. 2010;11(8):734–742. doi:10.1038/ni.1908.
16. Leon F, Contractor N, Fuss I, Marth T, Lahey E, Iwaki S, la Sala A, Hoffmann V, Strober W, Kelsall BL. Antibodies to complement receptor 3 treat established inflammation in murine models of colitis and a novel model of psoriasiform dermatitis. J Immunol. 2006;177(10):6974–6982. doi:10.4049/jimmunol.177.10.6974.
17. D'Agata ID, Paradis K, Chad Z, Bonny Y, Seidman E. Leucocyte adhesion deficiency presenting as a chronic ileocolitis. Gut. 1996;39(4):605–608. doi:10.1136/gut.39.4.605.
18. Guenther C, Faisal I, Fusciello M, Sokolova M, Harjunpää H, Ilander M, Tallberg R, Vartiainen MK, Alon R, Gonzalez-Granado JM. et al. β2-integrin adhesion regulates dendritic cell epigenetic and transcriptional landscapes to restrict dendritic cell maturation and tumor rejection. Cancer Immunol Res. 2021;9(11):1354–1369. doi:10.1158/2326-6066.CIR-21-0094.
19. Guenther C, Faisal I, Uotila LM, Asens ML, Harjunpää H, Savinko T, Öhman T, Yao S, Moser M, Morris SW. et al. A β2-Integrin/MRTF-A/SRF pathway regulates dendritic cell gene expression, adhesion, and traction force generation. Front Immunol. 2019;10:1138. doi:10.3389/fimmu.2019.01138.
20. Netea MG, Domínguez-Andrés J, Barreiro LB, Chavakis T, Divangahi M, Fuchs E, Joosten LAB, van der Meer JWM, Mhlanga MM, Mulder WJM. et al. Defining trained immunity and its role in health and disease. Nat Rev Immunol. 2020;20(6):375–388. doi:10.1038/s41577-020-0285-6.
21. Helft J, Böttcher J, Chakravarty P, Zelenay S, Huotari J, Schraml BU, Goubau D, Reise, Reis e Sousa C, Sousa C. GM-CSF mouse bone marrow cultures comprise a heterogeneous population of CD11c+MHCII+ macrophages and dendritic cells. Immunity. 2015;42(6):1197–1211. doi:10.1016/j.immuni.2015.05.018.
22. Lawless SJ, Kedia-Mehta N, Walls JF, McGarrigle R, Convery O, Sinclair LV, Navarro MN, Murray J, Finlay DK. Glucose represses dendritic cell-induced T cell responses. Nat Commun. 2017;8(1):15620. doi:10.1038/ncomms15620.
23. Argüello RJ, Combes AJ, Char R, Gigan JP, Baaziz AI, Bousiquot E, Camosseto V, Samad B, Tsui J, Yan P. et al. SCENITH: A flow cytometry-based method to functionally profile energy metabolism with single-cell resolution. Cell Metab. 2020;32(6):1063–1075.e7. doi:10.1016/J.CMET.2020.11.007.
24. Ponticos M, Lu QL, Morgan JE, Hardie DG, Partridge TA, Carling D. Dual regulation of the AMP-activated protein kinase provides a novel mechanism for the control of creatine kinase in

skeletal muscle. Embo J. 1998;17(6):1688–1699. doi:10.1093/emboj/17.6.1688.
25. Cytlak U, Resteu A, Bogaert D, Kuehn HS, Altmann T, Gennery A, Jackson G, Kumanovics A, Voelkerding KV, Prader S. et al. Ikaros family zinc finger 1 regulates dendritic cell development and function in humans. Nat Commun. 2018;9(1):1239. doi:10.1038/s41467-018-02977-8.
26. Boutboul D, Kuehn HS, Van de Wyngaert Z, Niemela JE, Callebaut I, Stoddard J, Lenoir C, Barlogis V, Farnarier C, Vely F. et al. Dominant-negative IKZF1 mutations cause a T, B, and myeloid cell combined immunodeficiency. J Clin Invest. 2018;128(7):3071–3087. doi:10.1172/JCI98164.
27. Oh K-S, Gottschalk RA, Lounsbury NW, Sun J, Dorrington MG, Baek S, Sun G, Wang Z, Krauss KS, Milner JD. et al. Dual roles for Ikaros in regulation of macrophage chromatin state and inflammatory gene expression. J Immunol. 2018;201(2):757–771. doi:10.4049/jimmunol.1800158.
28. Krönke J, Udeshi ND, Narla A, Grauman P, Hurst SN, McConkey M, Svinkina T, Heckl D, Comer E, Li X. et al. Lenalidomide causes selective degradation of IKZF1 and IKZF3 in multiple myeloma cells. Science. 2014;343(6168):301–305. doi:10.1126/science.1244851.
29. Wang F, Zhang S, Vuckovic I, Jeon R, Lerman A, Folmes CD, Dzeja PP, Herrmann J. Glycolytic stimulation is not a requirement for M2 Macrophage differentiation. Cell Metab. 2018;28(3):463–475.e4. doi:10.1016/j.cmet.2018.08.012.
30. Du H, Bartleson JM, Butenko S, Alonso V, Liu WF, Winer DA, Butte MJ. Tuning immunity through tissue mechanotransduction. Nat Rev Immunol. 2023;23(3):174–188. doi:10.1038/s41577-022-00761-w.
31. Griffiths KL, Tan JKH, O'Neill HC. Characterization of the effect of LPS on dendritic cell subset discrimination in spleen. J Cell Mol Med. 2014;18(9):1908–1912. doi:10.1111/jcmm.12332.
32. West MA, Wallin RPA, Matthews SP, Svensson HG, Zaru R, Ljunggren H-G, Prescott AR, Watts C. Enhanced dendritic cell antigen capture via toll-like receptor-induced actin remodeling. Science. 2004;305(5687):1153–1157. doi:10.1126/science.1099153.
33. Joshi I, Yoshida T, Jena N, Qi X, Zhang J, Van Etten RA, Georgopoulos K. Loss of ikaros DNA-binding function confers integrin-dependent survival on pre-B cells and progression to acute lymphoblastic leukemia. Nat Immunol. 2014;15(3):294–304. doi:10.1038/ni.2821.
34. Chan LN, Chen Z, Braas D, Lee JW, Xiao G, Geng H, Cosgun KN, Hurtz C, Shojaee S, Cazzaniga V. et al. Metabolic gatekeeper function of B-lymphoid transcription factors. Nature. 2017;542(7642):479–483. doi:10.1038/NATURE21076.
35. Krawczyk CM, Holowka T, Sun J, Blagih J, Amiel E, DeBerardinis RJ, Cross JR, Jung E, Thompson CB, Jones RG. et al. Toll-like receptor-induced changes in glycolytic metabolism regulate dendritic cell activation. Blood. 2010;115(23):4742–4749. doi:10.1182/blood-2009-10-249540.
36. Guak H, Al Habyan S, Ma EH, Aldossary H, Al-Masri M, Won SY, Ying T, Fixman ED, Jones RG, McCaffrey LM. et al. Glycolytic metabolism is essential for CCR7 oligomerization and dendritic cell migration. Nat Commun. 2018;9(1):2463. doi:10.1038/s41467-018-04804-6.
37. Gallucci S, Lolkema M, Matzinger P. Natural adjuvants: endogenous activators of dendritic cells. Nat Med. 1999;5(11):1249–1255. doi:10.1038/15200.
38. Morrison VL, MacPherson M, Savinko T, Lek HS, Prescott A, Fagerholm SC. The β2 integrin–kindlin-3 interaction is essential for T-cell homing but dispensable for T-cell activation in vivo. Blood. 2013;122(8):1428–1436. doi:10.1182/BLOOD-2013-02-484998.
39. Uetz-von Allmen E, Samson GPB, Purvanov V, Maeda T, Legler DF. CAL-1 as cellular model system to study CCR7-guided human dendritic cell migration. Front Immunol. 2021;12:702453. doi:10.3389/fimmu.2021.702453.

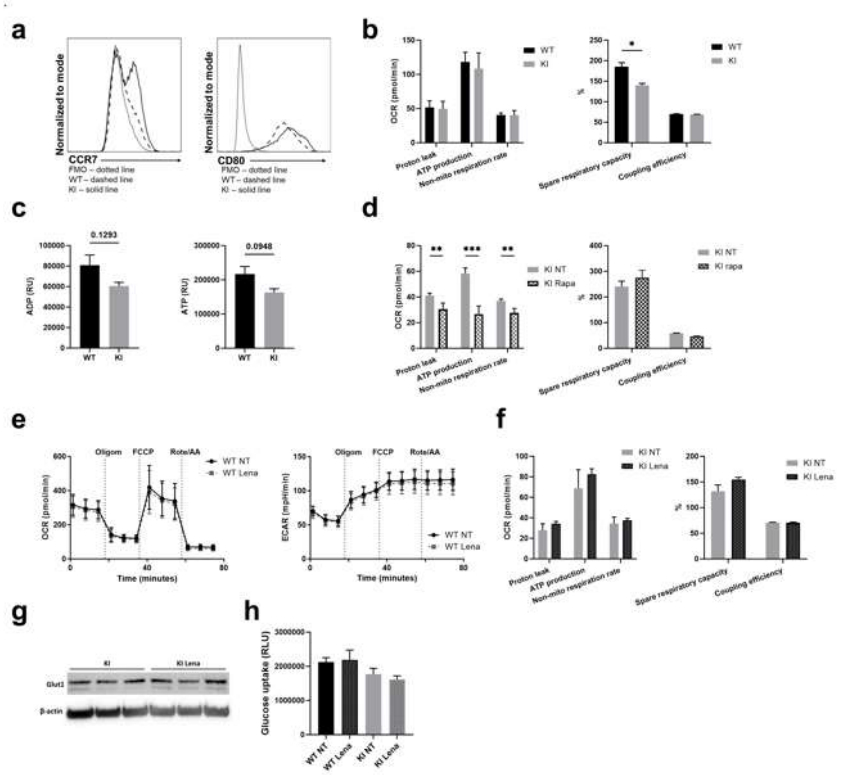

Supplementary 1

*Supplementary Fig 1. a) CCR7 and CD80 expression in WT and β2-integrin KI BM-DCs were measured by flow cytometry. Representative histograms are shown. b) Parameters of mitochondrial respiration in WT and β2-integrin KI BM-DCs were calculated based on OCR shown in Fig 2b (n=4). c) ATP and ADP concentrations in WT and β2-integrin KI BM-DCs were measured as described in Materials and Methods (n=3). d) Parameters of mitochondrial respiration in KI and rapamycin-treated KI BM-DCs were calculated based on OCR shown in Fig 4e (n=4). e) Extracellular acidification rate (ECAR) and oxygen consumption rate (OCR) of WT and lenalidomide-treated WT BM-DCs were measured real time by utilizing Seahorse Extracellular Analyser and Mito Stress Test Kit (n=4). f) Parameters of mitochondrial respiration in NT and lenalidomide-treated β2-integrin KI cells were calculated based on OCR shown in Fig 5d (n=3). g) Glut1 expression in NT and lenalidomide-treated β2-integrin KI cells was assessed by Western blotting (n=3). h) Glucose uptake in NT WT, lenalidomide-treated WT, NT β2-integrin KI and lenalidomide-treated β2-integrin KI cells was assessed by a glucose uptake kit, as described in Materials and Methods (n=3). P-values are shown as <0.05 *, <0.01 **, <0.005 ***.*

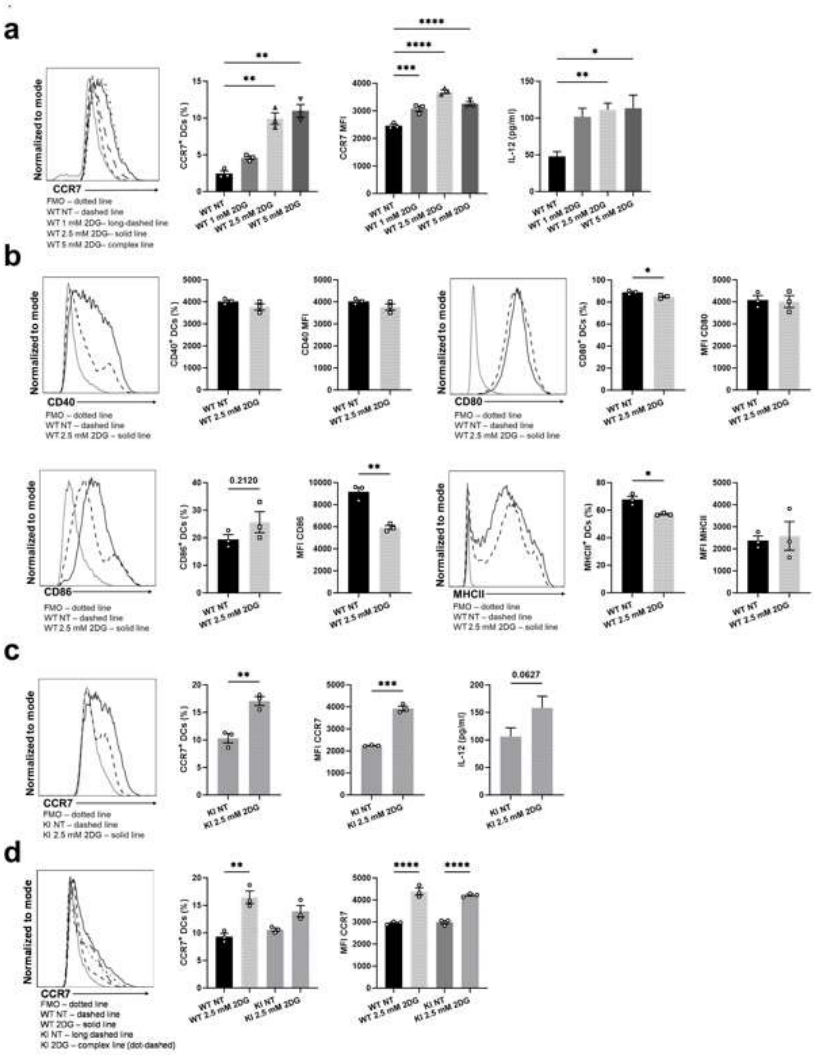

Supplementary 2

*Supplementary Fig 2. a) Effect of various concentrations of 2DG on CCR7 expression and IL-12 production in WT BM-DCs was measured by flow cytometry and ELISA, respectively (n=3). b) Effect of 2,5mM 2DG on expression of CD40, CD80, CD86 and MHCII in WT BM-DCs was assessed by flow cytometry (n=3). c) Effect of 2,5 mM 2DG on expression of CCR7 and IL-12 production in β2-integrin KI cells was assessed by flow cytometry (n=3) and ELISA (n=11), respectively. ELISA data is pooled from four independent experiments. d) Effect of 2,5 mM 2DG on CCR7 expression of WT and β2-integrin KI cells was assessed by flow cytometry (n=3). P-values are shown as <0.05 *, <0.01 **, <0.005 ***, <0.0001 ****.*

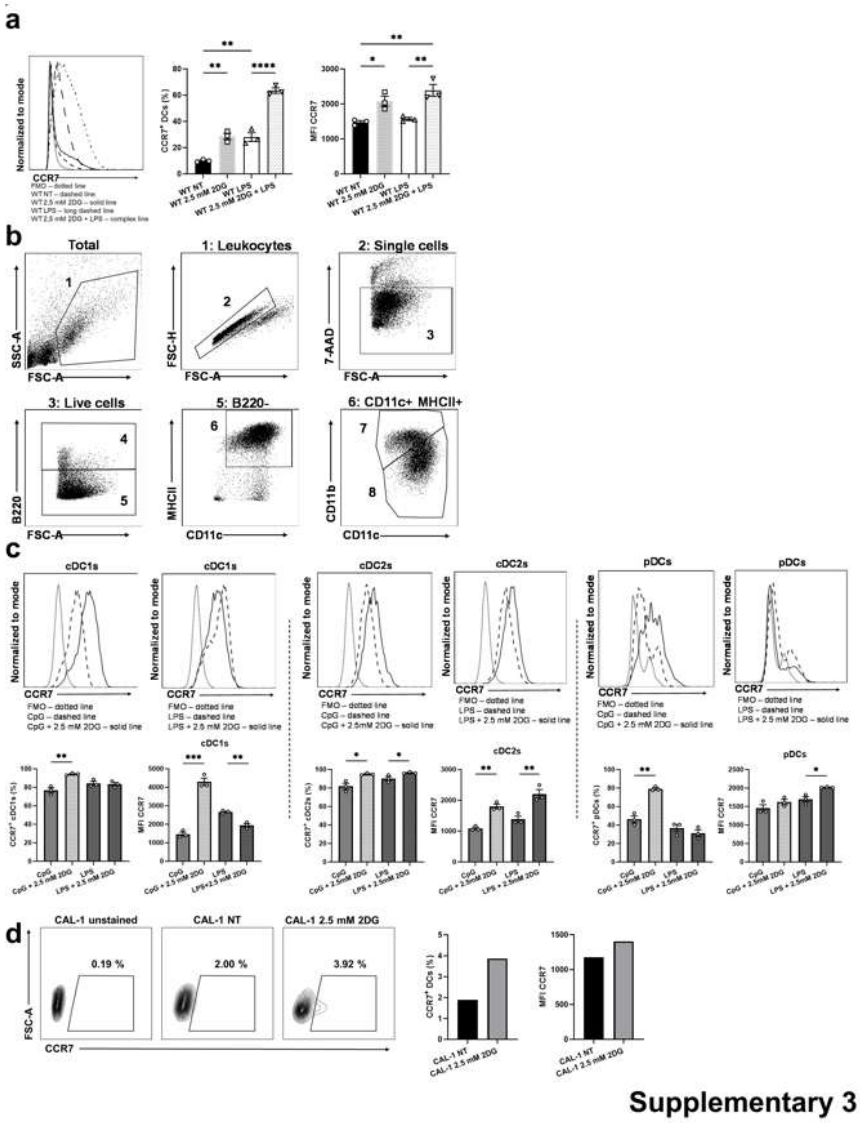

Supplementary 3

*Supplementary Fig 3. a) Effect of 2,5mM 2DG on expression of CCR7 in NT WT and LPS-treated WT BM-DCs was assessed by flow cytometry (n=3). b-c) Effect of 2,5 mM 2DG on CCR7 expression in Flt3L-induced BM-DCs was assessed by flow cytometry (n=3). Gating strategy is shown in b with gate 4 representing plasmacytoid DCs (pDCs), gate 7 conventional DCs type 2 (cDC2s) and gate 8 conventional DCs type 1 (cDC1s). Representative histograms and bar graphs for each cell population is shown in c. d) Effect of 2,5mM 2DG on CCR7 expression in the human DC cell line CAL-1 was assessed by flow cytometry (n=1). P-values are shown as <0.05 *, <0.01 **, <0.005 ***, <0.0001 ****.*

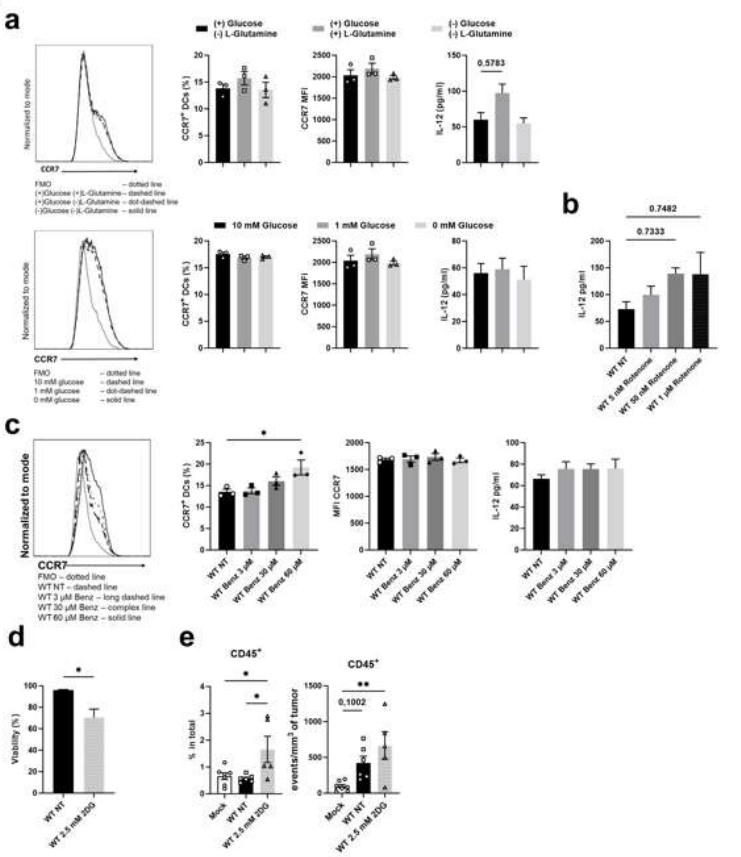

Supplementary 4

*Supplementary Fig 4. a) Effect of glucose and glutamine deprivation and also the effect of various concentrations of glucose on CCR7 expression and IL-12 production in WT BM-DCs was measured by flow cytometry and ELISA, respectively (n=3). b) Effect of varying concentrations of rotenone on IL-12 production was assessed by ELISA (n=3). c) Effect of varying concentrations of benserazide on CCR7 expression and IL-12 production in WT BM-DCs was assessed by flow cytometry (n=3) and ELISA (n=3-9), respectively. d) Viability of WT and 2.5mM 2DG-treated WT BM-DCs was assessed by Countess Automated Cell Counter (Invitrogen) (n=3). e) Proportion and number of CD45$^+$ cells in tumors were determined flow cytometrically (n=5-7). P-values are shown as <0.05 *, <0.01 **.*

Publication II

β_2-Integrins Regulate Microglial Responses and the Functional Outcome of Hemorrhagic Stroke In Vivo

Heidi Harjunpää,* Robert Tallberg,*,[1] Yunhao Cui,*,[1] Carla Guenther,* Hock-Kean Liew,[†,2] Anna Seelbach,[‡] Guillem Saldo Rubio,* Mikko Airavaara,[†] and Susanna C. Fagerholm*

Stroke is one of the leading causes of death and long-term disabilities worldwide. In addition to interruption of blood flow, inflammation is widely recognized as an important factor mediating tissue destruction in stroke. Depending on their phenotype, microglia, the main leukocytes in the CNS, are capable of either causing further tissue damage or promoting brain restoration after stroke. β_2-integrins are cell adhesion molecules that are constitutively expressed on microglia. The function of β_2-integrins has been investigated extensively in animal models of ischemic stroke, but their role in hemorrhagic stroke is currently poorly understood. We show in this study that dysfunction of β_2-integrins is associated with improved functional outcome and decreased inflammatory cytokine expression in the brain in a mouse model of hemorrhagic stroke. Furthermore, β_2-integrins affect microglial phenotype and cytokine responses in vivo. Therefore, our findings suggest that targeting β2-integrins in hemorrhagic stroke may be beneficial. ***The Journal of Immunology*****, 2024, 213: 519–525.**

Stroke is a major cause of mortality worldwide, and survivors often experience severe and lifelong disabilities (1, 2). Ischemic stroke is caused by the occlusion of cerebral arteries, preventing blood flow to the affected brain tissue, whereas hemorrhagic stroke is caused by the rupture of cerebral blood vessels, resulting in leakage of blood components into the brain. In addition to the disruption of blood flow, inflammation has been shown to play an important role in causing tissue damage in both stroke types (3, 4). Particularly in hemorrhagic stroke, the leakage of blood components such as thrombin and iron-containing proteins greatly enhances the inflammatory processes, often leading to severe secondary injuries. However, because ischemic stroke accounts for ∼87% of all stroke cases (5), research into the function of immune cells and pathways in stroke pathophysiology has largely been dictated by studies using animal models of ischemic stroke.

Microglia are resident cells and the major APCs of the CNS, accounting for ∼5–15% of the total cells (6–8). They are constantly in close interaction with other cells of the CNS, such as neurons, influencing their development, function, and repair (6, 8, 9). They also form the first line of defense against pathogens, tumors, and harmful self-proteins. In a resting state, microglia constantly monitor their environment to maintain homeostasis and to detect and respond to injury. The release of damage-associated molecular patterns, such as ATP and nucleic acid molecules from dying neurons (10, 11), and the released blood components, such as thrombin and chemokines, in hemorrhagic stroke lead to rapid activation of microglia (12, 13). Depending on the signals in the environment, microglial activation may result in a proinflammatory phenotype with increased production of proinflammatory cytokines (TNF-α, IL-6, IL-1β), reactive oxygen species, inducible NO synthase, and matrix metalloproteinases, contributing to tissue damage and disruption of the blood–brain barrier (BBB) (11–14). Alternatively, activated microglia may exhibit an anti-inflammatory type, which promotes brain repair by secreting growth factors and anti-inflammatory cytokines (IL-10, TGF-β) and prevents secondary inflammation by phagocytosing dead neurons, disabled synapses, and cellular debris. The anti-inflammatory function of microglia has been shown to be particularly important in preventing inflammation in hemorrhagic stroke because of microglial ability to phagocytose erythrocytes and other blood components (15).

Integrins are cell adhesion molecules consisting of one α- and one β-chain (16, 17). They span across the cell membrane and bind ligands in the extracellular matrix, on other cells, or in soluble form, thus mediating information from the surroundings to the cell interior. The expression of β_2-integrins is restricted to immune cells, and they play various critical roles in immunity, including immune cell trafficking, phagocytosis, T cell activation, and immune cell polarization (18). Both human and mouse microglia constitutively express β_2-integrins, and the expression has been shown to further increase following activation (19–22). In addition, the expression of β_2-integrins has been observed to increase on peripheral leukocytes in ischemic stroke patients compared with healthy control subjects (23), suggesting a role for β_2-integrins in stroke pathogenesis.

In this study, we investigated the putative role of β_2-integrins in hemorrhagic stroke, using a mouse model where β_2-integrins are expressed but dysfunctional (TTT/AAA-β_2-integrin knock-in [β_2-integrin KI] mice). We show in this study that the functional

*Molecular and Integrative Biosciences Research Programme, Faculty of Biological and Environmental Sciences, University of Helsinki, Helsinki, Finland; [†]Faculty of Pharmacy, University of Helsinki, Helsinki, Finland; and [‡]Neuroscience Center, HiLIFE, University of Helsinki, Helsinki, Finland

[1]These authors contributed equally to this work.

[2]Current address: Department of Medical Research, Hualien Tzu Chi Hospital, Buddhist Tzu Chi Medical Foundation, Hualien, Taiwan.

ORCIDs: 0000-0002-1380-9939 (H.H.); 0000-0002-8235-6785 (R.T.); 0009-0001-6887-042X (Y.C.); 0000-0001-7915-1028 (C.G.); 0000-0002-5981-4100 (H.-K.L.); 0000-0002-7908-7369 (A.S.); 0000-0002-9352-4326 (G.S.R.); 0000-0002-2026-1609 (M.A.).

Received for publication November 27, 2023. Accepted for publication June 10, 2024.

https://doi.org/10.4049/jimmunol.2300815

This work was supported by grants from Academy of Finland, E-RARE, Sigrid Juselius Foundation, Swedish Cultural Foundation, Magnus Ehrnrooth Foundation, and Liv och Hälsa (to S.C.F.); by a grant from Sigrid Juselius Foundation (to M.A.); and by a postdoctoral fellowship grant from Academy of Finland (to H.H.).

Address correspondence and reprint requests to Dr. Susanna C. Fagerholm, University of Helsinki, Viikinkaari 9, Helsinki, Uusimaa 00790, Finland. E-mail address: susanna.fagerholm@helsinki.fi

The online version of this article contains supplemental material.

Abbreviations used in this article: BBB, blood–brain barrier; KI, knock-in; MHCII, MHC class II; qRT-PCR, quantitative RT-PCR; WT, wild type.

outcome of hemorrhagic stroke is less severe in β_2-integrin KI compared with WT mice. Furthermore, the reduction in stroke severity is associated with decreased inflammatory cytokine expression (TNF-α and IL-6) and altered microglial reactivity in healthy brain (lower expression of MHC class II [MHCII], CD86, and CD16/32). Our results thus reveal a novel, to our knowledge, role for β_2-integrins in hemorrhagic stroke and microglial function.

Materials and Methods

Mice

C57BL/6N wild-type (WT) mice were purchased from Charles River and used as control animals for previously described TTT/AAA β_2-integrin KI mice (24). Mice were housed at the certified Laboratory Animal Center of the University of Helsinki under conventional conditions in groups of up to five animals per cage with food and water provided ad libitum. All the mice used in the study were between the ages of 12 and 30 wk. The experiments were performed according to the Finnish Act on the Protection of Animals Used for Scientific or Educational Purposes (497/2013) and according to the Directive 2010/63/EU of the European Parliament and of the Council of September 22, 2010, on the protection of animals used for scientific purposes and approved by the Finnish National Animal Experiment Board (Hankelupalautakunta – ELLA).

Isolation of leukocytes from the CNS

Brains and spinal cords were harvested and homogenized by hand between microscope glass slides in precooled 2% FCS (Life Technologies, catalog no. 10500-064) in PBS (Lonza, catalog no. 17-516F) and filtered through a 70-μm filter. The homogenized suspensions were centrifuged at 300 × *g* for 10 min at +4°C and resuspended in RPMI (Lonza, catalog no. 12-167F). Leukocytes were isolated from the homogenized suspension by Percoll density gradient centrifugation. Briefly, the cell suspension was mixed with 30% Percoll (Santa Cruz Biotechnology, catalog no. sc-500790A) and transferred on top of 70% Percoll solution in a 15-ml tube. The tubes were centrifuged at 500 × *g* for 30 min at room temperature without deceleration. The leukocytes were then carefully collected from the interphase of the 30% and 70% Percoll layers.

Microglial isolation by MACS

Microglial isolation was done essentially as described (25). Briefly, brain tissues were mechanically dissociated and treated with enzyme digestion mix: HBSS (without calcium/magnesium) (Life Technologies, catalog no. 14175-095), 5% FCS (Life Technologies, catalog no. 10500-064), 10 μM HEPES (VWR Chemicals, catalog no. 441487M), 2 mg/ml collagenase A (Roche, catalog no. 11088858001), and 28 U/ml DNase I (Invitrogen, catalog no. 11284932001) at 37°C for 40 min (agitate every 5 min, pipet up and down 20 times every 10 min). The samples were filtered through 70-μm nylon filters, followed by centrifugation at 300 × *g* for 10 min. Then, pellets were incubated with CD11b microbeads (Biotec, catalog no. 120-000-300) and MACS buffer (1 mM EDTA [Fluka Chemical Corp., catalog no. 03610], 1% BSA [Biowest, catalog no. P6154-100GR] in PBS [Lonza, catalog no. 17-516F]) on ice for 15 min. After incubation, the samples were mixed with MACS buffer and spun at 300 × *g* for 10 min. After discarding the supernatant, the pellets were resuspended in MACS buffer and filtered to MACS columns (Miltenyi Biotec) through 70-μm nylon filters. CD11b-positive cells were collected and centrifuged at 300 × *g* for 10 min. The pellets were resuspended in ice-cold PBS (Lonza, catalog no. 17-516F) and divided into two groups (the control and LPS-treated groups) and centrifuged at 300 × *g* for 10 min. After removing the supernatant, the cells were resuspended in 10% FCS (Life Technologies, catalog no. 10500-064) in 90% DMEM (Euroclone, catalog no. ECB9006L) with and without LPS (10 ng/ml) (Invitrogen, catalog no. 00-4976-93), respectively. After incubation for 3 h, all the samples were collected for quantitative RT-PCR (qRT-PCR), and cell culture supernatants were collected for ELISA.

Flow cytometry

Cell surface staining for single-cell suspensions of brain and spinal cord samples was performed using the following Abs: anti-CD45-BV650 clone 30-F11 (BD Biosciences, catalog no. 563410), anti-CD11b-FITC clone M1/70 (eBioscience, catalog no. 11-0112-82), anti-MHCII-allophycocyanin-eFluor780 (I-A/I-E) clone M5/114.15.2 (eBioscience, catalog no. 47-5321-82), anti-CD86-PE-cyanine (Cy)7 clone GL-1 (BioLegend, catalog no. 105014), anti-CD16/32-biotin clone REA377 (Miltenyi Biotec catalog no. 130-107-038), streptavidin-V500 (BD Biosciences catalog no. 561419), anti-CD45-PE-Cy7 clone 30-F11 (eBioscience, catalog no. 25-0451-81), F4/80-allophycocyanin-eFluor780 clone BM8 (eBioscience 47-4801-82), Ly6C-BV605 clone HK1.4 (BioLegend, 128035), Ly6G-PE clone 1A8-Ly6g (Invitrogen, 12-9668-82). Microglia were defined as $CD45^{low}CD11b^{+}$ (26, 27), lymphocytes as $CD45^{high}CD11b^{-}$, neutrophils as $CD45^{high}CD11b^{+}Ly6G^{+}F4/80^{-}$, and monocytes as $CD45^{high}CD11b^{+}Ly6C^{+}F4/80^{-}$. Microglial phenotype was further analyzed on the basis of MHCII, CD86, and CD16/32 expression. Unstained and fluorescence minus one controls were included in the experiments, and anti-CD16/CD32 (Fc block) clone 2.4G2 (BD Biosciences 553142) was added when CD16/32 expression was not being assessed. All data were collected using an LSRFortessa flow cytometer (BD Biosciences) and analyzed with FlowJo version 10 (FlowJo LLC).

In vivo hemorrhagic stroke experiment

The protocol for the hemorrhagic stroke animal model has been described elsewhere (28). Mice were used to administer microinfusions of bacterial collagenase VII-S (0.075 U in 0.5 μl sterile saline) (Sigma-Aldrich, catalog no. C2399) into the right striatum of the mouse. This was done at specific coordinates (0.2 mm anterior, 2.0 mm right, 3.7 mm ventral to bregma on the cranial surface) over a period of 10 min. The needle was then left in place for another 10 min to prevent reflux. The burr hole was then sealed with bone wax, and the mice were allowed to recover in individual cages at room temperature. Body weights of the mice were determined at three different time points. Mice were euthanized 72 h after surgery, and the entire brain was removed. The brains were then dissected, hematomas confirmed, and the right and left striata separated from the rest of the tissue and frozen.

Cylinder test

Functional impairment after hemorrhagic stroke was assessed by using the rodent cylinder test (29). The cylinder test was conducted 24 h after surgery as well as for untreated mice. The mice were placed individually in a transparent cylinder under infrared light for 5 min, and a camera was mounted underneath to record their behavior. The camera recording was then used to analyze the number of times the mice used their front paws to touch the cylinder wall. Because the stroke was induced on the right hemisphere, the contralateral side was expected to be affected by the injury. Two mice were excluded from the cylinder test and thus from Table I. One excluded mouse died 24 h after surgery, and the other one had a leakage of the hematoma following surgery.

qRT-PCR

Total RNA was isolated from frozen right striatum samples derived from WT and KI mice following intrastriatal hemorrhagic stroke with the Nucleospin RNA kit (Macherey-Nagel, catalog no. 740955) and converted into cDNA with the High-Capacity cDNA Reverse Transcription Kit (Thermo Fisher Scientific, catalog no. 4368814) according to the manufacturers' protocols. The qRT-PCR was performed by using TaqMan chemistry. Briefly, the cDNA was amplified in 11-μl volume containing 1× TaqMan Fast Advanced Master Mix (Thermo Fisher Scientific, catalog no. 4444557) and TaqMan primers and probes: TNF (Mm00443258_m1), IL-6 (Mm00446190_m1), and IL-10 (Mm01288386_m1). 18S rRNA (Eukaryotic 18S rRNA Endogenous Control; Thermo Fisher Scientific, catalog no. 4333760T) was used as a reference gene, and no template control was included in each assay. Each sample was run in duplicate or triplicate. Reactions were run with the CFX96 Touch Real-Time PCR Detection System (Bio-Rad Laboratories), and data were analyzed by using CFX Maestro (Bio-Rad Laboratories) and finalized with Excel (Microsoft). Relative units were calculated by using the comparative cycle threshold method, which has been described elsewhere (30). Samples were excluded from the analysis in case the differences in cycle threshold values between the duplicates or triplicates were >0.5.

ELISA

The levels of TNF and IL-10 from WT and β_2-integrin KI microglial supernatants were assessed with the mouse ELISA kit according to the manufacturer's instructions (R&D Systems, catalog nos. DY410 and DY417, respectively). Briefly, a 96-well MaxiSorp microplate (Thermo Fisher Scientific, catalog no. 442404) was first coated with capture Ab overnight. The next day, the wells were washed and blocked with reagent diluent (1% BSA [Biowest, catalog no. P6154] in PBS [Lonza, catalog no. 17-516F]) for a minimum of 1 h. The plate was then washed, and standards and samples were added. Following a 2-h incubation, the plate was washed and the detection Ab was added to the wells. After 2 h, the plate was washed and streptavidin-HRP (R&D Systems, catalog no. DY998) was added for 20 min. After washing, substrate solution (R&D Systems, catalog no. DY410) was added to the wells. Following visible color development (or latest after 20 min), sulfuric acid (Acros Organics, catalog no. 124645001; diluted 1:4 in water) was added to stop the reaction. The OD was immediately determined at 450nm and background at 540-nm wavelength using Multiskan GO

spectrophotometer (Thermo Fisher Scientific). The TNF concentration was determined on the basis of a standard curve using Excel and GraphPad Prism. All washing steps were performed by washing the plate first three times with 0.05% Tween (Fisher BioReagents, catalog no. BP337) in PBS and then once with PBS only.

Statistical analyses

The results in the graphs are indicated as the mean ± SEM, and the statistical analyses were performed using GraphPad Prism. Comparison of results between groups was performed using two-tailed unpaired *t* tests. The results were considered significant as follows: $*p < 0.05$, $**p < 0.01$, $***p < 0.001$, and $****p < 0.0001$.

Results

β_2-Integrins impact the functional outcome of hemorrhagic stroke

β_2-Integrins are crucial for the function of the immune system, and their expression has been shown to increase after ischemic stroke (23). However, their involvement in the pathophysiology of hemorrhagic stroke is currently poorly understood. To investigate this, we used previously generated β_2-integrin KI mice that express dysfunctional β_2-integrins on their immune cells because of a mutation in the β-chain of the integrin (24). First, a hemorrhagic stroke was induced by injecting bacterial collagenase into the right striatum of both WT and β_2-integrin KI mice. General well-being was monitored by measuring the weight of the animals at three time points following the surgery (Table I and Fig. 1A). As shown in Fig. 1a, both the WT and β_2-integrin KI mice had a similar weight loss after surgery, indicating that the surgery had a similar effect on nutritional aspects in both groups. The weight distribution of untreated WT and KI mice is shown in Supplemental Fig. 1A. The behavioral outcome of the stroke in the right striatum was determined by assessing the degree of forelimb injury in the contralateral paw of the animals by subjecting the mice to a cylinder test 1 d after surgery. Counting the paw touches revealed that the functional outcome of stroke was significantly less severe in the β_2-integrin KI mice than in the WT mice (Fig. 1B). There was no difference in paw use between WT and KI mice in untreated mice (Supplemental Fig. 1B). In conclusion, we found that β_2-integrins may be involved in the recovery of stroke-related injury and that a reduction in β_2-integrin functionality promotes neuroprotective aspects in the context of hemorrhagic stroke-related injury.

β_2-Integrins influence cytokine expression in the brain after hemorrhagic stroke

To assess whether the differences observed in the cylinder test between WT and β_2-integrin KI mice could be due to immunologic alterations, inflammatory cytokine expression was determined in the brain samples collected 3 d after stroke from the mice used in the cylinder test. RNA was extracted from the ipsilateral striatum samples, and the expression of TNF-α, IL-6, and IL-10 was determined by qRT-PCR. Interestingly, β_2-integrin KI mice showed significantly decreased expression of TNF-α ($p = 0.0055$) (Fig. 2A) and IL-6 ($p = 0.0067$) (Fig. 2B) compared with WT mice. There was also an average 45% decrease in IL-10 expression in β_2-integrin KI mice compared with WT mice (Fig. 2C). However, it did not reach statistical significance.

In conclusion, mice with dysfunctional β_2-integrins showed less severe behavioral deficits and decreased expression of inflammatory cytokines in the brain after induced hemorrhagic stroke.

β_2-Integrins affect microglial phenotype in vivo

Given that we observed a difference in the functional outcome and cytokine expression between β_2-integrin KI and WT mice following hemorrhagic stroke, we next aimed to investigate putative cellular components that could contribute to the results. Microglia are the main immune cells in the CNS, and they become rapidly activated after the incident of stroke (12, 13). In addition, microglia express β_2-integrins and further increase the expression following activation (19–22). Thus, to determine whether there are differences in the microglial population between β_2-integrin and WT mice, we assessed microglial phenotype in healthy brain by flow cytometry. We first identified microglia by gating the leukocyte populations using the markers CD11b and CD45 (Fig. 3A). The microglial population of the leukocytes is defined as $CD11b^{+}CD45^{low}$ (gate 3 in Fig. 3A) (26, 27). There were no statistically significant differences in the proportion of microglia in β_2-integrin KI compared with WT mouse brain (Fig. 3A). Further characterization of the microglial population was done by gating on markers associated with proinflammatory phenotype (MHCII, CD86, CD16/32). The proportion of microglia expressing MHCII ($p = 0.0176$ in microglial population; $p = 0.0137$ in leukocyte population), CD86 ($p = 0.0041$ in microglial population), or CD16/32 ($p = 0.0001$ in microglial population; $p = 0.0019$ in leukocyte population) was significantly higher in WT mice than in β_2-integrin KI mice (Fig. 3B–3D). Furthermore, the level of expression of CD16/32 in WT microglia was significantly higher than in β_2-integrin KI cells ($p < 0.0001$) (Fig. 3D). Of note, there were no differences in the proportions of lymphocytes ($CD45^{high}CD11b^{-}$) (gate 4 in Fig. 3A), neutrophils ($CD45^{high}CD11b^{+}Ly6G^{+}F4/80^{-}$) (included in gate 5 in Fig. 3A) (Supplemental Fig. 2) or monocytes ($CD45^{high}CD11b^{+}Ly6C^{+}F4/80^{-}$) (included in gate 5 in Fig. 3A) (Supplemental Fig. 2) between β_2-integrin KI and WT mice. Neutrophil and monocyte numbers in both WT and KI brains were very low, as expected. Altogether, compared with WT mice, microglia in mice with dysfunctional β_2-integrins express less MHCII, CD86, and CD16/32, markers generally associated with a proinflammatory phenotype.

β_2-Integrins influence microglial cytokine expression in vitro

To investigate cytokine production by microglia directly, microglia were isolated from healthy WT and β_2-integrin KI mice, and the levels of TNF-α in resting and LPS-activated cells were determined

Table I. Mouse details and weights used in in vivo stroke experiment

Mouse ID Number	Genotype	Surgery Number	Sex	Weight Day 1	Weight Day 2	Weight Day 3
2059	WT	1	Male	45.5 g	42.3 g	39.6 g
2061	WT	3	Male	41.4 g	38.8 g	36.1 g
2015	KI	4	Male	42.3 g	38.5 g	36.0 g
2016	KI	5	Male	42.5 g	42.0 g	40.1 g
2013	KI	6	Male	40.7 g	38.2 g	35.6 g
2062	WT	7	Male	40.0 g	39.5 g	38.1 g
2023	WT	9	Male	40.14 g	36.3 g	33.1 g
2041	KI	10	Male	32.49 g	29.6 g	28.4 g
2042	KI	11	Male	32.36 g	30.0 g	28.3 g
2043	KI	12	Male	30.52 g	28.4 g	27.1 g
2040	KI	13	Male	31.41 g	28.8 g	28.1 g

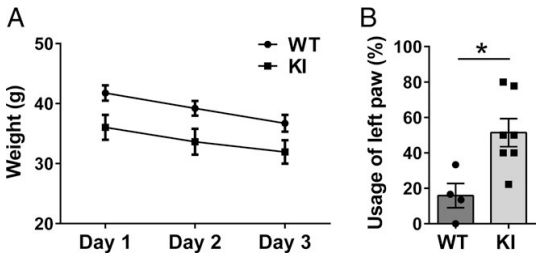

FIGURE 1. β2-Integrin KI mice show significantly higher use of left paw compared with WT mice 1 d after stroke. A hemorrhagic stroke was induced in the right striatum of groups of WT and β2-integrin KI mice (n = 4–7). General well-being of the mice was assessed by weight measurements 1, 2, and 3 d after surgery (**A**). The functional impairment was determined by assessing the use of the left paw in a cylinder test 24 h after surgery (**B**). Data are presented as the mean ± SEM. Statistical differences between WT and β2-integrin KI mice were determined by unpaired *t* test (*$p < 0.05$).

by qRT-PCR (Fig. 4A). Although there was no statistically significant difference in TNF-α expression under these experimental conditions, LPS-activated microglia isolated from β2-integrin KI mice showed an average 28% decrease in TNF-α expression compared with LPS-activated microglia isolated from WT mice (averages for WT, WT+LPS, KI, and KI+LPS: 1.00, 3.04, 0.68, and 2.20, respectively). To determine the effect of the β2-integrin mutation on TNF-α protein level, we assessed TNF-α levels from the culture supernatants from resting and LPS-activated WT and KI microglia by ELISA (Fig. 4B). Interestingly, TNF-α levels were significantly decreased in LPS-activated microglia isolated from β2-integrin KI mice compared with WT mice (Fig. 4B). In contrast, IL-10 levels in the culture supernatants were very low, and there were no statistically significant differences between the groups (Supplemental Fig. 3). In conclusion, β2-integrins influence the level of microglial reactivity to inflammatory stimulus.

Discussion

Inflammation is an important mechanism in the pathogenesis of stroke, and thus targeting leukocytes appears to be an attractive strategy for the development of novel therapies. Given that β2-integrins are constitutively expressed on leukocytes and have been shown to be upregulated in patients after ischemic stroke (23), targeting β2-integrins has been studied extensively in animal models of ischemic stroke. CD18 deficiency or blockade has demonstrated neuroprotective properties

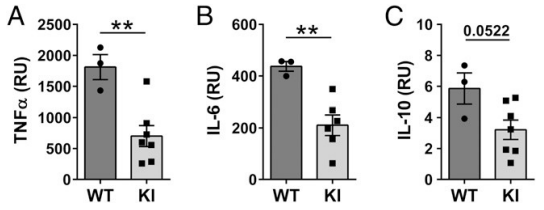

FIGURE 2. β2-Integrin KI mice show decreased expression of inflammatory cytokines 3 d following intrastriatal hemorrhagic stroke compared with WT mice. A hemorrhagic stroke was induced in the right striatum of groups of WT and β2-integrin KI mice. The mice were euthanized 3 d after surgery, and right striata were harvested and frozen. RNA was isolated, and relative expression of TNF-α (**A**), IL-6 (**B**), and IL-10 (**C**) was assessed by qRT-PCR from the brain samples (n = 3–7). Data are presented as the mean ± SEM, and each symbol represents an individual mouse. Statistical differences between WT and KI mice were determined by unpaired *t* test (**$p < 0.01$). RU, relative units.

such as reduced infarct volume, tissue injury, mortality, and improved motor function in various animal models of CNS ischemia (31–36). Furthermore, deficiency or blockade of either LFA-1 or Mac-1 has also shown beneficial effects in various studies involving animal models of cerebral ischemia with reduced infarct size, neuronal death, and mortality and improved motor function (33, 37–41). However, the effects of targeting β2-integrins in hemorrhagic stroke are less well understood. A study by Bavbek et al. showed that rabbits treated with anti-CD18 mAb after subarachnoid hemorrhage had less arterial constriction, an important cause of injury after hemorrhagic stroke, compared with controls (42). In this study, we also show that β2-integrin dysfunction results in improved functional outcome and decreased expression of proinflammatory cytokines, TNF-α and IL-6, in a mouse model of hemorrhagic stroke, suggesting that targeting β2-integrins may also be beneficial in the treatment of hemorrhagic stroke.

In the ischemic stroke models, most studies targeting β2-integrins have focused on neutrophil function and inhibition. Neutrophils infiltrate rapidly at the ischemic site (43), and they, as all other leukocytes, require β2-integrins as they migrate from the bloodstream into the tissues (44). Indeed, the accumulation of neutrophils at the site of ischemia has been implicated in the pathophysiology of stroke in both humans and mice (33, 43, 45–47), and several preclinical studies have associated successful β2-integrin blockade therapy with reduced neutrophil accumulation in the ischemic site (32, 33, 36, 38, 39, 47). It is possible that, also in our study, the improvement we observed in the behavioral test in β2-integrin KI mice compared with WT mice after hemorrhage is due to reduced infiltration of neutrophils and other peripheral leukocytes into the injury site. In support of this, the reduced expression of TNF-α and IL-6 that we observed in the β2-integrin KI mice compared with WT mice after hemorrhagic stroke suggests that the BBB, which is the main barrier preventing peripheral leukocytes from entering the brain, is less permeable in the β2-integrin KI mice. Interestingly, CD18 blockade has indeed been shown to reduce BBB damage (32) and to inhibit vascular permeability and leukocyte adherence after ischemia (48). In addition to their effects on the BBB, both TNF-α and IL-6 have been shown to increase the expression of ICAM-1 on endothelial cells (49). ICAM-1 is a ligand for β2-integrins and mediates leukocyte migration from the blood vessels to tissues (50). Therefore, the decreased expression of TNF-α and IL-6 in the β2-integrin KI brain may also have therefore inhibited peripheral leukocyte infiltration also via decreased expression of ICAM-1 on brain endothelial cells.

Given that microglia have been shown to be more activated and to produce more IL-1β and IL-6 in humans following hemorrhagic stroke (51), we wanted to determine whether the dysfunction of β2-integrins could in fact cause the beneficial effects observed in the cylinder test following hemorrhage via microglia. Therefore, we examined the expression of markers typically associated with a proinflammatory microglial phenotype in the healthy brain of β2-integrin KI versus WT mice. Indeed, we observed decreased expression of MHCII, CD86, and CD16/32 on microglia in β2-integrin KI versus WT mice, indicating less proinflammatory microglia in the brains of β2-integrin KI mice. In addition, we observed a significant reduction in TNF-α production in LPS-activated microglia isolated from β2-integrin KI mice compared with WT mice. Thus, our data demonstrate that targeting β2-integrins affects microglial phenotype and function. We can therefore hypothesize that microglia, either directly or indirectly by affecting peripheral leukocyte infiltration, may be responsible for the improved functional outcome and reduced inflammatory cytokine production in β2-integrin KI mice compared with WT mice after hemorrhagic stroke. As mentioned above, also other immune cells (neutrophils, macrophages, lymphocytes) may be involved in the milder stroke outcome reported in this study, because β2-integrins are expressed on all immune cells, not only on microglia. Microglia are one of the main

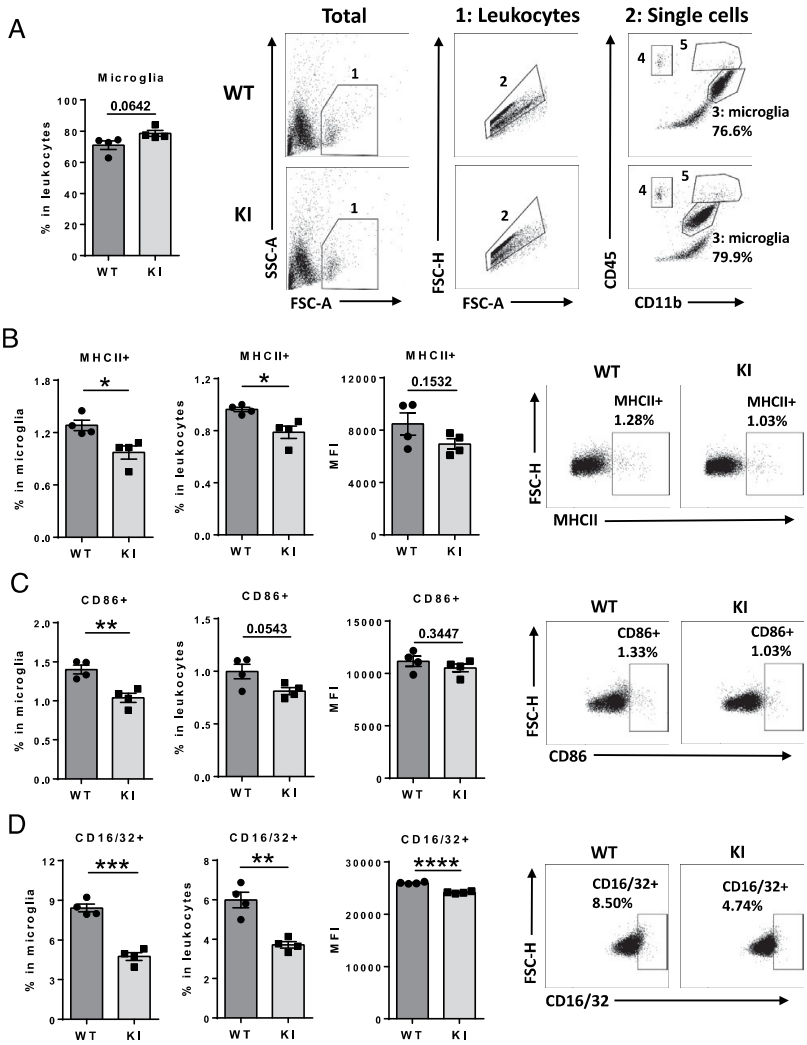

FIGURE 3. Microglia derived from β_2-integrin KI mice show decreased expression of markers associated with proinflammatory phenotype compared with WT mice. Microglial populations were assessed from the brains of male WT and β_2-integrin KI mice (21 wk) ($n = 4$) by flow cytometry. The proportion of microglia in leukocytes and the gating strategy are shown in (**A**). The proportions of $MHCII^+$, $CD86^+$, and $CD16/32^+$ cells in microglial and leukocyte populations, mean fluorescence intensities for $MHCII^+$, $CD86^+$, and $CD16/32^+$ cells, and representative dot plots for WT and β_2-integrin KI mice are shown in (**B–D**). Data in bar graphs are presented as the mean ± SEM, and for cell proportions, each symbol represents an individual mouse. Statistical differences between WT and β_2-integrin KI mice were determined by unpaired *t* test (*$p < 0.05$; **$p < 0.01$; ***$p < 0.001$; ****$p < 0.0001$).

producers of TNF-α and IL-6 cytokines in the brain, but a broad range of other cell types can also produce these cytokines (macrophages, endothelial cells, T cells, NK cells, and others). Other cell types than microglia may therefore also be involved in the reduced cytokine expression observed after hemorrhagic stroke in this study.

In previous stroke studies, targeting microglia has yielded conflicting results. In a study by Li et al., depletion of microglia reduced tissue damage and improved motor function in an ischemia model (52). Similarly, in two hemorrhage models, depletion of microglia by inhibition of colony-stimulating factor 1 receptor resulted in reduced brain injury and improved motor functions (51). However, there are also several studies showing that the presence of microglia or administration of exogenous microglia actually protects the brain from ischemia-induced neuronal damage (53–57). These conflicting results presumably represent the dual role of microglia in stroke pathogenesis and suggest that rather than being either present or absent, fine-tuning microglial function to promote anti-inflammatory functions and/or inhibit proinflammatory functions may be a more plausible approach.

Indeed, Zhao et al. demonstrated that the peroxisome proliferator-activated receptor-γ agonist, rosiglitazone, increased microglial phagocytic capacity in vitro and also improved hematoma clearance, reduced neuronal dysfunction, and promoted functional recovery in mice following intracerebral hemorrhage (58). In addition, several studies have shown minocycline, a tetracycline derivative, to inhibit microglial activation both in vitro and in vivo (59–61). However, the effects of minocycline on reducing brain damage or improving functional outcome have shown conflicting results in preclinical hemorrhage models (59–63). One aspect that may explain the conflicting results and that

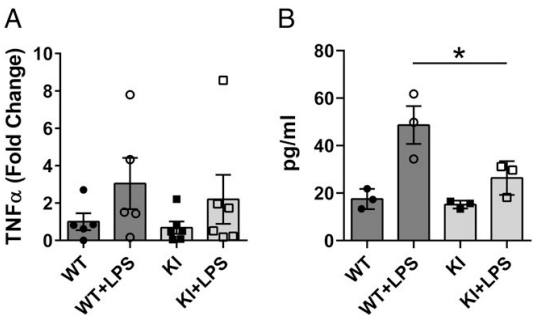

FIGURE 4. Isolated microglia from β_2-integrin KI mice show reduced levels of TNF-α compared with WT in response to an inflammatory stimulus in vitro. Microglia were isolated from the brains of healthy WT and β_2-integrin KI mice and activated with LPS in vitro. RNA was isolated from microglia, and the relative expression of TNF-α was assessed by qRT-PCR (n = 5–6) (**A**). TNF-α production by WT and β_2-integrin KI microglia activated with LPS in vitro was assessed by ELISA (n = 3) (**B**). Data in both graphs are presented as the mean ± SEM, with each symbol representing an individual mouse. Statistical differences between the groups were determined by one-way ANOVA. The graph in (A) is pooled from three independent experiments. *$p < 0.05$.

should be taken into account in the preclinical stroke studies is the timing of the treatment. Indeed, Szymanska et al. failed to observe any benefit of minocycline therapy in the functional outcome when treatment was started 3 h after induction of hemorrhage (60). In most of the preclinical studies, the drug is typically administered very shortly after the induction of hemorrhage, although in patients, the treatment is typically started hours after the stroke event. As a result, a drug that has shown benefit in animal models may not show benefit in the clinic. The effects of a potential drug, such as anti-CD18 mAb or minocycline, should therefore be tested in animal models at several different time points after the induction of hemorrhagic stroke. It should also be noted that the decrease of IL-6 observed in this study in β_2-integrin KI mouse brains after hemorrhagic stroke is not necessarily beneficial, given the newly described role of IL-6 in inducing repair-associated microglia (64).

In conclusion, we have demonstrated that β_2-integrins are involved in the pathophysiology of hemorrhagic stroke by modulating the inflammatory response. The link between neuroinflammation and β_2-integrins may be mediated by different microglial states. β_2-Integrins alter microglial polarization, thereby affecting the frequency of reactive microglial populations. Microglial function may modulate neuroinflammation directly or indirectly by affecting the infiltration of peripheral leukocytes in the brain, thereby influencing functional outcome and the degree of disability resulting from hemorrhagic stroke. The detailed mechanisms of how β_2-integrins affect the functional outcome in the context of hemorrhagic stroke is not yet understood. Therefore, further research on the involvement of β_2-integrins in the context of hemorrhagic stroke-related injury is needed. Studying the neuroinflammatory aspects of β_2-integrins may lead to a better understanding of the modulatory capacity of the immune system in the CNS and to the development of novel therapies for hemorrhagic stroke and also to other CNS diseases.

Acknowledgments

We thank Marjo Vaha for help with the cylinder experiments. Animals were kept at the Laboratory Animal Center of the University of Helsinki. Flow cytometry was performed at the Viikki HiLIFE Flow Cytometry Unit, University of Helsinki.

Disclosures

The authors have no financial conflicts of interest.

References

1. GBD 2019 Stroke Collaborators. 2021. Global, regional, and national burden of stroke and its risk factors, 1990–2019: a systematic analysis for the Global Burden of Disease Study 2019. *Lancet Neurol.* 20: 795–820.
2. Campbell, B. C. V., and P. Khatri. 2020. Stroke. *Lancet* 396: 129–142.
3. Alsbrook, D. L., M. Di Napoli, K. Bhatia, J. Biller, S. Andalib, A. Hinduja, R. Rodrigues, M. Rodriguez, S. Y. Sabbagh, M. Selim, et al. 2023. Neuroinflammation in acute ischemic and hemorrhagic stroke. *Curr. Neurol. Neurosci. Rep.* 23: 407–431.
4. Kleinig, T. J., and R. Vink. 2009. Suppression of inflammation in ischemic and hemorrhagic stroke: therapeutic options. *Curr. Opin. Neurol.* 22: 294–301.
5. Kuriakose, D., and Z. Xiao. 2020. Pathophysiology and treatment of stroke: present status and future perspectives. *Int. J. Mol. Sci.* 21: 7609.
6. Li, Q., and B. A. Barres. 2018. Microglia and macrophages in brain homeostasis and disease. *Nat. Rev. Immunol.* 18: 225–242.
7. Thion, M. S., F. Ginhoux, and S. Garel. 2018. Microglia and early brain development: an intimate journey. *Science* 362: 185–189.
8. Hickman, S., S. Izzy, P. Sen, L. Morsett, and J. El Khoury. 2018. Microglia in neurodegeneration. *Nat. Neurosci.* 21: 1359–1369.
9. Norris, G. T., and J. Kipnis. 2019. Immune cells and CNS physiology: microglia and beyond. *J. Exp. Med.* 216: 60–70.
10. Iadecola, C., and J. Anrather. 2011. The immunology of stroke: from mechanisms to translation. *Nat. Med.* 17: 796–808.
11. Rawlinson, C., S. Jenkins, L. Thei, M. L. Dallas, and R. Chen. 2020. Post-ischaemic immunological response in the brain: targeting microglia in ischaemic stroke therapy. *Brain Sci.* 10: 159.
12. Qin, J., Z. Ma, X. Chen, and S. Shu. 2023. Microglia activation in central nervous system disorders: a review of recent mechanistic investigations and development efforts. *Front. Neurol.* 14: 1103416.
13. Taylor, R. A., and L. H. Sansing. 2013. Microglial responses after ischemic stroke and intracerebral hemorrhage. *Clin. Dev. Immunol.* 2013: 746068.
14. Biswas, K. 2023. Microglia mediated neuroinflammation in neurodegenerative diseases: a review on the cell signaling pathways involved in microglial activation. *J. Neuroimmunol.* 383: 578180.
15. Liu, J., Z. Zhu, and G. K. Leung. 2022. Erythrophagocytosis by microglia/macrophage in intracerebral hemorrhage: from mechanisms to translation. *Front. Cell. Neurosci.* 16: 818602.
16. Kechagia, J. Z., J. Ivaska, and P. Roca-Cusachs. 2019. Integrins as biomechanical sensors of the microenvironment. *Nat. Rev. Mol. Cell. Biol.* 20: 457–473.
17. Takada, Y., X. Ye, and S. Simon. 2007. The integrins. *Genome Biol.* 8: 215.
18. Fagerholm, S. C., C. Guenther, M. Llort Asens, T. Savinko, and L. M. Uotila. 2019. Beta2-integrins and interacting proteins in leukocyte trafficking, immune suppression, and immunodeficiency disease. *Front. Immunol.* 10: 254.
19. Akiyama, H., and P. L. McGeer. 1990. Brain microglia constitutively express beta-2 integrins. *J. Neuroimmunol.* 30: 81–93.
20. Kloss, C. U., M. Bohatschek, G. W. Kreutzberg, and G. Raivich. 2001. Effect of lipopolysaccharide on the morphology and integrin immunoreactivity of ramified microglia in the mouse brain and in cell culture. *Exp. Neurol.* 168: 32–46.
21. Milner, R., and I. L. Campbell. 2003. The extracellular matrix and cytokines regulate microglial integrin expression and activation. *J. Immunol.* 170: 3850–3858.
22. Ullrich, O., A. Diestel, I. Y. Eyüpoglu, and R. Nitsch. 2001. Regulation of microglial expression of integrins by poly(ADP-ribose) polymerase-1. *Nat. Cell. Biol.* 3: 1035–1042.
23. Kim, J. S., M. Chopp, H. Chen, S. R. Levine, J. L. Carey, and K. M. Welch. 1995. Adhesive glycoproteins CD11a and CD18 are upregulated in the leukocytes from patients with ischemic stroke and transient ischemic attacks. *J. Neurol. Sci.* 128: 45–50.
24. Morrison, V. L., M. MacPherson, T. Savinko, H. S. Lek, A. Prescott, and S. C. Fagerholm. 2013. The β2 integrin-kindlin-3 interaction is essential for T-cell homing but dispensable for T-cell activation in vivo. *Blood* 122: 1428–1436.
25. Bordt, E. A., C. L. Block, T. Petrozziello, G. Sadri-Vakili, C. J. Smith, A. G. Edlow, and S. D. Bilbo. 2020. Isolation of microglia from mouse or human tissue. *STAR Protoc.* 1: 100035.
26. Pino, P. A., and A. E. Cardona. 2011. Isolation of brain and spinal cord mononuclear cells using Percoll gradients. *J. Vis. Exp.* (48): 2348.
27. Bedi, S. S., P. Smith, R. A. Hetz, H. Xue, and C. S. Cox. 2013. Immunomagnetic enrichment and flow cytometric characterization of mouse microglia. *J. Neurosci. Methods* 219: 176–182.
28. Tseng, K. Y., V. Stratoulias, W. F. Hu, J. S. Wu, V. Wang, Y. H. Chen, A. Seelbach, H. J. Huttunen, N. Kulesskaya, C. Y. Pang, et al. 2023. Augmenting hematoma-scavenging capacity of innate immune cells by CDNF reduces brain injury and promotes functional recovery after intracerebral hemorrhage. *Cell Death Dis.* 14: 128.
29. Schallert, T., S. M. Fleming, J. L. Leasure, J. L. Tillerson, and S. T. Bland. 2000. CNS plasticity and assessment of forelimb sensorimotor outcome in unilateral rat models of stroke, cortical ablation, parkinsonism and spinal cord injury. *Neuropharmacology* 39: 777–787.
30. Kankkunen, P., J. Rintahaka, A. Aalto, M. Leino, M.-L. Majuri, H. Alenius, H. Wolff, and S. Matikainen. 2009. Trichothecene mycotoxins activate inflammatory response in human macrophages. *J. Immunol.* 182: 6418–6425.

31. Clark, W. M., K. P. Madden, R. Rothlein, and J. A. Zivin. 1991. Reduction of central nervous system ischemic injury in rabbits using leukocyte adhesion antibody treatment. *Stroke* 22: 877–883.
32. Lindsberg, P. J., A. L. Sirén, G. Z. Feuerstein, and J. M. Hallenbeck. 1995. Antagonism of neutrophil adherence in the deteriorating stroke model in rabbits. *J. Neurosurg.* 82: 269–277.
33. Matsuo, Y., H. Onodera, Y. Shiga, H. Shozuhara, M. Ninomiya, T. Kihara, T. Tamatani, M. Miyasaka, and K. Kogure. 1994. Role of cell adhesion molecules in brain injury after transient middle cerebral artery occlusion in the rat. *Brain Res.* 656: 344–352.
34. Prestigiacomo, C. J., S. C. Kim, E. S. Connolly, Jr., H. Liao, S. F. Yan, and D. J. Pinsky. 1999. CD18-mediated neutrophil recruitment contributes to the pathogenesis of reperfused but not nonreperfused stroke. *Stroke* 30: 1110–1117.
35. Vedder, N. B., R. K. Winn, C. L. Rice, E. Y. Chi, K. E. Arfors, and J. M. Harlan. 1988. A monoclonal antibody to the adherence-promoting leukocyte glycoprotein, CD18, reduces organ injury and improves survival from hemorrhagic shock and resuscitation in rabbits. *J. Clin. Invest.* 81: 939–944.
36. Yenari, M. A., D. Kunis, G. H. Sun, D. Onley, L. Watson, S. Turner, S. Whitaker, and G. K. Steinberg. 1998. Hu23F2G, an antibody recognizing the leukocyte CD11/CD18 integrin, reduces injury in a rabbit model of transient focal cerebral ischemia. *Exp. Neurol.* 153: 223–233.
37. Arumugam, T. V., J. W. Salter, J. H. Chidlow, C. M. Ballantyne, C. G. Kevil, and D. N. Granger. 2004. Contributions of LFA-1 and Mac-1 to brain injury and microvascular dysfunction induced by transient middle cerebral artery occlusion. *Am. J. Physiol. Heart Circ. Physiol.* 287: H2555–H2560.
38. Chen, H., M. Chopp, R. L. Zhang, G. Bodzin, Q. Chen, J. R. Rusche, and R. F. Todd 3rd. 1994. Anti-CD11b monoclonal antibody reduces ischemic cell damage after transient focal cerebral ischemia in rat. *Ann. Neurol.* 35: 458–463.
39. Chopp, M., R. L. Zhang, H. Chen, Y. Li, N. Jiang, and J. R. Rusche. 1994. Postischemic administration of an anti-Mac-1 antibody reduces ischemic cell damage after transient middle cerebral artery occlusion in rats. *Stroke* 25: 869–876.
40. Garcia, J. H., K. F. Liu, and M. P. Bree. 1996. Effects of CD11b/18 monoclonal antibody on rats with permanent middle cerebral artery occlusion. *Am. J. Pathol.* 148: 241–248.
41. Soriano, S. G., A. Coxon, Y. F. Wang, M. P. Frosch, S. A. Lipton, P. R. Hickey, and T. N. Mayadas. 1999. Mice deficient in Mac-1 (CD11b/CD18) are less susceptible to cerebral ischemia/reperfusion injury. *Stroke* 30: 134–139.
42. Bavbek, M., R. Polin, A. L. Kwan, A. S. Arthur, N. F. Kassell, and K. S. Lee. 1998. Monoclonal antibodies against ICAM-1 and CD18 attenuate cerebral vasospasm after experimental subarachnoid hemorrhage in rabbits. *Stroke* 29: 1930–1936.
43. Jickling, G. C., D. Liu, B. P. Ander, B. Stamova, X. Zhan, and F. R. Sharp. 2015. Targeting neutrophils in ischemic stroke: translational insights from experimental studies. *J. Cereb. Blood Flow Metab.* 35: 888–901.
44. Conley, H. E., and M. K. Sheats. 2023. Targeting neutrophil β_2-integrins: a review of relevant resources, tools, and methods. *Biomolecules* 13: 892.
45. Akopov, S. E., N. A. Simonian, and G. S. Grigorian. 1996. Dynamics of polymorphonuclear leukocyte accumulation in acute cerebral infarction and their correlation with brain tissue damage. *Stroke* 27: 1739–1743.
46. Satoh, S., T. Kobayashi, A. Hitomi, I. Ikegaki, Y. Suzuki, M. Shibuya, J. Yoshida, and T. Asano. 1999. Inhibition of neutrophil migration by a protein kinase inhibitor for the treatment of ischemic brain infarction. *Jpn. J. Pharmacol.* 80: 41–48.
47. Vedder, N. B., R. K. Winn, C. L. Rice, E. Y. Chi, K. E. Arfors, and J. M. Harlan. 1990. Inhibition of leukocyte adherence by anti-CD18 monoclonal antibody attenuates reperfusion injury in the rabbit ear. *Proc. Natl. Acad. Sci. U. S. A.* 87: 2643–2646.
48. Gidday, J. M., T. S. Park, E. R. Gonzales, and J. W. Beetsch. 1997. CD18-dependent leukocyte adherence and vascular injury in pig cerebral circulation after ischemia. *Am. J. Physiol.* 272: H2622–H2629.
49. van de Stolpe, A., and P. T. van der Saag. 1996. Intercellular adhesion molecule-1. *J. Mol. Med. (Berl.)* 74: 13–33.
50. Harjunpää, H., M. Llort Asens, C. Guenther, and S. C. Fagerholm. 2019. Cell adhesion molecules and their roles and regulation in the immune and tumor microenvironment. *Front. Immunol.* 10: 1078.
51. Li, M., Z. Li, H. Ren, W. N. Jin, K. Wood, Q. Liu, K. N. Sheth, and F. D. Shi. 2017. Colony stimulating factor 1 receptor inhibition eliminates microglia and attenuates brain injury after intracerebral hemorrhage. *J. Cereb. Blood Flow Metab.* 37: 2383–2395.
52. Li, T., J. Zhao, W. Xie, W. Yuan, J. Guo, S. Pang, W. B. Gan, D. Gómez-Nicola, and S. Zhang. 2021. Specific depletion of resident microglia in the early stage of stroke reduces cerebral ischemic damage. *J. Neuroinflammation* 18: 81.
53. Faustino, J. V., X. Wang, C. E. Johnson, A. Klibanov, N. Derugin, M. F. Wendland, and Z. S. Vexler. 2011. Microglial cells contribute to endogenous brain defenses after acute neonatal focal stroke. *J. Neurosci.* 31: 12992–13001.
54. Imai, F., H. Suzuki, J. Oda, T. Ninomiya, K. Ono, H. Sano, and M. Sawada. 2007. Neuroprotective effect of exogenous microglia in global brain ischemia. *J. Cereb. Blood Flow Metab.* 27: 488–500.
55. Lalancette-Hébert, M., G. Gowing, A. Simard, Y. C. Weng, and J. Kriz. 2007. Selective ablation of proliferating microglial cells exacerbates ischemic injury in the brain. *J. Neurosci.* 27: 2596–2605.
56. Montero, M., B. González, and J. Zimmer. 2009. Immunotoxic depletion of microglia in mouse hippocampal slice cultures enhances ischemia-like neurodegeneration. *Brain Res.* 1291: 140–152.
57. Szalay, G., B. Martinecz, N. Lénárt, Z. Környei, B. Orsolits, L. Judák, E. Császár, R. Fekete, B. L. West, G. Katona, et al. 2016. Microglia protect against brain injury and their selective elimination dysregulates neuronal network activity after stroke. *Nat. Commun.* 7: 11499.
58. Zhao, X., G. Sun, J. Zhang, R. Strong, W. Song, N. Gonzales, J. C. Grotta, and J. Aronowski. 2007. Hematoma resolution as a target for intracerebral hemorrhage treatment: role for peroxisome proliferator-activated receptor gamma in microglia/macrophages. *Ann. Neurol.* 61: 352–362.
59. Power, C., S. Henry, M. R. Del Bigio, P. H. Larsen, D. Corbett, Y. Imai, V. W. Yong, and J. Peeling. 2003. Intracerebral hemorrhage induces macrophage activation and matrix metalloproteinases. *Ann. Neurol.* 53: 731–742.
60. Szymanska, A., J. Biernaskie, D. Laidley, S. Granter-Button, and D. Corbett. 2006. Minocycline and intracerebral hemorrhage: influence of injury severity and delay to treatment. *Exp. Neurol.* 197: 189–196.
61. Wu, J., S. Yang, G. Xi, G. Fu, R. F. Keep, and Y. Hua. 2009. Minocycline reduces intracerebral hemorrhage-induced brain injury. *Neurol. Res.* 31: 183–188.
62. Wasserman, J. K., and L. C. Schlichter. 2007. Minocycline protects the blood-brain barrier and reduces edema following intracerebral hemorrhage in the rat. *Exp. Neurol.* 207: 227–237.
63. Wasserman, J. K., and L. C. Schlichter. 2007. Neuron death and inflammation in a rat model of intracerebral hemorrhage: effects of delayed minocycline treatment. *Brain Res.* 1136: 208–218.
64. Choi, B. R., K. R. Johnson, D. Maric, and D. B. McGavern. 2023. Monocyte-derived IL-6 programs microglia to rebuild damaged brain vasculature. *Nat. Immunol.* 24: 1110–1123.

Publication III

INTERFACE

royalsocietypublishing.org/journal/rsif

Research

Cite this article: Askari S, Saldo Rubio G, Datar A, Harjunpää H, Fagerholm SC, Backholm M. 2025 Soft matter mechanics of immune cell aggregates. *J. R. Soc. Interface* **22**: 20250231.
https://doi.org/10.1098/rsif.2025.0231

Received: 18 March 2025
Accepted: 30 June 2025

Subject Category:
Life Sciences–Physics interface

Subject Areas:
biomechanics

Keywords:
immune cells, cellular aggregates, immune cell activation, soft matter mechanics

Authors for correspondence:
Susanna C. Fagerholm
e-mail: susanna.fagerholm@helsinki.fi
Matilda Backholm
e-mail: matilda.backholm@aalto.fi

†These authors contributed equally to the study.

Electronic supplementary material is available online at https://doi.org/10.6084/m9.figshare.c.7918150.

THE ROYAL SOCIETY PUBLISHING

Soft matter mechanics of immune cell aggregates

Shohreh Askari[1,†], Guillem Saldo Rubio[2,†], Anagha Datar[1], Heidi Harjunpää[2], Susanna C. Fagerholm[2] and Matilda Backholm[1]

[1]Department of Applied Physics, Aalto University, Espoo, Finland
[2]Molecular and Integrative Biosciences Research Programme, Faculty of Biological and Environmental Sciences, University of Helsinki, Helsinki, Finland

MB, 0000-0003-4501-8872

T-cells are a crucial subset of white blood cells that play a central role in the immune system. When T-cells bind antigens, it leads to cell activation and the induction of an immune response. If T-cells are activated by antigens *in vivo* or artificially *in vitro*, they form multicellular aggregates. The mechanical properties of such clusters provide valuable information on different T-cell activation pathways. Furthermore, the aggregate mechanics capture how T-cells are affected by mechanical forces and interact within larger conglomerates, such as lymph nodes and tumours. However, an understanding of collective T-cell adhesion and mechanics following cell activation is currently lacking. Probing the mechanics of fragile and microscopically small living samples is experimentally challenging. Here, the micropipette force sensor technique was used to stretch T-cell aggregates and directly measure their Young's modulus and ultimate tensile strength. A mechanistic model was developed to correlate how the stiffness of the mesoscale multicellular aggregate emerges from the mechanical response of the individual microscopic cells within the cluster. We show how the aggregate elasticity is affected by different activators and relate this to different activation pathways in the cells. Our soft matter mechanics study of multicellular T-cell aggregates contributes to our understanding of the biology behind immune cell activation.

1. Introduction

Cells are the fundamental building blocks of life. In multicellular organisms, individual cells work collectively to maintain the structural and functional integrity of tissues and organs. To study these multicellular living materials with the rigour of biological physics and mathematics, multicellular aggregates have been proposed as the ideal model system [1]. Decoding how cells behave and interact in an aggregate is key to understanding diverse biological processes, from tissue regeneration [2] and morphogenesis [3], to immune responses [4] and the progression of diseases like cancer [5].

Microscale force probes, such as atomic force microscopy, optical tweezers and micropipette-based techniques, have been widely used to measure the mechanical properties of single cells [6–13] as well as their adhesion to surfaces or other cells [14–23]. In addition, non-direct force measurements have been performed using, for example, the centrifugation assay, spinning disc and flow chamber, to probe the adhesion force of populations of single cells [24]. However, probing the biomechanics and dynamics of multicellular aggregates is challenging due to the mesoscale length scale of the system. This has led to the development of several new force probes and experimental approaches. For example, Foty *et al.* used a parallel plate compression apparatus to probe the interfacial tension of liver cell aggregates [25]. This approach was later adapted by several others [26,27]. Kalantarian *et*

al. used centrifugation to measure the surface tension of aggregates [28]. Ryan *et al.* probed the spreading rates of fibroblast cell aggregates to probe their cell–cell cohesion [29] and the group of Brochard–Wyart has further studied the spreading and flow of cellular aggregates [30–32]. In the same group, Guevorkian *et al.* also developed the micropipette aspiration technique to directly measure the viscoelastic mechanical properties of cancer cell aggregates [33] as well as the mechanosensitive 'shivering' of the aggregates under controlled aspiration [34]. Furthermore, Gonzalez-Rodriguez *et al.* measured the detachment and fracture of cellular aggregates using a force-calibrated glass slide as a cantilever [35]. As a final example, Lyu *et al.* have used a soft resistive force-sensing diaphragm to probe the tiny contractile force of cardiac organoids [36]. In general, experimental soft matter physics has been instrumental in forming a new understanding of these living multicellular materials.

From a soft matter mechanics perspective, T-cells are a particularly interesting cell type. These highly specialized, microscopically small immune cells are crucial in the adaptive response of the immune system of mammals [37]. T-cells originate in the bone marrow and migrate to the thymus for further development and maturation. The mature T-cells circulate in the blood stream, encounter antigens in lymph nodes, become activated and finally migrate to peripheral tissues to participate in the intricate functions of the whole immune system. Their main task is to recognize and destroy foreign invaders such as bacteria and viruses. They do this by recognizing and binding to a specific structure called an antigen on, for example, bacteria. Seminal biophysical studies have shown interesting mechanisms of how T-cells use mechanical forces in their immunological response [38,39].

Upon encountering a specific antigen, T-cells undergo activation and clonal expansion, that is, a rapid division to produce many identical cells that can respond to the same antigen [37]. To study the biology of T-cell activation, the activation process can be mimicked in an antigen-agnostic manner. This means that the T-cells are activated in a way that does not depend on recognizing a specific antigen but still triggers their activation and expansion. Such artificial activation can be done using chemicals such as phorbol myristate acetate (PMA) and ionomycin [40], or anti-CD3 antibodies [4,22]. These different activators work through distinct mechanisms (figure 1a). Anti-CD3 binds directly to the T-cell receptor (TCR), mimicking antigen binding and triggering a signalling cascade that results in T-cell activation. PMA and ionomycin stimulate elements of the intracellular signalling pathway that follow antigen recognition. Another important compound for the T-cell activation pathway is the inhibitor W-7, which inhibits the function of calmodulin (Ca^{2+}-binding protein) in cells [41].

When T-cells are activated, this leads to integrin activation and T-cell clustering into large aggregates of many cells (figure 1b). These aggregates are biologically important, as they allow the cells to efficiently share important soluble factors (interleukin-2) that allow for cell proliferation [42]. Integrins play a vital role in the immune cell function, particularly in T-cell adhesion, mediated by interactions with intercellular adhesion molecules (ICAMs) [21]. Atomic force microscopy studies have revealed time-dependent adhesion strengthening, with unbinding forces increasing from 140 to 580 pN over short time scales [21] as well as the effect of force generation on T-cell activation [43]. Advances in optical tweezers have provided further insights into integrin mechanics, enabling the quantification of cell–cell bond rupture forces [22].

These biophysical approaches collectively enhance our understanding of integrin function at molecular and cellular levels. However, an understanding of collective T-cell adhesion and mechanical forces in cell aggregates following cell activation is currently completely lacking. Such information is crucial because immune cells often interact within larger conglomerates, such as lymph nodes and tumours, and mechanical forces between cells are emerging as important regulators of immune cell programming, behaviour and function [44].

Here, we have used a soft matter mechanics approach to take a first step towards understanding the biology of T-cell interactions in mesoscale multicellular aggregates. In our experiments, we have activated mouse primary T-cells to study how the different activation pathways affect the resulting immune cell activity and multicellular aggregate properties. By using the micropipette force sensor (MFS) technique, we have directly measured the mechanical properties of the *in vitro* activated immune cell aggregates through stretching. To correlate the emergent macroscopic mechanical response of the multicellular system with the microscopic cell elasticity, we have developed a new mechanistic model. We have explored the effects of various factors, such as post-induction time, aggregate volume and pre-stretching, on the T-cell aggregate. Finally, we evaluated the influence of specific activators, including W-7 (a calmodulin antagonist) and anti-CD3, on aggregate stiffness. Our results showcase the importance of a multidisciplinary approach in the study of biological systems.

2. Methods

In this section, we concisely describe our experimental approach. For all technical details on methodology and materials, refer to §6 at the end of the article.

2.1. *In vitro* induced T-cell aggregation

To study the cohesion and mechanics of immune cell aggregates, primary T-cells were isolated from mice and activated using PMA and ionomycin, or by only anti-CD3. When the calmodulin inhibitor W-7 was used, it was added 30 min before the addition of PMA and ionomycin. These chemicals trigger intracellular signalling events that activate integrins, making the T-cells highly adhesive and causing them to aggregate into clusters (figure 1b). As shown in figure 1c,d, these treatments induce T-cell activation, as evidenced by increased CD69 expression at 5 h and CD25 expression after overnight incubation [45]. Of these *in vitro* activators, anti-CD3 most closely mimics the biological activation of T-cells, initiating intracellular signalling within the T-cell. PMA and ionomycin mimic these signalling effects by artificially activating the same pathways as

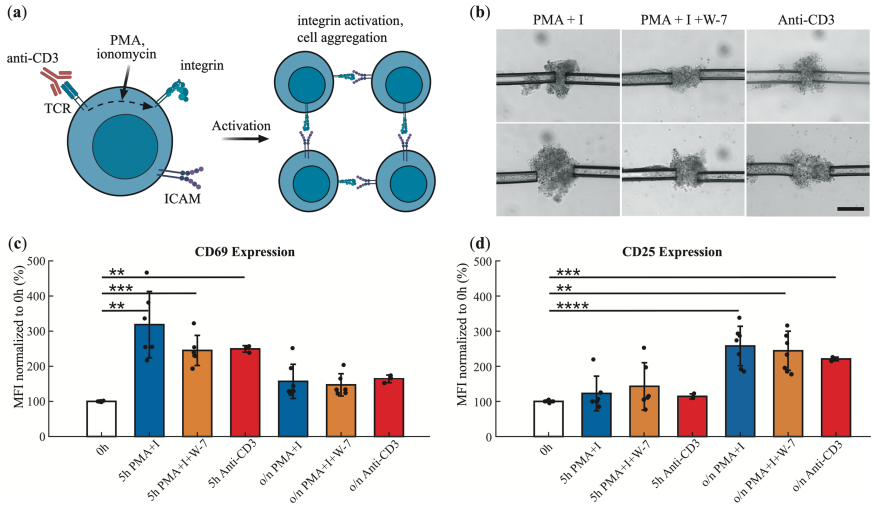

Figure 1. *In vitro* activation of T-cells. (a) Overview of *in vitro* activators: anti-CD3 binds the T-cell receptors (TCRs) and triggers the downstream activation signalling. PMA and ionomycin together mimic part of this signalling cascade. W-7, a calmodulin inhibitor, interferes with some effects of calcium influx into T-cells. T-cell activation leads to integrin activation, integrin binding to intercellular adhesion molecules (ICAMs), and cellular aggregation. It also induces various other cellular changes, including the expression of T-cell activation markers (not shown). (b) Optical microscopy images of T-cell aggregates (held by two micropipettes) following activation with PMA and ionomycin (PMA+I, left); PMA, ionomycin, and W-7 (PMA+I + W-7, middle); and anti-CD3 (right). Scale bar 50 µm. (c) Expression levels of the early T-cell activation marker CD69 after stimulation with PMA+ionomycin, PMA+ionomycin + W-7, or anti-CD3 at 5 h post-induction or overnight (o/n). Presented as mean fluorescence intensity (MFI) as measured using a flow cytometer. (d) Expression levels of the late T-cell activation marker CD25 under the same conditions. The stars in (c)–(d) indicate statistical significance of Welch's *t*-test of the mean of a pair of groups with $^{**}p < 0.01$, $^{***}p < 0.001$, $^{****}p < 0.0001$.

T-cell receptor activation [46]. W-7, a calmodulin antagonist, further modulates T-cell signalling and introduces an additional regulatory dimension to PMA+ionomycin-induced activation [47,48].

2.2. Stretching of T-cell aggregates

The MFS technique [49] was used to stretch the T-cell aggregates and measure their mechanical properties (figure 2). In this technique, the deflection x of a glass micropipette is used to measure and apply a force $F = k_p x$, where k_p is the spring constant of the cantilever, determined through calibration. The MFS technique has been extensively used to probe the biomechanical properties of single cells [8,9], including T-cells [39], as well as microbial flocs [50,51] and whole organisms [52,53].

The buffer solution containing T-cells was carefully injected between two glass slides, which were mounted in a custom-made holder on an inverted microscope. Two micropipettes were required for the stretching experiments: one straight holding micropipette mounted on a linear motor and one L-shaped, force-calibrated MFS mounted at a 90° angle on a manual *xyz*-micromanipulator (figure 2a). These micropipettes were moved into the chamber, ensuring that the entire lengths of the cantilevers were immersed in the buffer solution. Both micropipettes were used to hold on to an aggregate with gentle suction using syringes. To stretch the aggregate, the straight micropipette was moved to the left at a constant speed of $v = 20$ µm s^{-1} using a linear motor (figure 2b). This movement caused a deflection in the L-shaped micropipette, which applied an increasing force onto the aggregate, leading to its stretching.

3. Models

3.1. Mechanical properties

The T-cell aggregate was modelled as a cylinder with an initial radius R_0 and length L_0 (figure 2b). When stretched using MFS, the aggregate is under a stress $\sigma = F/\pi R_0^2 = k_p x/\pi R_0^2$ and strain $\varepsilon = \Delta L/L_0$, where $\Delta L = x_S - x = vt - x$ is the change in length of the aggregate. We have, in other words, used the engineering stress instead of the true stress to determine the mechanical properties. The same choice of definition was used in the cell aggregate stretching work of Gonzalez-Rodriguez *et al.* [35], allowing for direct comparisons between our findings. The Young's modulus is defined as $E = \sigma/\varepsilon$ for small deformations within the elastic regime [54]. This corresponds to the slope of the initial, linear regime in the standard stress–strain graph, illustrated with an example of our experimental data in figure 2c. As the aggregate is stretched further, the system transitions into the plastic regime, where material deformations become irreversible. From the stress–strain graph, the ultimate tensile strength σ_{UTS} was determined (figure 2c), which is an important measure of the mechanical properties of the aggregate, representing the maximum stress the material can sustain before breaking.

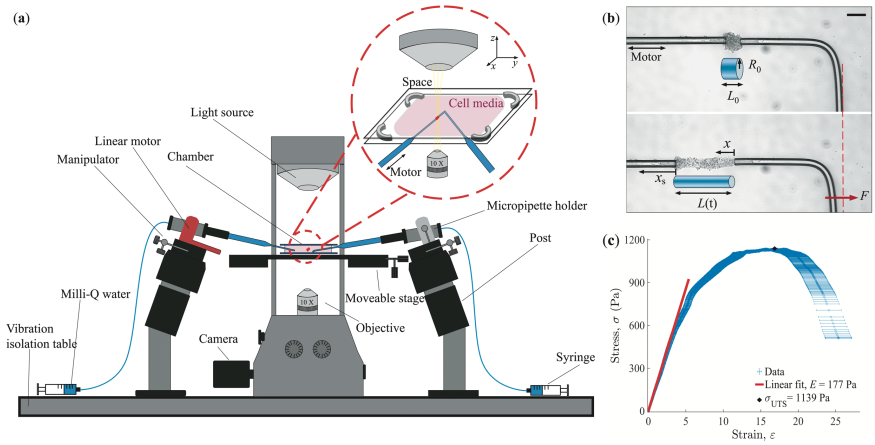

Figure 2. Cell aggregate stretching using the micropipette force sensor. (a) Schematic sketch (not to scale) of the set-up with the straight and L-shaped micropipettes holding on to the T-cell aggregate with suction. The straight micropipette is connected to a linear motor and the L-shaped is calibrated and used as a force sensor. (b) Examples of optical microscopy images from before (top) and after (bottom) the stretching. The aggregate is modelled as a cylinder with an initial radius R_0 and length L_0. During the experiment, the straight micropipette is moved to the left at a constant speed ($x_S = vt$), causing the L-shaped force sensor to deflect (x). This applies a Hookean force $F = k_p x$ onto the aggregate, which stretches, $L(t)$. Scale bar 50 µm. (c) Example of stress–strain graph from a typical stretching experiment. The Young's modulus E and ultimate tensile strength σ_{UTS} are determined from the graph. The error bars are error propagations of the stress and strain using the standard deviation of k_p, R_0 and L_0 (see §6 for details).

3.2. Mechanistic model

Various theoretical models, such as the geometry-based vertex model and lattice-based cellular Potts model [1], exist for describing a multicellular system. Most of these focus on epithelial morphology, topology, dynamics and mechanics in two dimensions [3,55–57]. A limited focus has been on modelling three-dimensional systems [57–62]. In our case, an advantage of a vertex model over the cellular Potts model would be that it allows for the treatment of the elastic response of a multicellular system under external loading [1]. However, the vertex-based model is not suitable for describing T-cell aggregates, where the randomly organized small cells do not deform into polyhedral shapes as required in a three-dimensional vertex geometry. To bridge the gap between individual cellular mechanical response and the emergent macroscopic mechanical properties (defined in §3.1), a new scaling law-based mechanistic model was developed (figure 3). A T-cell aggregate was assumed to consists of randomly arranged cells adhered to each other. The mechanical response of the cell (radius r_c) was modelled with an elastic spring with a stiffness of k_c. This effective cell stiffness includes the stiffness of the cell–cell adhesion bonds coupled with that of the cell itself, where we assume that the stiffness stems from the elastic cortical shell of the cell. The deformations of these springs contribute to the emergent mechanical response of the aggregate.

The force is applied in the x-direction, causing a mechanical response of the cells mostly along this axis. In response, each spring extends by Δl_c, forming a force chain in the aggregate, where neighbouring cells along the x-axis create a series connection of springs (figure 3b,c). For one such series connection along the entire aggregate length, the number of springs is $n_x \sim L_0/2r_c$. To stretch one such series-connected chain of springs, a force of $F_{series} = k_c \Delta l_c$ would be required [63]. The change in length of an entire chain upon stretching is the same as the change of length of the entire aggregate: $\Delta L \sim n_x \Delta l_c \sim (L_0/2r_c)\Delta l_c$.

The total number of series-connected chains within the cylindrical cross-sectional area ($A = \pi R_0^2$) of the aggregate is $n_A \sim R_0^2/r_c^2$. These chains of springs respond in parallel when the entire aggregate is stretched (figure 3c), requiring a total force of $F = n_A F_{series}$, according to the conventional rules of stretching parallel connected springs [64]. This gives an expression for the total force needed to stretch the aggregate: $F = k_c \Delta l_c R_0^2/r_c^2$.

Adding all of this together, the Young's modulus can thus be written as

$$E = \frac{\sigma}{\varepsilon} = \frac{F}{A}\frac{L_0}{\Delta L} \sim \frac{k_c}{r_c}. \tag{3.1}$$

This equation links the emergent mechanical response of the entire multicellular aggregate to the stiffness of the individual cells and their internal bonds. It shows that the elasticity of the aggregate scales linearly with the elasticity of the cells. This finding is critical for understanding the relationship between T-cell activation levels and aggregate mechanics, as higher T-cell activation can be hypothesized to create stronger adhesion within the aggregate as well as affect the cell stiffness. It is important to note that this mechanistic model is only valid in the initial elastic regime and cannot be extrapolated to the later stages of the stretching experiments.

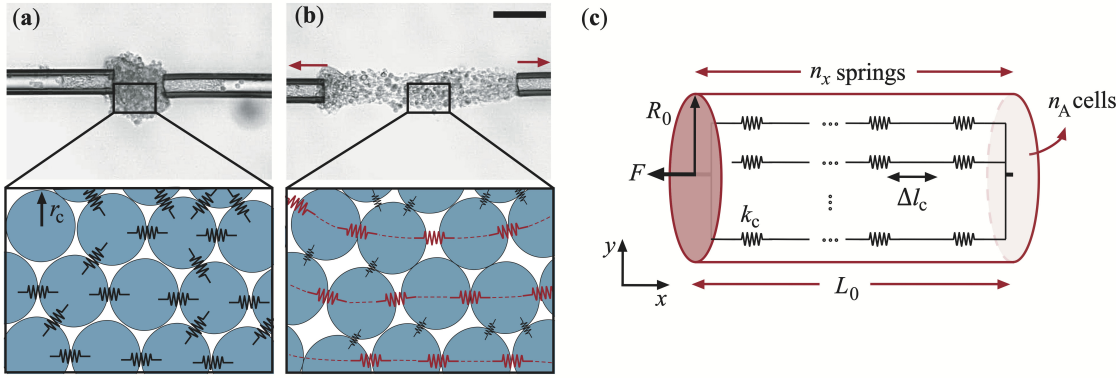

Figure 3. Mechanistic model. The cells are modelled as spheres with a radius of r_c and spring constant k_c. The aggregates with their modelled cell-spring structure are shown in (a) before and (b) during the stretching. Scale bar 50 µm. (c) Schematic drawing of the mechanistic model with parallel connections of series-connected springs acting as force chains through the aggregate. Each spring changes its length by Δl_c when the external force F is applied.

4. Results and discussion

4.1. Mechanics of T-cell aggregates

T-cell aggregates formed through activation with PMA and ionomycin were used as a model system in this study. The cells were activated in a biology laboratory and the aggregates were then transported to a physics laboratory for measurements. The activated T-cells remained viable for at least 24 h post-induction. A representative example of an MFS stretching experiment is shown in electronic supplementary material, video S1 and its resulting stress–strain curve is shown in figure 2c. The MFS technique is well suited for these measurements because of its ability to precisely measure nN-range forces while simultaneously stretching the sample and observing the resulting deformation. Since the sample is held through gentle suction with the micropipettes, no potentially harmful glue is needed. Several aggregates of varying volumes ($V = 10^4$ to 7×10^5 µm^3) were stretched (see electronic supplementary material, videos S2–S3). All experiments showed very similar stress–strain graphs with the clear traits of ductile material, indicating significant plastic deformations before rupture. In figure 4a, the Young's modulus is plotted as a function of time from when the activation was done. There is no effect of post-activation time on the stiffness of the clusters—as long as the cells remain viable, the Young's modulus remains constant.

Within error, the measured mechanical properties of the aggregates were independent of their volume (figure 4b). Experiments were initially also performed on aggregates with volumes much larger than 10^6 µm^3. However, these were found to be more irregular in shape with portions of the cluster not contributing to the stretching process. Since the cylindrical shape approximation did not properly account for the actual stretching of the large aggregates, these clusters were discarded from our results.

To hold on to the aggregate during the stretching experiment, a fraction of it was aspirated into both micropipettes, as seen clearly in the optical microscopy images of figure 3. In figure 4c, the measured Young's modulus is plotted as a function of the volume V of the aggregate (outside of the micropipettes) divided by the total volume V_{tot} of the aggregate (inside and outside of the micropipettes). Within experimental error, there is no mechanobiological effect of the aspiration on the measured stiffness.

The Young's modulus and ultimate tensile strength data are summarized in figure 5. The average values across 35 aggregates were determined as $E = 248 \pm 234$ Pa and $\sigma_{UTS} = 390 \pm 334$ Pa (median values shown with black lines in figure 5). In comparison, the stiffness of *individual*, non-activated T-cells has been measured as 80–100 Pa [65,66], whereas activated T-cells have stiffnesses in the range of 100–300 Pa [39]. The increase in stiffness during activation is due to drastic modifications of the actomyosin cytoskeleton. The stiffness of the aggregates is related mainly to changes in the actin cytoskeleton at the contact sites between the cells. Upon cell activation (through the T-cell receptor or with phorbol ester and ionomycin), the cells cluster together with the help of cell adhesion receptors, which leads to downstream signalling events. Integrin–actin linkages, actin polymerization and actin cross-linking (and later on centrosome and Golgi polarization) occurs at the contact sites between the cells, allowing for stiffening of the aggregates.

Our measured mechanical properties are lower than those reported for murine sarcoma aggregates [33,35]. Specifically, micropipette aspiration experiments on these yielded a Young's modulus of $E = 700 \pm 100$ Pa [33]. Measurements using glass slide-based cantilevers showed Young's modulus values ranging from $E = 1000 \pm 300$ Pa at very low speeds ($v < 0.02$ µm s^{-1}) to $E = 9000 \pm 2000$ Pa at higher speeds ($v = 1$ to 50 µm s^{-1}) [35]. Our T-cell aggregates may be softer due to the big differences in adhesion mechanisms and cytoskeletal architecture between immune cells and sarcoma cells. The latter study reported maximum stress values of $\sigma_{max} = 300$–700 Pa, which are similar, within error, to our measurements.

By combining the measured elastic modulus with our mechanistic model (equation (3.1)), the elastic response of one cell (including both the stretching of the cell as well as the deformation of the cell–cell bonds) $k_c \sim r_c E$ can be determined. The average T-cell radius was measured as $r_c = 3.3 \pm 0.8$ µm, giving an average cell spring constant of $k_c \approx 8 \times 10^{-4}$ N m^{-1}. This spring constant agrees well with the results in Lek *et al.* [21], where atomic force microscopy was used to measure the adhesion force

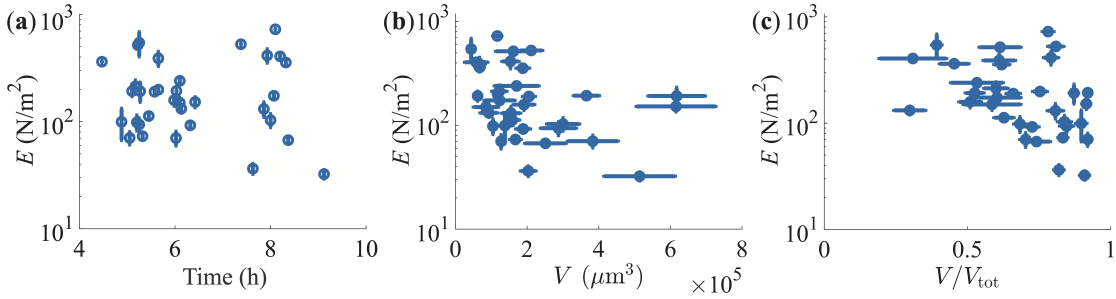

Figure 4. Effect of time, volume and aspiration. Young's modulus of T-cell aggregates (activated with PMA and ionomycin) as a function of (a) time after activation, (b) cluster volume and (c) relative cluster volume outside of the micropipettes. Within error, the stiffness remains constant for all cases.

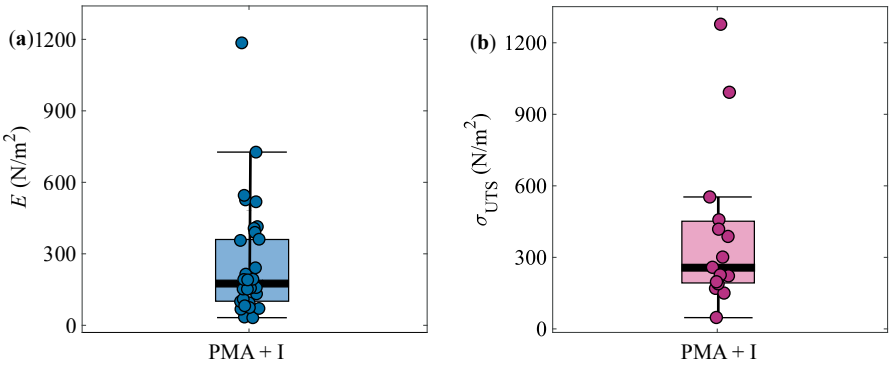

Figure 5. Mechanical properties. (a) The Young's modulus and (b) ultimate tensile strength of T-cell aggregates activated with PMA and ionomycin (i). The thick black line inside the box represents the median. The box spans the interquartile range (IQR), covering the middle 50% of the data. The error bars (whiskers) extend to the minimum and maximum values within 1.5 times the IQR, while points beyond this range are considered outliers.

between a single effector T-cell and an integrin ligand-coated surface. From their data, a spring constant of approximately 10^{-4} N m^{-1} was extracted, which captures both the deformation of the cell as well as the cell–cell adhesion bonds. This agreement underscores the reliability of our experimental and theoretical approach in quantifying T-cell mechanics within cellular aggregates.

In the mechanistic model, we assumed a purely elastic system and that the effect of the lateral bonds between the cells is much smaller than that in the direction of stretching. In the future, a more refined model could be developed to capture how the cells are interconnected. To reliably test such a new model, more advanced stretching experiments using confocal or fluorescence microscopy would be required to track the position and deformation of each cell during stretching as well as their connection points to nearest neighbours. Here, we only used one stretching speed ($v = 20$ μm s^{-1}) to deform the aggregates and probe the elastic response of these. This was to ensure a high enough number of successful experiments given the large variations in the biological sample. In future work, it would be interesting to perform the experiments at different stretching speeds to probe the viscoelastic response of the multicellular material. A more advanced mechanistic model, incorporating an elastic cell shell and its viscoelastic interior, would then be needed to describe the mechanical response.

Stretching experiments were also performed on cells containing a mutation in the β2-integrin that affects T-cell adhesion under flow conditions [67]. These knock-in cells were activated with PMA and ionomycin, but no difference was detected between the knock-in and the wild-type cellular aggregates (see electronic supplementary material). This indicates that the integrin mutation is not important for regulating cell–cell aggregate properties or activation under these activation conditions, as also shown in our previous work [67].

4.2. Pre-stretching of T-cell aggregates

Cells respond to mechanical stimuli by altering their properties. To investigate this in our aggregates, double-stretching experiments were performed. The aggregates were first pre-stretched to a maximum strain of $\varepsilon_1 \approx 0.2$–1, then returned to their initial configurations before being stretched again until rupture (see example experiment in electronic supplementary material, video S4). The average total waiting time between the successive stretches was 9.3 ± 2.1 s and was kept constant for all experiments. Some relaxation of the aggregate occurred during this time. The Young's modulus was measured in both elastic stretching phases, and the change in stiffness (E_2/E_1, where 1 and 2 refer to the first and second stretch, respectively) is plotted as a function of ε_1 in figure 6.

Our results show that aggregates soften in response to pre-stretching by a factor of 0.7 ± 0.3. This is in contrast to previous findings, where mechanical stimulation led to stiffening due to integrin–ICAM catch bond formation [68]. Instead, the viscoelastic relaxation of the aggregates during and after the first stretching phase is likely to have relaxed the aggregate modulus. The pre-stretch could have caused a disruption of the actin cytoskeleton, also known as 'fluidization' [69], which has been shown to occur at higher stretch amplitudes or rates, without affecting cell adhesion. Fluidization of the actin cytoskeleton is due to a broad effect on the whole cytoskeleton rather than a single molecular/signalling event.

4.3. Effect of T-cell activation pathway

When T-cells were treated with W-7 in addition to the standard PMA and ionomycin, the aggregates exhibited increased stiffness compared with those activated with only PMA and ionomycin (figure 7a, see example experiment in electronic supplementary material, video S5). This effect was more pronounced when comparing data from experiments conducted on the same day, using cells from the same mouse. Specifically, the addition of W-7 increased aggregate stiffness by a factor of $E_{PMA+I+W7}/E_{PMA+I} = 2.8 \pm 0.7$ (based on same-mouse experiments). This increase directly translates to a stiffening of the cells including the cell–cell adhesion bonds) by the same factor (equation (3.1)). Biologically, this suggests that T-cells become stiffer in response to W-7, probably due to its inhibition of Ca^{2+}-calmodulin, which itself is an inhibitor of caldesmon–actin bundle binding. By this mechanism, W-7 may be responsible for enhancing T-cell stiffness [70]. Interestingly, we also detected a small (not statistically significant) increase in metabolic activity in W-7-treated cells (see electronic supplementary material, [71]), indicating that altered mechanical responses of the aggregates may also be reflected in the activation response of the cells, for example altered cell proliferation, which we have not explored here.

To further explore the effect of different activation pathways, T-cells were activated using either anti-CD3 antibodies or PMA and ionomycin. Anti-CD3 antibodies provide a more physiologically relevant activation method, as they induce the same conformational change in CD3 (the T-cell antigen receptor) that occurs when it recognizes an antigen *in vivo*. This conformational change initiates the intracellular signalling cascade. The activation with anti-CD3 rendered a clear decrease in the aggregate stiffness as compared with cells activated with PMA and ionomycin (figure 7b, see example experiment in electronic supplementary material, video S6). Comparing the change in stiffness for aggregates with cells from the same mouse, $E_{Anti-CD3}/E_{PMA+I} = 0.30 \pm 0.02$. This suggests a lower level of activation of the T-cells with the antibody as compared with using the more artificial chemicals (which cause maximal activation of the cells). This correlates with lower CD69 expression in anti-CD3 treated cells compared with PMA/ionomycin activation, e.g. lower level of activation (figure 1c). Anti-CD3 is known to stiffen individual T-cells by a factor of two upon activation [39]. Our results indicate that PMA+ionomycin either stiffen the cells by a factor of *ca* 4 upon activation, or that the aggregate stiffness is primarily determined by cell–cell adhesion strength rather than individual cell elasticity.

The immune system is a complex cellular system that mediates functions such as protection against infection and tumour surveillance, but is also involved in pathological events, for example autoimmunity. To mediate these functions, immune cells interact both with other immune cells and non-immune cells, forming interconnected cellular communities. The human immune system consists of approximately 1.8 trillion cells, with a total weight of 1.2 kg. Of these, up to 40% are lymphocytes (T-cells and B-cells) [72]. These cellular communities interact in a highly coordinated manner for the immune system to perform its functions. However, lymphocytes are small and motile and mediate transient interactions with other immune cells and non-immune cells, making their analysis more challenging than the stable interactions found in other tissues and organs in the body.

Transient interactions between immune cells are mediated by cell surface proteins, and their complexity is beginning to be unravelled [73,74]. Immune cells communicate with each other through these cell surface receptors, which initiate intracellular signalling events within the cells, leading to cellular outcomes such as activation and effector functions. The intracellular signals consist of biochemical signals, but more recently, it has become apparent that also mechanical signals are important to determine outcome in immune reactions, such as lymphocyte activation [75]. Indeed, increased stiffness of the environment leads to stronger T-cell activation [76,77]. However, mechanical forces in larger immune cell communities have so far remained uncharacterized due to technical challenges to measure such forces in the small and transient cell groups. Here, we have made a first attempt to characterize mechanical properties of immune cell communities, starting with small T lymphocyte aggregates, and to correlate these with cellular activation outcomes by using novel methodology.

5. Conclusions

In this work, the micropipette force sensor technique was used to directly measure the mechanical properties of mesoscale (diameter approx. 30–120 μm) T-cell aggregates through stretching experiments. The multicellular aggregates were formed upon *in vitro* activation using PMA and ionomycin and their Young's modulus and ultimate tensile strength were determined as $E = 248 \pm 234$ N m^{-2} and $\sigma_{UTS} = 390 \pm 334$ N m^{-2}. These values are similar to the mechanical properties reported in the literature for aggregates made of other cell types. A mechanistic model was developed to couple the emergent mechanical response of the aggregate (Young's modulus E) with the intrinsic mechanical response of the cells (spring constant k_c): $E \sim k_c/r_c$, where r_c is the average cell radius. This rendered $k_c \approx 8 \times 10^{-4}$ N m^{-1} which agrees well with literature values from atomic force microscopy measurements on single T-cells. The addition of W-7 rendered stiffening of the aggregates by a factor of 2.8 ± 0.7, probably due to its inhibition of Ca^{2+}-calmodulin. Conversely, T-cell activation with anti-CD3 rendered softening of the clusters by a factor of

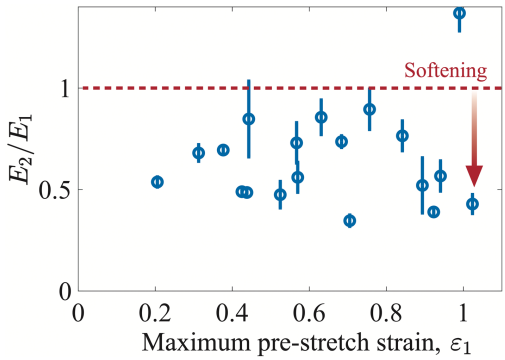

Figure 6. Effect of pre-stretching. The ratio between the Young's modulus in the second (E_2) and first (E_1) stretching experiment as a function of maximum strain ε_1 during the pre-stretching. The aggregates soften after the pre-stretching.

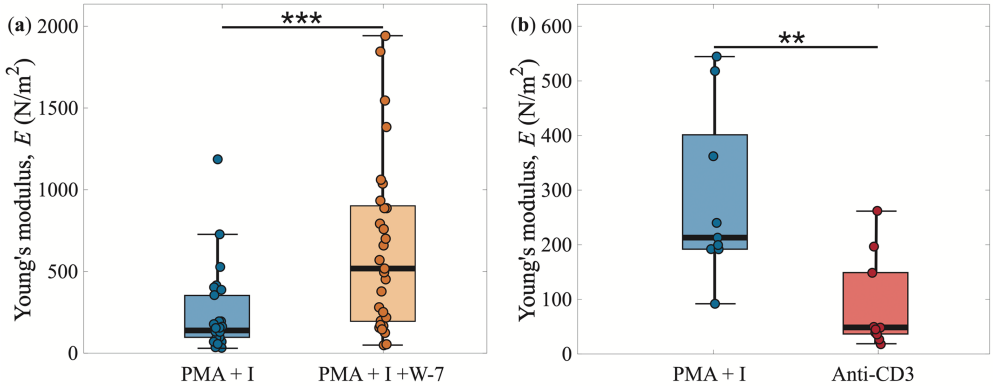

Figure 7. Activation pathways. The Young's modulus of T-cell aggregates activated with PMA+ionomycin compared with (a) aggregates activated also with W-7 and (b) only with anti-CD3. The addition of W-7 makes the aggregates stiffer, whereas anti-CD3 produces softer aggregates than PMA+ionomycin. The stars indicate $^{**}p < 0.01$ and $^{***}p < 0.001$.

0.30 ± 0.02 compared with aggregates activated with PMA and ionomycin. This suggests a lower level of activation of the T-cells with the antibody as compared with using the more artificial chemicals, which cause stronger activation of the cells.

6. Experimental details

6.1. T-cell isolation

The day before an extraction the MACS buffer was prepared following Miltenyi's instructions: phosphate buffered saline (PBS, Lonza, cat. no. 17-516F), 0.5% bovine serum albumin (BSA, Biowest, cat. no. P6154) and 2 mM ethylenediaminetetraacetic acid (EDTA). After the BSA was fully dissolved, the solution was sterilized through filtration through a 22 µm nylon mesh filter (Fisher Scientific, cat. no. 2263548).

Spleens from C57BL/6 N mice were extracted and mechanically dissociated by grinding the tissue between the back of a sterile syringe and a 70 µm cell strainer (Fisher Scientific, cat. no. 22363548) placed over a 50 ml falcon after the cell strainer was wetted using 1 ml of ice-cold PBS (Lonza, cat. no. 17-516F) supplemented with 2% fetal bovine serum (FBS, Gibco, cat no. 10500-064). After the tissue was dissociated, the syringe back and the strainer were rinsed using a further 5 ml of ice-cold PBS + 2% FBS. The cell strainer was discarded, and the cell suspension was centrifuged at 330g for 5 min. The supernatant was discarded, and the pellet was resuspended in room temperature ammonium-chloride-potassium (ACK) lysis buffer (0.15 mol l^{-1} NH_4Cl, 0.01 mol l^{-1} $KHCO_3$ and 0.1 mmol l^{-1} EDTA in milli-Q water) to perform red blood cell lysis. With our aliquot the time needed to do so was 50 s. After this time the cell suspension was diluted to a final volume of 20 ml with PBS + 2% FBS. The cell suspension was passed through a 70 µm cell strainer and into a new falcon. The suspension was then centrifuged at 330g for 5 min and the supernatant discarded. The pellet was resuspended in 40 µl of de-gassed MACS buffer + 10 µl of the biotinylated antibody cocktail from the CD4+T cell enrichment kit (Miltenyi, cat. no. 130-104-454) and placed on ice for 5 min. After the initial incubation on ice, 30 µl of MACS buffer and 20 µl of the anti-biotin magnetic beads from the same kit were added, mixed well and incubated on ice for 10 min.

During the incubation, the magnetic separation column (Miltenyi, cat. no. 130-042-401) was placed on the magnet over a 15 ml falcon and capped with a 70 µm cell strainer and primed by adding 3 ml of MACS buffer. After the 10 min incubation

of the magnetic beads was done, the cell suspension and beads were resuspended in 1 ml of MACS buffer and transferred to the magnetic separation column. After the cell suspension flows through the column, the falcon is rinsed with 1 ml of MACS buffer and the liquid was added to the column. After this, the column was washed with more MACS buffer until 10 ml of MACS buffer and CD4+T cell enriched cell suspension made it through the column. The cell suspension was then counted and centrifuged at 330*g* for 5 min. The supernatant was discarded, and the cell pellet was resuspended in RPMI (Lonza, cat. no. 12-167F/EuroClone, cat. no. ECB9006L) supplemented with 10% FBS (Gibco, cat no. 10500-064), 100 U ml^{-1} penicillin–streptomycin (penicillin, Orion, cat. no. 465161; streptomycin Thermo Fisher Scientific, cat. no. D7253-100 g), 2 mM L-glutamine (Thermo Fisher Scientific, cat. no. BP379-100) and 50 µM 2-mercaptoethanol (Fluka biochemika, cat. no. 63690) at a concentration of 4 million cells ml^{-1} and plated in a 24-well plate (CellStar, cat. no. 662160) and incubated at 37°C before proceeding to the different experiments.

6.2. T-cell treatments

The T-cell suspension was activated using anti-CD3 2.5 µg ml^{-1} (Sigma-Aldrich, cat. no. MAB484) or PMA 10 ng ml^{-1} (Sigma-Aldrich, cat. no. P81389) + Ionomycin 0.5 µg ml^{-1} (Thermo Fisher Scientific, cat. no. J62448.M). In the cases where the calmodulin inhibitor W-7 (Sigma-Aldrich, cat. no. 681629) was used, it was added at 50 µM 30 min before the addition of PMA + Ionomycin.

6.3. Flow cytometry

The following conjugated antibodies were used for flow cytometric analysis of Puromycin-PE (BioLegend, cat. no. 381503, clone 2A4): CD4-PE-Cy7 (BioLegend, cat. no. 100528, clone RM4-5), CD25-APC-Cy7 (BioLegend, cat. no. 102026, clone PC61), CD69-APC (BioLegend, cat. no. 104514), clone H1.2F3. Fc-receptor block (BD Pharmingen, cat. no. 553142 clone 2.4G2) was used in all experiments assessing mouse cells, and unstained and fluorescence minus one (FMO) controls were included in all panels. 7-AAD (eBioscience, cat. no. 00-6993-50) was used to detect dead cells. Acquisition was performed on an LSR Fortessa flow cytometer (Becton Dickinson), and data were analysed using FlowJo software (Tree Star).

6.4. Translation rate analysis

Puromycin (Gibco, cat. no. A11138-03) is incorporated into nascent proteins in a manner that prevents the further extension of said proteins and assayed through flow cytometry using an anti-Puromycin PE conjugated antibody (BioLegend, cat. no. 381503) after fixing and permeabilizing the cells using the Foxp3 permeabilization kit (eBiocience, cat. no. 00-5523-00). To determine the total background for puro-PE fluorescence we used Harringtonine (Sigma-Aldrich, cat. no. SML1091-10MG) at 2 µg ml^{-1} for 30 min before the addition of Puromycin. To determine the maximum energy level of the cells, dimethyl sulfoxide (DMSO, Fisher Scientific, cat. no. BP231-1) 0.08% was used as a negative control and added for 30 min before the addition of Puromycin. To determine the contribution of mitochondrial energy pathways to the total, the mitochondrial ATP synthase inhibitor Oligomycin (Sigma-Aldrich, cat. no. 04876-5MG) was used at 1 µM for 30 min before the addition of Puromycin. To determine the contribution of glucose-related energy production to the total, the phosphoglucoisomerase inhibitor 2-Deoxy-D-Glucose (Sigma-Aldrich, cat. no. D8375-5G) was used for 30 min before the addition of Puromycin. To determine the contribution of glycolysis alone to the cell's energy level a combination of Oligomycin and 2-Deoxy-D-Glucose can be used. In all cases, Puromycin was added at 10 µg ml^{-1} for 45 min after 30 min of incubation with the different inhibitors. The incorporation of puromycin was then assayed via flow cytometry.

6.5. Micropipette force sensor

The MFS was manufactured and calibrated as described in detail in [49]. Briefly, the MFS was made of a hollow glass capillary (World Precision Instruments, TW100-6) with an inner diameter of 0.75 mm and an outer diameter of 1 mm. The cantilever was pulled using a micropipette puller (Narishige, PN-31) and shaped with a microforge (Narishige, MF-900).

Prior to use, the MFS requires calibration to determine its spring constant, k_p. We calibrate our cantilevers using the water droplet method developed by Colbert *et al.* [9] and described in detail in [49], using water drops of different sizes as control weights. The cantilever was mounted horizontally, and a droplet of Milli-Q water (Millipore Direct-Q 3 UV) was pushed out to rest on the cantilever end using a syringe connected with a plastic tube to the micropipette holder (IM-H3 Injection Holder Set by Narishige Lifemed Co., Ltd.). A camera was used to image the experiment from the side at a frame rate of 30 frames s^{-1}. Using an in-house MATLAB (MathWorks) image analysis script, the shape of the drop was modelled as an ellipsoid with a volume of V. The drop weight was then calculated as $W = \rho g V$, where ρ is the density of water. The cantilever deflection Δx was measured as a function of time through image analysis in MATLAB, and the micropipette spring constant was determined using Hooke's law: $k_p = W/\Delta x$. The calibration was repeated several times for each cantilever. In this study, micropipettes with spring constants ranging from 10 to 40 nN μm^{-1} were used.

6.6. Stretching experiments

6.6.1. Microscope set-up

An inverted wide-field microscope (Nikon ECLIPSE Ts2-FL) equipped with a manually adjustable *xy*-stage was used to securely position the sample chamber. A 10× objective (Nikon 10×/0.25 Ph1 DL Objective Lens) was used to ensure sufficient resolution as well as a big enough field of view to observe the cluster deformation and micropipette motion. Image acquisition was performed using a FLIR camera (GS3-U3-23S6M-C, Integrated Imaging Solutions, Inc.) mounted on the microscope. An image sequence of the experiment was recorded at 30 frames s^{-1}, a frame rate chosen to match the experimental speed and ensure adequate temporal resolution.

6.6.2. Experimental chamber

The sample chamber was constructed using aluminium and designed to hold two untreated glass slides at a fixed spacing. Depending on the volume of the cell solution media, two sizes of glass slides were used (Plain Pre-Cleaned Microscope Slides, 75 × 50 mm, thickness of 0.96 to 1.06 mm, and VWR Ground Edge Microscope Slides, 75 × 25 mm, thickness of 0.8 to 1.2 mm). Spacing between the slides was maintained using four plastic spacers, each 2 mm thick, placed at the corners of the slides to create a uniform 2 mm gap (figure 2a). The cell culture media was injected into the chamber using a plastic pipette, with the tip widened by cutting it with scissors to minimize disruption of the clusters during injection. Surface tension prevented leakage from the chamber, while strong intercellular bonds ensured the integrity of the clusters during their transfer from a 24-well plate to the sample chamber.

6.6.3. Micropipette set-up

Cantilevers of two micropipettes were positioned parallel to the *xy*-plane, situated between the glass slides and submerged in the cell culture medium. Each micropipette was connected to a micropipette injection holder (IM-H3 Injection Holder Set by Narishige Lifemed Co., Ltd.), which was linked via plastic tubing (i.d. = 1 mm; Narishige, model no. CT-1) to syringes (sizes ranging from 10 to 20 ml) filled with water. The holders were securely mounted on optical bases (Dynamically Damped Post, 14′ Long, Metric, Ø1.5′, Thorlabs, model no. DP14A/M) fixed to an active vibration isolation stage (MVIS 30 × 30 model by Newport Corporation), minimizing interference from environmental vibrations or nearby movement. Suction pressure, controlled via the syringes, was used to enable the micropipettes to firmly grasp the clusters.

A straight micropipette was attached to a linear motor (Thorlabs Kinesis Brushed Motor Controller) to enable controlled motion along the *x*-axis, with an initial acceleration of 1 mm s^{-2} and a constant velocity of 20 µm s^{-1}. An L-shaped micropipette was positioned such that the bent portion of its cantilever was parallel to the cantilever of the straight micropipette. The L-shaped micropipette remained stationary throughout the experiment and functioned as a force sensor.

6.6.4. Experimental procedure

T-cells were extracted and activated at the University of Helsinki and moved to Aalto University for mechanical analysis in 6-well cell culture plates in a Styrofoam box at 37°C. All samples were analysed within 12 h of activation. The prepared cell media contained a high density of single T-cells and a small number of aggregates. Since the cells and aggregates were denser than the surrounding medium, they settled onto the bottom slide of the experimental chamber. To allow for proper settling, the sample was left undisturbed for a few minutes before beginning the experiment. Once an aggregate had stabilized on the bottom slide, the straight micropipette was used to lift it from the surface and position it between the slides. Both micropipettes then grasped the aggregate, ensuring that neither of them made contact with the slides. The linear motor was activated, causing the straight micropipette to move backward and stretch the cluster. This induced deflection in the stationary L-shaped micropipette, which served as a force sensor. The applied force and cluster deformation were determined by analysing the recorded images using MATLAB.

In the cell culture medium, a limited number of aggregates were present, exhibiting variations in size and shape. For the experiments, aggregates with a somewhat uniform shape, structure and density were selected. Experiments were deemed invalid, and their results were excluded if any of the following conditions occurred: aggregate rotation, vertical displacement of the straight micropipette, rupture of the aggregate at the onset of the test without any observed stretching or deformation, or the appearance of jumps in the stress–strain graph. These jumps in the measured force were attributed to fluctuations in suction pressure during the experiment, leading to inconsistent data. Keeping the aspirated part of the aggregate fixed typically required less suction at the beginning of the experiment compared with when the cluster was fully stretched and close to rupture. As a result, the applied suction pressure was not constant throughout the experiment and was instead adjusted to maintain a stable aspiration length. However, in some instances, the cluster was drawn further into the micropipette due to excessive suction, or it slipped out because of insufficient suction. In such cases, we discarded the ultimate tensile strength from our measurements and only reported the Young's modulus.

6.6.5. Analysis of measurements

MATLAB was used to determine the initial dimensions of the aggregate by measuring the distance between designated points in the experimental frames. In particular, the initial radius (R_0) and length (L_0) of the aggregate were determined from the first

frame. The initial length was measured as the distance between the openings of the two micropipettes. To ensure measurement accuracy, each measurement was repeated five times across different positions of the cluster, with the mean and standard deviation calculated and reported for subsequent calculations. The error bars in figure 2c are error propagations based on the formula used to calculate the stress–strain relationship using these standard deviations for R_0 and L_0 as well as the standard deviation for k_p (from several calibration measurements on the same micropipette). The errors for the stress are so small that they are not visible in the graph. We also used MATLAB to determine the deflection of the L-shaped micropipette as a function of time, $x(t)$. This deflection was used to calculate the applied force as a function of time, $F(t)$. Additionally, the change in the length of the cluster as $\Delta L = x_s - x$, where $x_s = vt$ is the motion of the straight micropipette. The Young's modulus was determined by fitting a line to the first 10–30 data points in the stress–strain graph.

6.6.6. Validation and replication

To ensure consistency and accuracy, stiffness measurements were performed on 5 to 25 clusters from each prepared cell media sample.

6.7. Statistical analysis

We performed Welch's *t*-test (MATLAB 'ttest2') to statistically validate the difference between (i) unactivated and activated T-cells with respect to expression levels of CD69 and CD25 (figure 1c–d) and (ii) Young's moduli of aggregates activated by different agents (figure 7).

Ethics. All the experiments were performed according to the Finnish Act on the Protection of Animals Used for Scientific or Educational Purposes (497/2013) and to the Directive 2010/63/EU of the European Parliament and of the Council of 22 September 2010 on the protection of animals used for scientific purposes and approved by the Finnish National Animal Experiment Board (Hankelupalautakunta—ELLA).

Data accessibility. The datasets used for plotting all graphs in the paper and examples of raw data files are shared on Zenodo [78].

Supplementary material is available online [79].

Declaration of AI use. We have not used AI-assisted technologies in creating this article.

Authors' contributions. S.A.: formal analysis, investigation, methodology, software, visualization, writing—original draft, writing—review and editing; G.S.R.: formal analysis, investigation, methodology, visualization, writing—original draft, writing—review and editing; A.D.: formal analysis, investigation, methodology, software, visualization, writing—review and editing; H.H.: conceptualization, investigation, supervision, writing—review and editing; S.C.F.: conceptualization, funding acquisition, methodology, project administration, supervision, writing—original draft; M.B.: conceptualization, formal analysis, investigation, methodology, project administration, supervision, writing—original draft.

All authors gave final approval for publication and agreed to be held accountable for the work performed therein.

Conflict of interest declaration. We declare we have no competing interests.

Funding. This research was funded by the Väisälä project grant RESOLVE by the Finnish Academy of Science Letters (M.B.), the Jane and Aatos Erkko Foundation grant ROOTS (M.B.), and by Research Council of Finland (S.C.F., H.H.), Livoch Hälsa foundation (S.C.F.) and Magnus Ehrnrooth foundation (S.C.F.).

Acknowledgements. We thank Dr. Maja Vuckovac for her help in the laboratory.

References

1. Ackermann J, Ben Amar M, Joanny JF. 2021 Multi-cellular aggregates, a model for living matter. *Phys. Rep*. **927**, 1–29. (doi:10.1016/j.physrep.2021.05.001)
2. Bassi G, Grimaudo MA, Panseri S, Montesi M. 2021 Advanced multi-dimensional cellular models as emerging reality to reproduce *in vitro* the human body complexity. *Int. J. Mol. Sci*. **22**, 1195. (doi:10.3390/ijms22031195)
3. Fletcher AG, Osterfield M, Baker RE, Shvartsman SY. 2014 Vertex models of epithelial morphogenesis. *Biophys. J*. **106**, 2291–2304. (doi:10.1016/j.bpj.2013.11.4498)
4. Fagerholm SC, Prescott A, Cohen P, Gahmberg CG. 2001 An essential role for calmodulin in regulating human T cell aggregation. *FEBS Lett*. **491**, 131–136. (doi:10.1016/s0014-5793(01)02182-2)
5. Nunes AS, Barros AS, Costa EC, Moreira AF, Correia IJ. 2019 3D tumor spheroids as *in vitro* models to mimic *in vivo* human solid tumors resistance to therapeutic drugs. *Biotechnol. Bioeng*. **116**, 206–226. (doi:10.1002/bit.26845)
6. Radmacher M, Fritz M, Kacher CM, Cleveland JP, Hansma PK. 1996 Measuring the viscoelastic properties of human platelets with the atomic force microscope. *Biophys. J*. **70**, 556–567. (doi:10.1016/s0006-3495(96)79602-9)
7. Sleep J, Wilson D, Simmons R, Gratzer W. 1999 Elasticity of the red cell membrane and its relation to hemolytic disorders: an optical tweezers study. *Biophys. J*. **77**, 3085–3095. (doi:10.1016/s0006-3495(99)77139-0)
8. Colbert MJ, Raegen AN, Fradin C, Dalnoki-Veress K. 2009 Adhesion and membrane tension of single vesicles and living cells using a micropipette-based technique. *Eur. Phys. J. E* **30**, 117–121. (doi:10.1140/epje/i2009-10514-7)
9. Colbert MJ, Brochard-Wyart F, Fradin C, Dalnoki-Veress K. 2010 Squeezing and detachment of living cells. *Biophys. J*. **99**, 3555–3562. (doi:10.1016/j.bpj.2010.10.008)
10. Van Vliet KJ, Bao G, Suresh S. 2003 The biomechanics toolbox: experimental approaches for living cells and biomolecules. *Acta Mater*. **51**, 5881–5905. (doi:10.1016/j.actamat.2003.09.001)
11. Mitrossilis D, Fouchard J, Guiroy A, Desprat N, Rodriguez N, Fabry B, Asnacios A. 2009 Single-cell response to stiffness exhibits muscle-like behavior. *Proc. Natl Acad. Sci. USA* **106**, 18243–18248. (doi:10.1073/pnas.0903994106)
12. Mitrossilis D, Fouchard J, Pereira D, Postic F, Richert A, Saint-Jean M, Asnacios A. 2010 Real-time single-cell response to stiffness. *Proc. Natl Acad. Sci. USA* **107**, 16518–16523. (doi:10.1073/pnas.1007940107)

13. Urbanska M, Guck J. 2024 Single-cell mechanics: structural determinants and functional relevance. *Annu. Rev. Biophys*. **53**, 367–395. (doi:10.1146/annurev-biophys-030822-030629)
14. Coman DR. 1944 Decreased mutual adhesiveness, a property of cells from squamous cell carcinomas. *Cancer Res*. **4**, 625–629.
15. Evans EA. 1980 Analysis of adhesion of large vesicles to surfaces. *Biophys. J*. **31**, 425–431. (doi:10.1016/S0006-3495(80)85069-7)
16. Evans EA. 1980 Minimum energy analysis of membrane deformation applied to pipet aspiration and surface adhesion of red blood cells. *Biophys. J*. **30**, 265–284. (doi:10.1016/s0006-3495(80)85093-4)
17. Francis GW, Fisher LR, Gamble RA, Gingell D. 1987 Direct measurement of cell detachment force on single cells using a new electromechanical method. *J. Cell Sci*. **87**, 519–523. (doi:10.1242/jcs.87.4.519)
18. Evans E, Ritchie K, Merkel R. 1995 Sensitive force technique to probe molecular adhesion and structural linkages at biological interfaces. *Biophys. J*. **68**, 2580–2587. (doi:10.1016/s0006-3495(95)80441-8)
19. Benoit M, Gabriel D, Gerisch G, Gaub HE. 2000 Discrete interactions in cell adhesion measured by single-molecule force spectroscopy. *Nat. Cell Biol*. **2**, 313–317. (doi:10.1038/35014000)
20. Litvinov RI, Shuman H, Bennett JS, Weisel JW. 2002 Binding strength and activation state of single fibrinogen-integrin pairs on living cells. *Proc. Natl Acad. Sci. USA* **99**, 7426–7431. (doi:10.1073/pnas.112194999)
21. Lek HS, Morrison VL, Conneely M, Campbell PA, McGloin D, Kliche S, Watts C, Prescott A, Fagerholm SC. 2013 The spontaneously adhesive leukocyte function-associated antigen-1 (LFA-1) integrin in effector T cells mediates rapid actin- and calmodulin-dependent adhesion strengthening to ligand under shear flow. *J. Biol. Chem*. **288**, 14698–14708. (doi:10.1074/jbc.m112.430918)
22. McDonald C, Morrison VL, McGloin D, Fagerholm SC. 2022 Examining the effect of Kindlin-3 binding site mutation on LFA-1-ICAM-1 bonds by force measuring optical tweezers. *Front. Immunol*. **12**, 792813. (doi:10.3389/fimmu.2021.792813)
23. Petit J *et al*. 2018 A modular approach for multifunctional polymersomes with controlled adhesive properties. *Soft Matter* **14**, 894–900. (doi:10.1039/c7sm01885a)
24. Ungai-Salánki R, Peter B, Gerecsei T, Orgovan N, Horvath R, Szabó B. 2019 A practical review on the measurement tools for cellular adhesion force. *Adv. Colloid Interface Sci*. **269**, 309–333. (doi:10.1016/j.cis.2019.05.005)
25. Foty RA, Forgacs G, Pfleger CM, Steinberg MS. 1994 Liquid properties of embryonic tissues: measurement of interfacial tensions. *Phys. Rev. Lett*. **72**, 2298–2301. (doi:10.1103/physrevlett.72.2298)
26. Norotte C, Marga F, Neagu A, Kosztin I, Forgacs G. 2008 Experimental evaluation of apparent tissue surface tension based on the exact solution of the Laplace equation. *Europhys. Lett*. **81**, 46003.
27. Mgharbel A, Delanoë-Ayari H, Rieu J. 2009 Measuring accurately liquid and tissue surface tension with a compression plate tensiometer. *HFSP J*. **3**, 213–221. (doi:10.2976/1.3116822)
28. Kalantarian A, Ninomiya H, Saad SMI, David R, Winklbauer R, Neumann AW. 2009 Axisymmetric drop shape analysis for estimating the surface tension of cell aggregates by centrifugation. *Biophys. J*. **96**, 1606–1616. (doi:10.1016/j.bpj.2008.10.064)
29. Ryan PL, Foty RA, Kohn J, Steinberg MS. 2001 Tissue spreading on implantable substrates is a competitive outcome of cell–cell vs. cell–substratum adhesivity. *Proc. Natl Acad. Sci. USA* **98**, 4323–4327. (doi:10.1073/pnas.071615398)
30. Douezan S, Guevorkian K, Naouar R, Dufour S, Cuvelier D, Brochard-Wyart F. 2011 Spreading dynamics and wetting transition of cellular aggregates. *Proc. Natl Acad. Sci. USA* **108**, 7315–7320. (doi:10.1073/pnas.1018057108)
31. Douezan S, Brochard-Wyart F. 2012 Spreading dynamics of cellular aggregates confined to adhesive bands. *Eur. Phys. J. E* **35**, 116. (doi:10.1140/epje/i2012-12116-8)
32. Beaune G *et al*. 2014 How cells flow in the spreading of cellular aggregates. *Proc. Natl Acad. Sci. USA* **111**, 8055–8060. (doi:10.1073/pnas.1323788111)
33. Guevorkian K, Colbert MJ, Durth M, Dufour S, Brochard-Wyart F. 2010 Aspiration of biological viscoelastic drops. *Phys. Rev. Lett*. **104**, 218101. (doi:10.1103/physrevlett.104.218101)
34. Guevorkian K, Gonzalez-Rodriguez D, Carlier C, Dufour S, Brochard-Wyart F. 2011 Mechanosensitive shivering of model tissues under controlled aspiration. *Proc. Natl Acad. Sci. USA* **108**, 13387–13392. (doi:10.1073/pnas.1105741108)
35. Gonzalez-Rodriguez D, Bonnemay L, Elgeti J, Dufour S, Cuvelier D, Brochard-Wyart F. 2013 Detachment and fracture of cellular aggregates. *Soft Matter* **9**, 2282. (doi:10.1039/c2sm26648b)
36. Lyu Q *et al*. 2022 A soft and ultrasensitive force sensing diaphragm for probing cardiac organoids instantaneously and wirelessly. *Nat. Commun*. **13**, 7259. (doi:10.1038/s41467-022-34860-y)
37. Janeway CA, Travers P, Walport M, Shlomchik MJ. 2001 *Immunobiology: the immune system in health and disease*, 5th edn. New York, NY: Garland Science.
38. Basu R *et al*. 2016 Cytotoxic T cells use mechanical force to potentiate target cell killing. *Cell* **165**, 100–110. (doi:10.1016/j.cell.2016.01.021)
39. Sawicka A, Babataheri A, Dogniaux S, Barakat AI, Gonzalez-Rodriguez D, Hivroz C, Husson J. 2017 Micropipette force probe to quantify single-cell force generation: application to T-cell activation. *Mol. Biol. Cell* **28**, 3229–3239. (doi:10.1091/mbc.e17-06-0385)
40. Larsen CS. 1990 Activation of human T lymphocytes by phorbol-12,13-dibutyrate and ionomycin. *Scand. J. Immunol*. **31**, 353–360. (doi:10.1111/j.1365-3083.1990.tb02778.x)
41. Pan F, Means AR, Liu JO. 2005 Calmodulin-dependent protein kinase IV regulates nuclear export of Cabin1 during T-cell activation. *EMBO J*. **24**, 2104–2113. (doi:10.1038/sj.emboj.7600685)
42. Sabatos CA, Doh J, Chakravarti S, Friedman RS, Pandurangi PG, Tooley AJ, Krummel MF. 2008 A synaptic basis for paracrine interleukin-2 signaling during homotypic T cell interaction. *Immunity* **29**, 238–248. (doi:10.1016/j.immuni.2008.05.017)
43. Hu KH, Butte MJ. 2016 T cell activation requires force generation. *J. Cell Biol*. **213**, 535–542. (doi:10.1083/jcb.201511053)
44. Du H, Bartleson JM, Butenko S, Alonso V, Liu WF, Winer DA, Butte MJ. 2023 Tuning immunity through tissue mechanotransduction. *Nat. Rev. Immunol*. **23**, 174–188. (doi:10.1038/s41577-022-00761-w)
45. Darzynkiewicz Z, Juan G, Li X, Gorczyca W, Murakami T, Traganos F. 1997 Cytometry in cell necrobiology: analysis of apoptosis and accidental cell death (necrosis). *Cytometry* **27**, 1–20. (doi:10.1002/(sici)1097-0320(19970101)27:13.3.co;2-x)
46. Chatila T, Silverman L, Miller R, Geha R. 1989 Mechanisms of T cell activation by the calcium ionophore ionomycin. *J. Immunol*. **143**, 1283–1289. (doi:10.4049/jimmunol.143.4.1283)
47. Osawa M, Swindells MB, Tanikawa J, Tanaka T, Mase T, Furuya T, Ikura M. 1998 Solution structure of calmodulin-W-7 complex: the basis of diversity in molecular recognition. *J. Mol. Biol*. **276**, 165–176. (doi:10.1006/jmbi.1997.1524)
48. Hidaka H, Sasaki Y, Tanaka T, Endo T, Ohno S, Fujii Y, Nagata T. 1981 N-(6-aminohexyl)-5-chloro-1-naphthalenesulfonamide, a calmodulin antagonist, inhibits cell proliferation. *Proc. Natl Acad. Sci. USA* **78**, 4354–4357. (doi:10.1073/pnas.78.7.4354)

49. Backholm M, Bäumchen O. 2019 Micropipette force sensors for *in vivo* force measurements on single cells and multicellular microorganisms. *Nat. Protoc.* **14**, 594–615. (doi:10.1038/s41596-018-0110-x)
50. Yeung AKC, Pelton R. 1996 Micromechanics: a new approach to studying the strength and breakup of flocs. *J. Colloid Interface Sci.* **184**, 579–585. (doi:10.1006/jcis.1996.0654)
51. Poppele EH, Hozalski RM. 2003 Micro-cantilever method for measuring the tensile strength of biofilms and microbial flocs. *J. Microbiol. Methods* **55**, 607–615. (doi:10.1016/s0167-7012(03)00198-2)
52. Backholm M, Ryu WS, Dalnoki-Veress K. 2013 Viscoelastic properties of the nematode *Caenorhabditis elegans*, a self-similar, shear-thinning worm. *Proc. Natl Acad. Sci. USA* **110**, 4528–4533. (doi:10.1073/pnas.1219965110)
53. Backholm M, Ryu WS, Dalnoki-Veress K. 2015 The nematode *C. elegans* as a complex viscoelastic fluid. *Eur. Phys. J. E* **38**, 36. (doi:10.1140/epje/i2015-15036-1)
54. Gere JM, Goodno BJ. 2011 *Mechanics of materials*. Boston, MA: Cengage Learning.
55. Gibson MC, Patel AB, Nagpal R, Perrimon N. 2006 The emergence of geometric order in proliferating metazoan epithelia. *Nature* **442**, 1038–1041. (doi:10.1038/nature05014)
56. Nagpal R, Patel A, Gibson MC. 2008 Epithelial topology. *BioEssays* **30**, 260–266. (doi:10.1002/bies.20722)
57. Hannezo E, Prost J, Joanny JF. 2014 Theory of epithelial sheet morphology in three dimensions. *Proc. Natl Acad. Sci. USA* **111**, 27–32. (doi:10.1073/pnas.1312076111)
58. Stott EL, Britton NF, Glazier JA, Zajac M. 1999 Stochastic simulation of benign avascular tumour growth using the Potts model. *Math. Comput. Model.* **30**, 183–198. (doi:10.1016/s0895-7177(99)00156-9)
59. Bielmeier C, Alt S, Weichselberger V, La Fortezza M, Harz H, Jülicher F, Salbreux G, Classen AK. 2016 Interface contractility between differently fated cells drives cell elimination and cyst formation. *Curr. Biol.* **26**, 563–574. (doi:10.1016/j.cub.2015.12.063)
60. Cerruti B *et al*. 2013 Polarity, cell division, and out-of-equilibrium dynamics control the growth of epithelial structures. *J. Cell Biol.* **203**, 359–372. (doi:10.1083/jcb.201305044)
61. Okuda S, Inoue Y, Adachi T. 2015 Three-dimensional vertex model for simulating multicellular morphogenesis. *Biophys. Physicobiology* **12**, 13–20. (doi:10.2142/biophysico.12.0_13)
62. Lawson-Keister E, Zhang T, Nazari F, Fagotto F, Manning ML. 2024 Differences in boundary behavior in the 3D vertex and Voronoi models. *PLoS Comput. Biol.* **20**, e1011724. (doi:10.1371/journal.pcbi.1011724)
63. Serna JD, Joshi A. 2011 Studying springs in series using a single spring. *Phys. Educ.* **46**, 33–40. (doi:10.1088/0031-9120/46/1/003)
64. Rao SS, Fah YF. 2011 *Mechanical vibrations*, 5th edn. Singapore: Prentice Hall/Pearson.
65. Bufi N, Saitakis M, Dogniaux S, Buschinger O, Bohineust A, Richert A, Maurin M, Hivroz C, Asnacios A. 2015 Human primary immune cells exhibit distinct mechanical properties that are modified by inflammation. *Biophys. J.* **108**, 2181–2190. (doi:10.1016/j.bpj.2015.03.047)
66. Guillou L, Babataheri A, Saitakis M, Bohineust A, Dogniaux S, Hivroz C, Barakat AI, Husson J. 2016 T-lymphocyte passive deformation is controlled by unfolding of membrane surface reservoirs. *Mol. Biol. Cell* **27**, 3574–3582. (doi:10.1091/mbc.e16-06-0414)
67. Morrison VL, MacPherson M, Savinko T, San Lek H, Prescott A, Fagerholm SC. 2013 The β2 integrin–kindlin-3 interaction is essential for T-cell homing but dispensable for T-cell activation *in vivo*. *Blood* **122**, 1428–1436. (doi:10.1182/blood-2013-02-484998)
68. Chen W, Lou J, Zhu C. 2011 Forcing switch from short- to intermediate- and long-lived states of the αA domain generates LFA-1/ICAM-1 catch bonds. *J. Biol. Chem.* **286**, 18344. (doi:10.1074/jbc.a110.155770)
69. Andreu I *et al*. 2021 The force loading rate drives cell mechanosensing through both reinforcement and cytoskeletal softening. *Nat. Commun.* **12**, 4229. (doi:10.1038/s41467-021-24383-3)
70. Kokate SB, Ciuba K, Tran VD, Kumari R, Tojkander S, Engel U, Kogan K, Kumar S, Lappalainen P. 2022 Caldesmon controls stress fiber force-balance through dynamic cross-linking of myosin II and actin-tropomyosin filaments. *Nat. Commun.* **13**, 6032. (doi:10.1038/s41467-022-33688-w)
71. Argüello RJ *et al*. 2020 SCENITH: A flow cytometry-based method to functionally profile energy metabolism with single-cell resolution. *Cell Metab.* **32**, 1063–1075.(doi:10.1016/j.cmet.2020.11.007)
72. Sender R *et al*. 2023 The total mass, number, and distribution of immune cells in the human body. *Proc. Natl Acad. Sci. USA* **120**, e2308511120. (doi:10.1073/pnas.2308511120)
73. Nakandakari-Higa S *et al*. 2024 Universal recording of immune cell interactions *in vivo*. *Nature* **627**, 399–406. (doi:10.1038/s41586-024-07134-4)
74. Shilts J *et al*. 2022 A physical wiring diagram for the human immune system. *Nature* **608**, 397–404. (doi:10.1038/s41586-022-05028-x)
75. Huse M. 2017 Mechanical forces in the immune system. *Nat. Rev. Immunol.* **17**, 679–690. (doi:10.1038/nri.2017.74)
76. Blumenthal D, Chandra V, Avery L, Burkhardt JK. 2020 Mouse T cell priming is enhanced by maturation-dependent stiffening of the dendritic cell cortex. *eLife* **9**, e55995. (doi:10.7554/elife.55995)
77. Saitakis M, Dogniaux S, Goudot C, Bufi N, Asnacios S, Maurin M, Randriamampita C, Asnacios A, Hivroz C. 2017 Different TCR-induced T lymphocyte responses are potentiated by stiffness with variable sensitivity. *eLife* **6**, e23190. (doi:10.7554/elife.23190)
78. Askari S, Rubio GS, Datar A, Harjunpää H, Fagerholm SC, Backholm M. 2025 Data from: Soft matter mechanics of immune cell aggregates. Zenodo. (doi:10.5281/zenodo.15672310)
79. Askari S, Saldo Rubio G, Datar A, Harjunpää H, Fagerholm Susanna SC, Backholm M. 2025 Supplementary material from: Soft matter mechanics of immune cell aggregates. Figshare. ()

Supplementary Material for

Soft matter mechanics of immune cell aggregates

S. Askari,[1,†] G. Saldo Rubio,[2,†] A. Datar,[1] H. Harjunpää,[2] S. C. Fagerholm,[2,‡] and M. Backholm[1,*]

[1]Department of Applied Physics, Aalto University, Espoo, Finland
[2]Research Program of Molecular and Integrative Biosciences, Faculty of Bio- and Environmental Sciences, University of Helsinki, Helsinki, Finland
[†]Equal contribution

Knock-in cells

There is a mouse model which has a knock-in (KI) TTT/AAA mutation in the β2 integrin that prevents the binding of Kindlin 3 to the cytoplasmatic tail of the protein and impairs part of its function, especially under conditions of shear flow. However, we found that the mutation has no effect on T-cell aggregate stiffness (**Fig. S1**), which correlates well will previous experiments that it also does not impact T-cell activation under these conditions (*67*).

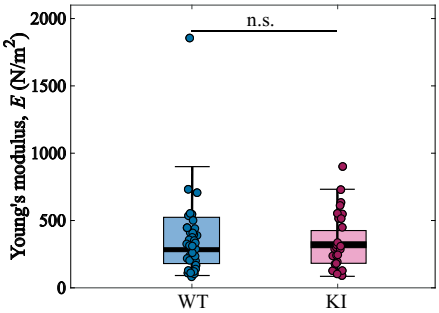

FIG. S1. Young's modulus of wild-type (WT) and knock-in (KI) T-cell aggregates 4 and 10h post-induction with PMA (10 ng/mL) and ionomycin (0.5 µg/ml). No significant difference was found between these two groups (n.s., $p > 0.05$).

Metabolic activity

T-cell activation leads not only to cell aggregation and increased expression of activation markers, but also to changes in cellular metabolism. To investigate whether increased aggregate stiffness of W-7-treated cells was associated with an increased rate of cellular metabolism, we investigated protein translation rates of PMA+ionomycin-treated cells versus those treated also with W-7, by utilizing a puromycin-incorporation assay (*78*). Interestingly, we observed a minor (not significant) increase in cell metabolism of W-7-treated cells (**FIG. S2**), indicating that aggregate stiffness may correlate with altered cellular responses during activation.

[‡]susanna.fagerholm@helsinki.fi
*matilda.backholm@aalto.fi

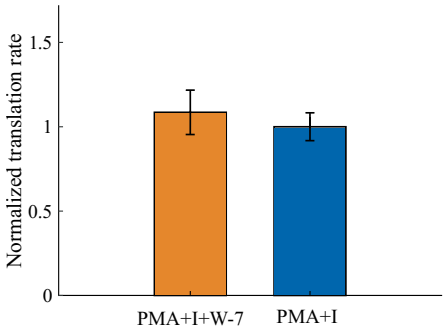

FIG. S2. Translation rate of T-cells at 24h post-induction with either PMA (10 ng/mL) and ionomycin (0.5 μg/ml) or with the same after a 30 min incubation with W-7 (50 μM). The results are normalized to the translation rate without W-7 ($n = 5$). No significant difference was found between these two groups.

Supplementary Movies

Movie S1 | Stretching experiment of T-cell aggregate

Movie (S1.mp4) from a representative MFS stretching experiment on a T-cell aggregate (volume $V = (20 \pm 2) \times 10^4\ \mu\text{m}^3$) activated with PMA+I (same as plotted in **Fig. 2c**).

Movie S2 | Stretching experiment of small T-cell aggregate

Movie (S2.mp4) from a representative MFS stretching experiment on a small T-cell aggregate (volume $V = (15 \pm 2) \times 10^4\ \mu\text{m}^3$) activated with PMA+I.

Movie S3 | Stretching experiment of large T-cell aggregate

Movie (S3.mp4) from a representative MFS stretching experiment on a large T-cell aggregate (volume $V = (51 \pm 10) \times 10^4\ \mu\text{m}^3$) activated with PMA+I.

Movie S4 | Pre-stretching experiment of T-cell aggregate

Movie (S4.mp4) from a representative MFS pre-stretching experiment on a T-cell aggregate (volume $V = (32 \pm 2) \times 10^4\ \mu\text{m}^3$) activated with PMA+I. The aggregate is pre-stretched to a maximum strain of $\varepsilon_1 \approx 0.7$, after which it is returned to the initial configuration to finally be stretched again until rupture.

Movie S5 | Stretching experiment of T-cell aggregate activated with W-7

Movie (S5.mp4) from a representative MFS stretching experiment on a T-cell aggregate (volume $V = (52 \pm 6) \times 10^4\ \mu\text{m}^3$) activated with PMA+I+W-7.

Movie S6 | Stretching experiment of T-cell aggregate activated with Anti-CD3

Movie (S6.mp4) from a representative MFS stretching experiment on a T-cell aggregate (volume $V = (26 \pm 2) \times 10^4\ \mu\text{m}^3$) activated with Anti-CD3.